ANALYSIS AND SOLUTIONS FOR RFID TAG AND RFID READER DEPLOYMENT IN WIRELESS COMMUNICATIONS APPLICATIONS

MAJID SALIM AL KHAMBASHI

Ph.D.

2012

ANALYSIS AND SOLUTIONS FOR RFID TAG AND RFID READER DEPLOYMENT IN WIRELESS COMMUNICATIONS APPLICATIONS

Simulation and Measurement of Linear and Circular Polarised RFID Tag and Reader Antennas and analysing the Tags radiation efficiency when operated close to the human body

Majid Salim AL KHAMBASHI
H.Dip.Lab.S., H.N.Dip.Eng., M.Sc.

Submitted for the Degree of

Doctor of Philosophy

School of Engineering, Design and Technology

University of Bradford

2012

Abstract

ANALYSIS AND SOLUTIONS FOR RFID TAG AND RFID READER DEPLOYMENT IN WIRELESS COMMUNICATIONS APPLICATIONS

Simulation and Measurement of Linear and Circular Polarised RFID Tag and Reader Antennas, and analysing the Tags radiation efficiency when operated close to the human body

Majid Al khambashi

Keywords

Radio Frequency Identification (RFID); Sensor Antennas; Genetic Algorithms (GA); Antennas; Antenna Polarisation; Radiation Pattern; Finite-Difference Time-Domain (FDTD); Method of Moments (MoM); Balun.

The aim of this study is to analysis, investigate and find out the solutions for the problems associated with the implementations of antennas RFID Reader and Tag for various applications. In particular, the efficiency of the RFID reader antenna and the detection range of the RFID tag antenna, subject to a small and compact antenna's design configuration have been studied.

The present work has been addressed directly to reduce the cost, size and increase the detection range and communication reliability of the RFID framework antennas. Furthermore, the modelling concept of RFID passive tags mounted on various materials including the novel design of RFID reader antenna using Genetic Algorithm (GA) are considered and discussed to maintain reliable and efficient antenna radiation performances.

The main benefit of applying GA is to provide fast, accurate and reliable solutions of antenna's structure. Therefore, the GA has been successfully employed to design examples: meander-line, two linear cross elements and compact Helical-Spiral antennas.

In addition, a hybrid method to model the human body interaction with RFID tag antenna operating at 900*MHz* has been studied. The near field distribution and the radiation pattern together with the statistical distribution of the radiation efficiency and the absorbed power in terms of cumulative distribution functions for different orientation and location of RFID's tag antenna on the human body have been demonstrated.

Several tag antennas with symmetrical and unsymmetrical structure configurations operating in the European UHF band 850-950 *MHz* have been fabricated and tested. . The measured and simulated results have been found to be in a good agreement with reasonable impedance matching to the typical input impedance of an RFID integrated circuit chip and nominal power gain and radiation patterns..

Acknowledgements

This report could not have written without ***Prof Raed A. Abd-Alhameed and Dr HS Rajamani*** who are not only served as my supervisors but also encourage me throughout my academic program. They also guided me through the project process, never accepting less than my best efforts.

In addition, I would like to take this opportunity to thank ***Dr D. Zhou, Dr C. H. See*** **and** ***Mr M. B. Child*** for their excellent assistance in the model process and taking the measurements, and my deepest gratitude to ***Prof Raed's students.***

I would like to express my deepest appreciation to **my wife, my kids (Mjed, Malk, Maha and Miar), my parents and cousins.**

I am grateful to great support of all my friends.

Finally, I'd like to thank everyone who helped and support this research project in terms the practical implementation of all RFID samples.

TABLE OF CONTENTS

CHAPTER EIGHT
CONCLUSIONS AND SUGGESTIONS FOR FUTURE WORK

List of Tables

LIST OF FIGURES

LIST OF ABBREVIATIONS

2D	Two dimensional
3D	Three dimensional
ABC	Absorbing Boundary Condition
ADS	Advanced Design System
AR	Axial Ratio
ASIC	Application Specific Integrated Circuit
ASCII	American Standard Code for Information Interchange
Auto ID	Automatic Identification
Balun	Balanced Unbalanced
BEM	Boundary Element Method
BW	Bandwidth
CD	Compact Disc
CDF	Cumulative Distribution Function
CEM	Computational electromagnetic
CP	Circular Polarisation
CPU	Central processing Unit
CST	Computer Simulation Technology
CR	Cognitive radio
DARPA	Defence Advanced Research Projects Agency in USA
DC	Direct current
DDA	Discrete Dipole Approximation
DMLRT	Double Meander Line RFID Tag
EEPROM	Electrically Erasable Programmable Read Only

	Memory
EIPR	Effective Isotropic Radiation Power
EPC	Electronic Product Code
EM	Electromagnetic
EMC	Electromagnetic Compatibility
ESRMLA	Equal Space Rectangular Meander Line Antenna
FCC	Federal Communications Commission
FDTD	Finite-Difference Time-Domain
FEM	Finite-Element Method
GA	Genetic Algorithm
HF	High Frequency
HFSS	High Frequency Structure Simulator
IC	Integrated Circuit
IEEE	Institute of Electrical and Electronics Engineers
IETD	Integral-Equation Time-Domain technique
ISO	International Standard Organization
ID	Identification
LF	Low Frequency
MLRT	Meander Line RFID Tag
MIT	Massachusetts Institute of technology
MoM	Method of Moment
MLA	Meander Line Antenna
NEC	Numerical Electromagnet Code
NFC	Near Field Communication System
$P_{absorbed}$	Absorbed power
$P_{radiated}$	Radiated power
PC	Personal computer
PCB	Printed Circuit Board
PDE	Partial Differential Equations

PDF	Probability Density Function
PEC	Perfect Electric Conductor
PML	Perfectly Matched Layer
PP.	Pages
RF	Radio Frequency
RFID	Radio Frequency Identification
RL	Return Loss
ROM	Read Only Memory
RX	Receiver
SAR	Specific Absorption Rate
SARS	Severe Acute Respiratory Syndrom
SDR	Software Defined Radio
SRAM	Static Random Access Memory
SMLRT	Single Meander Line RFID Tag
TX	Transmitter
UHF	Ultra High Frequency ($300MHz - 3GHz$)
USA	The United States of America
VSWR	Voltage Standing Wave Ratio
WWII	Second World War

LIST OF SYMBOLS

$\varepsilon r, eff$	The effective permittivity of the dielectric material
Γ	Complex Reflection Coefficient
Ω	Ohm
λ	Wavelength (m)
t	time (s)
H	magnetic field strength [A/m]
E	Electric field strength [V/m]
B	Magnetic flux density
D	Electric flux density
dBm	Logarithmic measure of power, related to $1mW$($0dBm$=$1mW$, $30dBm$=$1W$)
Er	The electrical field component in direction of radius r
$E\theta$	The electric field component in direction of θ
$E\varphi$	The electric field component in direction of φ
Q	The antenna quality factor
F	Critical frequency
C	Light Speed c = 3x 108 m/s
$\rightarrow$	Sign of the vector
Wb	Weber = J/A
Ω	ohm
Hz	hertz
m^2	square metre
A	ampere
V	volt
C	coulomb
V	Speed of light in free space (2.9979×10^8) $m.s^{-1}$
H	henry

F	farad
W	watt
s	second
N	newton
T	tesla = $W/m^2 = Vs/m^2$
S	Siemens = $1/\Omega$
$\nabla.$	Divergence operator
$\partial/\partial t$	Partial derivative with respect to time
ρ	total charge density (free & bound charge)
J	total current density (free & bound current)

CHAPTER ONE

INTRODUCTION AND RESEARCH MOTIVATION

1.1 BACKGROUND AND OBJECTIVES

Radio Frequency Identification (RFID) is a form of wireless data transfer which does not require a line-of-sight channel as is required with infra-red linked terminals. Typically, it comprises of small, discreetly placed transponder tags and a transceiver unit that is usually referred to as the reader which interrogates the sent data as well as providing linkage to a wider network [1, 2]. Moreover, the RFID system in its basic form transmits a target identity in the form of a unique serial number. In term of classification, RFID naturally generalises as a flexible component within an Automatic Identification technology (Auto-ID) in which several target objectives and applications could be analysed subject to achievable sensitivity in the hardware implementation [3, 4].

To simply the picture, RFID tags are small electronic widgets, nodes in network terms, which are adhered, embedded or otherwise fixed to the target structure. Naively, it may be seen as a replacement for certain areas of, for example, optically read barcode systems, whilst deepening and extending both the density and range of available information. In term of installation, the essential hardware comprises of an integrated circuit (IC) and an antenna. Various levels of integration and control devices are possible

within an RFID system. RFID systems may be broadly divided into passive and active systems, but in this work the passive RFID has been concerned [4].

The most convenient realisation tends to favour the passive approach owing to the system uses the coupling effect between two or more antennas through which a communications channel is established. Usually, the transceiver unit is a fixed node or base with the transponders acting as rovers. For most practical purposes, their operation is based on magnetic coupling and in addition the base provides the power required by the tags through coupling radiated induction zone fields. So, the antennas will require precise tuning to the operating frequency or resonance which will typically be featured into any practical design. In other words, this must be an intrinsic feature of the design. By modulating these fields, the base station is able to transmit a signal to the tags to power them up and consequently return energy on-chip data to the base [4, 5]. On the other hand, the detection range of the tags will be effectively bounded by the power received from the base station. Consequently, for long detection ranges, active tags should be considered. Since the active RFID is used throughout the conventional high frequency domains including UHF and VHF microwave and millimetre wave. In return, on active RFID system requires more complex electronics and share comparable size constraints with their passive counterparts, so in spite of memory functions, as well as

the potentially high data rates, the successful realisation should be consider the signal integrity as well as taking noise issues into account [6].

For both passive and active RFID devices, the broad environmental conditions are significant factors in the antenna design, therefore, RFID readers need to be able to cope with dielectric mixtures and various material composites. To some extent, positioning will be determined by the presence of conducting materials. Furthermore, designing strategies for overcoming the constraints imposed by strong conducting layers and liquids such as water are a matter of continuous review and improvement. In a passive RFID set, the reader powers up the tags, so that information can be passed on by the chip using a low power radio wave. However, for ease of use, RFID readers may be fitted with an additional interface. Thus, passing on the data to another sub-system such as a PLC (programmable logic controller) [3, 4].

Many identification methodologies may be followed, but the most common operation is to store an ID or serial number that identifies a specific product or data type. Precisely, the stored information on the tag can range from just the ID, to several kilobytes of read-write data, to dynamic updates on specific aspects of environmental response for example temperature profiles. In fact, the RFID tags could be read-only or read-write depending on their data storage capability; most read-only types have no data storage capacity beyond their unique ID. Hence, the data for monitoring the process

and analysing the data may be accessed from a mobile terminal such as a smart phone or PDA or host computer; overall, the process will be fully automated [7, 8].

The RFID system is characterised by the detection range and a variety of the mostly second order effects such as the magnitude of the information to be passed, the transmit rate and the physical space available on the tag. This last point gives rise to a fundamental physical constraint: antenna selection and construction. The fitness may now be measured in terms of the stiffness of the network with respect to its material and electromagnetic environment. This final statement carries a lot of assumed information regarding to the system parameters such as the operating frequency and the system performance metrics as a function of acceptable data transfer [9, 10, 12].

Seen from a logistical or commercial perspective RFID is an empowering technology. For example, a customer's data may be extracted from the network as a set: the unique tag ID, the reader ID, the transaction status code and the error code [12]. Consequently, RFID is expected to boost supply chain efficiencies and security of supply through increased asset visibility and inventory controls. It is possible to see this in a rather more abstract manner, as suggested by the system fitness concept alluded to previously with applications appearing in medical physics and broad clinical practice [13]. Physically, the tag is a packaged assembly with an embedded thin film medium [12, 13].

Unlike conventional wireless communications, there is no market dominance for RFID technologies; although, this is really a reflection of the pervasive and ubiquitous nature of the technology. Thorough reading around this topic, shows that many specialist applications are very much the concern of specific leading industries (e.g. WalMart, Gillette), laboratories (e.g. MIT Media Lab) and the more niche applications are more the preserve of entrepreneurs and small companies [14].

An RFID system simply consists of tags, readers and an application system. Typically, when a tag is attached to a person or object passing through an electromagnetic field generated by a reader and detects a signal from the reader, it identifies itself in terms of its serial number, a model number, colour, place of assembly, or other stored information. Furthermore, the RFID tags can be classified as chip and chip-less tags based on the way the tags store their data [15, 16]. In particular, chip-less tags do not contain an integrated chip, therefore unique patterns are encoded on the surface of materials/tags. On the other hand, tags containing microchips are called chip tags, in which the Integrated circuit (IC) has been used to store the unique data.

Throughout a wireless sensor network environment, the RFID method is considered as the dominant wireless identification for the next generation capable of recording or reading using RFID core technology [16]. Presently, the network aims at the communication using IP between entities of the

converged network like Broadband Convergence Network (BcN). Among many suggested networks, the BcN network seeks the convergence of existing diverse communication networks and one of its convergence areas is the service convergence, in which the RFID system is the core technology for comprising the most existing networks. In fact, the IP networking address cannot be done by the RFID tag ID itself. Therefore, a special mechanism is used for generating the IPv6 address by using the RFID tag ID for the IP networking as the one generated by using Electronic Product Code (EPC) of EPC global standards [17].

The RFID operating frequency has been raised into the high frequency band. Eventually, any problems that may occur in the design of the system such as impedance matching, inductive coupling range and the antenna type become more complicated and acute [13, 18]. For example, a multi-turn loop antenna at microwave band is not recommended as the number of windings decreases as the frequency increases (1000-100)turns between (100-400) *kHz* and (10-3) turns at (<13.56) *MHz*. For more information retrieval, the antenna size at high frequency rates must be small with Omni-directional properties or hemispherical coverage. It is clear that the problem of gain and polarisation must also be taken into account to provide the maximum possible signal [15]. There are several possible antenna designs that can be developed at high frequency which can be classified into two main types:

- Omni-directional Antennas: some of these antennas are characterised by low input impedance between (50-80)Ω, such as a dipole, or high input impedance between (100-300)Ω, such as a in closed loop, and between (10-200)Ω for open loop structures such as a folded dipole. In general, they have linear polarisation with low gains [2].
- Directional antennas: to achieve good matching impedance the printed board antenna (50-100)Ω and micro-strip technology (30-100)Ω are becoming more popular in RFID antenna systems. In bandwidth terms, the printed dipole and patch antennas achieve low relative bandwidths (10-15)% and (2-3)% respectively while the log spire antennas have wideband frequency which is up to 100%.

For RFID antenna matching, the tuning procedure for the same antenna varies depending on the application type in use. This problem becomes very clear when an object is placed closed to the antenna as it will degrade the return loss spatially when the antenna used is Omni-directional. In some cases, when the object is dielectric the change occurs in the resonance frequency as well. However, directional antennas do not suffer from this problem; they are recommended to be used rectify the problem. In addition to this, objects close to the antenna also affect the radiation pattern for glass or plastic by up to 10 dB reduction in pattern at 100mm. This problem occurs wherever the antenna is directional or Omni-directional [15].

Furthermore, the radiation pattern of the antenna for both the tag and the interrogator antennas when the hand-held systems are used will be seriously distorted [15, 16]. However, it should be clearly noted that for a fixed transmitted power the range decreases by increasing the operating frequency. Therefore, an active antenna system is required to compensate for this constraint and achieve better detection ranges. On the other hand, antenna overwhelmingly emit in the proximity of complex models that could considerably influence the transmitter performance. Therefore, the antenna problems could be analysed, evaluated and solved via accepting full-wave numerical methods e.g., Finite-difference time-domain (FDTD), Method of Moments (MoM) or Finite Element Method (FEM)) [21].

The FDTD technique has been adopted from the differential equation formularization which gives direct results through the moving in discretised time of Maxwell's curl equations. In other words, the design model is done through continuous transfer of the equations into discrete counterparts in both space and time. In addition, this method is normally executed as an initial stage across building a suitable structure for numerical evaluation and implementation on digital computers [22, 25].

In comparison to the FDTD, the MoM has been created using the integral equations, which is appropriate for testing electromagnetic performance of transmitting and/or scattering models. In addition to this, MoM is simply modelling the arranged metallic bodies embedded in a homogeneous

environment. In case of addressing the possibility of collecting the FDTD and MoM to solve antenna problems, a hybrid numerical method could be modified in the event of the possibility of dividing an electromagnetic problem into sub-problems [26, 27].

1.2 AIMS AND OBJECTIVES

Much time and effort is spent in generating RFID tag and reader antennas' model in order to achieve the best simulation and measurement results. Particularly, the reading attempt could be estimated by how such knowledge might be captured. In contrast, the practical parts which have been implemented give the certainty in the results after comparing the simulation and measurements results. Observance that the readers antenna operate at (866-867)MHz, therefore, all of the designs in this report have been modulated to work in the RFID European UHF band frequency standard range (865-868)MHz as well as the most of them operate with high efficiency using Alien reader's antenna.

This research is allied to design new radiating elements that support the operation of the RFID systems that includes the development of tag and reader sensors based on various applications. Recently, RFID technology has been successfully implemented in various industrial, public and government sectors. The main inspiration of this research could be summarised as follows:

- To implement, new tag and reader antennas to improve the detection range for various expected applications. This includes the use of genetic algorithms to design new compact structures in order to satisfy several constraints.
- Improve the tag antenna operation when placed on surface objects having different electric properties. This concerns the problem of reducing the mutual coupling between the antenna and the object.

An initial parametric study approach of the tag and reader design concept has been carried out in this research to support the idea of implementing small sized systems, taking into consideration the aim of maximising the transfer power into and out of the device when the tag mounted on different materials.

The antenna design concept based on polarisation diversity has been highlighted in this work to help and improve the system performance. A new design idea of a compact circular polarised antenna has been considered and tested to achieve better detection distance and acceptable working bandwidth.

The research work has intensively investigated and discussed the modelling of and measurement process of these newly design of sensors such as the mounting of the IC chip on the RFID antenna tag.

The research also to considers how to establish statistical measurements on predicting the maximum detection range of the prototype antennas for evaluation purposes, subject to the various orientations and mounting of the RFID tags with respect to the reader location.

With this work, several antennas have been successfully designed and tested. A comprehensive study of the enhanced detection range has been investigated at UHF frequency band.

1.3 THE NEW RESEARCH CONTRIBUTIONS FOR THE PRESENT THESIS

The main research contributions include the following:

- Adopting the Genetic Algorithm (GA) to design linear and circular RFID tag's antennas.
- Deployment the RFID tags to operate stable on the multiple items surface with different electric properties.
- Model a novel Helical-Spiral RFID reader's antenna using Genetic Algorithm (GA).
- The cost and the reliability of the RFID tags have been considered and evaluated in this research; this includes the selection process of passive tag and the dielectric material properties.

- The human body interaction with RFID tag has been studied using a hybrid method technique.
- Several new RFID tags sensors were implemented analysed and tested covering various applications.
- A compact balun operated at 900MHz has been implemented to support the measurements of antenna's radiation performances.
- For the validation process the achieved results of the genetic algorithm (GA) software have been compared to two well known software packages. These are Computer Simulation Technology (CST) and High Frequency Structure Simulator (HFSS),
- A conceptual RFID antenna's structure is proposed exploring from the variations of several antenna parameters through the using of the parametric study.

1.3.1 AUTHOR PUBLICATION CONTRIBUTION

Some of the outcomes of the present work have been transformed to several papers publications that reflect the impact of the results achieved among the technology found nowadays in this interesting research area. The following list presents the Journals and the Refereed Conference papers that I have contributed during the time of my study.

JOURNALS PAPERS:

[1] M. S. Alkhambashi, R. A. Abd-Alhameed, D. Zhou, C. H. See, P. S. Excell, M.M. Abusitta, et al., "Design of Dual-Band Quadrifilar Spiral Antennas for Satellite-Mobile Handsets", Microwave and Optical Technology Letter, MOP-09-0944, vol.52, no.4, pp. 987-990, April. 2010.

[2] M. S. Alkhambashi, R. A. Abd-Alhameed and C. Hwang, "Printed planer RFID Tag Antenna Design to be Mounted on Metallic Objects", IET in Microwave, Antennas and Propagation, under review, 2012.

REFEREED CONFERENCE PAPERS:

[1] M. S. Alkhambashi, D. Zhou, R. A. Abd-Alhameed, C Zhang and J. D. Zu, "Design and Optimisation of Compact Hybrid Quadrifilar Helical-Spiral Antenna in GPS Applications Using Genetic Algorithm", Presented at EUCAP 2012, Prague, March 2012.

[2] M. S. Alkhambashi, R. A. Abd-Alhameed, C. H. See, A. S. Hussaini, J. M. Noras, M. B. Child, et al. "A Novel RFID Tag Antenna Mountable on Metallic Objects", Presented at EUCAP 2012, Prague, March 2012.

[3] M. S. Alkhambashi, M. Bin-Melha, C. H. See, R. A. Abd-Alhameed, D. Zhou, S. Jones, et al., "Two miniaturised printed dual-band spiral antenna designs for satellite communication systems", Presented at

PSATS 2012 - 4th International Conference on Personal Satellite Services, Bradford, UK, , Technical Session 2, Paper 5, 22-23 March 2012, pp. 1-6.

[4] M. S. Alkhambashi, K. N. Ramli, R. A. Abd-Alhameed, Y. A. S. Dama, M. B. Child, P. S. Excell, et al.," Interaction of EM fields to the human body using MoM-FDTD-SGFDTD hybrid computational method", Presented at Proc. of the 10th Int. Symposium on Electromagnetic Compatibility (EMC Europe 2011), York, UK, Sept.2011, pp.571-574.

[5] M. S. Alkhambashi, R. A. Abd-Alhameed, D. Zhou, Y. Ma. C. H. See, M. M Abusitta, et al., "EQUAL-SPACED RECTANGULAR MEANDER-LINE ANTENNA RFID TAG DESIGN FOR UHF BAND ", Presented at Centre for Applied Internet Research, Glyndŵr University, Wrexham, LL11 2AW, Wales, UK, Sept. 2009, pp. 426-430.

[6] M. S. Alkhambashi, D. Zhou, R.A. Abd-Alhameed, C. H. See, Z. Zainal Abidin, K. N. Ramli, et al. , "Meander-line antenna design for UHF RFID tag using a genetic algorithm", Progress In Electromagnetics Research Symposium, PIERS Proceedings, Beijing CHINA, March 2009, pp.1253-1256.

[7] M. S. Alkhambashi, K. N. Ramli, R. A. Abd-Alhameed, D. Zhou, P. S. Excell, C. H. See, et al., "Accurate hybrid computational electromagnetics techniques", Presented at In proceedings of the ninth informatics workshop for research students (ISBN: 978-1-85143-251-6), University of Bradford, Bradford, UK, June 2008, pp. 198-199.

[8] M.S. Alkhambashi, "Hidden Cameras", School of Engineering conference, Caledonian College of Engineering, Oman, Muscat, 17-05-2003.

1.4 ORGANISATION OF THE THESIS

The remainder of this thesis is organised as follows:

Chapter Two provides an overview of RFID technology and applications based on a detailed literature review; it then goes on to provide a perceptual setting for the rationale and scope of the proposed research. Moreover, the RFID system history, the types, the operation frequency and environment, the types of chips and memory used in RFID have been studied and discussed.

In Chapter Three, a critical appraisal of a planar meander line and cruciform RFID tag model and cross-shape RFID tag antenna has been made for the UHF band. These antennas are designed to meet the required aspects of linear and circular polarised antennas operation (LP and CP). The intention is to set a flexible design strategy which combines the selective capability of a heuristic optimiser. In this case, a generic algorithm with the accuracy of physics based model defined through an electromagnetic simulation code. The NEC2 code was selected for this task as it is universal rigorously benchmarked and may be combined with the GA driver into an efficient machine code. The nominal operating frequency in these sample designs was set at 900*MHz* and the simulated impedances of the GA-optimised tag antennas are compared vs. target impedance values and actual prototypes

have been realised and measured. Including in the final measurements is a preliminary evaluation of detection range.

In Chapter Four, the class of LP-antennas studied in Chapter Three, is extended through a detailed analysis of equally spaced, with single and double rectangular, meander line antennas. Symmetrical antenna structures have been examined using a balanced feeding network in the balun feed. In addition, the effects of looping in the chip mount neighbourhood have been studied. Several antenna tags are subsequently modelled and then prototypes created and measured. The modelling of these antennas is carried out using Ansoft's High Frequency Structure Simulator (HFSS) and Computer Simulation Technology (CST) and concentrating on the identification and tuning of the critical structure parameters rather than attempting to locate a global minimum. Once again, physically realised structures have been built, measured, and assessed for detection range.

Chapter Five tackles the problem of proximity of antenna tags with metal or metal-composite surfaces. Modified 'S' and 'T' structures are proposed as test structures. The purpose was to extend the modelling capability further, mostly using HFSS and CST, to characterise the antenna in its operating environment. Experimental investigations are carried out on this basis with lessons learned in the attempted realization being fed back into the simulation. Initial results appear consistent, but several practical build

related and system performance issues cannot be inferred directly from this style of simulation.

Chapter Six presents the design and optimisation of compact hybrid quadrifilar helical-spiral RFID Reader's antenna using GA. The radiation performance of the new proposed antenna is presented. The symmetry of antenna geometry features of balanced feeding, high power gain and its capability to mission circular polarisation for a broad angular area suggests that this antenna is a good applicant to RFID reader applications.

Chapter Seven describes the design investigation of the interaction between electromagnetic field and the human body for RFID tag's antenna using a hybrid MoM/FDTD computational method. In order to facilitate the present work, the optimum RFID tag's antenna (meander and cross shape) has been modelled in free space using NEC [29-31], then the results fed to the hybrid code that links MoM and FDTD, in which it has been written as a platform in Fortran 90. Indeed, the designing method has been applied to implement a typical on human body scenario at the frequency of 900*MHz*. Ultimately, the near as well as far fields and the cumulative distribution function of the radiation efficiency at thirty two locations on back and front of human body have been well studied and analysed.

Chapter Eight presents integrated conclusions of the research work done and suggestions for future work based on the results presented in this thesis.

CHAPTER TWO

LITERATURE REVIEW AND OBJECTIVES OF THE RESEARCH

2.1 INTRODUCTION

Automatic Identification systems (Auto-ID) are an enabling class of technologies that are used for the identification of objects and collections of data linked to these objects without the need of human intervention [3, 33]. Figure 2.1 shows a possible family of Auto-ID technologies including bar-coding, biometrics, optical character recognition (OCR) and radio frequency identification (RFID). Some concepts are plainly more generic than others and there is a potential for a degree of polymorphism in this classification.

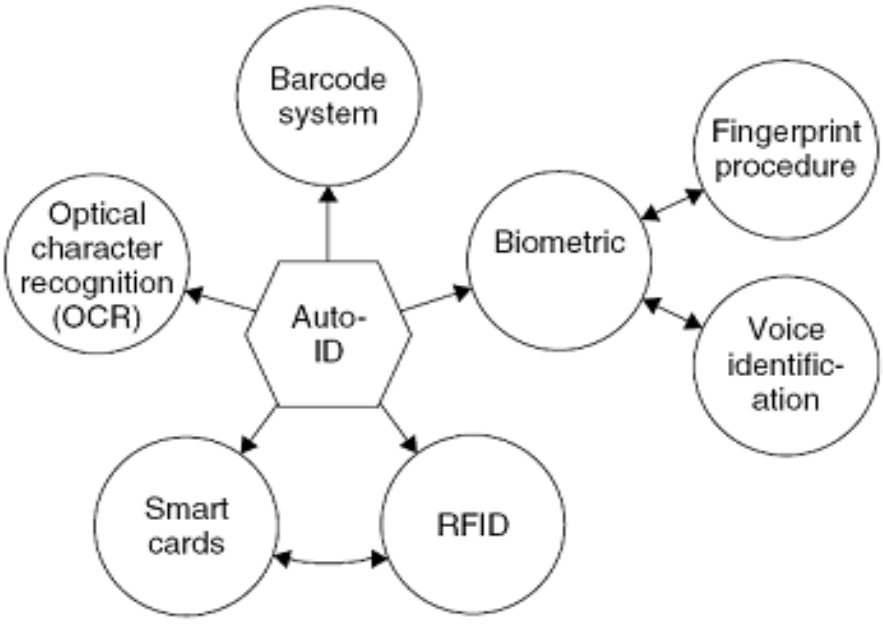

Figure 2.1: Auto-ID systems

RFID uses radio waves to identify physical objects [3] in contrast with barcode systems which are read by fixed line of sight readers and can only work individually. Generally, the barcode systems are substantially degraded by even minor damage or obscured targets and cannot be updated [34]. In terms of accuracy of work, bar-coding often requires manual tracking and therefore it is susceptible to human error. In contrast, the RFID could cope with dirty or harsh conditions and could read multiple tags not necessarily requiring line of sight transmission; finally, the raw detection is not subject to human error [3, 34].

2.2 CONCEPT AND EXISTING IMPLEMENTATION OF RFID SYSTEMS

In many aspects, RFID technology is a natural evolution of technologies developed in WWII starting with early modern development might be traced to the Auto-ID and Media labs at MIT, both of which remain major centres of innovation and development in the field and their applications. There were parallel developments in the USA including projects through DARPA, the Department of Defence and the Department of Homeland Security [3, 35]. In 2003, RFID tracking was used within the Alexandra Hospital (Singapore) during the SARS outbreak. The RFID tags were equivalent to ID cards with the networked data being used to create an infection map which could be centred around individual cases [3, 35]. A tangible law enforcement application was implemented by the European Central Bank in

2005 in which RFID has been used as a tracking mechanism for Euro bank notes [33]. Retail sector applications are now quite pervasive that early deployments are well documented both in academic and trade journals [3, 33].

A generic RFID setup comprises four main elements:

- Transponder tags are located on target objects.
- The transceiver (reader) interface communicates between the microcontroller and transponder, the precise details depends on the specification of the technology.
- Data processor – microcontroller.
- Reader and tag antennas.

RFID technology provides a quick, flexible and reliable way to electronically detect, track and control a different range of items. As well as these characteristics, the RFID has advantages which are not available with other identification technologies such as programmability and adaptation; it could achieve response times of less than $100ms$ even under harsh conditions [7]. A recent study by A. R. J. Ruiz, et al. [9] presents a novel technique to precisely locate persons inside by fusing inertial navigation system (INS) methods with an active RFID system. The RFID hardware and software technologies incorporate the electronic product code (EPC) global standards which is a product numbering standard which could be considered

as the ID number of the chip. Each tag is assigned a unique EPC which allows any change occurring on the targets to be recorded [36]. Using the EPC, the information stored on the tag can range from as little as a simple ID number to several kilobytes of read-write data [22, 37]. Typically, header, EPC manager number, object class and serial number are an example set or data where these represent:

- Header: length, type, structure and generation of EPC.
- EPC manager number: maintains subsequent partitions.
- Object class: a protocol class defined by EPC Global.
- Serial number: identifies instance, encoded in bits on the tag.

The information from the tag/reader may be presented to a human operator over a mobile terminal or a host computer which manages the data automatically. Unfortunately, the tags cannot be reprogrammed using state machines or ROM. Typically the active RFID tags use EEPROM whilst passive such as back scatter tags typically store their digital codes using SRAM. In a large longitudinal study, Stefano et al. (2011) [38] investigated a dual band symmetrical UWB-RFID transceiver for high capacity wireless NV-Memory application.

The memory requirements of an RFID tag are affected by the distance between the reader antenna and the tag antennas, as well as the transmission medium assumed to be described by the air interface standard (ISO – 18000,

Class 0, Class 1, Generation1 and Generation2) [39, 40]. Furthermore, Class 0 and Class 1 is known as the Electronic product code (EPC) tag. Moreover, the reader could also write and read Class 0 and Class 1 tag i.e. ISO 18000-6B. To clarify, EPC Class 1 is Generation 1 and Generation 2 (Gen1 and GEN2). Recent evidence [41] demonstrates an improved UHF RFID reader can be created based on the reduction of the baseband noise using the captured TX signal after filtering. Technically, the frequency plays a pivotal role along with the transmission medium for the effective communication between tag and reader. Each country is assigned its own frequency according to universal standards. Note that the ISO frequency band for UHF RFID operations in European countries is (865-868)*MHz*. In this research, a key aim is to carefully match the antennas to free space for this band. The detection (read) range may be defined as the maximum distance between the reader antenna and tag antenna; in general, this will vary according to system configuration [42]:

- Operating frequency
- Q-factor of antenna (and tuning circuit)
- Orientation of the antenna
- Excitation (current)
- Coding (modulation) / decoding (demodulation) algorithm
- Number of data bits and detection algorithm
- The condition of the electromagnetic environment.

In addition to the chip specification, the physical size of the tag, the ability of the transceiver to cope with multiple tags and its immunity to interference will influence the quality of test and measurement results [43]. Figure 2.2 illustrates the real-time environmental factors which should be kept in mind. Other factors would include the suitability of dielectrics as substrates and construction materials, and shape of the tag.

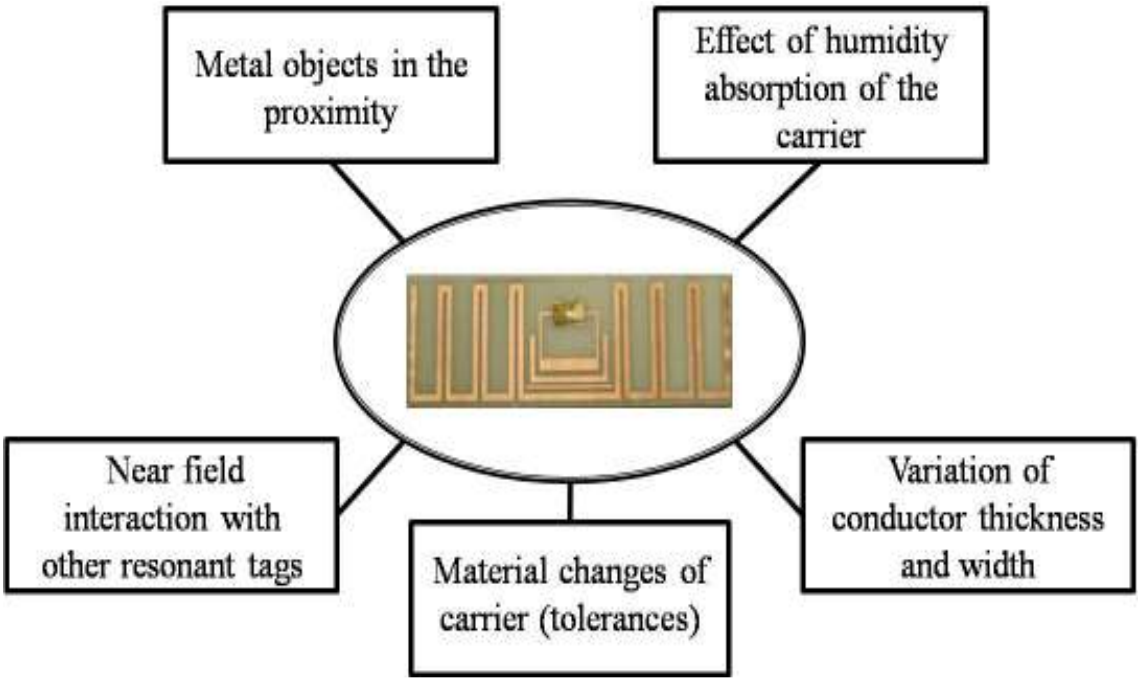

Figure 2.2:Tags antenna simulations factors

Figure 2.3 shows the action of the data transfer from the transponder tags. In practical terms, the ‘tag’ is an object which can be attached to a target thereby allowing the remote ID operation and more abstractly to track state changes.

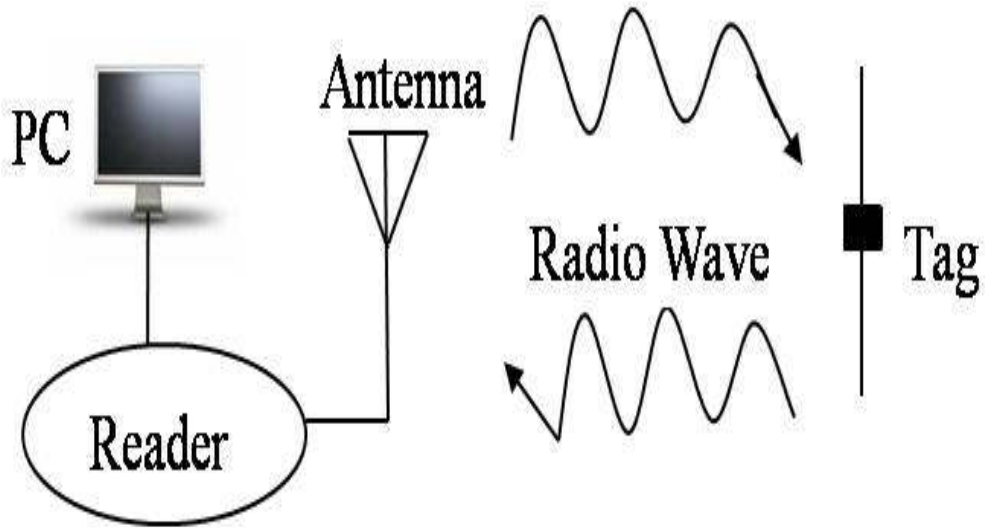

Figure 2.3:Reader antenna communications with tags

The main concepts regarding the anti-collision problem in dense RFID networks have been studied by Nikolaos [44]. However, the most significant factor affecting passive RFID performance is the fundamental antenna design. Reflections from the ground, scattering objects and absorption all affect communications performance; scattering and guided wave effects from target objects must be taken into account for a successful design strategy [44, 45].

In general, the reader antenna should be as close as possible to the tag antennas. However, if all the tags respond to the reader at once then data collisions are inevitable leading to interrupted or unsuccessful transmissions [46]. However, L. Kang, et al. [47] redesigns Randomly Number (RN) generator to make the collided RNs decidable by leaving the collision slots. In addition, directly decode the collisions (DDC) reduce the information carried by each RN to enable concurrent transmission of multiple tags has been used. Improved

propagation models, particular for indoor build environments are needed for better system performance and model validation. Antennas which are in close proximity or close to conducting media will suffer from mutual coupling effects which affecting their gain, radiation pattern and polarisation state [3, 47]. Preferential, absorber screens may be used to mitigate interference but the absorber material (and shape) must be properly evaluated.

The deployment of absorbers or screens may effectively support in reducing any interference. Simply put, there should be a comprehensive evaluation of the absorber and its materials in order to gain good absorbing properties [48]. Having discussed the communication process between the RFID reader and RFID tags and all of the expected problems during it and their suggested solutions to minimise the negative effect of such problems, the RFID tags should be discussed and analysed in details.

Discussing the concept of RFID tags brings the issues of its components comparison of its different types and its characteristics. Regarding the actual structure of the RFID tags, there are two main components present in it. To begin with, there is a small chip or integrated circuit (IC) where a unique identification number (ID) is located. Particularly, this chip plays the role of the memory where the information is stored and it is embedded in a thin medium film [23, 49]. Significantly, the task of antenna in functionalising the chip can never be ignored. In addition, the

characteristics of the stored information in the chip whether they are read only (Read only), or read and written, with a limit extent a write-once-read-many (WORM), or with a free one (Read/Write) has an influence on improving the performance of the RFID tag. [50] was discussed the changing resistance of WORM after exposure to moisture or water. Through the study has been found that the WORM suits for operating as a humidity sensor at room temperatures owing to it's sensitivity to high temperatures.

It is worth mentioning that the power consumption of the IC should be taken in to account. If the power consumption of the chip is low, the communication range would be longer and vice versa. Another significant point that should be taken in consideration is the importance of being aware of the impedance of the chip. To make the chip communicate clearly, the chip receives power from the reader antenna and responds by varying its input impedance and thus modulating the backscattered signal with data. In order to achieve optimum operating condition, the reader antenna impedance should be match correctly to the chip impedance. As the frequency of the chip is very important, it is taken into account when manufacturing chips according to the universal standards which shows the specific and suitable frequency for each group of countries. For instance, chip seller supplied constant values of chip frequency in Europe which is 866.5 *MHz*. Importantly, the chip can never work or function without a suitable attached antenna, therefore, a detailed discussion of antenna is needed [7, 51].

Generally, it is commonly known that the aim of tag antenna designer is to design an antenna that could increase the maximum detection range of the RFID system. The job of the antenna is sending and receiving signals in the shape of radio waves. Simply, the RFID antenna is a flat structure containing a metallic conductive coil while the chip is less than half a millimetre thick. In addition, the type and characteristic of the dielectric is a vital factor in improving the performance of the tag. Basically, the chip and antenna tags are usually attached to a dielectric substrate that can be made of foam, plastic or other materials. Knowing the main components of the tag, there are two main types of tags: passive and active [13, 52]. However, passive tags are currently the most widely deployed as they are the cheap to produce. The research work in this thesis, therefore, is concerned with the design concept of passive tag antennas.

Active and passive RFID tags are two different systems, each with their own unique advantages. As explained in Figure 2.4 which shows the power recourse differs from an active tag to a passive one. This figure also indicates the eligibility of communications access of these types of tags.

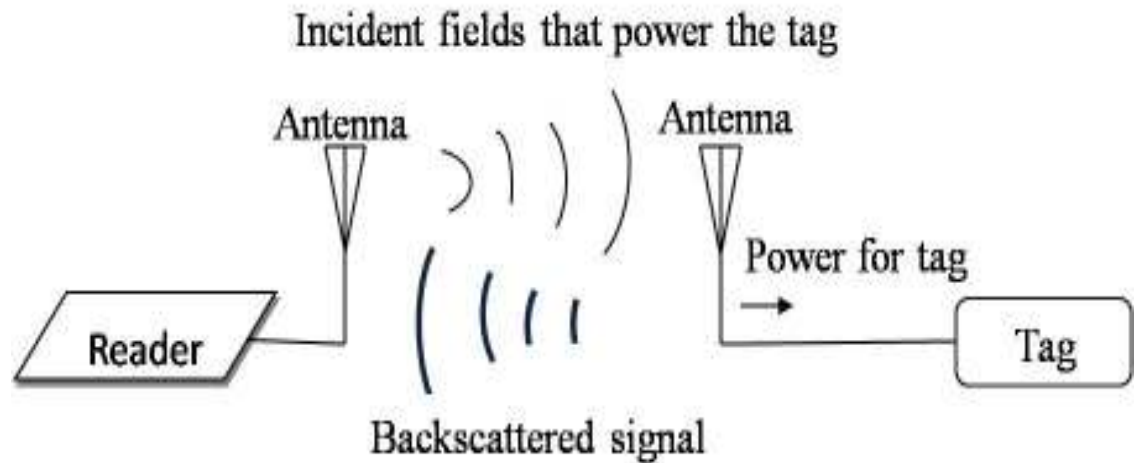

(a)

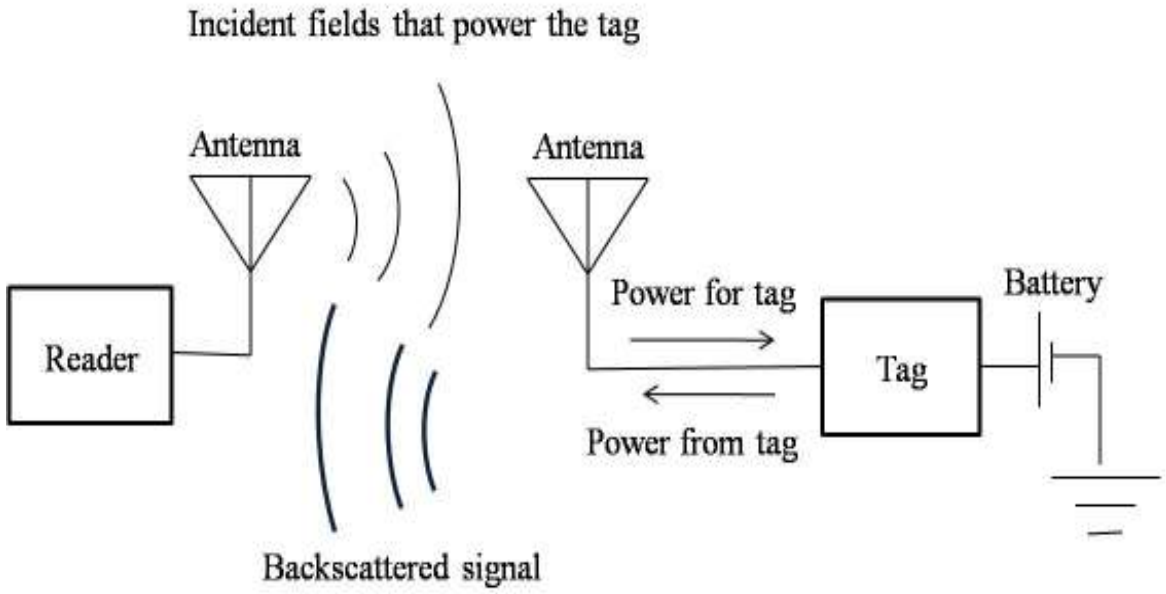

(b)

Figure 2.4: The power transmission mechanism between the RFID reader and RFID tag; a) passive tags and b) active tags.

To begin with, passive tags do not have a unified power source and are powered by the signal sent from the RFID reader antenna. In fact, an electrical field is induced in the tag antenna due to the incident fields from the reader. This field is responsible for generating a small voltage potential across the output port of the RFID tag i.e. the input port for the IC chip.

This generated power is used by the IC to transmit a signal back to the reader in terms of transmitting a modulated signal or encoded identification signal.

Figure 2.4(a) shows clearly that the passive tags are powered by direct energy provided by the radiating antenna of the reader. In other words, the passive tags can be considered as in a “sleep” state until being awakened by the reader’s emitted field. When a passive tag is “wakeup” it will start broadcasting its individual EPC. Generally, the ability of the passive tags to send the target IDs to longer distance seems to be dependent on the strength of the reader antenna power [53]. To sum up the communication process between reader and the tags, two main steps can be identified which are:

- The forward communication where there is a clear direct link from the reader to the tags. In such a case, the chip on the tag is powered up by the electromagnetic field which the tag received from the reader.
- The backward communication begins from the tags to the reader as a backward action. So, signal modulation is achieved by the switching between different impedance states and the backscattering field strength.

In contrast, the active tags are commonly powered by an internal battery which is small and light-weight. Therefore, such a tag would be always in

the active state and ready to communicate as shown in Figure 2.4 (b) in which the tag can send signals continuously. The main advantage of such a tag is its ability to communicate with every reader at any time and at longer distances. However, the lifespan of the used batteries and the possibility of being destroyed might be considered as the main disadvantage of such a type of tags.

It is worth mentioning that there is a third type of tags which combine the advantages of the two types that previously mentioned above. Such a kind of tag is called either semi-passive or semi-active according to whether the tag can regenerate the necessary power from the reader or use the additional power provided by the combined batteries.

However, in this research work the active and semi-active tags are not going to be considered to avoid the design complexity and the costs of batteries. In addition, the possibility of varying batteries characteristics are another threat that prevents such type of tags to be used in this research [13]. Therefore, passive tags seem to be the suitable candidate for RFID application to be used in this research. In order to simplify the comparisons between the three kinds of tags, Table 2.1 has been presented.

Table 2.1:The characteristics of passive, semi-passive / semi-active and active RFID tag.

PASSIVE	SEMI-PASSIVE/SEMI-ACTIVE	ACTIVE
Powered by reader radio frequency field	Powered by a small battery (less power consumption)	Powered by a battery (need a battery, crystal and some external parts)
Shortest read range (usually less than 1m)	Shorter read range than active tag (less than 10m)	Longer read range (more than 10 m)
Unlimited lifetime	Limited lifetime (More lifetime than active)	Limited lifetime (need to battery)
Smallest and lightest	Not that big	Big
Cheaper	More expensive than passive	More expensive than passive and semi-passive
Required much higher power reader	Require much higher power reader than active tag	Required lower power reader than passive and semi-passive

However, reviewing the table contents, it can be easily noticed that passive tags seem to be easier to be designed and most suitable choice to be used in a different applications owing to the unneeded for the batteries; therefore, there won't have an expiry date.

In fact, the idea of having three different types of tags appears as a result of the need of having specific types of tags with specific characteristics subject to specific applications. However, as a result of not having a continuous power source in the passive tags they have a longer lifespan. Therefore, such a characteristic can recommend this type of tag to be the

most appropriate one to be used in different investigation in this research, as examples: in supermarket checkouts and smart cards.

Having so many designs and forms of tags, the most appropriate design should be chosen according to the target applications. To make it clearer, if the communication distance is the most essential point to be taken into account then the active tags would be the most suitable one for such a case. On the other hand, passive tags would be better in the case of automatic picking process.

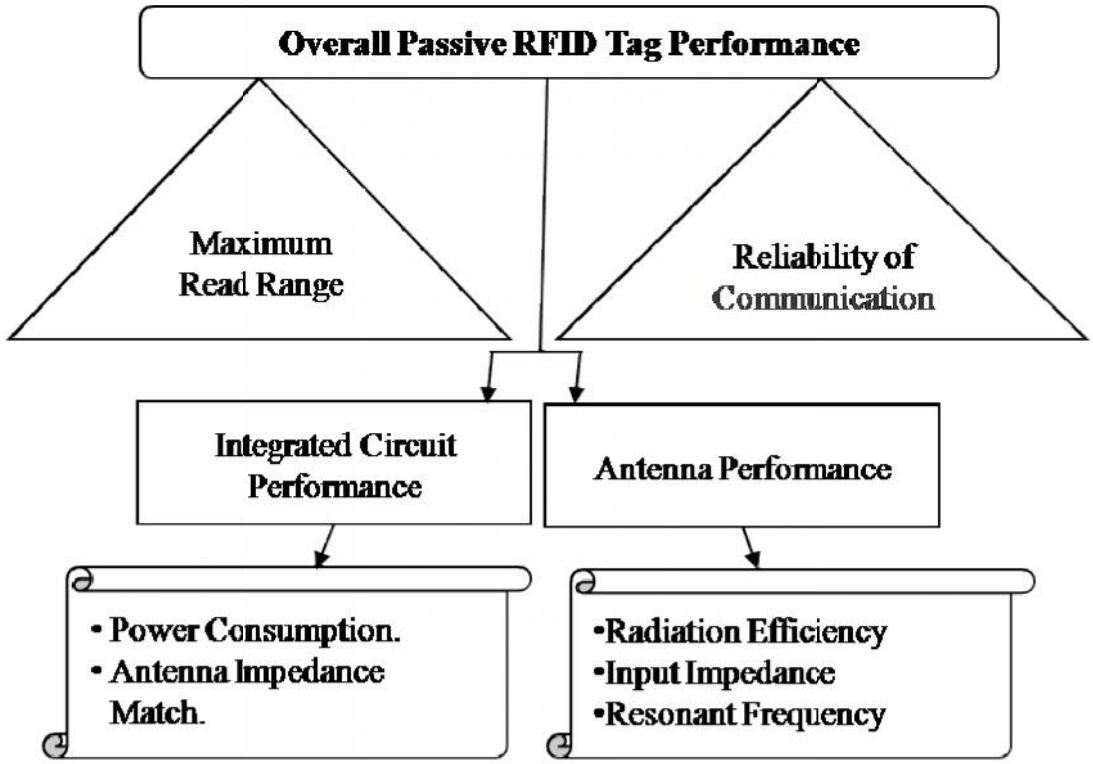

Figure 2.5: Passive RFID tag performance metrics

Figure 2.5 presents the tag performance metrics for passive tags. However, being aware of the most suitable frequencies that can be used with different

distances is essential. For example, if a high rate of frequency is used then the communication distance will be minimised because of the effects of the channel characteristics and vice versa when the transmitted power unchanged. At the same time, it should be noted that low frequency (LF) and ultra high frequency (UHF) operations of RFID system are near field coupling (ex. 125 *kHz*, and 13.56 *MHz*) and far field operation (ex. 433 *MHz*, 868 *MHz*, 915 *MHz*, and 2.45 *GHz*) [14], as the communication between the reader and the tags occur by using near electric fields or magnetic fields, or far field electromagnetic radiation respectively.

In order to measure the performance of the designed tags, a simple geometrical set up is shown in Figure 2.6. The RFID reader used in this research has two antennas: one for transmitting the signal to the tags (TX) and the other as a receiver (RX). In fact, the detection range can be simply known by measuring the distance (in metres) between the tag and the reader antenna location.

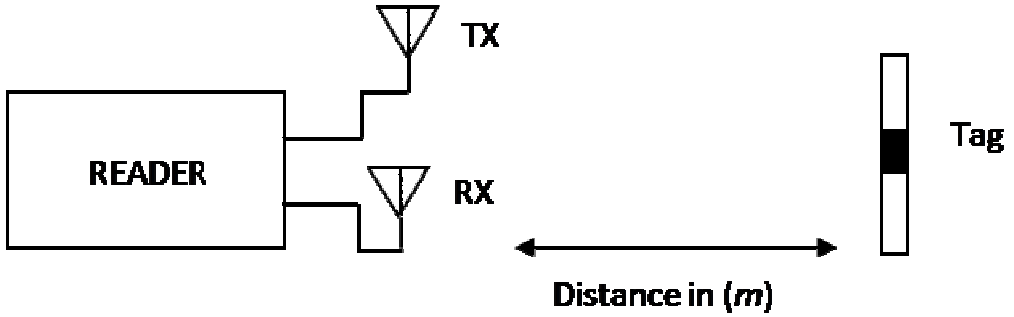

Figure 2.6: Test setup for detecting range measurements.

All measurements have been carried out using the alien technology reader ALR-8800 [54]. This reader has been designed to work in the frequency range from 865.6 *MHz* to 867.6 *MHz* with 5.5*dBi* gain. The detection range is measured and tested for several RFID tags in which the experiments setup was done in two different lab environmentally. The theoretical maximum detection rang *r* can be expressed as in following according to Friis Transmission Equation [14]:

$$r = \frac{\lambda}{4\pi}\sqrt{\frac{P_t G_t G_r (1-|S|^2)}{P_{th}}} \tag{2.1}$$

where λ is the wavelength in free space, P_t is the transmitted power of a reader, G_t is the antenna gain of a reader (P_tG_t is the EIRP of a reader), G_r is the antenna gain, P_{th} is the minimal power to activate the RFID tag chip, and $|s|^2$ is the power reflection coefficient. The coefficient '*s*' is the input return loss and is given by:

$$|s|^2 = \left|\frac{Z_c - Z_a}{Z_c + Z_a}\right|^2 \quad for\ 0 \le |S|^2 \le 1 \tag{2.2}$$

where $Z_c = R_C + jX_c$ and $Z_a = R_a + jX_a$ are the impedances of the RFID chip and the antenna, respectively.

The main components of the ALR-8800 are shown in Figure 2.7, they are: reader, two reader antennas, software tools, standard 120 VAC power and sample tags. To begin with, software tools are simply stored software (Alien

demo software) in a CD that can be downloaded in the PC (host) to configure the communication between the reader and the computer.

Such a communication process between the data processing data device and reader can be achieved by different ways such as cable or wireless networks. Furthermore, after being connected to the PC and assigned an IP address for identification process then an automatic connection process can be established. However, in the case of not being recognised the MAC address can be easily found on the side of the reader or in the CD's manual. Moreover, the used antennas are supported with six metres cable each in order to locate them in a suitable position and make communication process more flexible. After such a briefly discussion, the advantages and disadvantages of RFID system could be addressed as follows.

Figure 2.7: Alien Technology Kit

An RFID system has its own advantages including:

- Having the characteristic of not requiring line of sight communication may ease and speed up the process of reading.
- Being able to read many tags at the same time.
- Having a fast ability to read that might be up to 1000 tags per second.
- Having a memory where data can be stored or saved.
- Being able to read/write operations and could repeat them depending on the used memory type.
- Having a low manufacturing price.

On the other hand, there are several disadvantages of this technology which are:

- Not having a very strong security base.
- Encountering difficulties to read when the tag is attached to conducting surface, such as metal.
- High cost of the readers.

2.3 ANTENNA CHARACTERISTICS AND MEASURMENTS

Antennas are devices which efficiently transmit and receive radiated electromagnetic waves. There are several important antenna characteristics

which should be considered when selecting or specifying an antenna including:

- Antenna radiation patterns.
- Transducer power gain.
- Antenna directivity.
- Polarisation state.

Antenna radiation patterns are normally specified in two ways: elevation and azimuthal patterns. The elevation pattern is the graph of the energy radiated from the antenna in profile and the azimuthal pattern is the graph of the energy radiated from the antenna as seen from directly above. The power gain is the ratio of the input power to the output power for the antenna, whilst the directivity measures the concentration of radiated power in a particular direction. The polarisation state encodes the inner orientation of the electromagnetic waves far from the source. This research considers both linear and circular polarisation states denoted as LP and CP respectively. In simple terms possible LP-states are vertical, horizontal and oblique radiation whilst CP-states are left handed (LH) or right handed states (RH) and are related to the more general elliptic case. It will become apparent in subsequent chapters that polarisation will be a significant factor for the realization of a properly working antenna and hence RFID sub-system [55, 56]. Figure 2.8 presents diagrammatically LP and CP antennas.

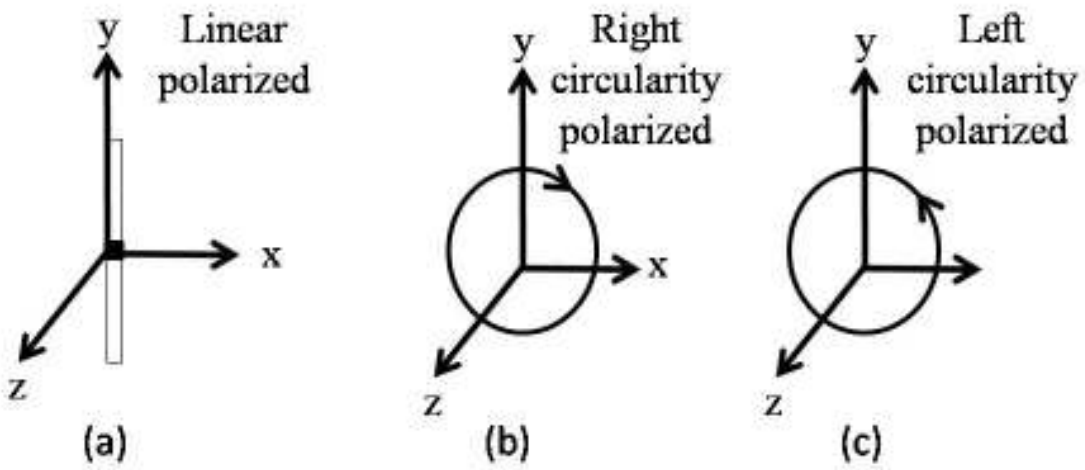

Figure 2.8:Wave polarisation; a) linear polarisation, b) Right circular polarisation and c) left circular polarisation.

CP is generated by the combination of two orthogonal linear polarised antennas with equal amplitudes and having 90 degrees phase shift between their time signals. The phase shift polarity will define the type of the circular polarisation either right or left handed [56].

According to the concept of radiation pattern, the academic isotropic antenna has a global radiation pattern, but physically do not exist. In summary, the radiation pattern of an antenna can be presented in two wave forms: these are E-plane (Electric field) and the H-plane (Magnetic field).

Conceptually, it is useful to think of the tag antenna as an electrically small dipole with a gain of$\approx 2dBi$. In practise, there is little scope for improvement without jeopardising the antenna's Omni-directional property. In particular, the directivity gain is a far field quantity which is defined as

the ratio of the radiation density in a particular angular direction in space to the radiation density of the same power radiated isotropically:

$$D(\emptyset, \theta) = \frac{Sa}{P_t} \qquad (2.3)$$

where

Sa=4π power per unit solid angle in direction Ø and θ, and P_i== Total power radiated by antenna

Theoretically, antenna gain is defined as the ratio of the radiation density in a particular angular direction in space to the total input power to the antenna:

$$G(\emptyset, \theta) = \frac{Sa}{P_i} \qquad (2.4)$$

where

Sa=4π power radiated per unit solid angle in direction Ø and θ, and P_i= Total input power radiated to antenna

Note, the effective isotropic radiation power (EIRP) is the product of the input power to the antenna and its maximum gain. An UHF antenna resonates at a unique or particular frequency and is sized carefully according to the wavelength of the operating EM wave.

The return loss is a significant factor of antenna because of its accuracy in measuring the reflection waves to and from antennas performance. In

practice, the return loss can be affected by several factors such as: size, shape, choice and manufacturing of the insulation or dielectric and so forth.

2.4 TARGET APPLICATIONS

This research aims to design, implement and operate passive RFID systems relevant to different environments and applications. In addition, both the RFID tag and reader antennas discussed in this work have been successfully shown to produce good simulation and measurement results to use in many applications. Seemingly, the applications of RFID system might be limitless; some of the target applications of the optimum RFID tag and reader antennas have been described below:

- To provide unique services for delivering more qualified in workflow control whether inside a building i.e. enclosed surrounded volume, or the movements of the objects similar to that used in healthcare for monitoring patients inside or outside hospitals and transport trucks.
- Providing comprehensible analyses of the activities of the staff within the organization which could be easily account the day work of the staff and the extent of work. For example, such a benefit could be noticed in many cases especially in emergency rooms such as measuring the flow of doctors and nurses including the time periods they spend on dealing with patients or waiting for some conditions such as resource conflicting before doing anything. Therefore,

bottlenecks might be identified and improvements with high parallelism and reducing resource conflicts would be achieved. Furthermore, the people who inside the building are very significant in case of fire happen.

- In hospital, providing analyses of patient access services are very important. This can be also performed in different cases, such as measuring patient flow including the time periods of patients spending on each stage of their treatment process such as registration, waiting in the room, and waiting in the bed, etc. practically, the RFID tags can track their locations and times spent on these locations as well as some medical tests. In addition, the patients could be monitored in the ambulances and the activities of the elderly at home as well as in disaster cases.
- Easing the way of identifying all different kinds of items in the store such as medicines in pharmacies (e.g. bottles or tablets), the equipments in science laboratory and so forth.
- Avoiding missing any other equipments or/and facility in the whole building, however, the forgetting of some of the equipments and tools used in the operations such as scissors, forceps, cutters and etc inside the human body is a serious issue. Therefore, any missing equipment would be easily identified.
- There are things that are in dire need to make sure it accurately from the correct material such as the organising and providing the suitable kinds of food for different patients. For instance, if a diabetic patient

is given a food with a lot of sugar, the reader will start the alarm because the container's ID will not match the one specified for diabetic patients.

- Away from the indoor, such IDs is very helpful in organising the parking process. For example, disabled parking places can be easily limited to be used by the holders of disabled IDs. Specifically, if a person use disabled parking places without having the disabled IDs on his/her vehicle, the reader would immediately recognise him/her and open the alarm. Actually, there is no need to worry about ambulances in such a case because normally ambulances have their own parking places in another area (the emergency entrance).
- Checking the levels of the used containers in the house, hospitals, industry and so forth wither they are used for water or/and other things by attaching tag sensors for different levels in order to know the target levels.
- In the case of having electrical problems, RFID sensors can used to switch between the spare electric generators and batteries, which can minimise the time used to start the generator basically because batteries will replace these generators and will not need the thirty seconds as generators do.
- For other future applications, RFID systems can be used to help in creating capsule cameras, which are very helpful in having a pervious knowledge of patients' conditions by having a complete scan of their bodies.

- Even sanitation needs passive RFID tag to check and report the blocking drainage hole to the control room through GPRS. Precisely, the idea of sensor without battery in this case is a great plan.

2.5 CONCLUSION

In summary, several perspectives of RFID systems have been discussed and investigated in this chapter, in terms their operation definition, components, structure and communication strategy. This also includes the advantages and disadvantages of RFID technology and their associated applications. In addition, the differences between the passive and active tags have been addressed in details.

A brief review on the measurement kits used through this course of research work has been presented. The antenna operation concept and their characteristics also have been given.

To sum up, the issues discussed or/and mentioned in this chapter will be tackled in details in the following chapters.

CHAPTER THREE

LINEAR AND CIRCULAR POLARISATION ANTENNA DESIGN FOR UHF TAG USING A GENETIC ALGORITHM

3.1 INTRODUCTION

Interoperable wireless communications are an everyday reality, experiencing dramatic increases in the volume and complexity of data traffic. They support applications including mobile internet access, healthcare monitoring, generic smart environments, and logistical location based operations [2, 16]. Much attention is therefore directed at spectrum efficiency and spectrum management, but there is a corresponding drive to create robust and functional miniaturised hardware designs. This has a special significance for the antenna designer. Radio frequency identification (RFID) technologies are a modern outgrowth of the logistical applications.

It should be understood that the antenna's orientation is significant in achieving the maximum benefits. In addition, the ground signal radiation is often utilised in medium and low frequency designs, therefore, it makes sense to use vertical polarisation. In contrast, horizontal polarisation is limited because the Earth works as a near ideal conductor at low frequencies. In all events, high frequency radiation is strongly affected by

antenna polarisation, UHF and VHF frequency ranges are satisfied in both polarisations [2, 57].

RFID tag efficiency is affected by the position of the tag relative to the reader, hence, in order to receive maximum power on the tags, the both antenna planes must be considered in parallel with one another. The tag's antenna should be small compared with object size [2, 56], low profile and have a simple low cost construction; printed monopole, dipole and folded dipole radiators are all suitable candidate types. Miniaturization issues must be addressed objectively; meander lines provide an obvious option for reduced antenna sizes whilst maintaining suitable bandwidth performance. However, there is an eventual trade-off between the size reductions and required compensation for the effects of a large resonant (wire) length, various types of meander can be considered [40].

The meander and folded dipole antennas are usually characterised as Omni-directional; the features and the benefits have been studied and discussed in [59]. In addition, the meander antenna has been used frequently in recent times, and proved to have the best features and results of the potential antennas. Chen [62] argues that the meander-line antenna has been used for mobile handsets with simple structure and could be fabricated at low cost. Reference [61] proposes a small broadband antenna which composed of meander, folded loop and disk loaded monopole model. Elsewhere, Occhizzi [62] has use of the meander-line antenna as a strain sensor. However, the

flexibility of form depending on the place of installation and the low cost to implement are the two important aspects in choosing such a design.

It is worth pointing out that when creating the tags antenna, it is not important to make it on the radiation shape of circular polarisation as the reader antennas are already in that radiation shapes. In order to expand the use of the tag, the studied antenna in this chapter is considered in both linear and circular polarisation.

Linear polarised (LP) antennas have more power transmitted on a single plane compared to circularly polarised ones, therefore, longer read range could be obtained on the plane which has been used. In CP-antennas, the power is spread equally across the two positions; the tag's received power could be not as much as received from LP-antennas. However, a major benefit of using CP-antennas is that the tracking objects do not necessarily have to be in a specific orientation. In a variable environment, the CP-antenna will be the better choice; in contrast the LP-antenna is better when position i.e. orientation can be guaranteed [1, 2]. In contrast, an effective progress of composite right/left handed spongy wave design for polarisation flexible antenna applications has been demonstrated by Dong [63].

The feed mechanism is an essential feature for the practical design; this chapter will concentrate on obtaining suitably miniaturised tag antennas with useful gain characteristics. The issue of feed mechanisms has been

outlined in the previous chapters and will be reconsidered in following chapters along with other design requirements.

The design strategy adopted here made of a Genetic Algorithm (GA) optimisation within an electromagnetic simulation engine. In this case, the optimiser is a FORTRAN driver run with the NEC2 source code. Furthermore, the simulation and stopping criteria are set to provide a fast and reliable parameter set for the candidate structure; these results move in some cases been cross validated with commercial EM codes such as HFSS and Microwave Studio. Finally, benchmarked results are then created from the fabricated antennas and a standard performance is established for each prototype [64].

3.2 GENETIC ALGORITHM (GA)

In the recent years, the major advances in design optimisation, particularly for complex systems, have been using heuristic methods. Some are based on physical analogies such as the Boltzmann machine, i.e. simulated annealing, whilst others are based on establishing cooperative or emergent behaviour, possibly with an underlying dynamical model such as particle swarm optimisers. Here, generic algorithms (GA) have been employed with an electromagnetic simulation engine as part of a well established design strategy. Practically, GA functions are a global optimisation which operates on genes which are binary sequences that define chromosomes.

Subsequently, these chromosomes undergo selection, mating and modification to reach the final solution of a global minimum [65]. The precise details of the simple genetic algorithm might be understood in specific terms as a dynamical system which may then be generalised, but this detail is not needed for our purposes. In the target work, the GA has been successfully used to obtain complex wire and microstrip antenna designs. In addition, the NEC2 source code is used for the electromagnetic simulation as it is fully accessible and can be easily modified to work with the GA optimiser. Several examples of GA aided antenna design might be found in the literature [2, 65].

In [66] the GA method is used successfully for designing a low cost, with high performance, focal plane horn array. Coelho [67] presents a chaotic approach of differential evolution optimization applied to loudspeaker design problem [67]. Furthermore, extensive performance evaluation results display that the GA is able to achieve lower Peak Side-lobe Level (PSL) and leads to saving on computational efforts of up to 90% compared to the previous published work [68]. In mobile communications area, Kim [69] presents a high gain wideband resonant type mobile communication base station antenna using a GA.

The GA design strategy which is employed here is summarised by the flow chart in Figure 3.1.

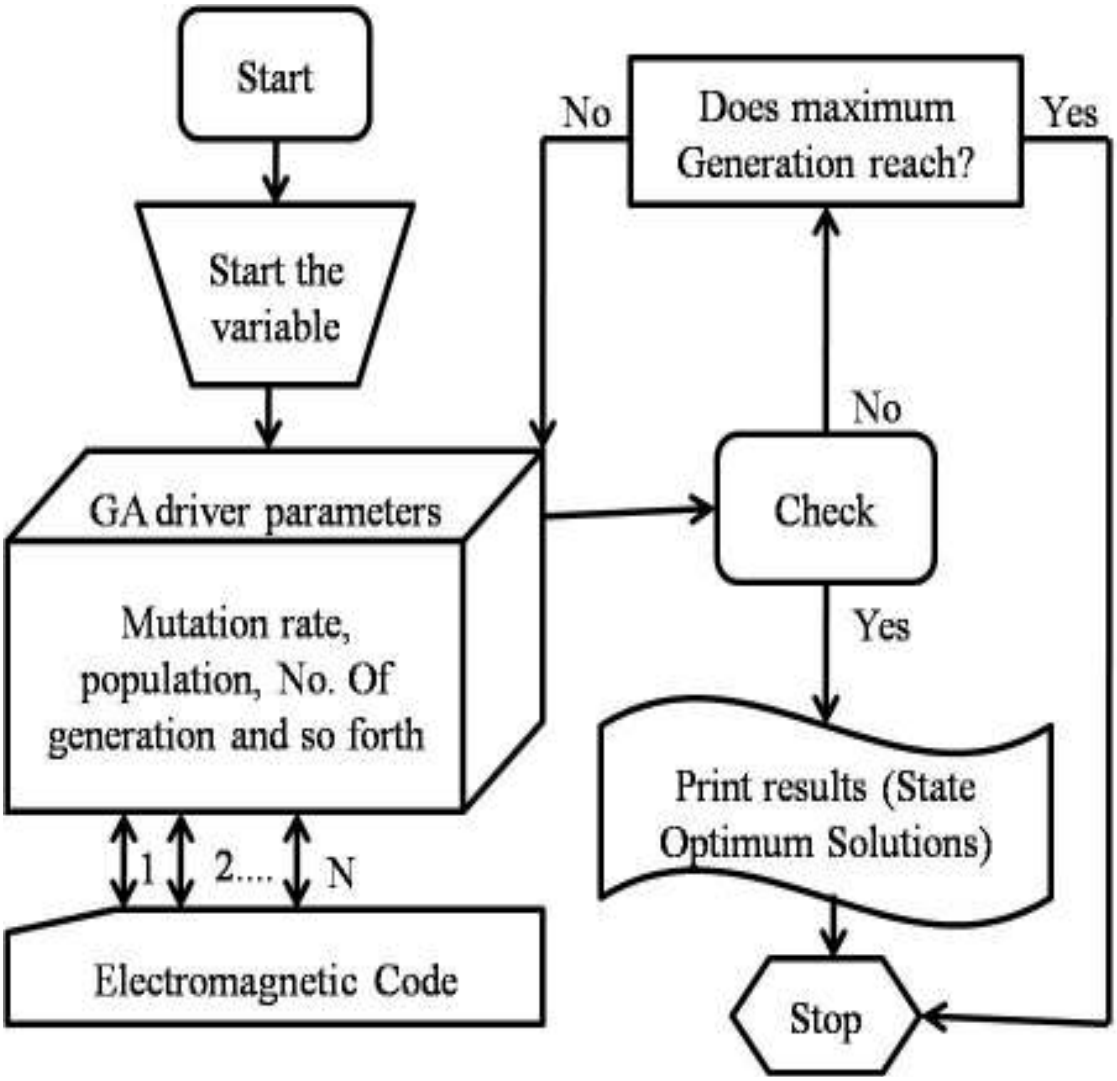

Figur 3.1:Flow chart of the genetic algorithm used in this study

Once a candidate configuration is presented, the GA converts the parameters into a file which can be called from NEC2. As a result, the sub-sequence geometries are fed into the GA engine for analysis versus. the constraints of the cost function, and then analysed individually until the most favourable design candidate is reached. The computed input impedance of the radiator for the 900*MHz* band is considered within the cost function.

3.3 CONFIGURATION OF THE PROPOSED RFID TAG

A generic planar meander line tag antenna template is shown in Figure 3.2. The final tag configuration has been optimised using the GA method for the UHF band. Obviously, the design optimisation is aided through a parallel meander line arrangement which is used to enhance the bandwidth.

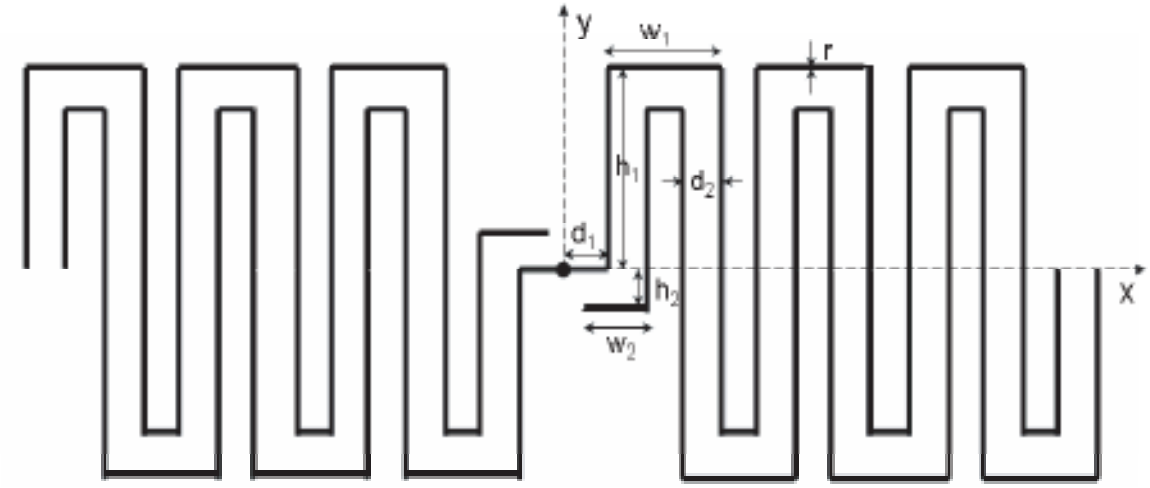

Figur 3.2:The optimum RFID antenna tag model

It is clear to observe them there are two parallel meander lines running together side by side where they are fed from the centre. In fact, the meander lines are used to minimise the antennas' size. In such a case, the assumption of having folded wires affects the antennas' performance. The cost function is targeting a specified return loss for acceptable antenna power gain. The time for taken hundreds of generations to reach optimum solutions was very encouraging to do more investigation [40].

The structure of the optimum tag antenna has been found within the maximum generations and the best solutions are listed in Table 3.1. They are the GA input parameters in which the possible ranges of parameters magnitudes have been shown. There are seven parameters have been used to define the proposed tag antenna including matching circuit elements i.e. parameters $w2$ and $h2$. For this optimisation, the procedure a real-valued of GA chromosomes has been used. Besides, the proposed tag antenna has been designed with 50Ω input impedance at 900MHz.

Table 3.1:Summary of GA input parameters, antenna variables and best solutions.

GA parameters	**GA- RFID passive tag antenna**	
	Parameters(*m*)	**Optimal (*m*)**
	Feeding wire length (d_1) (0.0025-0.0030)	0.0025
No. of population size =4,	Spacing between wires (d_2) (0.001-0.003)	0.00222
No. of parameters = 7,	Outer wire width (w_1) (0.006-0.01)	0.00651
Probability of mutation =0.02,	Matching wire width (w_2) *(0.0015-0.0055)*	0.00372
Maximum generation =250,	Outer wire height (h_1) (0.005-0.015)	0.01110
No. of possibilities=32768,	Matching wire height (h_2) *(0.001-0.003)*	0.00214
	Wire radius (r) (0.0001-0.0002)	0.0002

The reader antenna has been built in the form of the dipole antenna to examine the tag's antenna communication efficiency; Figure 3.3 presents

the position of the reader antenna (dipole) to the proposed antenna with distance (*d*) in metres.

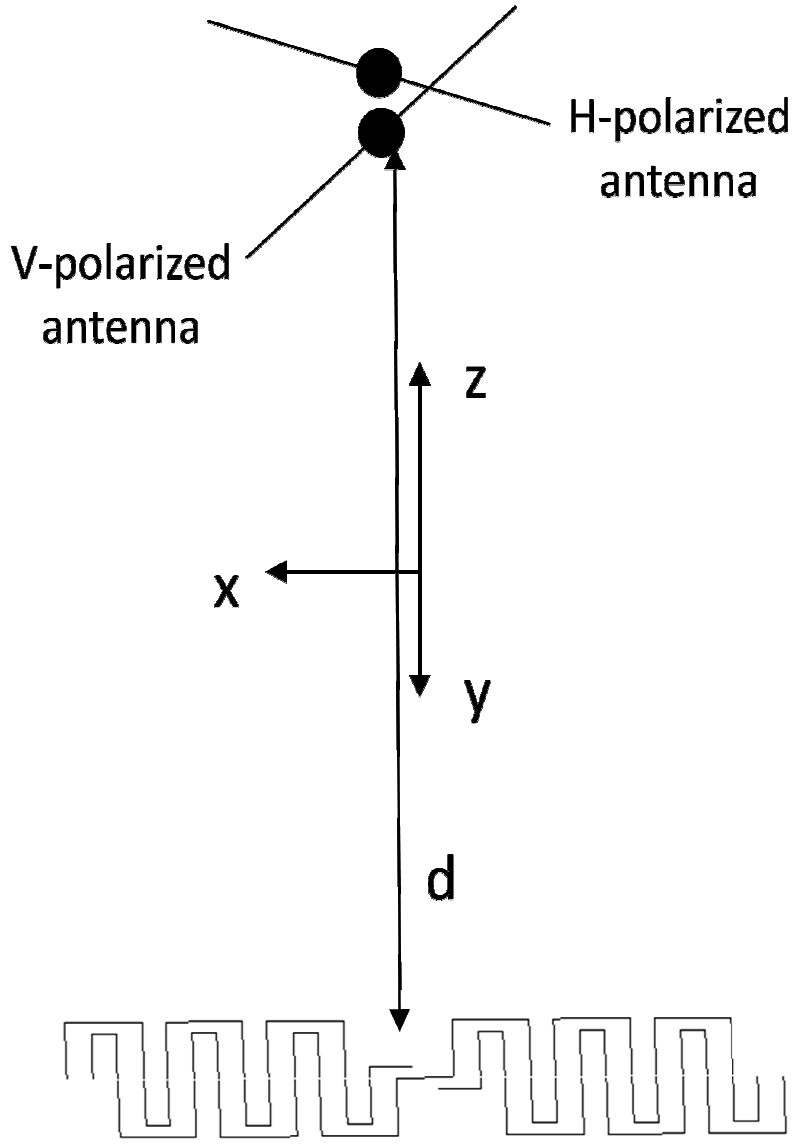

Figur 3.3:The optimum antenna direction regarding to reader antenna

The current induced on the central segment on the RFID tag (r=0.0005*mm* for *λ/2* dipole at 900*MHz*) has been demonstrated in Table 3.2.

Table 3.2: Comparison of the antenna power received/transmitted in vertical and horizontal planes

	Horizontal			**vertical**		
	(RP) normalised to mW	Received power (mW)	Transmitted power (mW)	(RP) normalised to 1 mW	Received power (mW)	Transmitted power (mW)
$\lambda/4$	0.2275	0.0010	4.8268	74.600	0.3511	4.7064
$\lambda/2$	0.0451	0.0002	4.8057	31.267	0.1523	4.8710
λ	0.0113	0.0001	4.8110	9.4411	0.0456	4.8299
2λ	0.0028	0.0001	4.8127	2.3663	0.0114	4.8176
3λ	0.0028	0.0001	4.8131	1.1214	0.0054	4.8151

$P_r/P_t=P_{r(1w)}/1$

In addition, the transmitted (TP) and received (RP) power in horizontal and vertical planes ($\lambda/4$ to 3λ) studied and Table 3.2 presents the results of this study.

It is worth mentioning that the received power of the optimum design in horizontal plane has been measured and found to be almost equal to zero as shown in Figure 3.4. The maximum power has been obtained in the vertical plane which is more than $70mW$ at 0.5 wavelengths. Clearly, the proposed antenna tag is operating as a linear polarisation sensor which can be easily deduced from the above table. Precisely, the received power of the antenna when it is in the horizontal polarised position is nearly negligible.

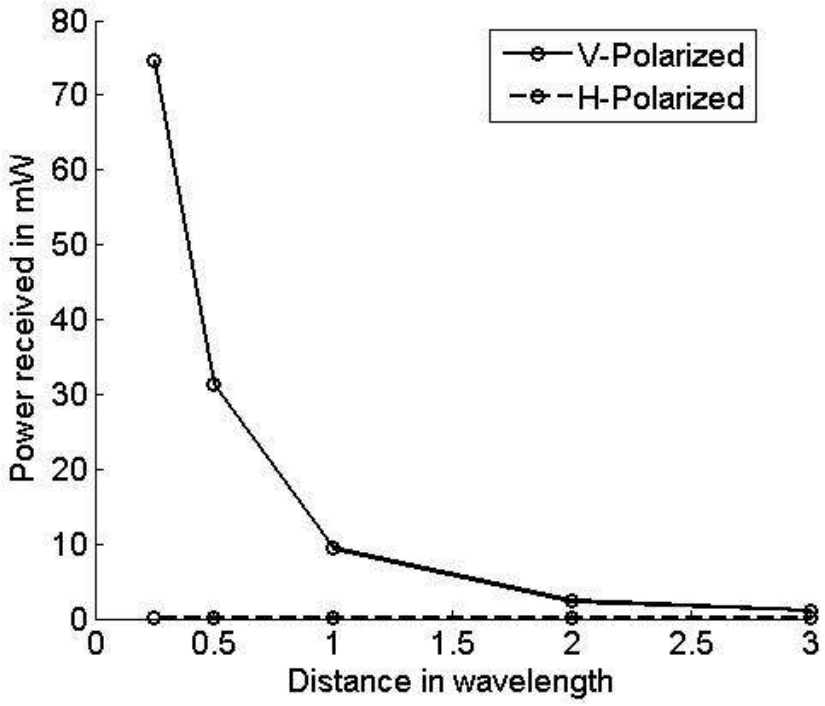

Figur 3.4: The variation of power received with optimum tag's antenna wavelength in vertical and horizontal position

From Figure 3.4, it can be clearly proven that the optimum antenna has successfully been designed with linear polarisation. In addition, the proposed sensor works in cross-polar position with full antenna performance whilst in the co-polar plane there is a big mismatch.

3.3.1 SIMULATION AND MEASURED RESULTS

After investigating the geometry of the proposed antenna, it is clear that the most appropriate dimension ($l \; x \; w$) has been found to be $62mmx22mm$. The target frequencies have been chosen to work in a UHF band (860-960)MHz. For validation, the optimum tag as shown in Figure 3.2 has been designed

and simulated on the HFSS software and the results are compared with those from the NEC software. Figure 3.5 demonstrates the close agreement in terms of the return loss with both software packages predicting a return loss of 40*dB*at 900*MHz*. In particular the simulated results show that the optimal tag antenna has a wide impedance bandwidth with respect to the tag IC impedance and enables it to fully cover the allocated UHF frequency band for RFID application from 860*MHz* to 960*MHz*. At 30*dB* return loss, the simulated bandwidth is 5 *MHz*, and across the entire frequency range the return loss is better than 10*dB* according to the simulated results. In addition, better antenna adaptations have been achieved by increasing the bandwidth and reducing the return loss.

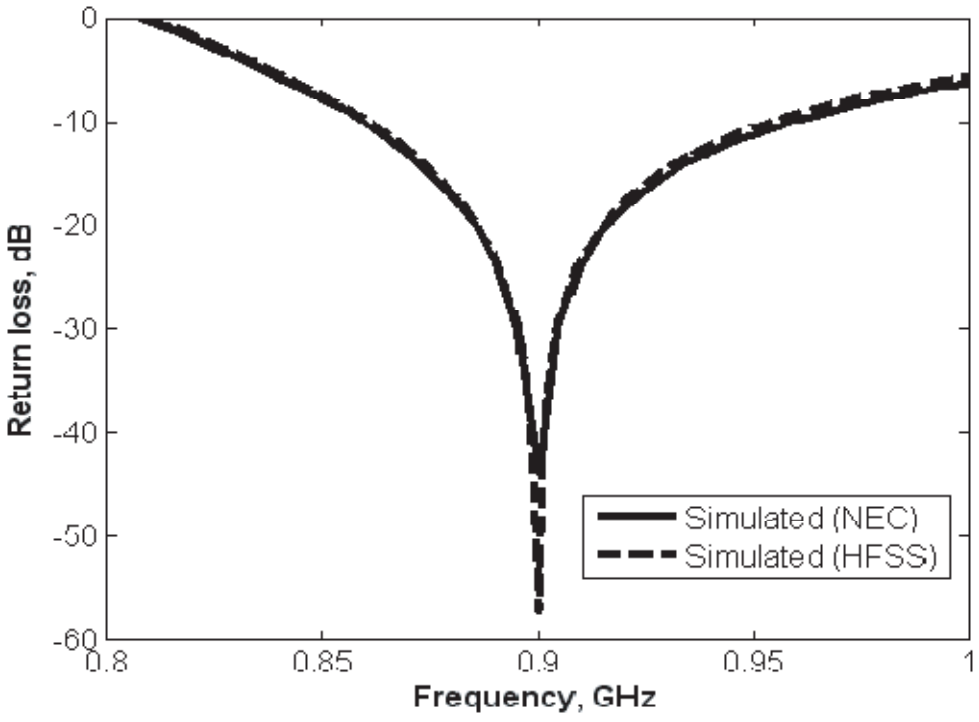

Figur 3.5:Comparison of return loss for the optimal RFID tag antenna

As it can be noticed in Figure 3.6, the obtained input impedance results for both software packages has been examined within the frequency range of 800*MHz* to 1000*MHz*. The simulated input impedance of the optimal tag antenna is found to be (12.2+*j*135)*Ω* at *900MHz*, for both packages.

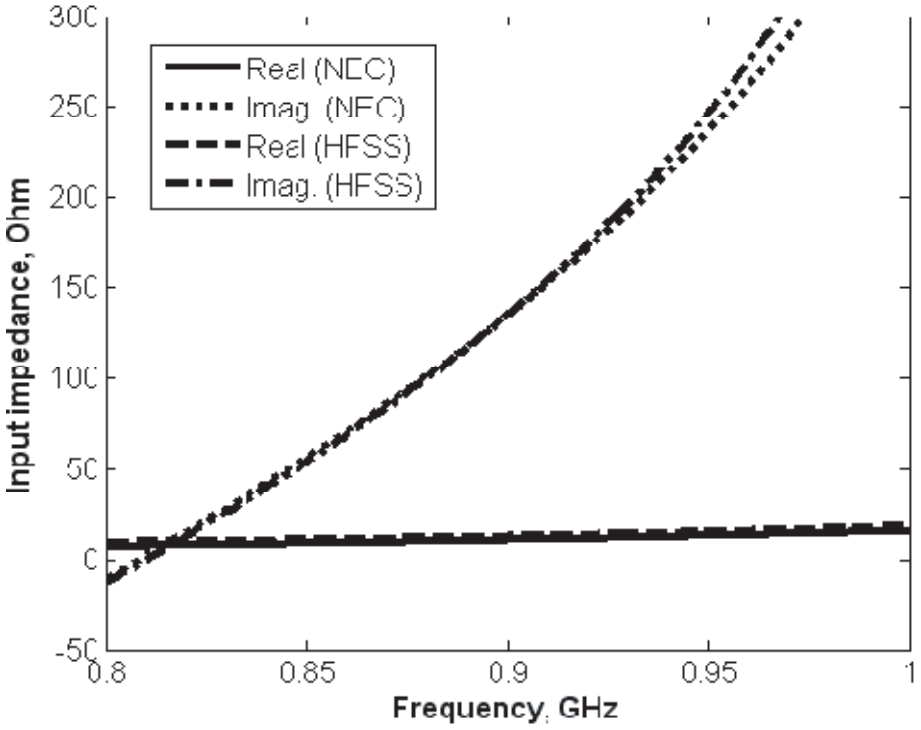

Figur 3.6:Simulated input impedance of the optimal RFID tag antenna

The antenna produces two fields when power is radiated to it from the reader: the inducting field which is related to storing the power and the radiating field which transmits the data back to the reader. The radiation field patterns of the proposed tag antenna have been investigated. In particular, the radiation patterns of the horizontal and vertical plane at 900*MHz* have been studied and the corresponding normalised results are displayed in Figure 3.7 and 3.8. Figure 3.7 demonstrates the radiation

patterns in the *z-x* plane at 900*MHz* and the vertical antenna power has been indicated equally in all directions (Omni-directional).

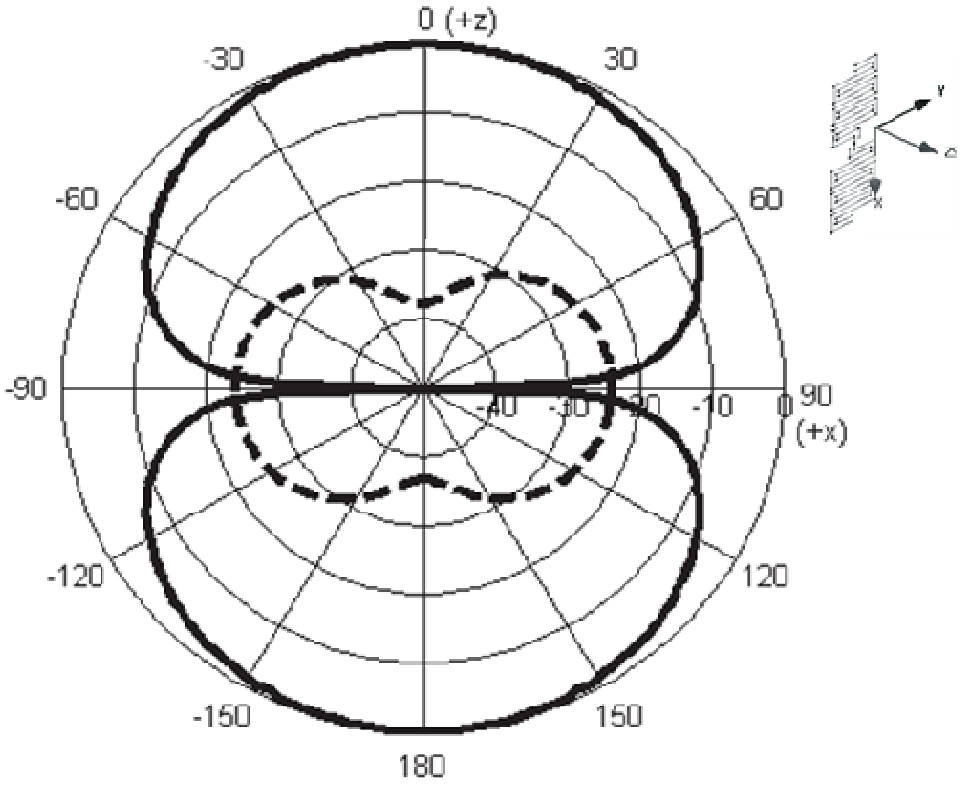

Figur 3.7:Radiation patterns of the proposed GA-optimised tag antenna for 900*MHz* at (*z-x* plane); '—— ' measured E_θ and `- - - -' measured E_ϕ

From the above figure, the optimum tag antenna's emitted power is concentrated into an area that looks like a donut (isotropic radiator). In addition, the maximum far field E_θ has been emission between ± 40 degrees with around 3*MHz*. In the other sides, the highest far field at E_ϕ has been radiated in the vertical plane is perpendicular to the dipole and zero in the direction of the antenna.

As it can be seen from below figure, below the horizontal antenna radiation (*z-y*) plane is essentially bidirectional. By turning the antenna 90 degrees, it is easily to obtain that the *E*-field is parallel to the purposed antenna and perpendicular to the floor.

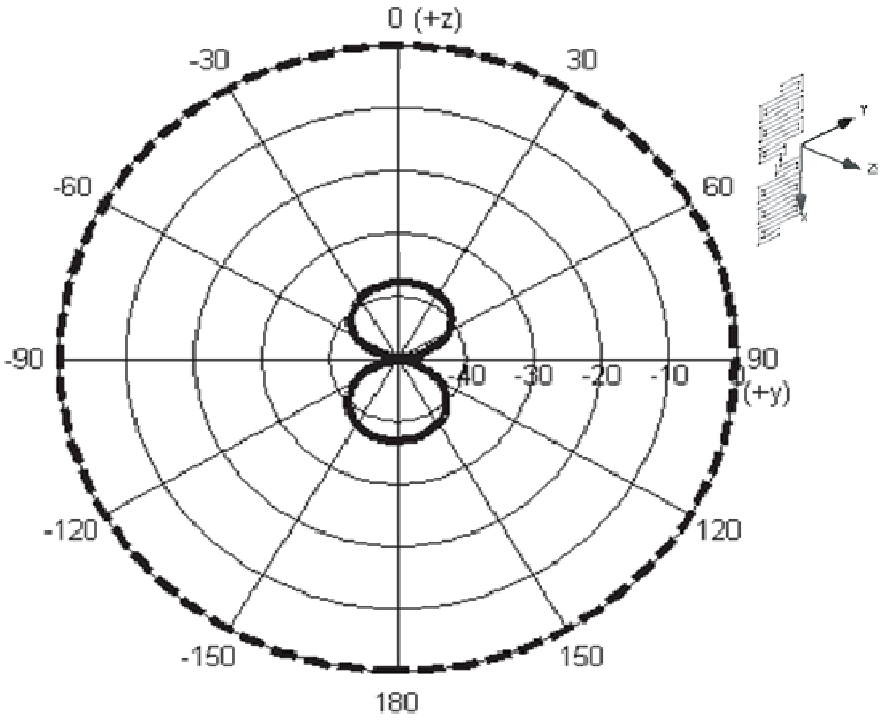

Figur 3.8:Radiation patterns of the proposed GA-optimised tag antenna for 900*MHz* at (z-y plane); `——' measured $E_\theta$ and `- - - -' measured E_ϕ

To sum up this section, a novel design for the design and optimisation of RFID tag antennas with linear polarisation by use of genetic algorithms has been presented. A FORTRAN code genetic algorithm driver was adopted in this work in conjunction with the industry-standard NEC-2 FORTRAN source code which has been used to evaluate the randomly generated antenna samples. The results of the optimum designs of the proposed antennas exhibit good input impedance matching as required by the RFID

IC. In addition, the powered received in vertical and horizontal plane has been studied. The presented examples show the capability of the proposed program in antenna design using GA and the results are encouraging for practical implementation of this tag antenna for UHF RFID applications.

3.4 CROSS- SHAPE RFID TAG ANTENNA

Wireless communication technologies are used in a variety of devices of varying sizes extending from small hand-held systems to devices installed on planes. For high speed data access, these technologies need wide bandwidth antennas, but also ideally they should be small size, simple, low-loss impedance matching and have high transmission performance. Circular polarised antennas have many properties that make them a strong candidate in wireless applications [2, 70].

In order to increase the reading range of passive RFID systems, readers and tags working in UHF band with highly sensitive signal detection abilities can be investigated. As mention previously, the limitation of the reader's transmitted power by the local EIRP regulations has reduced the possibility of increasing the radiation power of the reader. Therefore, the choice to increase the polarisation efficiency between the tag and the reader antennas is a good option to expand the detection rate. In fact, in most RFID technology the reader's antenna works with CP to detect the tag's antenna type. Commonly, mismatch between the tag and reader antennas occurs and

the reading range is minimised as a consequence, thus, the CP tag antenna is essential to increase the range [2, 71].

A novel CP tag antenna (cross-shape model) has been investigated and analysed using the genetic optimization algorithm and the geometry displayed in Figure 3.9. However, the algorithm has been repeated until sufficient new chromosomes have been formed, and an acceptable condition is reached, or a predefined number of iterations/generations have occurred. The studied method in this section is based on the well-known cross tag design and the optimization of the structure and feed point location of the CP tag antenna is performed via the genetic optimization algorithm, to reach a suitable antenna operation around the resonance frequency. In addition, the aim of designing a CP tag antenna is to reduce the mismatch polarisation between reader and tags. Therefore, the reading range should be twice that of linearly polarised tags. A highly axial ratio (AR) is displayed that shown near to the targeted operating frequency 900MHz. The antennas designed by this efficient design procedure have been realised experimentally, and the simulated results have been compared. In addition, the received power in horizontal and vertical planes has been analysed.

The configuration of the proposed antenna in the NEC-2 model and a total view of the complete assembly with the design parameters is presented in Figure 3.9.

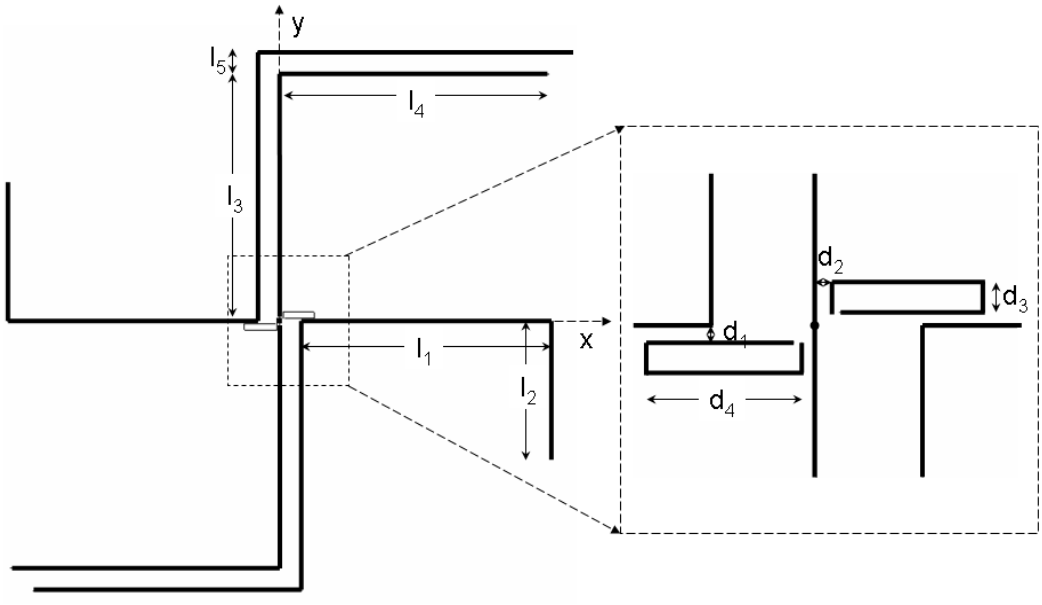

Figur 3.9: The CP tag antenna (cross model) dimensions

The photo of the realisation of proposed tag antenna is shown in Figure 3.10.

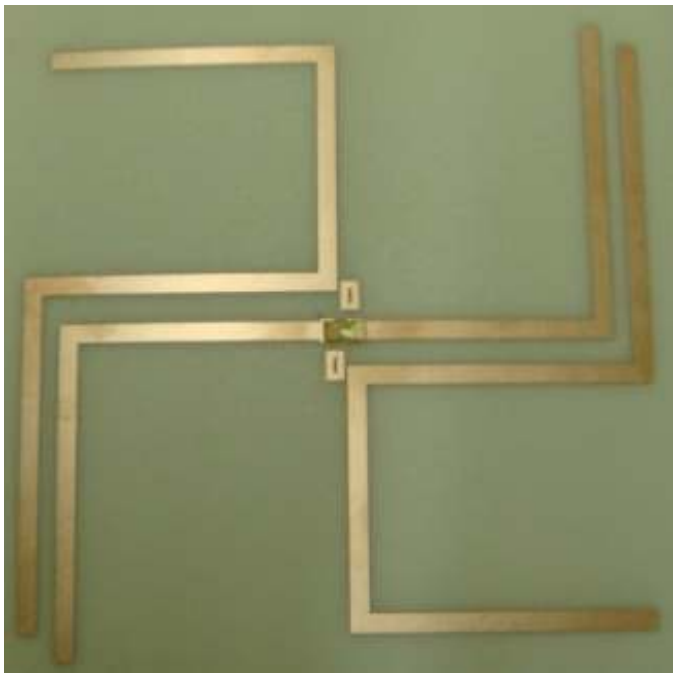

Figur 3.10: The proposed tag's antenna prototype

Table 3.3 shows the GA input parameters, their restrictions in term of allowed ranges and the optimal values for each particular dimension of the structure. It has to be mentioned that the weighted coefficient *W* has been found as 0.2*mm* as fixed value after a few efforts. It has to be mentioned that the weighted coefficient W has been found as 0.2mm as fixed value after a few efforts and under the maximum number or generation is 1000.

Table 3.3:Summary of GA input parameters, antenna variables and best solutions.

GA parameters	**GA-optimised RFID tag antenna with CP**	
	Parameters (*m*)	**Optimal (*m*)**
	Antenna wire length 1 (l_1) (0.025-0.05)	0.046629
No. of population size = 6,	Antenna wire length 2 (l_2) (0.015-0.04)	0.025503
No. of parameters = 9,	Antenna wire length 3 (l_3) (0.025-0.05)	0.046038
Probability of mutation =0.02,	Antenna wire length 4 (l_4) (0.0015-0.0055)	0.050454
Maximum generation =1000,	Antenna wire length 5 (l_5) (0.001-0.005)	0.004194
No. of possibilities=32768,	Matching loop distance 1 (d_1) (0.0005-0.001)	0.000618
	Matching loop distance 2(d_2) (0.0005-0.001)	0.000636
	Matching loop distance 3 (d_3) (0.001-0.003)	0.001200
	Matching loop distance 4 (d_4) (0.002-0.0075)	0.005826
	Wire radius (r) (fixed)	0.0002

Figure 3.11, demonstrates the location and position of the CP antenna tag comparing to the dipole antenna which has been used as the reader antenna. The horizontal and vertical position of the reader's antenna with different orientations of the proposed tag antenna has been studied. Clearly, from Figure 3.11 (a) shows the antenna position when θ is equal to 90^0 the state of the optimum antenna when θ is equal to 0 degrees is shown in Figure 3.11 (b). The distance between the reader and the tag antennas (d) are measured in metres and the tag antenna is also shown in the figure below.

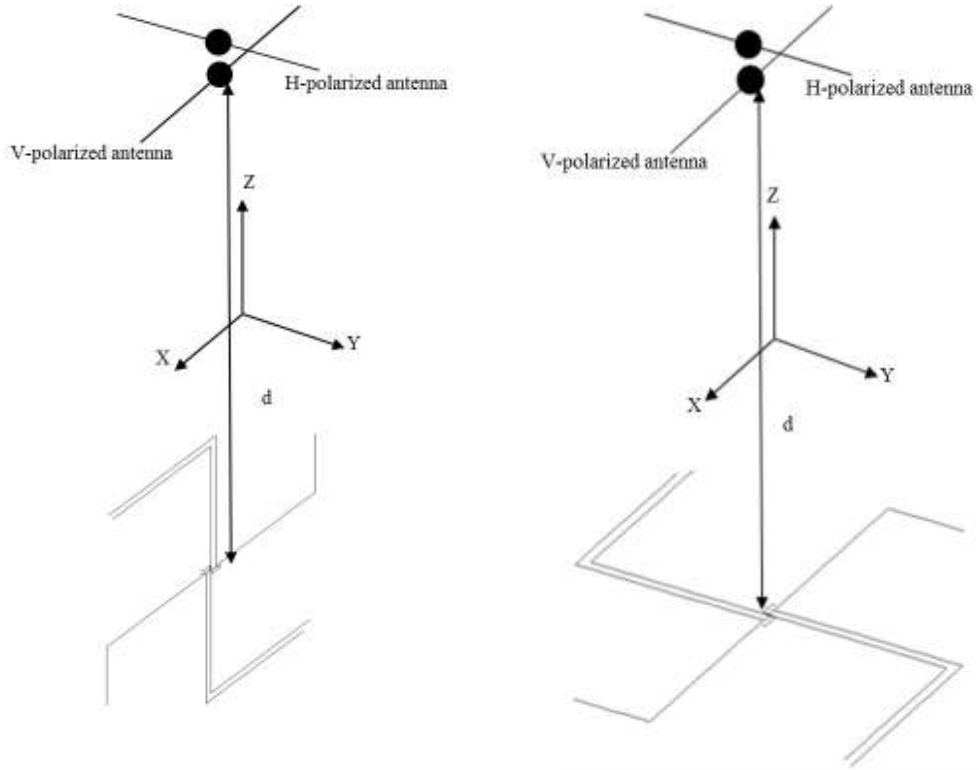

(a) (b)

Figur 3.11: The optimisation setup of proposed antenna tag and reader antenna; a) θ = 90^0, b) θ = 0^0.

The electrical power of the CP RFID tag antenna which is received/transmitted in horizontal and vertical plain has been measured and shown in Table 3.4. According to the obtained results, the transmitted and received powers in both planes are similar.

Table 3.4:The optimisation results of the power received/transmitted by the optimum tag

	Horizontal			**Vertical**		
	(RP) normalised to $1mW$	Received power (mW)	Transmitted power (mW)	(RP) normalised to $1mW$	Received power (mW)	Transmitted power (mW)
$\lambda/4$	68.7470	0.2434	3.5405	76.2650	0.3341	4.3808
$\lambda/2$	0.0244	0.1223	5.0197	30.9120	0.1523	4.9269
λ	7.6184	0.0366	4.8041	9.4471	0.0456	4.8269
2λ	1.9029	0.0092	4.8137	2.5321	0.0122	4.8181
3λ	0.9129	0.0044	4.8088	1.1217	0.0054	4.8140

$$P_r/P_t=P_{r(1w)}/1$$

These results show that the proposed tag antenna has circular polarised properties. In particular, the received powers in co and cross planes have been normalised and plotted in Figure 3.12. In addition, the current induced on the central segment on the RFID tag (r = 0.0005mm for $\lambda/2$ dipole at 900MHz) has been measured.

The maximum electrical power received has been found to be about 77mW in the horizontal plane and 94mW in the vertical ones at λ wavelength.

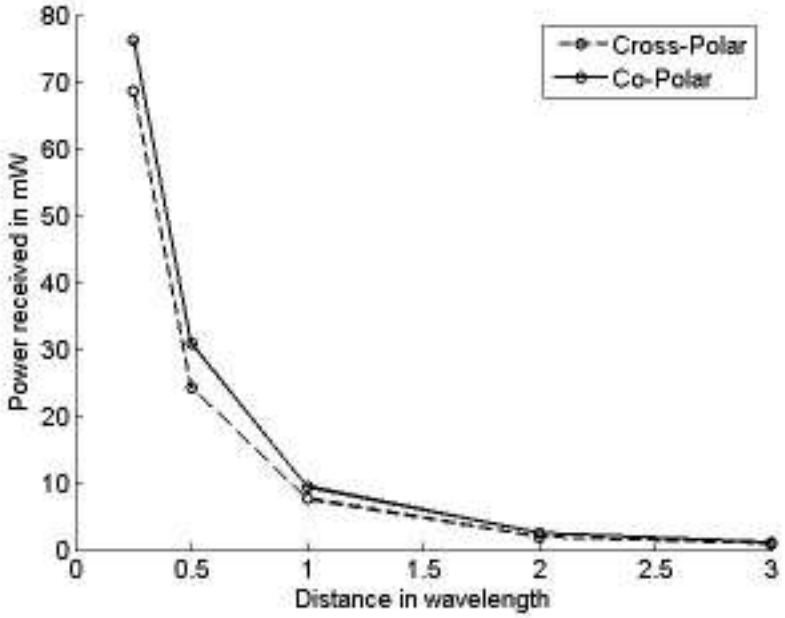

Figur 3.12: The power received in vertical and horizontal planes for 1W normalised input power

3.4.1 SIMULATION RESULTS

The configuration of the proposed CP RFID tag antenna, with excellent AR, has been found within the maximum generations and the antenna parameters of the best design as presented in Table 3.3. For validation, a model of the GA-optimised CP RFID antenna tag has been made and tested. The CP RFID tag arms are made of copper wires with radius of 0.2mm. The narrow bandwidth of the designed antenna bandwidth has been not considered in the GA cost function. The optimal antenna appears to have excellent impedance matching that covers the bandwidth requirements at 900MHZ band for RFID system communications as shown in Figure 3.13. The input impedance has been found to be about (10 - j130)Ω at 900MHz.

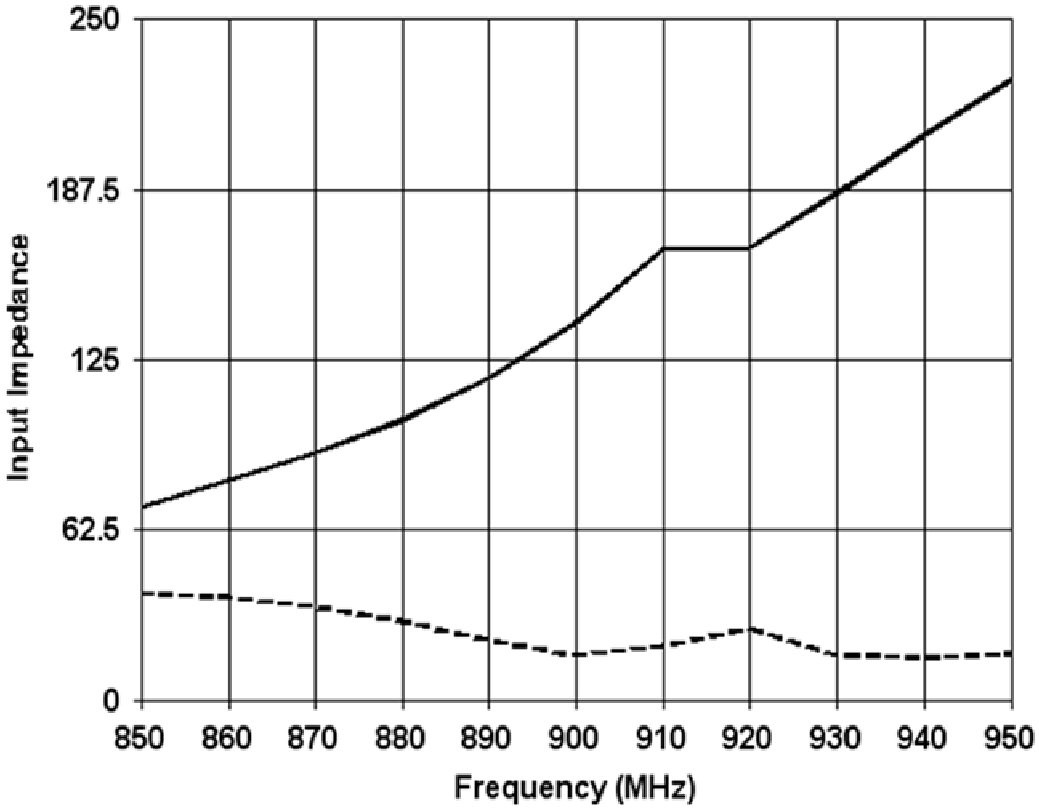

Figur 3.13: Antenna's tag input impedance; dashed line: real and solid line: imaginary.

Figure 3.14 displays the AR simulation of the optimum tag antenna at 900*MHz* (less than 1*dB*), which show an acceptable characteristic of circular polarisation. Although small differences are present between the two planes, a high AR nearly to one in the surrounding area of 900*MHz*. The proposed tag antenna orientation of the AR (< 0.7*dB*) is about ± 50 degrees, which is working much in big area as CP. The polarisation matching between the tag and reader antennas (AR) at the bore-sight ($\theta = 0^0$) is indicated by solid line; the dashed line shows the matching at the bore-sight (θ=90^0). Clearly, the axial ratio in vertical and horizontal polarisation is in fairly close agreement to each other at 900*MHz*.

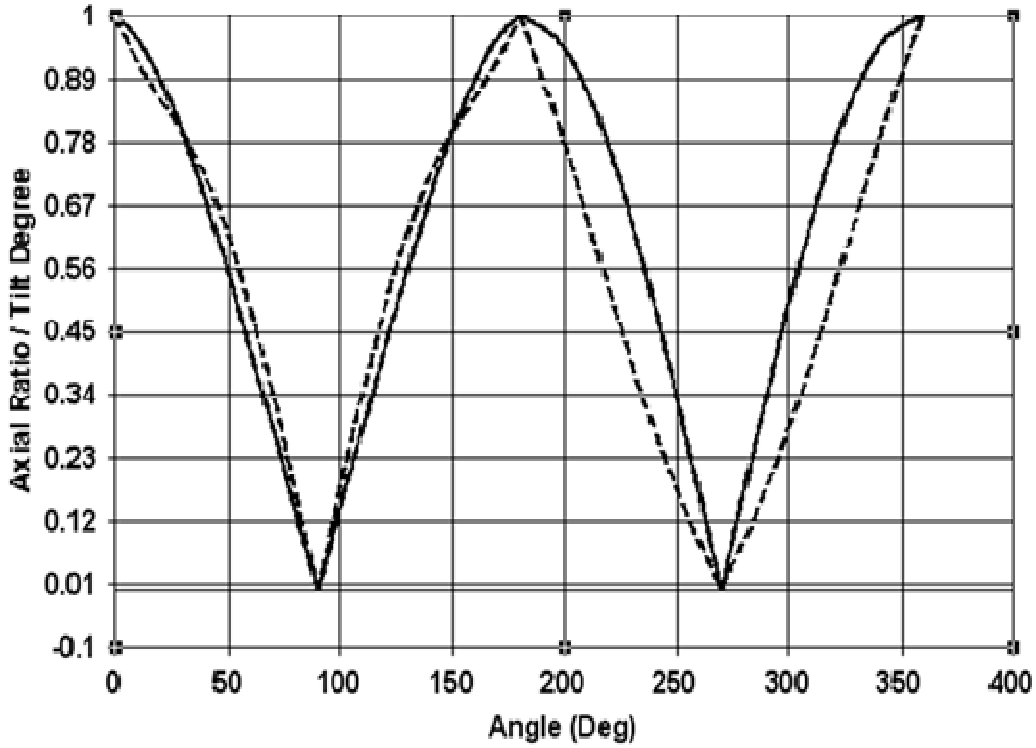

Figur 3.14: The Axial Ratio of the optimum tag antenna at 900MHz; dashed line: AR, $\phi=90^0$ and Solid line: AR, $\phi=0^0$.

According to [72], the minimum polarisation loss is about 2.54*dB* and the maximum ones is 3.54*dB*, where the smallest polarisation loss occurs when the stronger linear field component of the circularly polarised wave is correspondently associated with the linearly polarised wave. On the other hand, the maximum polarisation occurs when the weakest linear field component of the circularly polarised wave is united with the linearly polarised wave.

As can be seen from Figure 3.15, the proposed antenna has a smallest axial ratio at frequency 900*MHz* band. This shows that the optimum antenna has a quite interesting results, as this can be noted, from the power receiving

study when the antenna is in a vertical position is nearly the same as when it's in a horizontal polarised position and it's found nearly to 75*mw* at 900*MHz*.

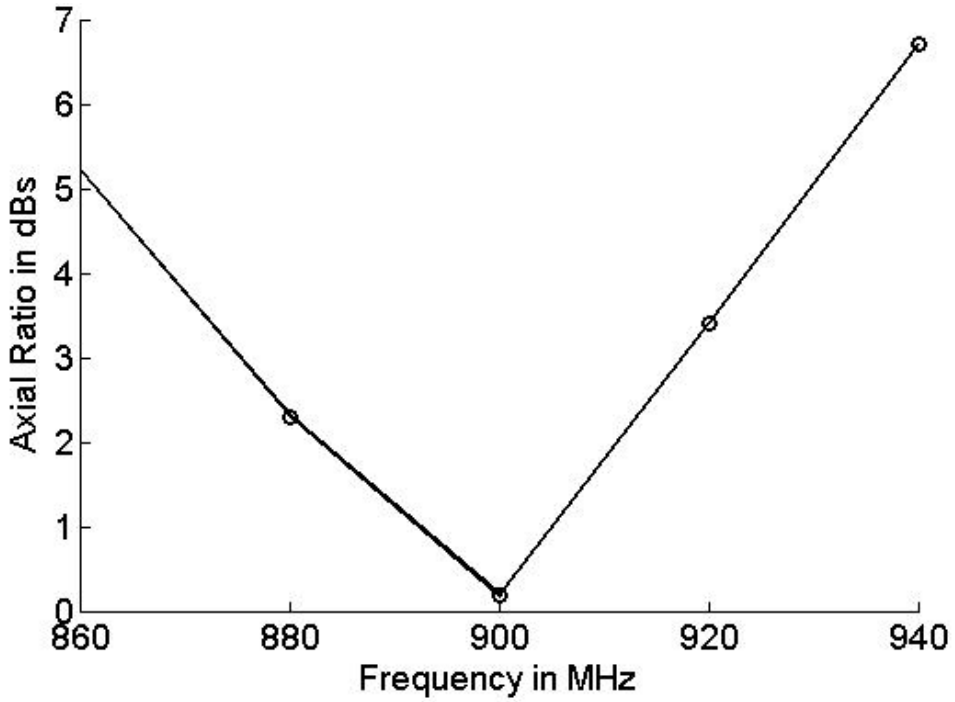

Figur 3.15: AR in *dBs* of the proposed CP tag antenna related with frequency in 900*MHz*

The observations verify the greater circular polarised characteristic of the proposed optimal design. Figure 3.16 and 3.17 present the radiation pattern of the optimal antenna at 900*MHz* for both polarisations i.e. copular and cross-polar. The symmetrical and identical variations have been obtained for all the radiation patterns.

The results confirm that an axial ratio of less than 5.5*dB* over ±50° elevation angle can be achieved. Therefore, the GA has proven its advantage for quickly finding solutions for optional antenna design.

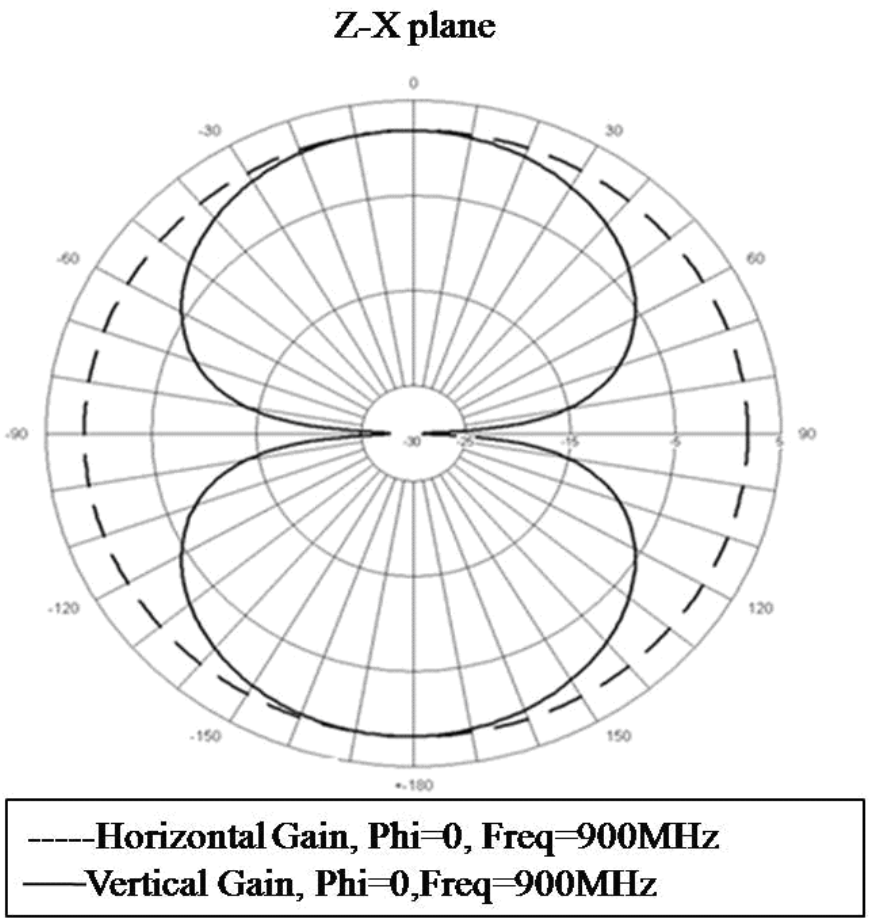

Figur 3.1: The radiation diagram at (z-x) plane

Figure 3.16 shows that the proposed design operates as a circular polarised antenna in (*z-x*) plane when the antenna's position is about ± 50^0 within a 3*MHz* bandwidth. On the other hand, the circular polarisation occurs in (*z-y*) plane when the antenna's orientation is about ±45 within a 3*MHz* bandwidth

as clearly seen in Figure 3.17.

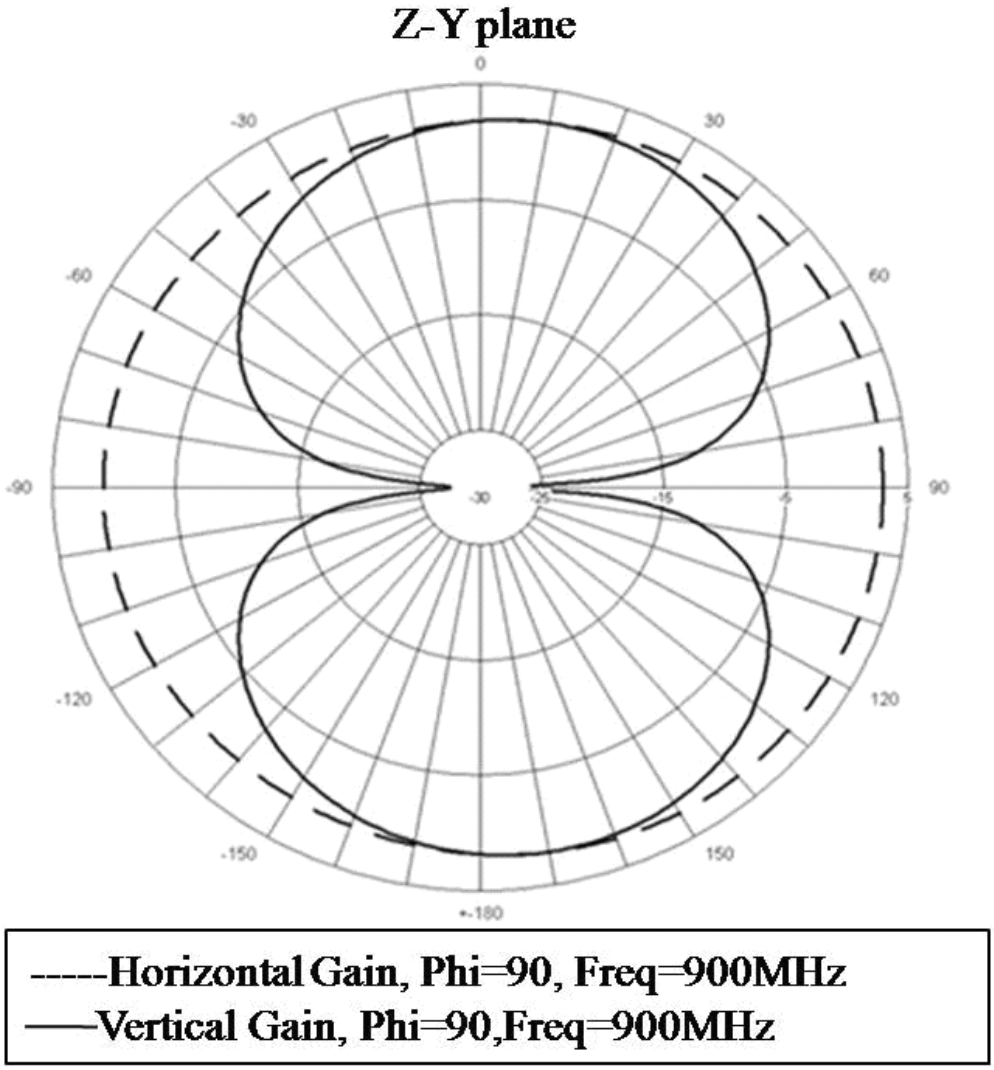

Figur 3.2: The radiation diagram at (*z*-*y*) plane

Novel CP cross –shape has been found to give less than 1*dB* axial ratio and the CP operation can be obtained according to the results when the antenna position is between $\pm 45^0$ to $\pm 50^0$ in both plane within a 3*MHz* bandwidth.

3.5 CONCLUSIONS

In conclusion, this chapter can be considered to be the first step on setting the design procedures. The main motivation of the work presented is its contribution towards others antenna design features for the coming chapters. In brief, the features of GA developed have been a great help in designing of the new proposed linear and circular polarised antennas in this chapter. Beside this, the HFSS software is used to confirm and compare the gained results for these antennas' configurations. To sum up, both proposed antennas have shown good and acceptable radiation performances and thus they might be recommended as excellent candidates for tag designs.

CHAPTER FOUR

LINEAR POLARISED RFID TAG SENSORS DESIGN FOR UHF BAND

4.1 INTRODUCTION

An important requirement for any wireless communication technology is to have antennas with high efficiency and excellent overall performance [73]. Specifically, antennas by themselves are not intelligent and need some other facility to acquire such features. For example, in the RFID systems when the chips are amounted on antennas then the passive RFID tags are configured and the device becomes “intelligent”. Information may now be obtained and transmitted. In particular, the conjugate matching method is used to maximise the power transmission between the antenna/IC assembly when RFID tags are configured. Generally, the reactance of this chip is commonly much smaller than the usual 50Ω [2, 7].

RFID tag antennas are usually etched on thin dielectric which is integrated onto mounted on or adhered to the relevant surface. Many current designs employ materials such as Foam Clad R/F 100 (Arlon) which has a relative permittivity close to that of air. Being a foam material this varies slightly [74]; tags mounted on metallic targets typically use variants of FR4 [75]. These dielectrics are used to support the additional circuitry for the feed network and required for testing purposes.

Chip mounting to foam materials could be awkward as standard soldering operations require good surface contact and temperatures $\geq 250℃$. In addition, some foam materials are difficult to cut, or bend due to their fragility. A practical solution is to use a good electrical conductivity paste (conductive epoxy) for soldering between the chip and antenna tag ports. The paste is actually a binary composite of epoxy (bright silver) and hardener (gray silver); they need to be mixed with equal density for two minutes and then used within eight minutes [76].

Most contemporary designs use foam, or composite materials. [77] proposes a novel Ψ-shaped microstrip patch antenna providing a wide-impedance bandwidth, in addition to acceptable radiation patterns. In [78] a WLAN chip antenna has been presented which the antenna is mounted above the system ground plane of the mobile terminal cavity by folding a metal plate onto a foam base. In [79] a single feed quad-band PIFA is presented with some novel features; a foam dielectric substrate is used to provide a rigid structure and shielding. USB dongles use an internal antenna fabricated from bending a metal plate over a foam base [40].

In this chapter, single and double meander-line RFID tag antennas for the UHF band $(860-960)MHz$ have been studied and investigated over specific design frequencies that cover the European variant of the band$(865-868)MHz$. Initial design studies are made using HFSS; the parameter space being made up of the obvious structure parameters and data relating to the

location of the chip and the geometry of the looping around the chip. The geometry is simplified using rectangular lines of the version presented in [75]. The measurement kits used in this study are manufactured by Alien Corp. [80]; in which the input impedance is $(12.2 - j135)\Omega$ at $900MHz$. In order to test the antenna radiation pattern, a balun operating at $900MHz$ has been modeled using advanced design system (ADS) [54] and HFSS [81]. Moreover, the measurement of the far-field pattern has been obtained and compared with the simulation results.

4.2 BALUN DESIGN CONSIDERATIONS

In fact, the balun word is a short word that comes from the combination of bal(ance) and un(balance). A balun is employed to convert an unbalanced port to balanced port feeding network or vice versa. This device is employed for balanced feeding input ports network such as that used for dipole and loop antennas, in which a balance feeding current with equal amplitudes and have 180 degrees phase difference. The balun also provide the basis to exclude the conducting ground from the radiating structures.

Mathematically, the balun is composed from two 90^0 phasing lines which easily could be calculated from the 180^0 split [73].In contrast, numerous balun structures have been demonstrated for RFID devices application such as that reported in [82] in which a robust ultra high frequency near-field

RFID reader antenna has been tested; in addition, to [83] that investigated a simple shape broadband planar antenna adaptable to RFID tag.

To assist the balun model and characterization, the ADS software has been used to model the performance of the design structure and to achieve the optimum dimensions required as observed in Figure 4.1. The layout of the initial design then optimised using HFSS to include all possible coupling between the transmissions lines used for which a new layout model is presented in Figure 4.2. The optimum balun dimensions have been found after several attempts as shown in Table 4.1. In contrast, the simulation results of the target model i.e. ADS and HFSS have been compared to the measured results and have been found with quite reasonable agreement.

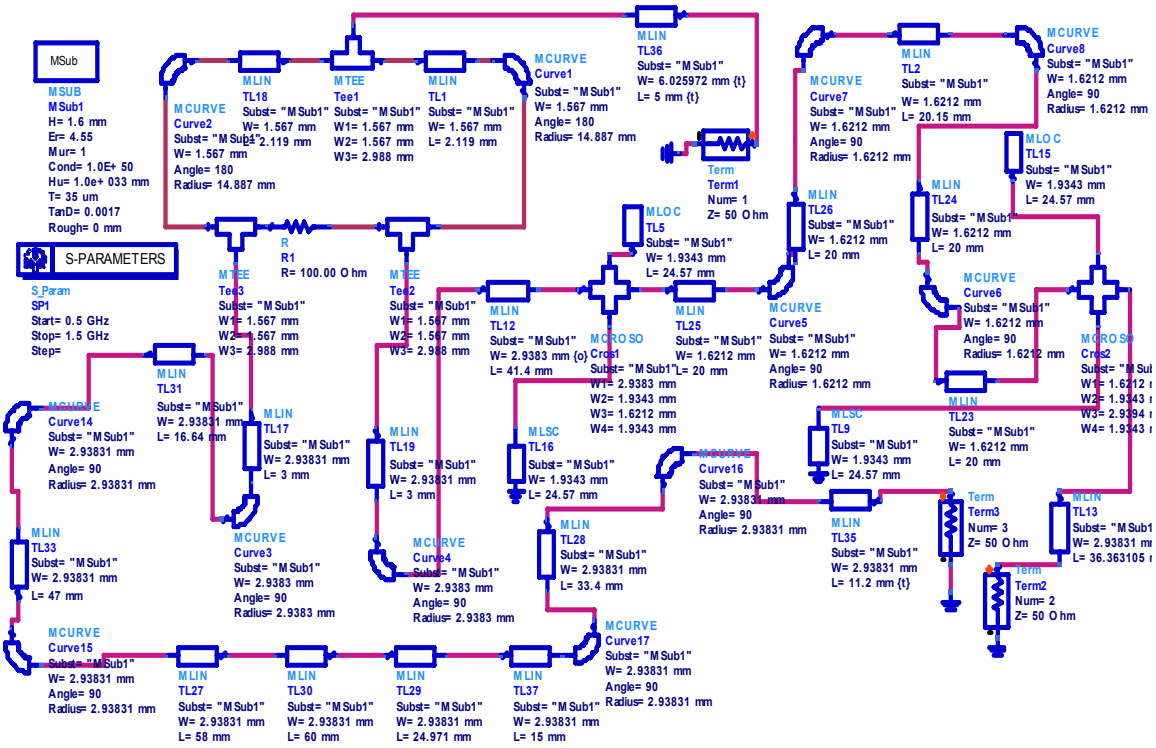

Figure 4.1:Balun circuit is design by ADS software

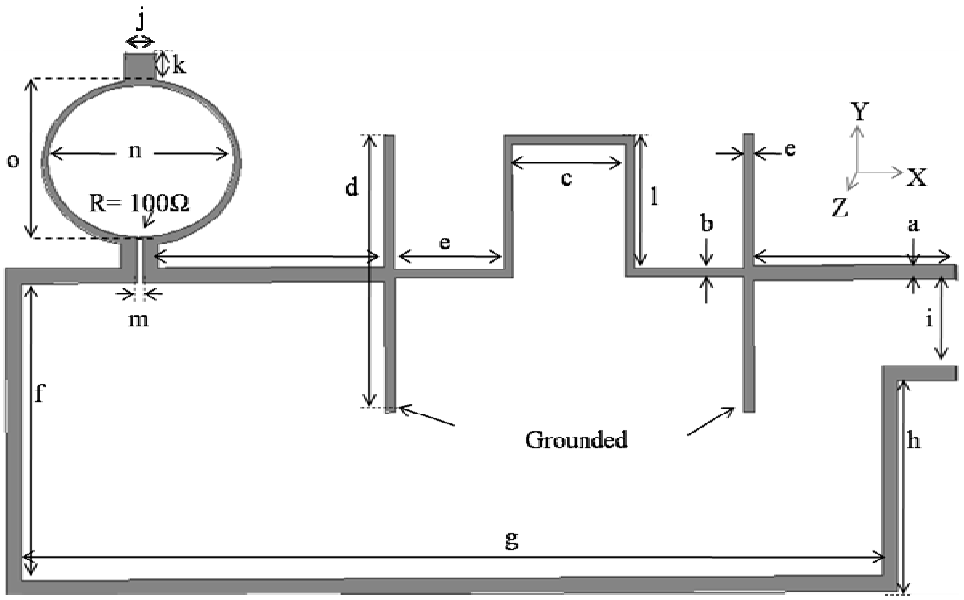

Figure 4.2:Layout of the target balun

Table 4.1:The balun parameters

a	2.9384	**i**	16.0469
b	1.6	**j**	5.06224
c	21.7706	**k**	5.06224
d	52.0778	**l**	25.0836
e	1.9343	**m**	1.2998
f	55.815	**n**	35.433
g	163.8475	**o**	28.43
h	39.5467		

4.2.1 SIMULATION AND MEASURED RESULTS

The balun has been designed to operate at 900*MHz* and the feeding ports are normalised to Z_0=50Ω. In. addition, the balun has been simulated using ADS

and HFSS, fabricated in a microstrip and tested. The photograph of the optimum balun during the measurement test is shown in Figure 4.3.

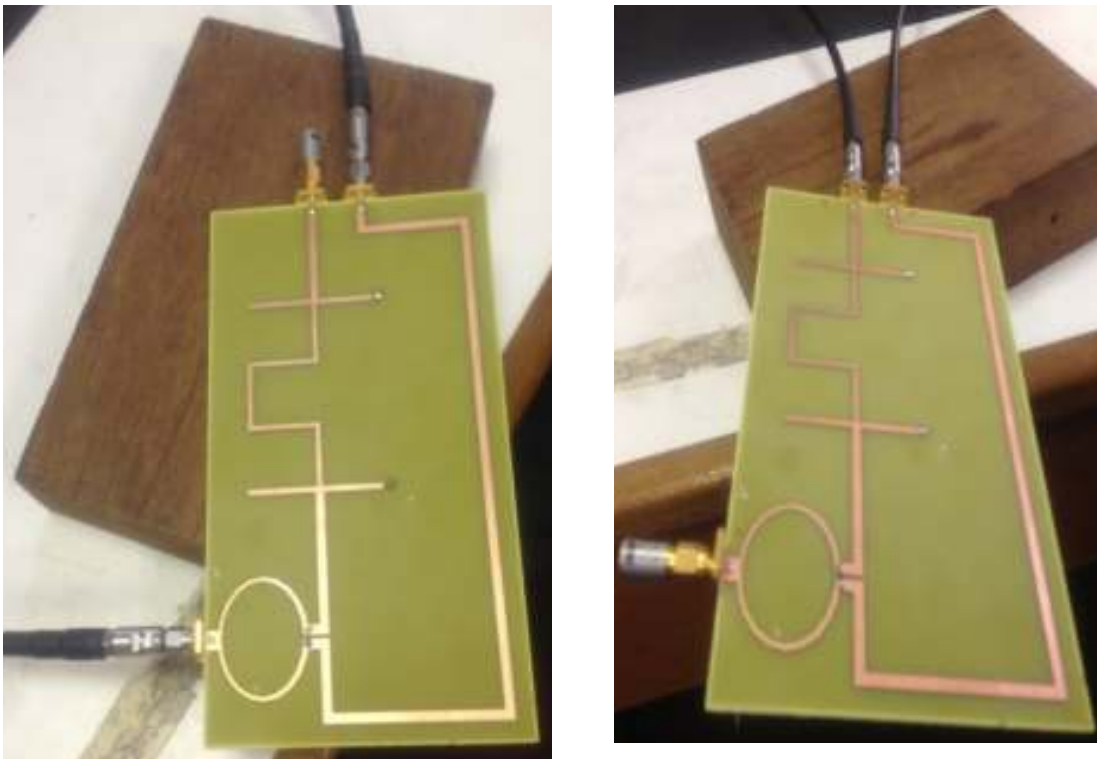

Figure 4.3:The photo of the optimum balun design in position of measurement

The simulated ADS results have been presented in Figure 4.4. In particular, the refection coefficient $|S_{11}|$, $|S_{22}|$ and $|S_{33}|$ have been indicated in Figure 4.4 (a) and the phase difference between the outputs ports has been presented in Figure 4.4 (b).

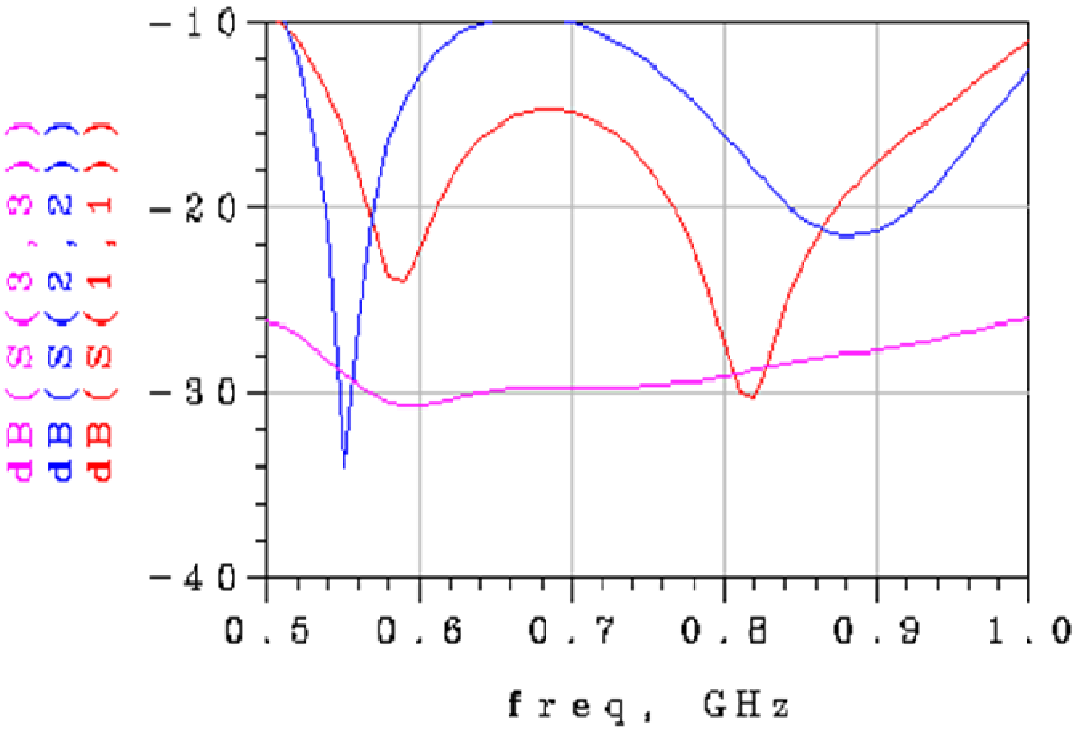

(a)

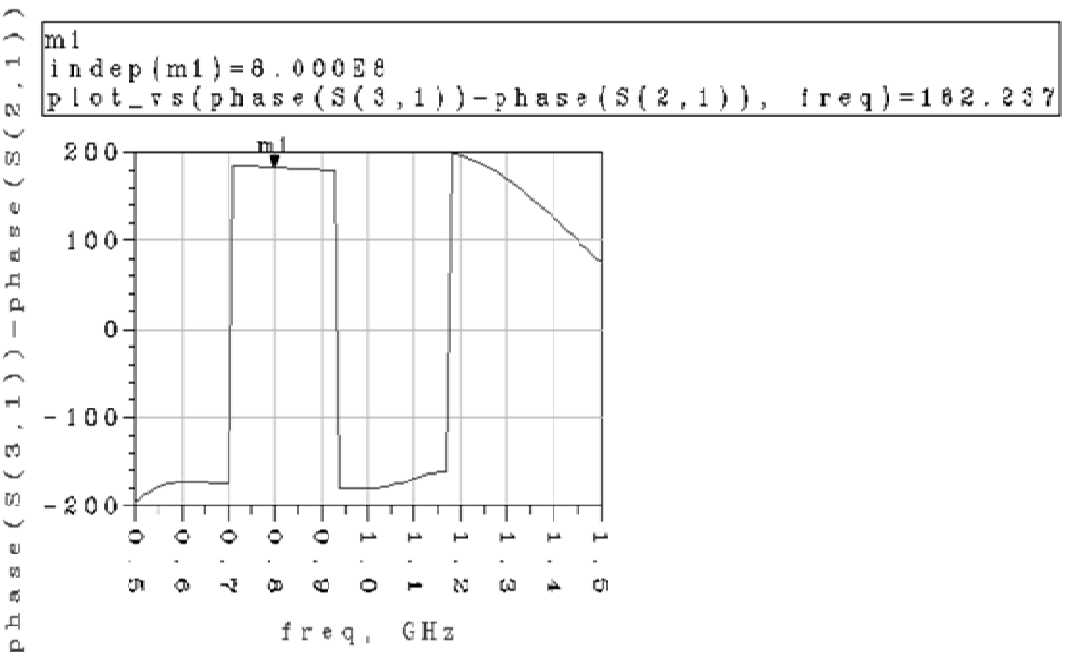

(b)

Figure 4.4:The ADS results a) the Simulated input and output Refection coefficient $|S_{11}|$, $|S_{22}|$, $|S_{33}|$ and b) the phase shift between the output ports

The simulated and measured results in terms of the return loss and insertion loss between the three ports are presented in Figures 4.5 and 4.6 respectively. There were more than 12dB in a return loss was achieved and acceptable insertion loss difference around ± 0.05dB at 900MHz.

In addition, the simulated and the measured of the phase difference between the two outputs ports are presented in Figure 4.7. A good agreement can be seen over the required bandwidth around 900MHz. The results encourage the employ this feeding network to the new designed tags presented in the following sections.

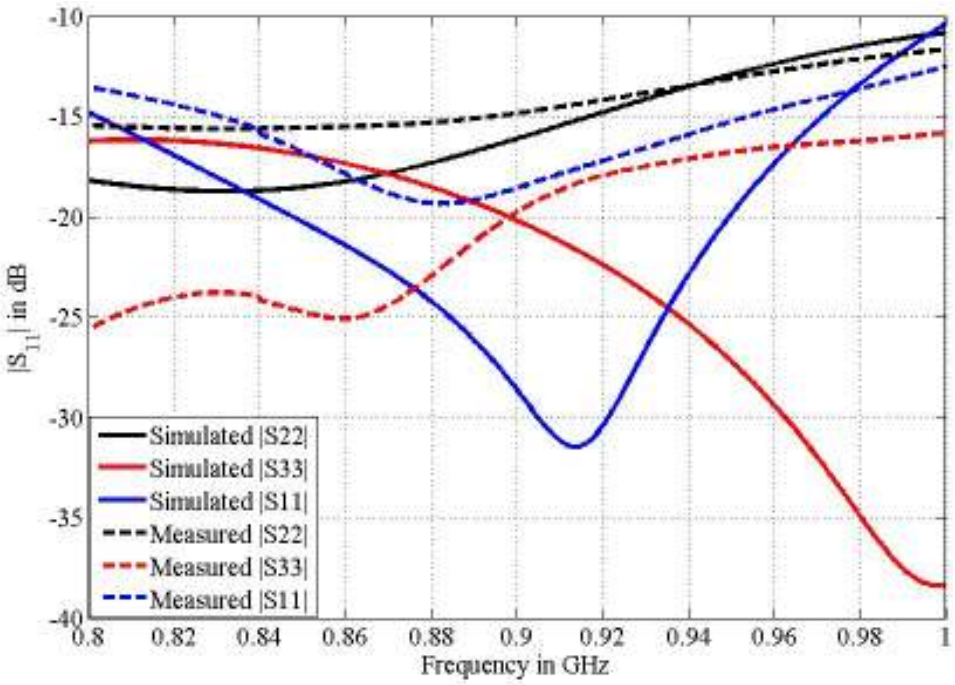

Figure 4.5:The Measured and simulated Refection coefficient of the input and output parameters result in term of dB

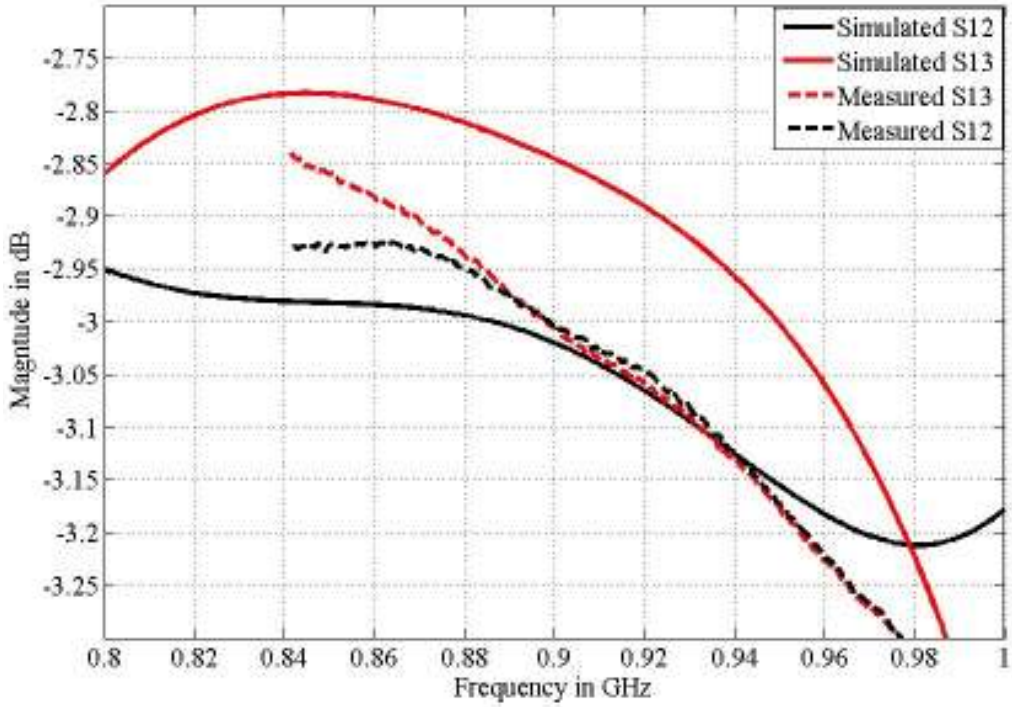

Figure 4.6:The simulated and the measured insertion loss coefficients

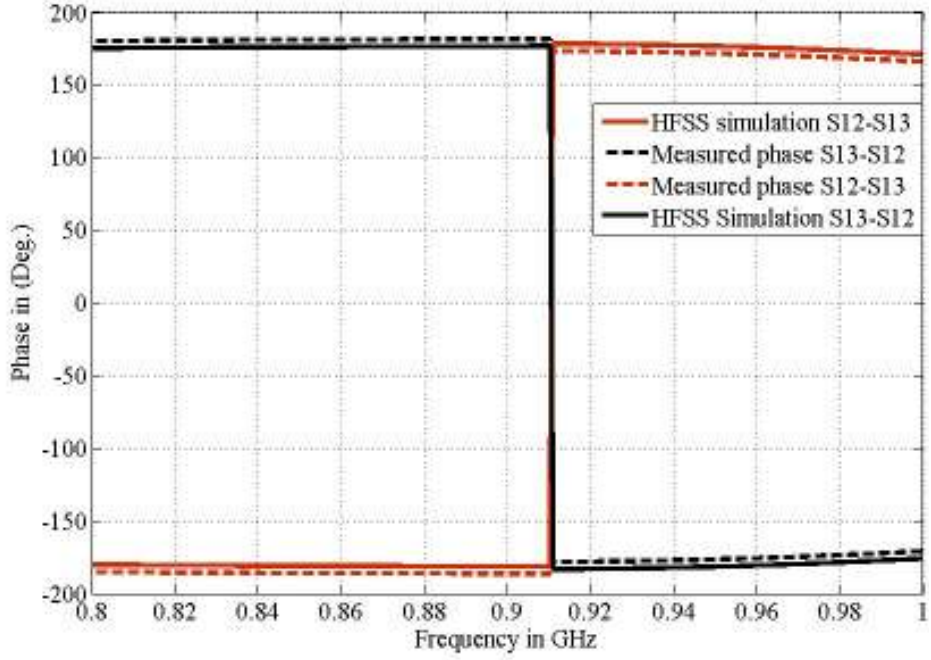

Figure 4.7:Simulated and measured the phase difference between the two output ports

4.3 MEANDER LINE RFID TAG (MLRT) – 1st DESIGN

In this section, the design and operating principles of a double rectangular meander line RFID tag are investigated. The design strategy is intended to minimise the antenna's size while improving its overall performance. Eventually, the most significant metric will be judged in terms of successful read/write capabilities, with in well defined transmission bounds. The recent literature places emphasis on passive RFID tags even for long detection lengths [75].

The design schematic is shown in Figure 4.8.

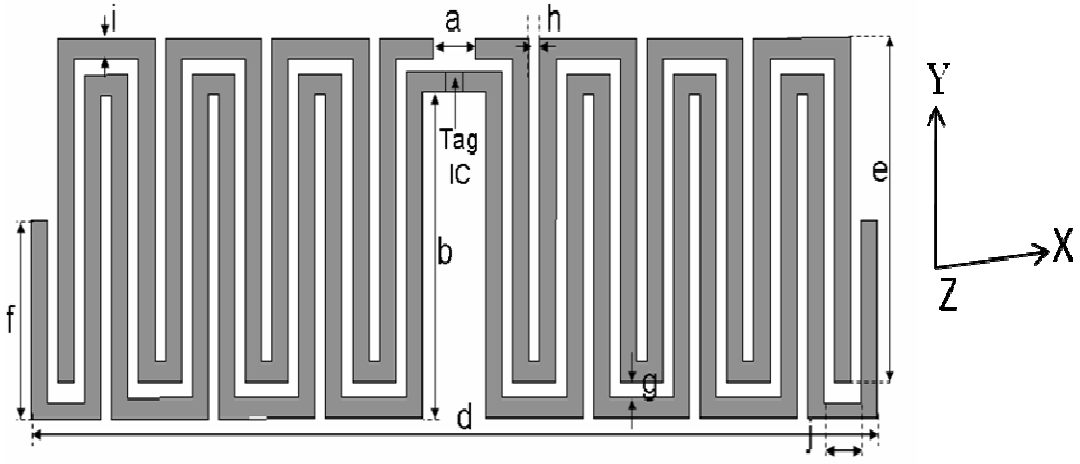

Figure 4.8:Geometry of the proposed RFID tag's sensor

The antenna is formed from two rectangular parallel folded lines. The design frequency is 867*MHz* with a 3*MHz* bandwidth. The schematic in the geometric modeller in HFSS is converted into a DXF file which defines a mask for both prototyping and further circuit analysis in Advanced Design

System software (ADS) [54]. From Figure 4.9 shows a realised candidate structure; the structure parameters are listed in Table 4.2 (cross reference with Figure 4.8). The lineal dimensions of the prototype are $63.2mm \times 19.8mm$.

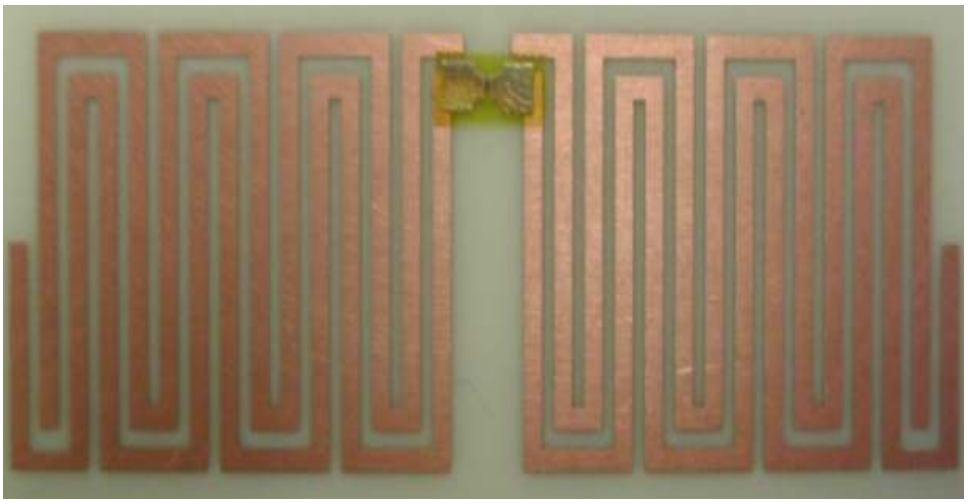

Figure 4.9:RFID tag construction (Antenna, IC and foam dielectric)

Table 4.2:Antenna dimensions in *mm*

a	3.2	**e**	19.8	**h**	0.8
b	19	**f**	11.5	**i**	1.2
c	4.8	**g**	0.9	**j**	2.8
d	63.2				

Tuning the parameter set $\{e, f \text{ and } g\}$ allows the opportunity to study the antenna performance in a controlled fashion. This allows design optimisations to be introduced in a semi-empirical fashion, incorporating lessons learned from the actual realisation. These can be used subsequently to seed more detailed HFSS analysis of more realistic structures [81].

4.3.1 SIMULATION AND MEASUED RESULTS

The input impedance of the prototype antenna has been calculated from the image theory and the advantage of the inherent symmetry of the structure has been taken. In Figure 4.10, the structure is cut into two parts, one of which is mounted over a $60cm \times 60cm$ ground plane. The grounded antenna is then connected to a fully calibrated Vector Network Analyser (VNA) to measure the input impedance. For the operating frequency, the length of each side of the ground represents 2λ which is acceptable in practical terms. The electromagnetic analysis has been cross validated with CST Microwave Studio using a transient analysis [84].

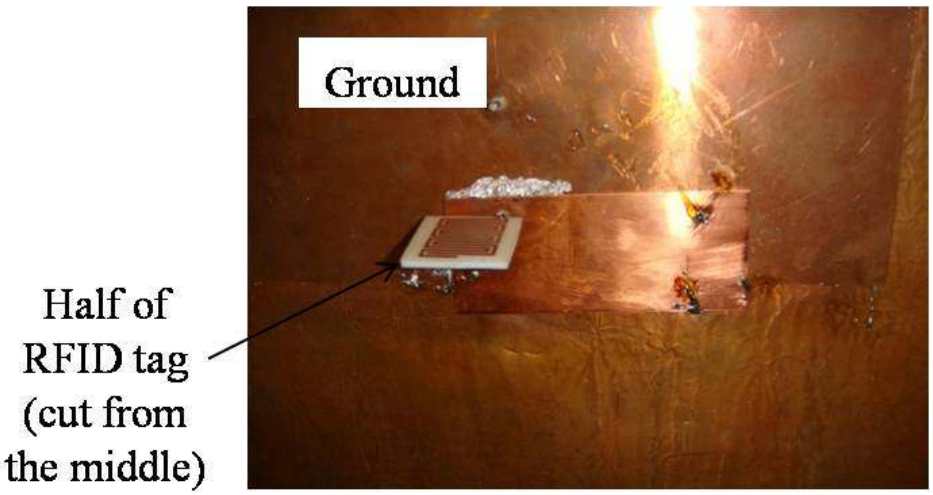

Figure 4.10:RFID tag monopole antenna on a finite conducting ground plane ($60cm$x$60\ cm$).

The comparative results are visualised in the Smith Chart in Figure 4.11. All of the results are in close proximity to one another; the transient analysis

input impedance is calculated as $(11.2 - j80)\Omega$ (CST) and the corresponding frequency domain reduced order calculation is $(14.4 - j134.8)\Omega$ by HFSS simulation results.

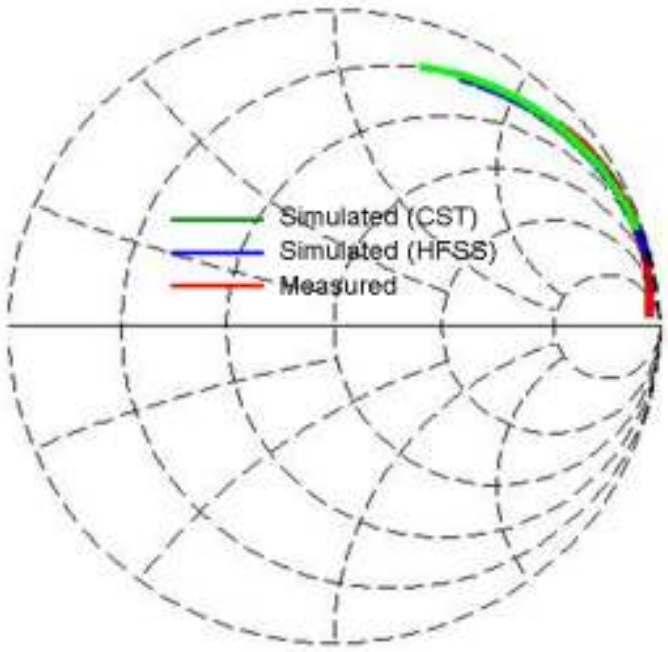

Figure 4.11:Smith chart of input impedance using HFSS, CST (simulations) and analyser signal result (measurement).

From image theory it can be assumed that the structure operates as a monopole over a large square ground plane. Only half the antenna $\{e\}$ is used in this measurement, where each lateral length of the ground plane is $> 3\lambda$ in free space. Figure 4.12 shows a return loss peak output from HFSS at $867MHz$ of $34.3dB$ with an approximate $3MHz$ bandwidth. In addition, the measured$|S_{11}|$ has been presented and clearly observed from both curves that the convergence between them.

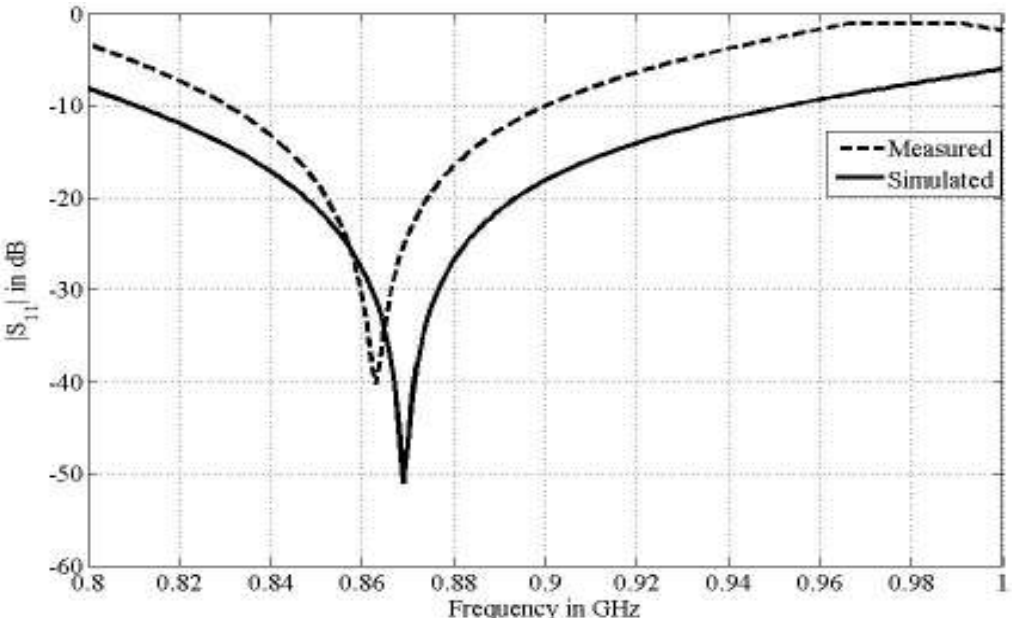

Figure 4.12:The Measured and simulated Refection coefficient $|S_{11}|$ for the target radiator

The input impedance for this simulation is given in Figure 4.13; the calculated input impedance is $(14.3 - j134.8)\Omega$ at $867MHz$.

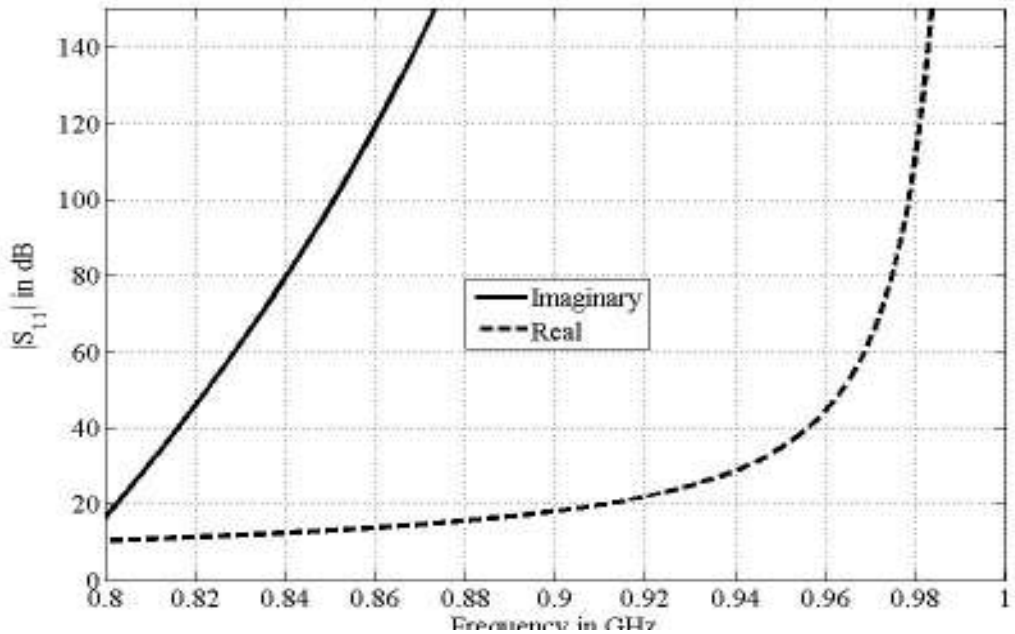

Figure 4.13: Input impedance versus frequency

The radiation patterns in the E-plane i.e. the (*z*-*x*) plane is given in Figure 4.14; the optimal performance for the radiator is ±60° in the (*z*-*x*) plane with a 4*MHz* frequency range.

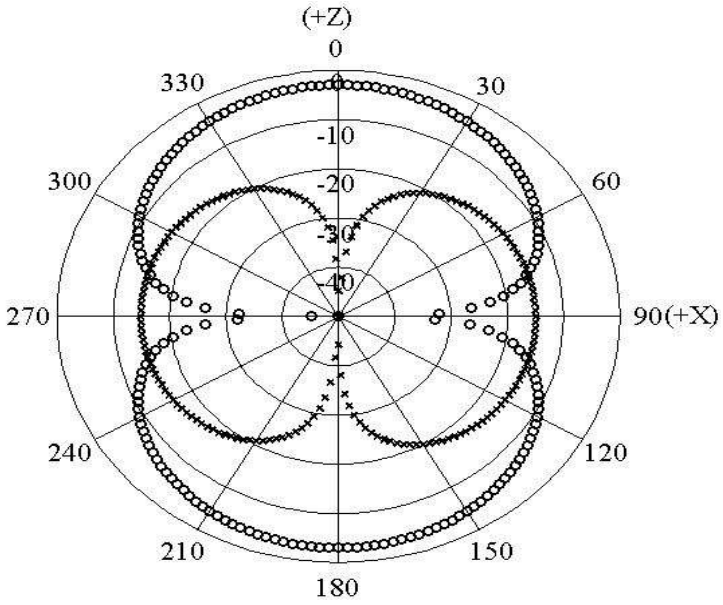

Figure 4.14:Normalised radiation pattern (*x*-*z*) plane at 867*MHz*
'000' simulated co-polarisation and 'xxx' simulated cross-polarisation.

The pattern has a characteristic doughnut shape. The vertical and horizontal patterns have also been studied at this frequency. The result is omni-directional. The H-plane (*z*-*y*) result is shown in Figure 4.15.

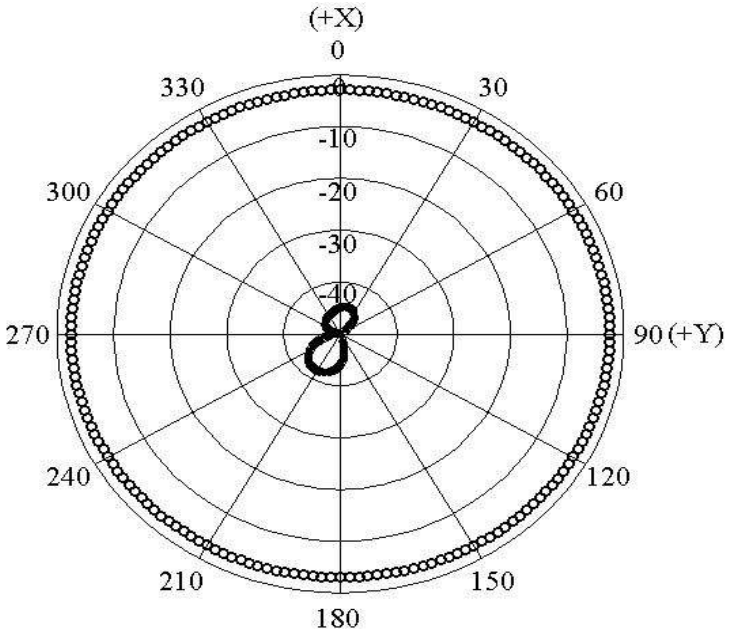

Figure 4.15:Normalised pattern (*z-y*) plane at 867*MHz*
'000' simulated co-polarisation and 'xxx' simulated cross-polarisation.

This candidate structure has a dipole-like radiation pattern which will be present in the implementation of the tag that will operate as a LP-antenna; so the RFID reader will be located diametrically opposite. The maximum detection range seems to have an upper bound of about $5m$ when a $72mm \times 32mm \times 2mm$ foam substrate is used. More detailed analysis of the materials composition, notably the solder paste, needs to be incorporated into the final design optimisation.

4.4 MEANDER RFID TAG (DMLRT) - 2nd DESIGN

The design process is essentially as in the above discussion. The schematic is shown in Figure 4.16. The main tuning parameters are $\{k, l\}$ and the

structure parameters are listed in Table 4.3. Variations in the other parameters appear to be second order effects.

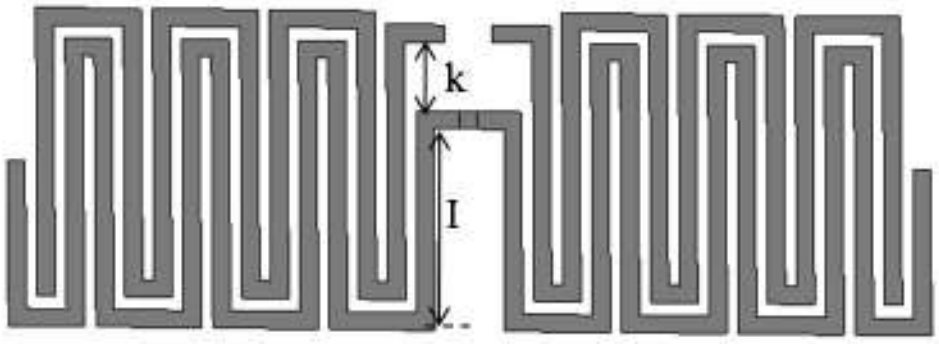

Figure 4.16: The proposed compact DMLRT antenna (modify of Figure 4.1)

Table 4.3:List of assumed parameters in *mm* for Figure 4.9

a	3.2	**e**	19.8	**i**	1.2
b	19	**f**	11.5	**j**	2.8
c	4.8	**g**	0.9	**k**	4.8
d	63.2	**h**	0.8	**l**	14

Figure 4.17 (a and b) compares the HFSS schematic with a realised candidate structure including the dielectric and chip.

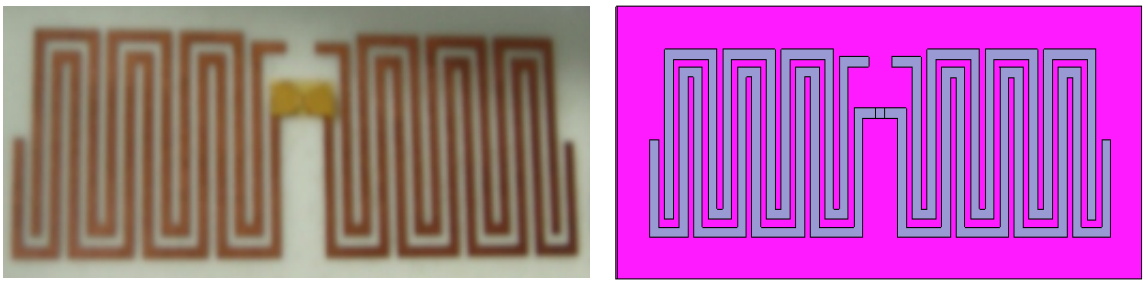

(a) (b)

Figure 4.17:DMLRT antenna; a) A prototype: RFID tag with configured antenna and integrated IC, b) HFSS model

The actual size of the IC and its enclosure are larger than in the initial simulations. However, any major discrepancies between the simulated and realised performance will be clarified in the following section.

4.4.1 SIMULATION AND MEASUED RESULTS

The HFSS output shows a return loss peak at 867*MHz* of 39.9*dB* as shown in Figure 4.18.

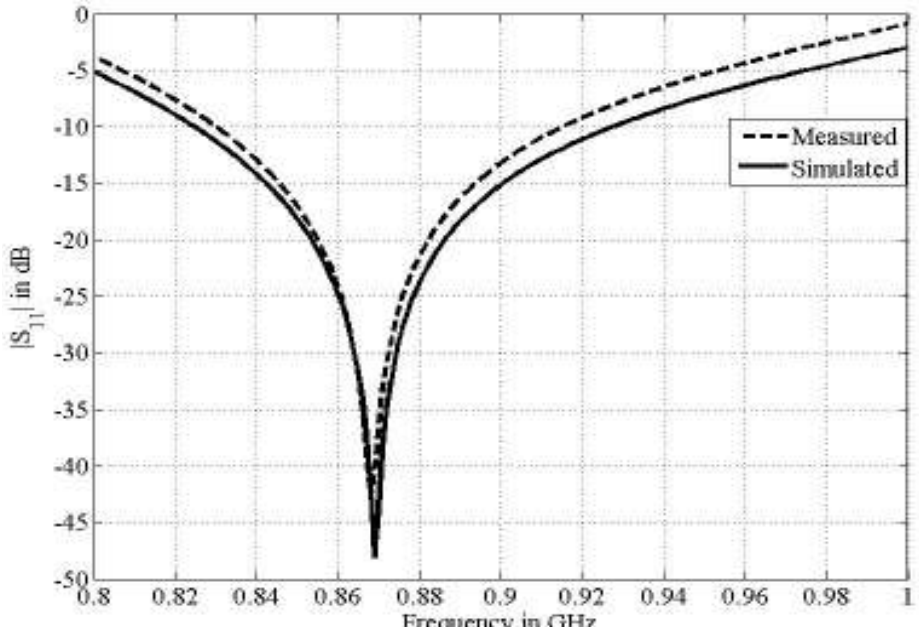

Figure 4.18:The Refection coefficient $|S_{11}|$ characteristics of the proposed tag's antenna

The real and imaginary components of the input impedance have been presented in Figure 4.19 and the result being found as (15.4-j136.8)Ω.

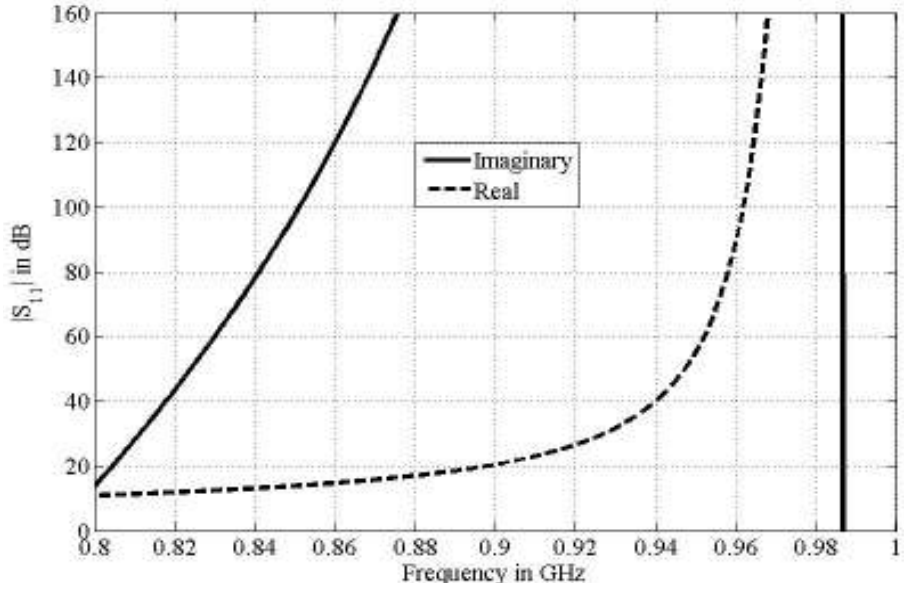

Figure 4.19: The input impedance plot

The approximate characteristic dipole radiation pattern could be seen in Figures 4.20 and 4.21 i.e. E-plane and H-plane.

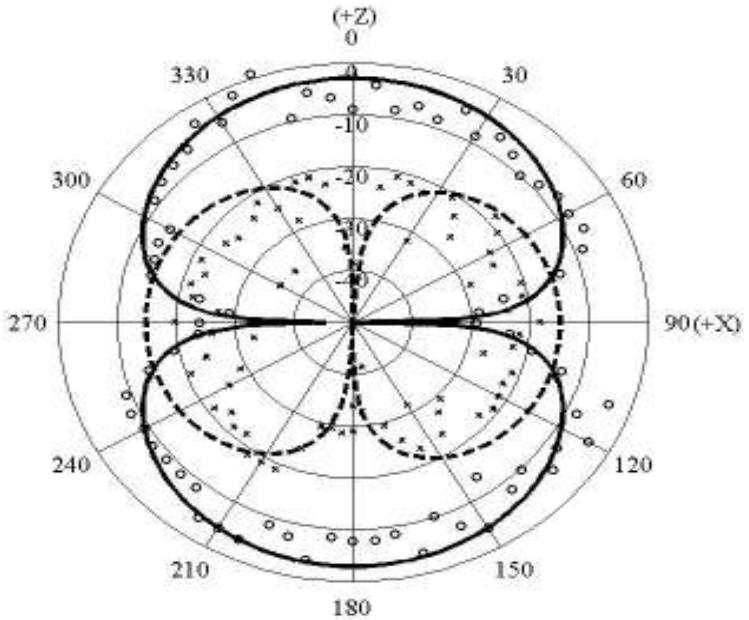

Figure 4.20:Simulated antenna patterns in (z-x) plane
'—' simulated co-polarisation and '---' simulated cross-polarisation
'ooo' measured co-polarisation and 'xxx' measured cross-polarisation

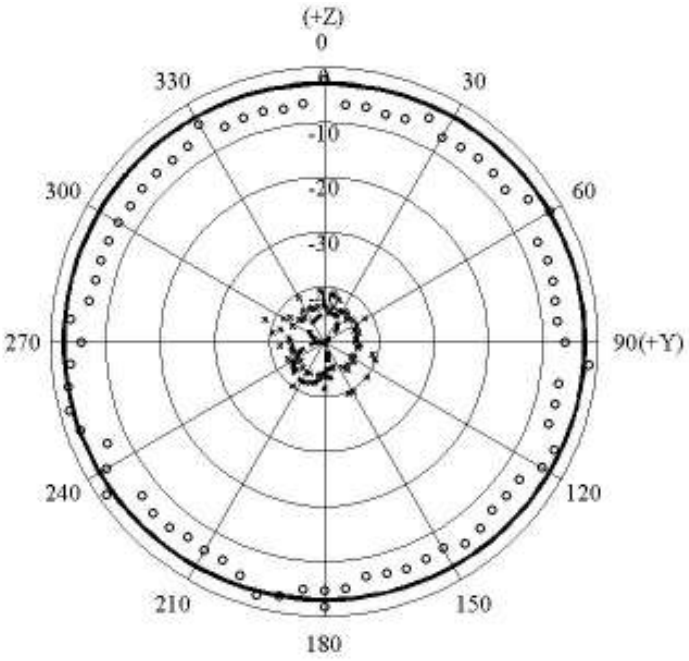

Figure 4.21:Radiation pattern of a printed DMLRT antenna (z-y) plane
'—' simulated co-polarisation and '---' simulated cross-polarisation
'ooo' measured co-polarisation and 'xxx' measured cross-polarisation

This is comparable with the previous design. The measurement of the detection range gives a range of 4 to 6.5m.

4.5 DMLRT ANTENNA (INNER LOOP)

The sample RFID tags coming with the reader kit from the Alien technology company have been used to test the tag samples implemented. Noticeably, those samples have loops around the chip which seem to improve the chip's ability to be read and written on [73].Therefore, several research papers concerning the role of the loop have been read.

- In fact, some of the effects of the loop can be summarised in the following points [7-73]. Similar to a transformer, the inner loop works as impedance match easing the designer's job to matching the chip to the antenna.
- The inner loop join point to the antenna can be raised or lowered to shift the antenna impedance to the target location on the Smith Chart. The antennas impedance level can be changed by making the inner loop line thinner or thicker.
- The inner loop has a DC short circuit resistance which helps to remove high voltage discharge, working as electrostatic discharge securing the die (chip).Obviously, in Figure 4.22, the parameters (i and b) are taken in consideration while designing the loop.

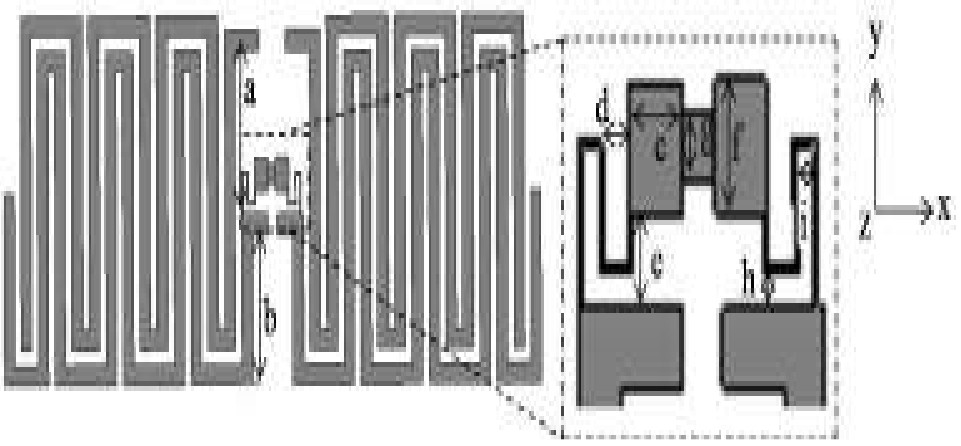

Figure 4.22:Relevant antenna parameters

In addition, the discussed parameters are shown in Table 4.4. However, the dimension of the chip in the antenna is considered to be around 3*mm* long which was found quite acceptable to fit the chip.

Table 4.4:Design parameters

a	9.52*mm*	**d**	0.9*mm*	**g**	1*mm*
b	9.28*mm*	**e**	1.4*mm*	**h**	0.6*mm*
c	1.5*mm*	**f**	2*mm*	**i**	0.5*mm*

Again, Figures 4.23 (a and b) shows the differences between the real design and the one designed using HFSS package.

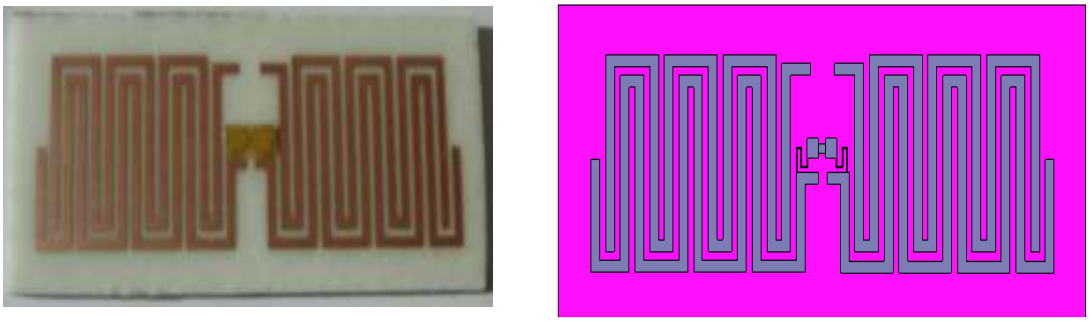

(a) (b)

Figure 4.23:Double line meander antenna; a) Photo of the real design (antenna and die), b) simulated design.

It is worth mentioning that the RFID tag's size is 72*mm*x32*mm*x2*mm*.

4.5.1 SIMULATION AND MEASUED RESULTS

The assumption of the current distribution has been studied within the HFSS simulation as shown in Figure 4.24.

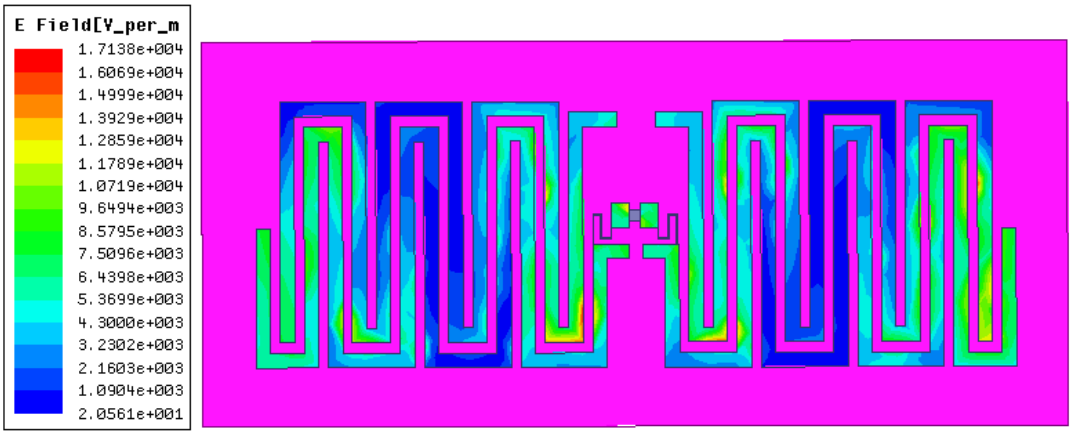

Figure 4.24:The simulated electric field distribution of the optimum antenna

From the simulation results, it has been found that the return loss is 41 *dB* at the frequency range of 867*MHz* as it can be easily noticed in Figure 4.25. In addition, the optimum antenna has 3*MHz* bandwidth when the return loss is 38*dB* at 867*MHz*.

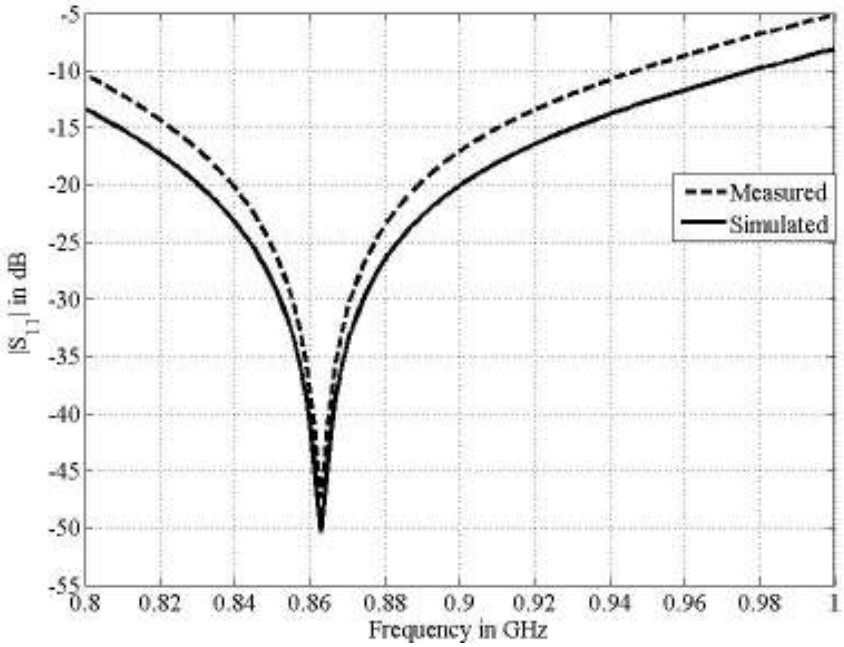

Figure 4.25:The HFSS simulated and measured Refection coefficient $|S_{11}|$ of the above antenna

Commonly, the real and the imaginary input impedance can be presented as (15.5-j140.3)Ω as shown in Figure 4.26.

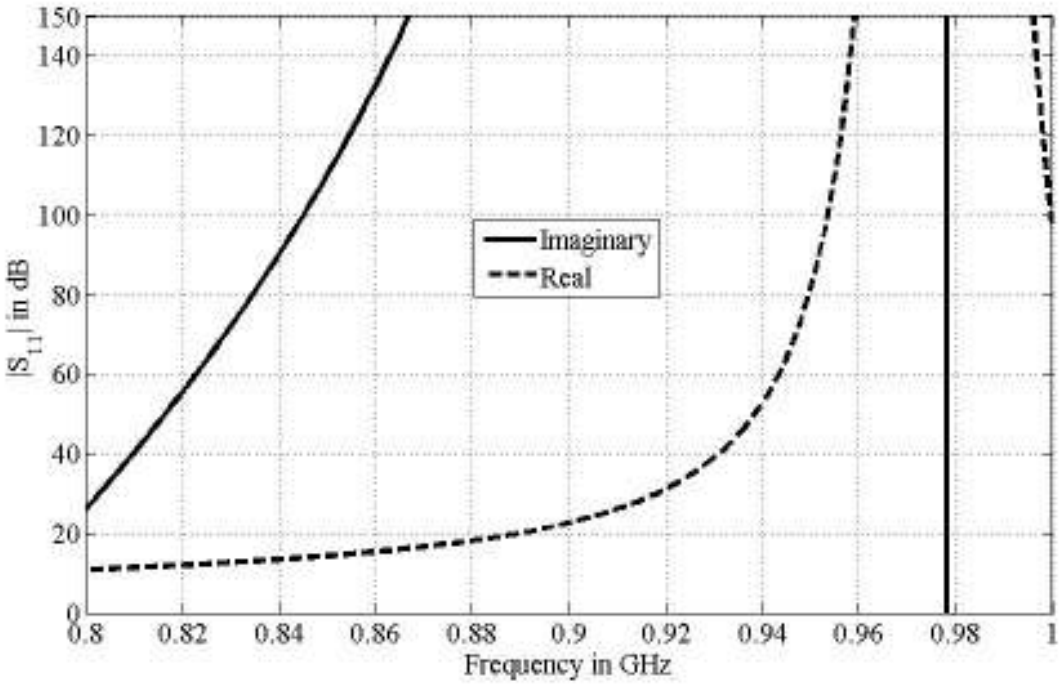

Figure 4.26:The impedance of tip off design

The simulated directivity patterns results of the optimum RFID tag's antenna in: a) *z-x* plane, b) *z-y* plane and c) *x-y* plane at 900*MHz* have demonstrated in Figure 4.27.

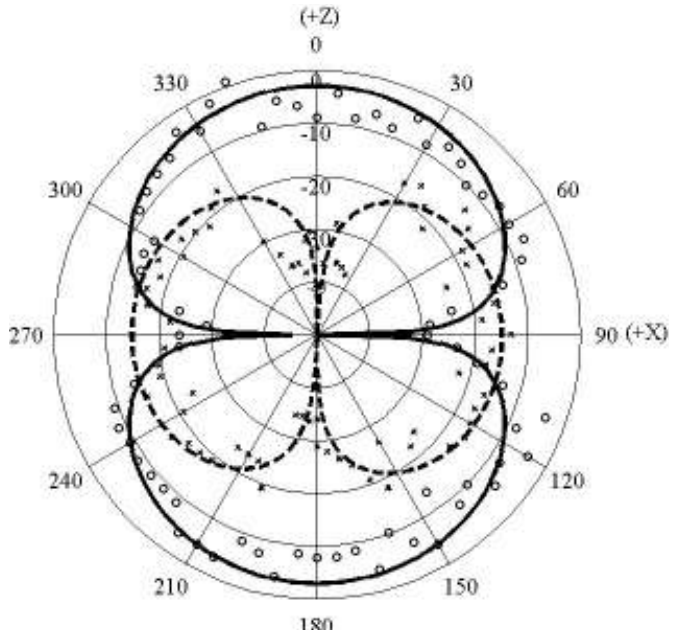
(+Z)
0
30
60
90 (+X)
120
150
180
210
240
270
300
330
-10
-20
-30
-40

(a)

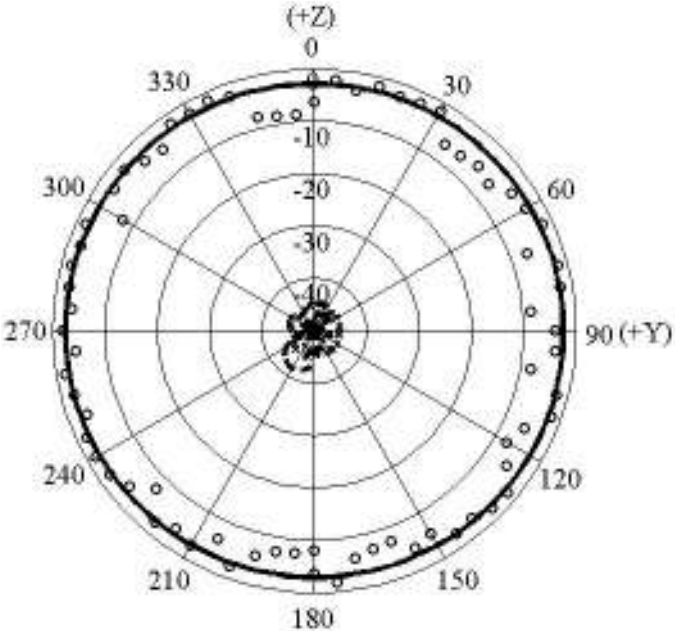
(+Z)
0
30
60
90 (+Y)
120
150
180
210
240
270
300
330
-10
-20
-30
-40

(b)

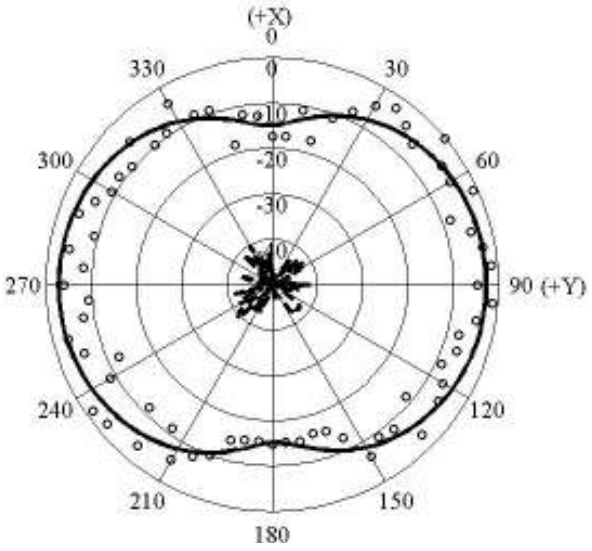

(c)

Figure 4.27:The simulated directivity patterns results of the optimum RFID tag's antenna in: a) *z-x* plane, b) *z-y* plane and c) *x-y* plane at 900*MHZ*.
'—' simulated co-polarisation and '----' simulated cross-polarisation
'ooo' measured co-polarisation and 'xxx' measured cross-polarisation

Similarly, the detection range measurement has been applied using the Alien reader and found to be up to six metres. Furthermore, the operational efficiency of the RFID tag antenna has been tested when it's stick on many volunteers at various locations on their cloths and bodies. .

4.6 SINGLE RECTANGULAR MEANDER- LINE RFID TAG (SMLRT) -1st DESIGN

In this section, a single meander rectangular line design with a narrow chip place has been presented. However, in this design, this space is one millimetre only. Figure 4.28 demonstrates the shape of the design, the place of the chip and some other parameters.

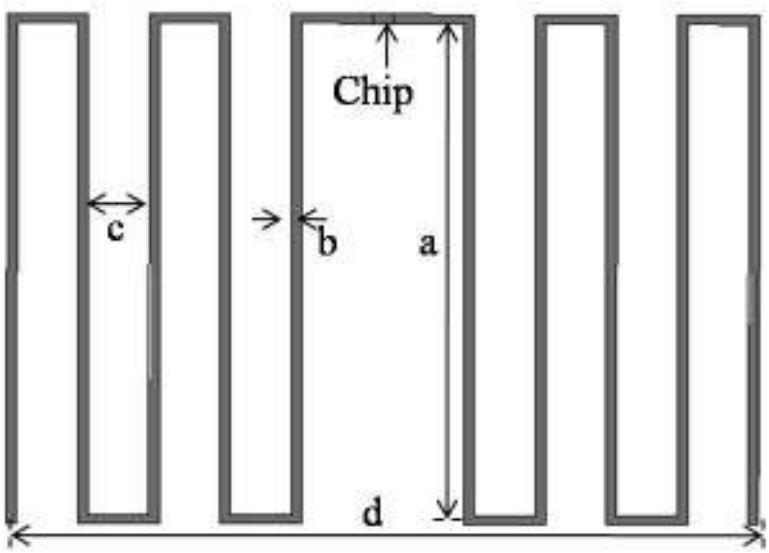

Figure 4.28:SMLRT antenna geometry

For more understanding, those parameters are presented in Table 4.5. It is worth mentioning that the line width has been used 0.5*mm*.

Table 4.5:Detailed parameter for proposed antenna

a	28*mm*	**d**	37*mm*
b	0.5*mm*	**Chip place**	0.5*mm* x1*mm*
c	3*mm*		

Clearly, Figure 4.29 (a and b) displays the suggested design in reality and after being done by HFSS. Noticeably, the space allocated for the chip in HFSS design is much smaller to fit the chip in.

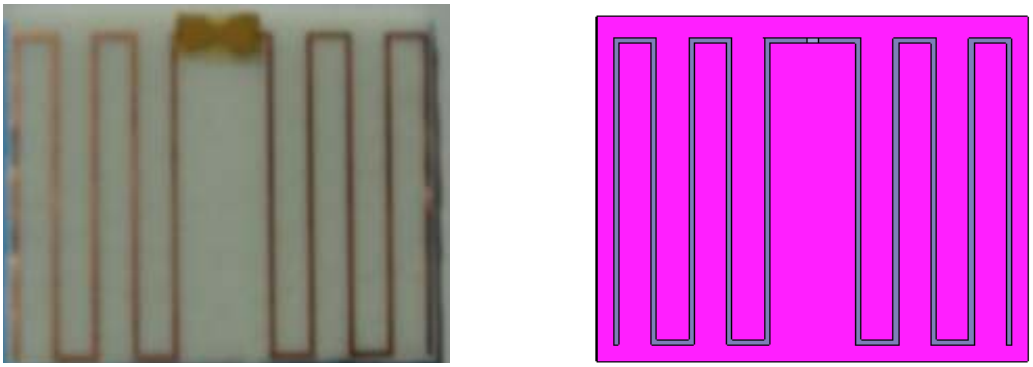

(a) (b)

Figure 4.29:SMLRT antenna 1st design; a) Photo of the proposed tag, b) HFSS design

The used foam surface size is 43.5*mm*x35*mm*x2*mm*.

4.6.1 SIMULATION AND MEASUED RESULTS

To avoid redundancy, each design has its own simulation results which are presented in the same way. As it is clear in Figure 4.30, the return loss result is found to be 36*dB* at the frequency value 867.5*MHz*.

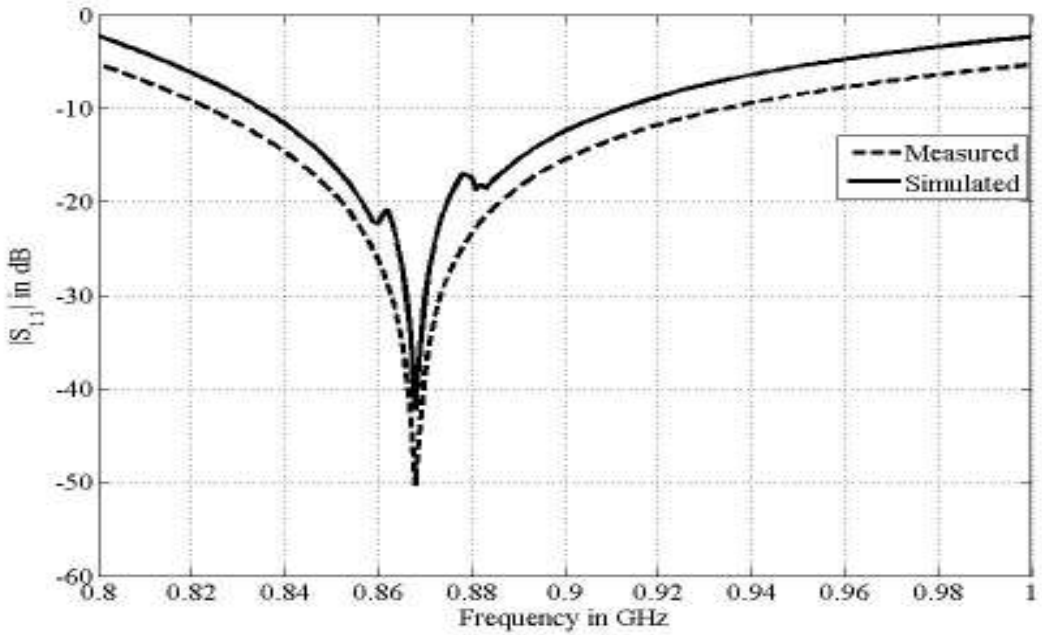

Figure 4.30:Refection coefficient$|S_{11}|$ in *dB*

In addition, the input impedance is found to be (7.6-j139.7) Ω at 867*MHz* as shown in Figure 4.31.

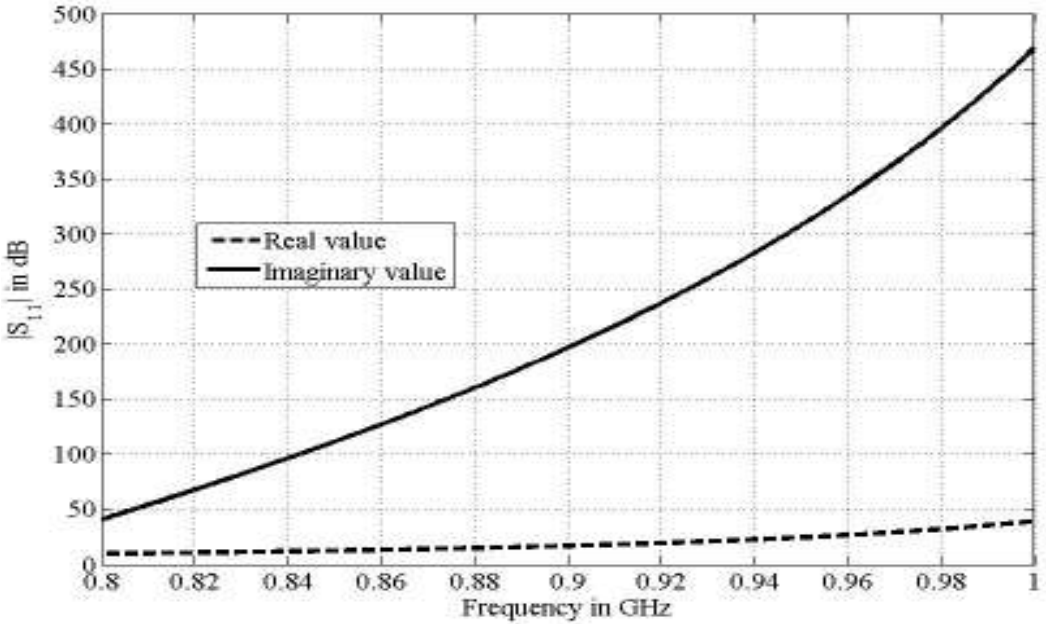

Figure 4.31:Impedance plot of optimum design

The (*z*-*x*) plane presented in Figure 4.32.

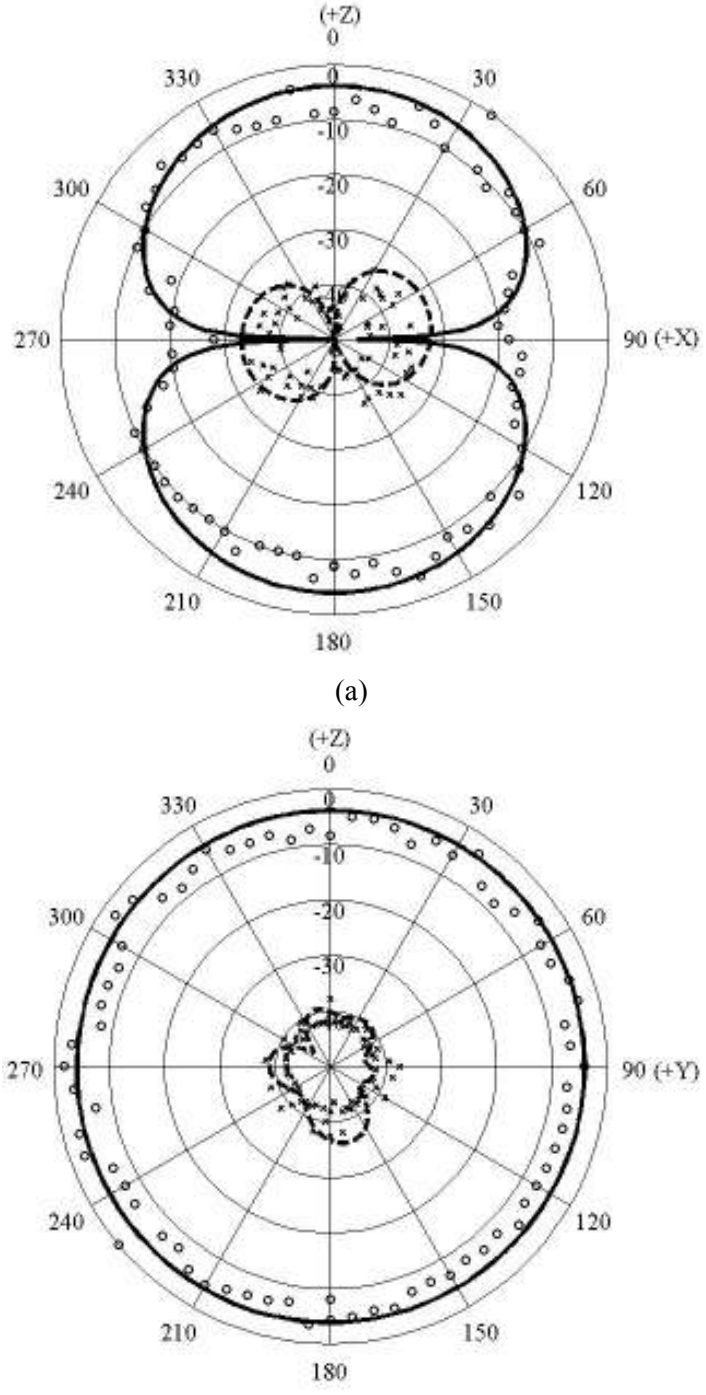

Figure 4.32:Radiation patterns of the antenna, a) x-z plane and b) y-z plane
'—' simulated co-polarisation and '----' simulated cross-polarisation
'ooo' measured co-polarisation and 'xxx' measured cross-polarisation

Generally, in this design the detection distance is found to be around six metres.

4.7 SMLRT ANTENNA, (WIDER CHIP PLACE) – 2nd DESIGN

In this design, the space specified for the chip has been modified and made bigger than the previous one. In particular, Figure 4.33 shows the designs parameters. In addition, the optimum antenna tag design has been investigated and simulation results have been carefully studied. The proposed design has been printed in term to implement and the detection range has been measured and found to be more than 5 metres. In terms of the results, the optimum tag and the previous design simulation results can be compared and it can clearly be seen that the chip place size does not have that much effect on the obtained results.

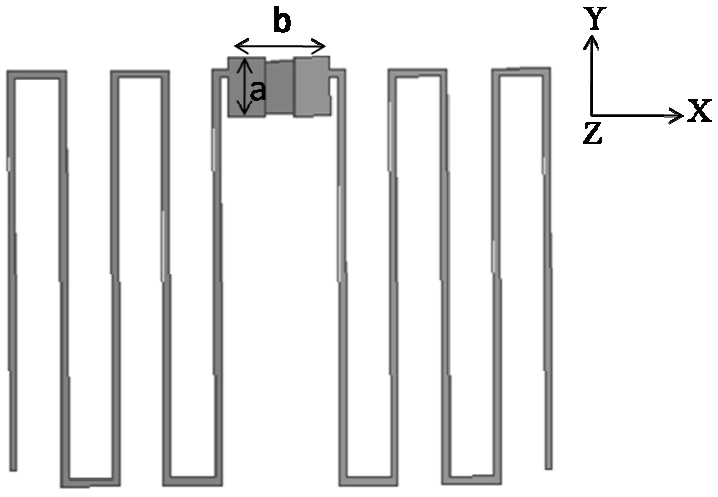

Figure 4.33:SMLRT antenna observation geometry

To make it clearer, the design's parameters are presented in Table 4.6. As can be seen from previous figure, (f and g) are the chip place dimensions which are 7*mm*x4*mm* length.

Table 4.6:Dimensions of SMLRT antenna

a	7*mm*	**b**	4*mm*
c	3*mm*	**d**	37mm
Chip place		0.5*mm* x1*mm*	

Looking at Figure 4.34 (a and b), the substrate dielectric spongy box is 43.5*mm*x35*mm*x2*mm*. Through out those two figures, it can be noticed that the place of the chip is bigger than the one in the previous design.

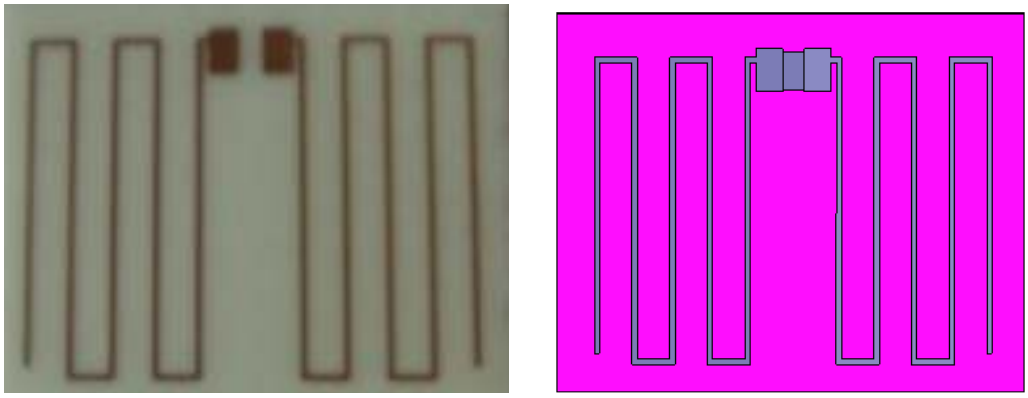

(a) (b)

Figure 4.34:SMLRT antenna 2nd design; a) The original RFID tag with setup antenna, b) The Ansoft HFSS design.

4.7.1SIMULATION AND MEASUED RESULTS

The sensor's return loss result is found to be 34.3*dB* at the frequency 867*MHz*. Figure 4.35 depicts that the input impedance is (7.6-j139.7)*Ω*.

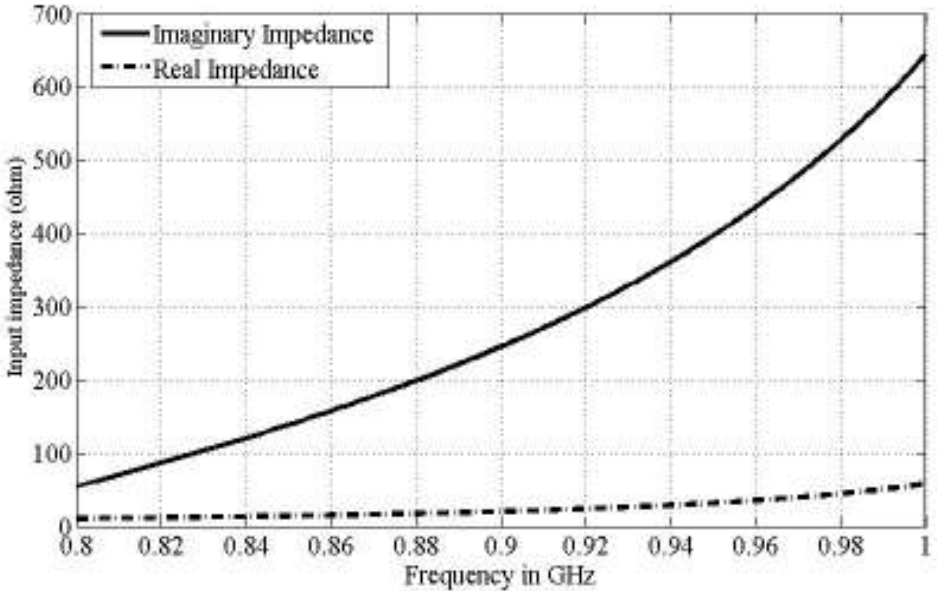

Figure 4.35:The impedance of proposed antenna was found to be (7.6-j139.7)Ω.

As Figure 4.36 indicates that the radiation pattern of (*z-x*) plane.

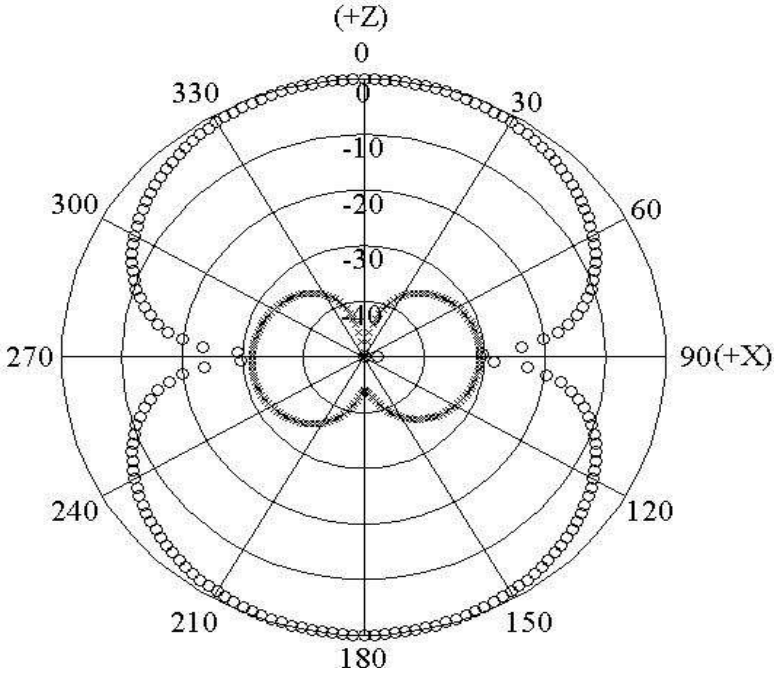

Figure 4.36:Polar plot of the radiation pattern (*z-x* plane)
'000' simulated co-polarisation and 'xxx' simulated cross-polarisation.

However, the pattern diagram of the (*z*-*y*) plane is displayed in Figure 4.37.

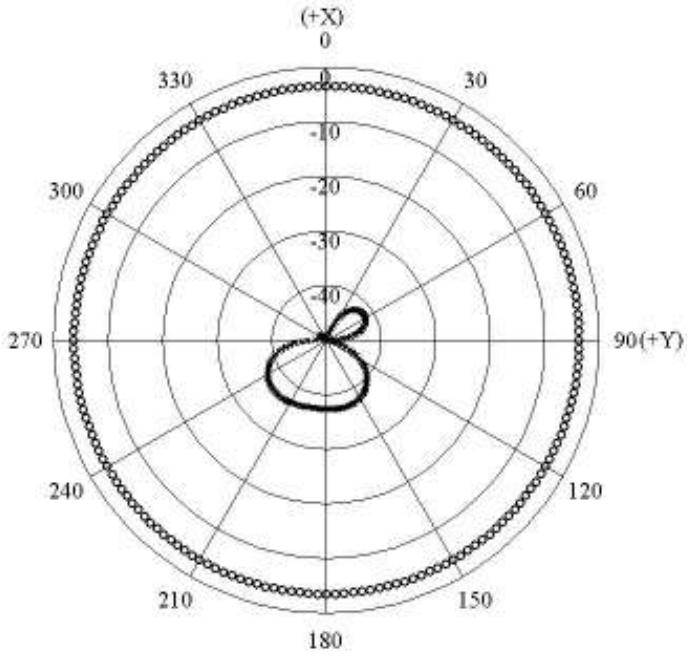

Figure 4.37:Polar plot of the radiation pattern (*x*-*y* plane)
'000' simulated co-polarisation and 'xxx' simulated cross-polarisation.

As can be observed from measurements, the detection range has been studied for vertical and horizontal antenna polarisation and is found to be between five to seven metres.

4.8 RECTANGULAR MEANDER LINE RFID TAG (MLRT) WITH MULTI-LOOPING AROUND THE CHIP

The previous designs have been significant regarding the importance of the shape of the designs and the allocated places for the chip in determining the

detection range. Therefore, the design shown in Figure 4.38 was designed in order to overcome such problems.

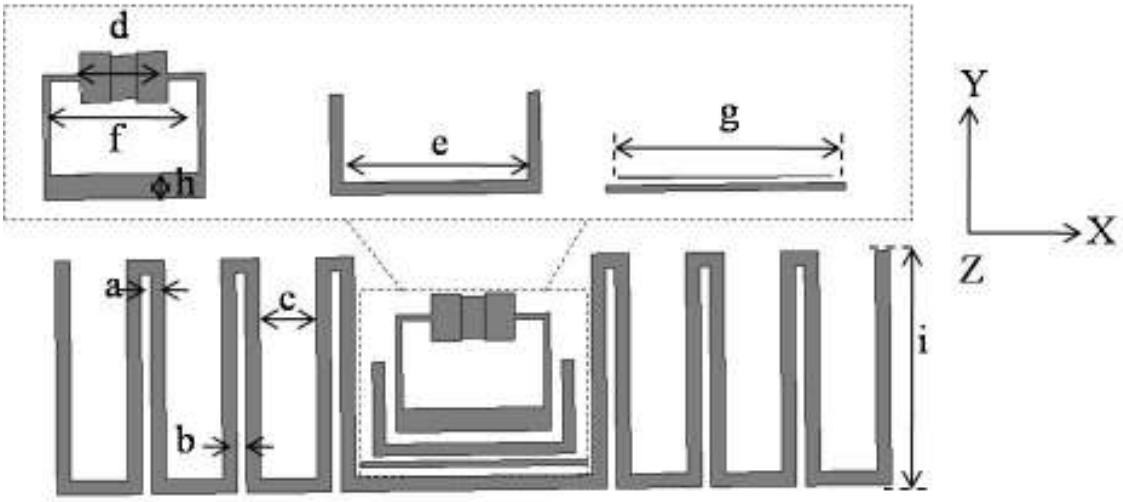

Figure 4.38:Elementary printed MLRT antenna with multi-looping around the chip.

The parameters of the novel figure are demonstrated in Table 4.7.

Table 4.7:Parameters of meander antenna with multi looping around chip

a	1.2*mm*	**d**	7mm	**g**	18*mm*
b	0.8*mm*	**e**	15*mm*	**h**	2mm
c	4*mm*	**f**	12*mm*	**i**	18.5*mm*

Moreover, Figure 4.39 (a and b) displays the real image of the proposed RFID tags and the one done by software.

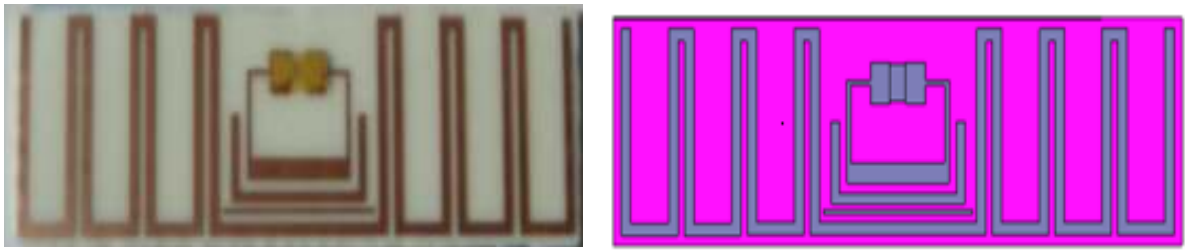

(a) (b)

Figure 4.39:MLRT antenna with multi loop; a) The framework RFID tag with antenna and chip, b) The electromagnetic numerical HFSS software design

4.8.1SIMULATION AND MEASURED RESULTS

Further evidence of this model is that the proposed design has been investigated by simulation and measurement. To better understand the simulation has been performed by HFSS of the return loss curve for the RFID tag antenna design, as shown in Figure 4.40 and it is found to be 29.9*dB* at frequency 865*MHz*.

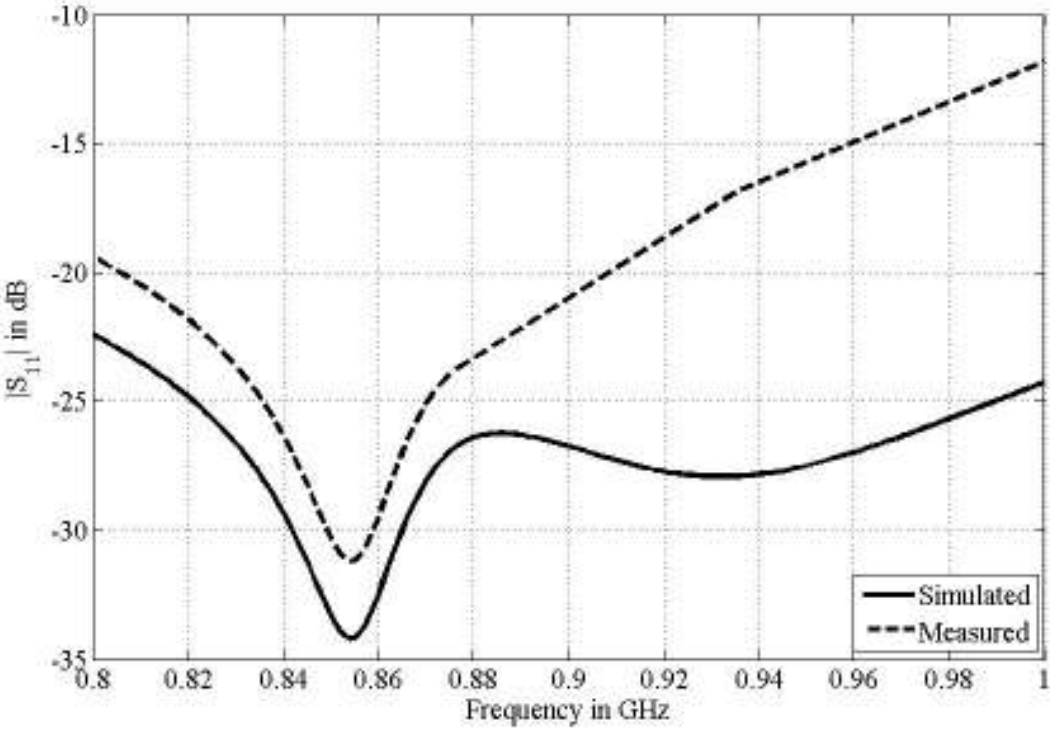

Figure 4.40:Simulated and measured Refection coefficient: modified RFID tag with multi loop around the IC

In the graph bellow, Figure 4.41, the input impedance of the optimal tag antenna is found to be (14.3 - j131.5) Ω at 865MHz.

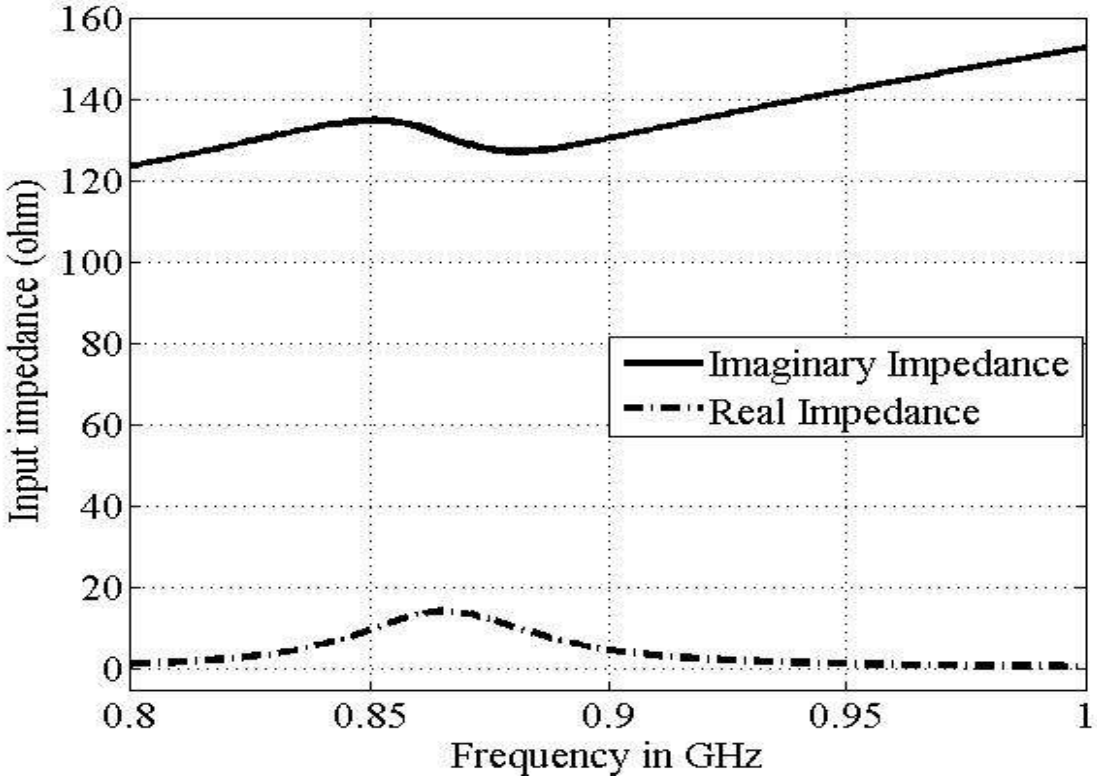

Figure 4.41:The impedance plot to meander-line with die looping

Emphasising the accuracy of the simulated results, the radiation patterns in the *E*-plane (*z-x* plane) and H-plane (*z-y* plane) at 865*MHz* have been studied and the corresponding normalised results are presented in Figure 4.42(a and b).

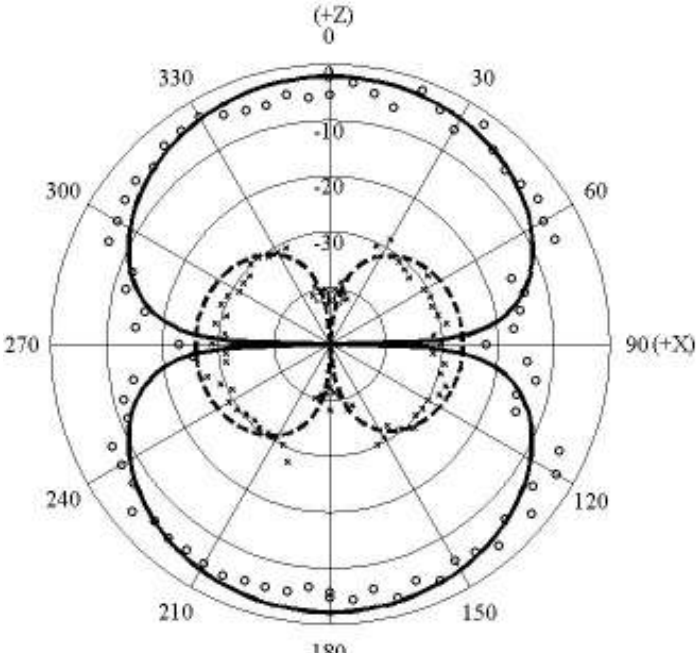

(a)

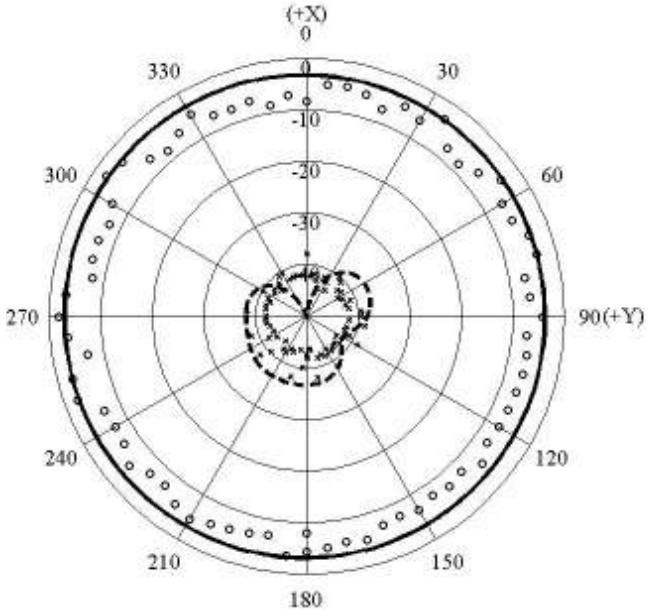

(b)

Figure 4.42:MLRT antenna normalised radiation pattern in a) x-z plane and b) x-y plane)
'—' simulated co-polarisation and '----' simulated cross-polarisation
'ooo' measured co-polarisation and 'xxx' measured cross-polarisation

Finally, the design and measured results of the proposed antenna are discussed. As stronger as the magnetic field is as the larger the detection

range is. After simulation and modelling, it can be observed that the loop around the antenna motivates the magnetic field. To conclude, the measuring steps are repeated until the results show a maximum reading range of more than five metres in the vertical direction.

Table 4.8 summarises the simulation results of the discussed design, such as: return loss, input impedance as well as detection distances. .

Table 4.8: Summarise of the linear polarisation antenna RFID tag results

Antenna	**$\|S_{11}\|$ at 876 *MHz* (*dB*)**	**Input impedance (*Ω*)**	**Reading range (*m*)**
Figure 4.8	-34.3	14.3 – j134.8	Up to 5
Figure 4.16	-39.9	15.4 – j136.8	4 to 6.5
Figure 4.22	-41	15.5 – j 140.3	Up to 6
Figure 4.28	-36	7.6 – j139.7	Up to 6
Figure 4.38	-29.9	14.3 –j 131.5	Up to 6

4.9 CONCLUSION

In conclusion, this chapter has discussed and analysed several linear polarised of RFID tag antennas throughout several developmental designs. Moreover, the effect of the antenna's shape and size have been optimised and the role of the loop rounding the chip as well. Furthermore, a balun operating at 900*MHz* has been designed successfully and fabricated. The phase between unbalances ports has been found as 180^0 with almost equal magnitudes at wide bandwidth of 900*MHz*.

It is worth mentioning that all tags considered in this chapter are proposed for non- conducting surfaces. The simulated and measured results for all the target designs have been found in good agreement in terms the return loss and radiation performances at 876*MHz*.The following chapters concerns the tag designs attached to conducting objects.

CHAPTER FIVE

RFID TAG ANTENNA MOUNTABLE ON METALLIC OBJECTS

5.1 INTRODUCTION

RFID tagging technologies are a rapidly becoming a ubiquitous type of auto-identification in a variety of applications in logistics, commerce and environmental infrastructure. Obviously, this popularity stems from the capability to track items and associated information on static or moving objects speedily as well as in multiple data types; the typical data transfer times could be less than 100 *ms* [85]. In contrast, RFID strategies might be deployed in awkward environments, although practical limitations. Thus far commercial and logistic applications have tended to dominate the field, e.g. access control (tollgates) and product or component tracking; there is also a rapidly developing biomedical applications field [53].

RFID methods involve a radio transponder (the 'tag') and reader or interrogator. The RF antenna can be considerd a key part of the system and often presents a serious design challenge as it must have a direct connection to the tag's ASIC (Application Specific Integrated Chip). Moreover, the ASIC input impedance always presents a capacitive reactance. In particular, it follows that the reactive nature of the tag antenna must be properly

realised as the complex conjugate of the ASIC input impedance to enable the maximum transmission using the RF power induced from the tag. Through analysing the previous antenna designs, microstrip antennas have an obvious attraction for such applications. They may be easily constructed with the given radiation and polarisation properties and made to work in most normal operating environments [87, 89]. This work is concerned with overcoming the difficulties of identifying a given passive tag in close proximity with metal surfaces. Recent work in this area includes the possible use of EBG material [90] and the integration of a tag with aluminium foil packaging [91].

On the other hand, the RFID frequency range extends into the microwave region which has consequences for antenna in maximising the detection range of the technology. Moreover, RF signals may be absorbed by liquids and reflected by metals; thus constraining the reading distance. Hence, at least the material of the objects at the level of the surface on which the tag is mounted must be taken into account within the design process. Conductive surface mountings are unavoidable in a range of large applications and the performance of label style tags are substantially affected by metallic objects [88]. This is a major design challenge.

One of the more important difficulties for passive tags mounted on conducting surfaces is the absence of an internal power source as well as the RFID communication protocol. In such cases, the radiation pattern,

efficiency, input impedance and resonant frequency will change. These factors will depend on the distance of the antenna from the surface as well as the size and the shape of the antenna [85, 90]. Most of the incident electromagnetic radiation will reflect from the surface with a 180° phase reversal effectively minimising the detection distance ($\approx 50cm$) [85]. These reflected signals cancel the incident wave and reduce the power needed by the tag to excite the RFID chip [53]. RFID tags might be mounted on random objects with features which are only partially accounted for some of which will directly affect the tag's reading ability [85].

RFID metallic tag configurations have incorporated patch type antennas, inverted F-type antennas and so forth which all utilise the action of a ground plane structure [90-91]. In this way, [94] reports a slim RFID antenna tag design; whilst [95] proposes a UHF band device which makes use of an artificial magnetic conductor (AMC) as the ground plane. In [96], Griffin et al, propose two useful forms of the radio link budget which describe the power link with the tag attached to a target. In this chapter, we review some of the design options aimed at overcoming this difficulty; also, two novel designs are introduced – the S and T forms.

An apparently obvious solution to this problem, as mentioned early in this chapter, would be to use microstrip antennas. Such antennas could be made to work efficiently in a general environment tuning the operating frequency, radiation patterns and polarisation states. In addition, they have favourable

mechanical features and are easily adhered to conducting surfaces with curvature if necessary [47, 97].

In summary, the antenna designer frequently has to compensate for the proximity of the antenna to awkward materials or environments which will have a direct impact on the effective range. Dry goods provide the least challenging environment for the designer but in general high permittivity media such as liquids and metal are far more problematic [98]. In some RF sensors it may be helpful to minimise the width of the radiator, thus limiting the contact area with a high dielectric material. Flexible substrates tend to be composed of high pressure thermosetting plastic laminates these work well in both dry and humid conditions. HFSS is used to investigate a variety of possible antenna layouts and is well suited when needed to robustly handing inhomogeneous material boundaries. Where necessary the designs are normalised to the standard cable impedance of 50Ω, although, the cable with impedances of 75Ω or 300Ω might be used in some applications. The antennas under discussion in this chapter need to achieve optimal conjugate impedance matching with the tag IC input impedance [43, 99].

The test structure is built on a $1.6mm$ FR4-epoxy substrate with dielectric properties at $867MHz$: $\epsilon_r = 4.6, \tan\delta_{\epsilon} = 0.017$. The tag antenna has been tested using an Alien ALR8800 RFID reader. In particular, the **S** and T RFID tags' antennas discussed in the sequel are intended to compensate for

the presence of metal placement objects and should anticipate degradation in available read distances.

5.2 S-SHAPE RFID TAG ANTENNA

This section proposes a novel RFID antenna tag design which could be mounted on a conducting surface; the basic template for this structure is shown in Figure 5.1(a). The antenna consists of an inner spiral line, an outer bent line and a double S-matching network. The ideal structure is printed on a single-layer substrate with a ground plane. This passive structure receives, reinforces and retransmits a back-scattered signal to the reader.

The target frequency band and RF specification is the European UHF RFID band which has a centre frequency of 900*MHz* and a bandwidth of 3*MHz*. The ASIC selected for this tag IC design is a Higgs IC that has been designed to follow the EPCglobal Class-1 Gen-2 specification, therefore, the used input impedance is (15 + j140)Ω. Instead of a standard meander line antenna, an S-shaped printed line antenna has been designed using the FR4-epoxy substrate which has a permittivity of 4.5 and loss tangent of 0.017 at 900*MHz*. Moreover, 1.6*mm* substrate thickness has been employed. Consequently, the first cut dimensions have been found from simulation using HFSS. Indeed, a candidate structure with principal linear dimensions of 32.5*mm*×19.5*mm* has been prototyped and illustrated in Figure 5.1(b).

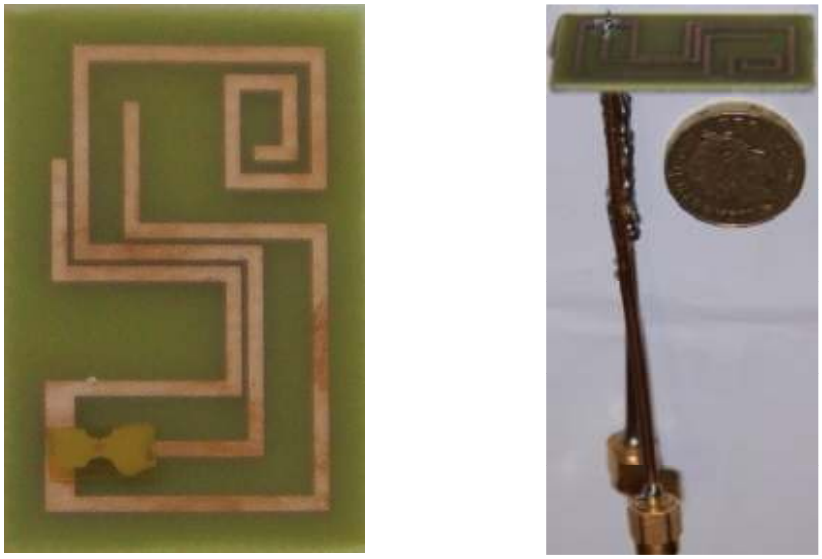

(a) (b)

Figure 5.1:RFID tag antenna for metal surface; a) The original model with Alien chip (Higgs-2), (b) antenna prototype with Alien chip (Higgs-2).

The first cut dimensions for this structure are obtained from HFSS parameter studies and a candidate structure with lineal dimensions 32.5*mm*x19.5*mm* has been fabricated as presented in Figure 5.2.

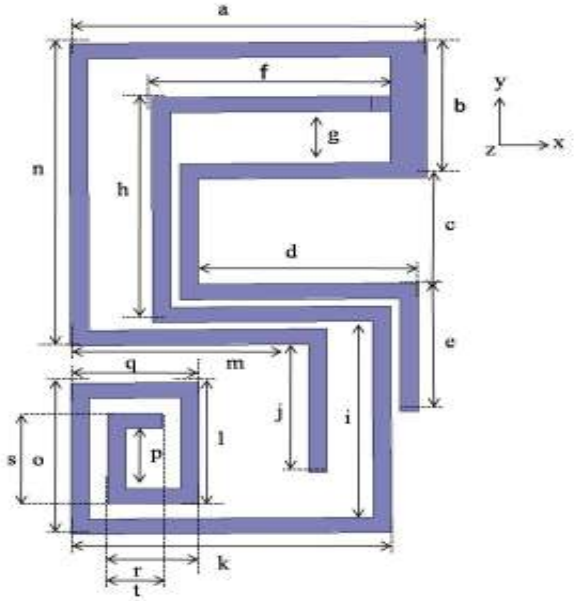

Figure 5.2:RFID tag antenna for metal surface: the proposed (S) Shape antenna's geometry.

The optimum structure parameters are presented in Table 5.1.

Table 5.1:Parameters of the proposed RFID tag's antenna

Parameter	**Value *mm***	**Parameter**	**Value *mm***
A	19.5	**k**	17.5
B	9	**l**	8
C	0.5	**m**	13
D	12	**n**	20
E	8.5	**o**	10
F	13	**p**	4
G	0.5	**q**	7
H	14.9	**r**	5
I	13	**s**	6
J	8.5	**t**	2

5.2.1 SIMULATION AND RESULTS

The antenna was connected with the tag IC and preliminary distance detection tests were carried out. As a result of the tag radiator input impedance is found as $(14.3 - j\ 140.9)\Omega$ at $900MHz$ which is commonly normalised to 50Ω throughout the whole RFID band. In contrast, the detection rate has been measured and found is greater than $75cm$.

For comparison, the simulated (HFSS) and measured antenna's result of the amplitude of a reflected wave reflected wave relative to an incident wave (reflection coefficients) are visualised and depicted in Figure 5.3. It can be seen that the measured results agree well with simulated results. The simulated gain performance has been given in Figure 5.4.

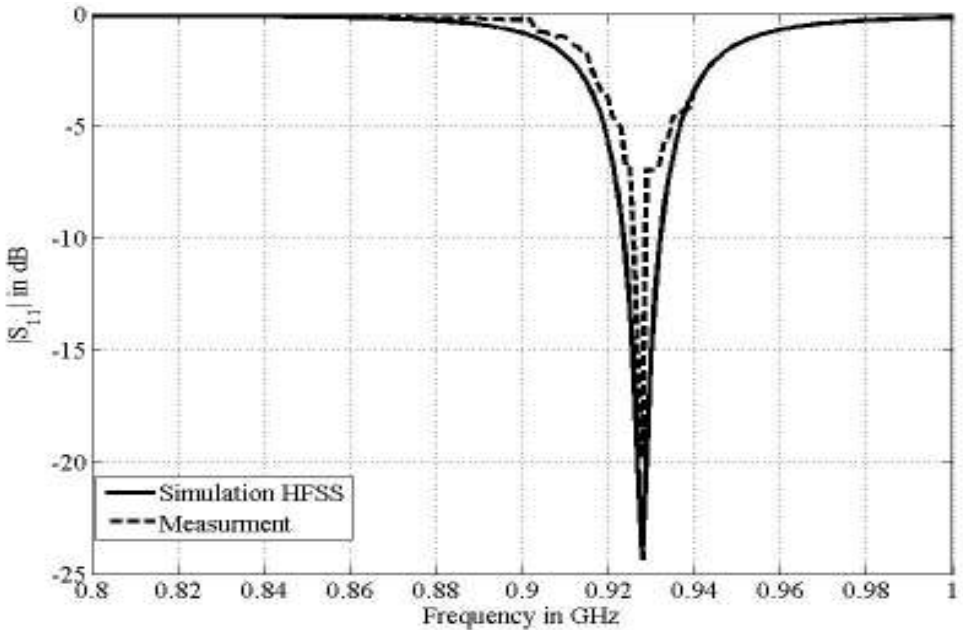

Figure 5.3:Refection coefficient $|S_{11}|$ for the optimised design

As observed from Figure 5.4, the gain factor of such a tag antenna when placed on the metallic surface has been presented.

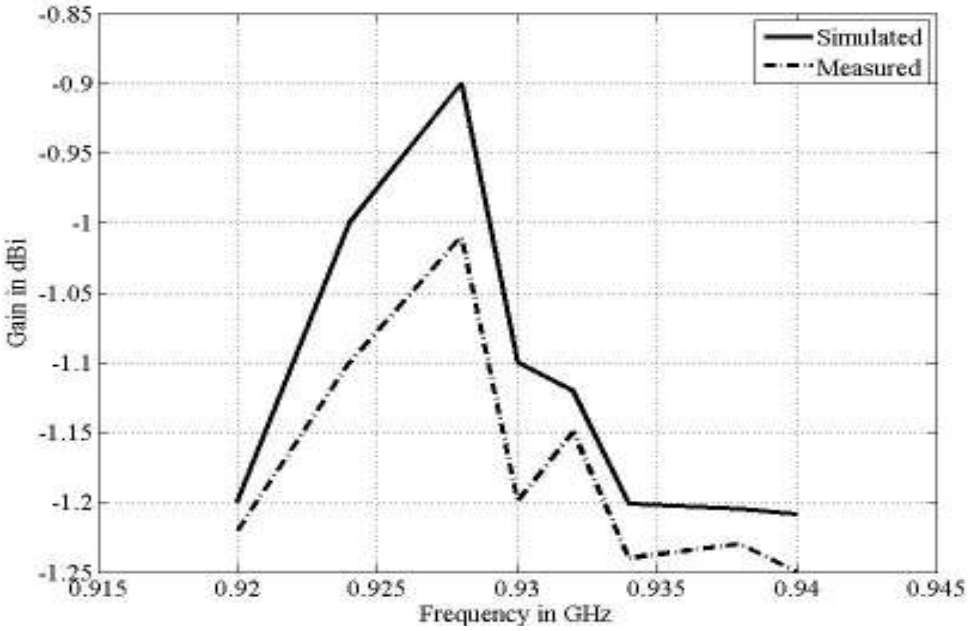

Figure 5.4:Simulated gain of proposed RFID tag's antenna design

The RFID operating distance in the conducting items has been decreased compared to the normal working range of tag when its operating on the non-conducting surfaces. Indeed, the simulated and measured results have been obtained and looked closer to each other. The measured directivity patterns, in other words the H-plane and E-plane, of the optimum antenna at the frequency $f = 900MHz$ are depicted in Figure 5.5.

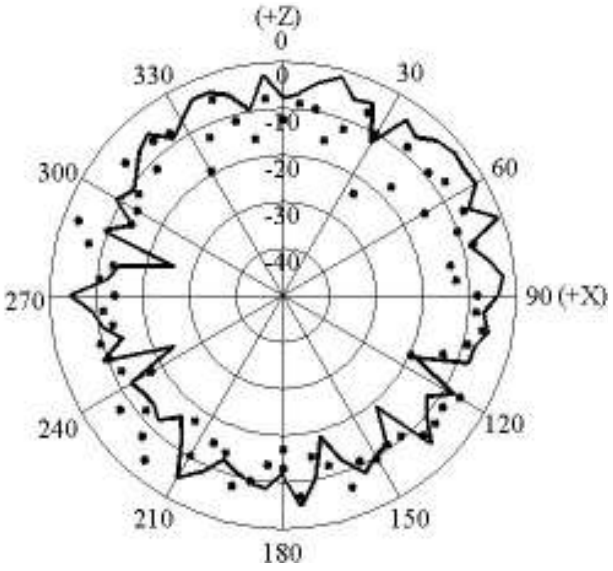

(a)

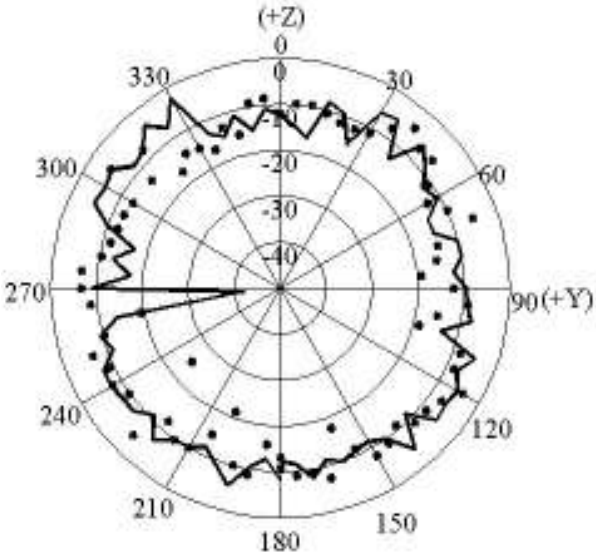

(b)

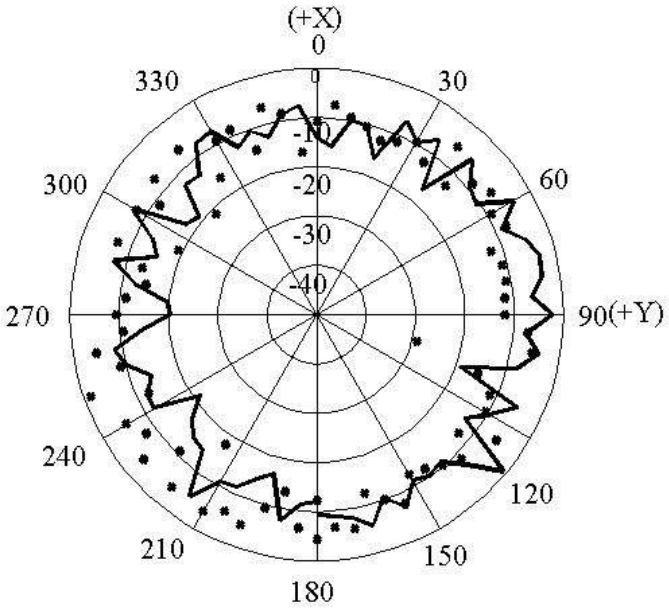

(c)

Figure 5.5:The measured normalised directivity patterns results of the optimum RFID tag's antenna in: a) *z-x* plane, b) *z-y* plane and c) *x-y* plane at 900*MHz*.
'—' measured co-polarisation and ''xxx' 'measured cross-polarisation.

The concept of the current distribution has been computed within the simulation as shown in Figure 5.6. It can be seen that the maximum current is distributed about the feed point.

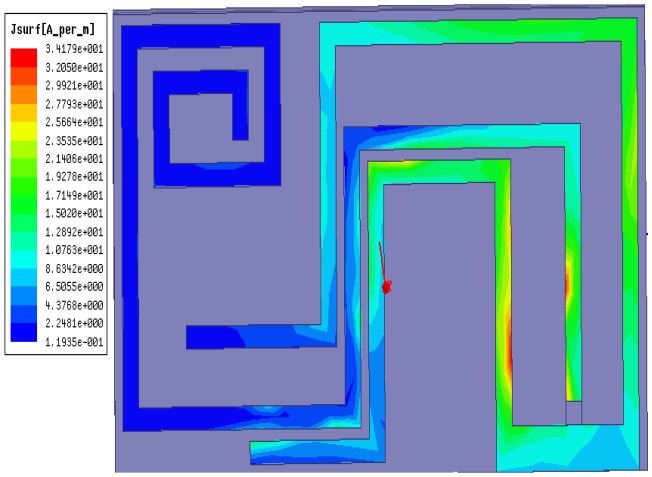

Figure 5.6:The concept of the simulated excited surface currents in the tag's antenna at 900*MHz*.

The design of a mountable RFID tag has been presented for UHF frequencies and situations where the tag is expected to be in close proximity of metallic surfaces. Detailed electromagnetic simulation of the antenna tag sub-system indicated an impedance of $(14.3 - j140.9)\Omega$ at $900MHz$. The detection range is found to be better than $75cm$.

5.3 CONFIGURATION OF T-SHAPE RFID TAG ANTENNA

This section proposes a second design with the same objectives as above and for the same operating frequency. This design is more basic and seems to deliver improved results. Once again a first cut design has been generated from a parameter study in HFSS from which a candidate structure has been fabricated. The basic configuration is given in Figure 5.7

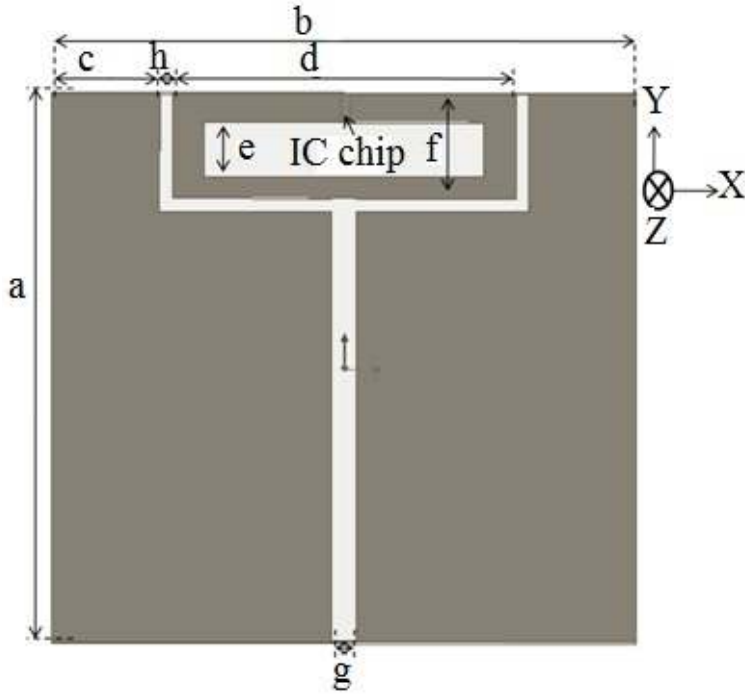

Figure 5.7:The dimensions of metallic T-shape RFID tag antenna

The structure parameters are summarised in Table 5.2. The HFSS schematic is given in Figure 5.7. The feed point (chip placement) has been generated with a $(14 - j130)\Omega$ input impedance which is normalised to 50Ω.

Table 5.2:The dimensions listed for antenna structure shown in Figure 5.7

a	43.5*mm*	**e**	0.25*mm*
b	46*mm*	**f**	7.9*mm*
c	8.5*mm*	**g**	4*mm*
d	26*mm*	**h**	1*mm*

The optimum micro-strip antenna tag has been carefully analysed and studied and the simulation results have been obtained as in the following section.

5.3.1 SIMULATION AND RESULTS

The simulated current distribution has been analysed as presented in Figure 5.8; it is clearly seen that the maximum current is spread closely around the floating feeding port.

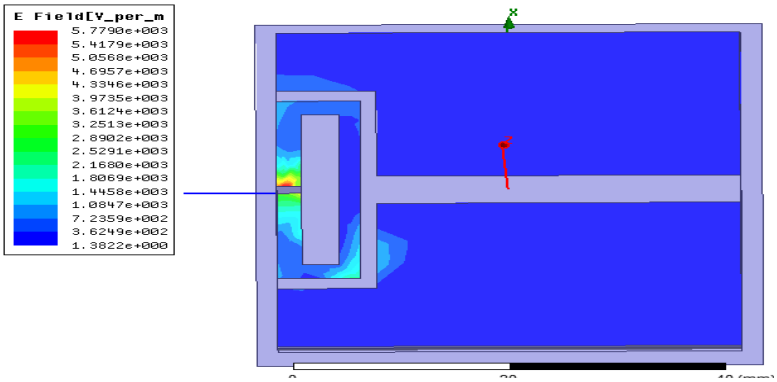

Figure 5.8:The surface current distribution of the antenna shown in Figure 5.7.

The return loss, coupling and radiation pattern of the radiator have been measured and the results have been verified to ensure adequate performance. As demonstrated in Figure 5.9, the intensity of a reflected wave relative to an incident wave i.e. reflection coefficient at 867*MHz* is -26.9*dB*. It is worth mentioning that the best geometry sizes with a highest reflection coefficient at the specified frequency were studied, analysed and tested before the optimum RFID tag antenna was implemented. Through the simulations, the (e, h and g) lengths have been found that the more influential to the antenna properties. From these parameters, the study analyses have been focused on their size and the remaining sizes have been kept constant.

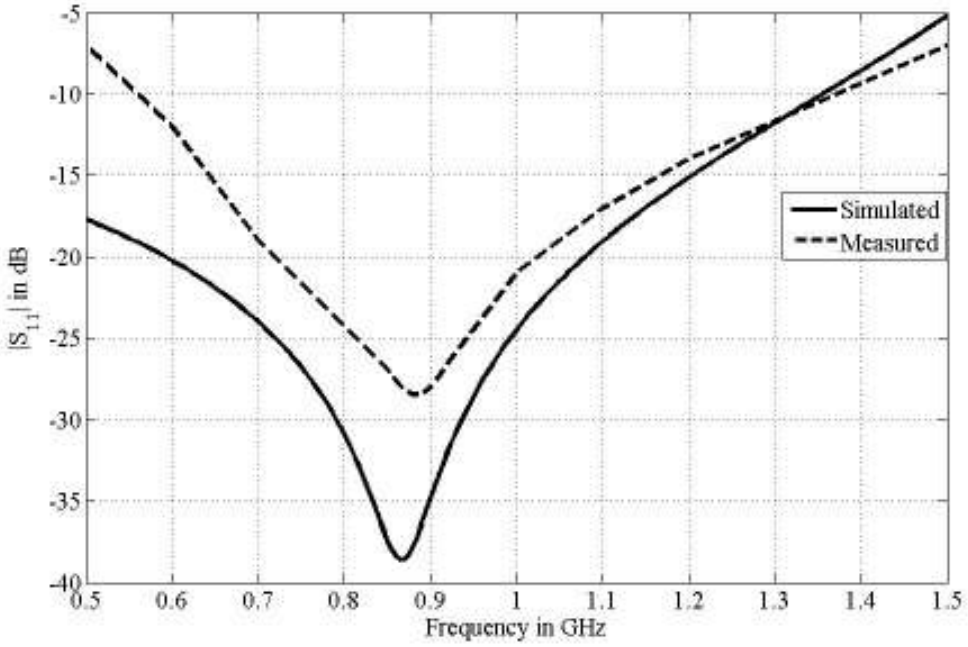

Figure 5.9:The reflection coefficient $|S_{11}|$ for Metallic T-shape RFID tag antenna.

As is clear from the Figure 5.10 (a) the e-parameter could be used to adjust the great antenna efficiency to the specific point of frequency.

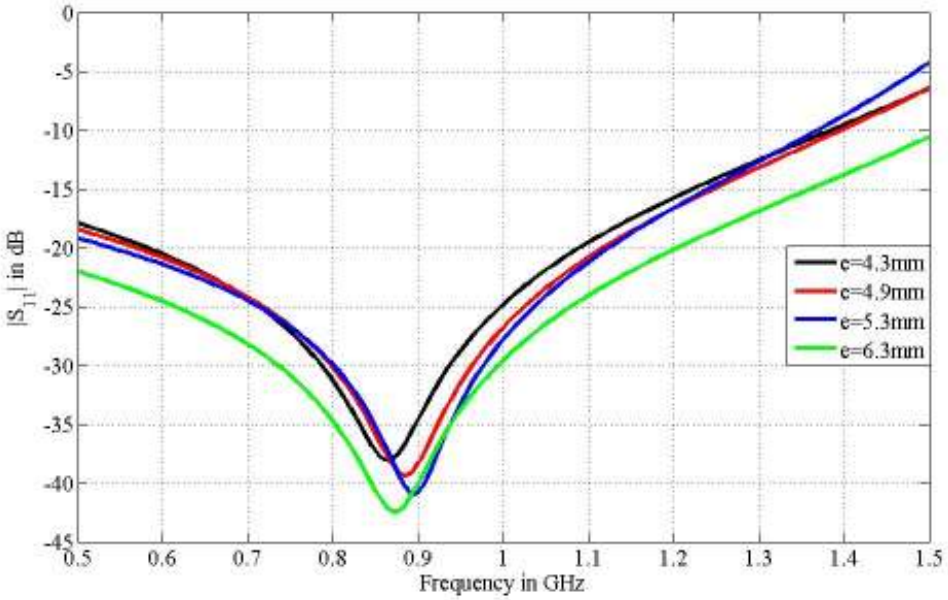
0
-5
-10
-15
-20
-25
-30
-35
-40
-45
0.5
0.6
0.7
0.8
0.9
1
1.1
1.2
1.3
1.4
1.5
|S11| in dB
Frequency in GHz
e=4.3mm
e=4.9mm
e=5.3mm
e=6.3mm

(a)

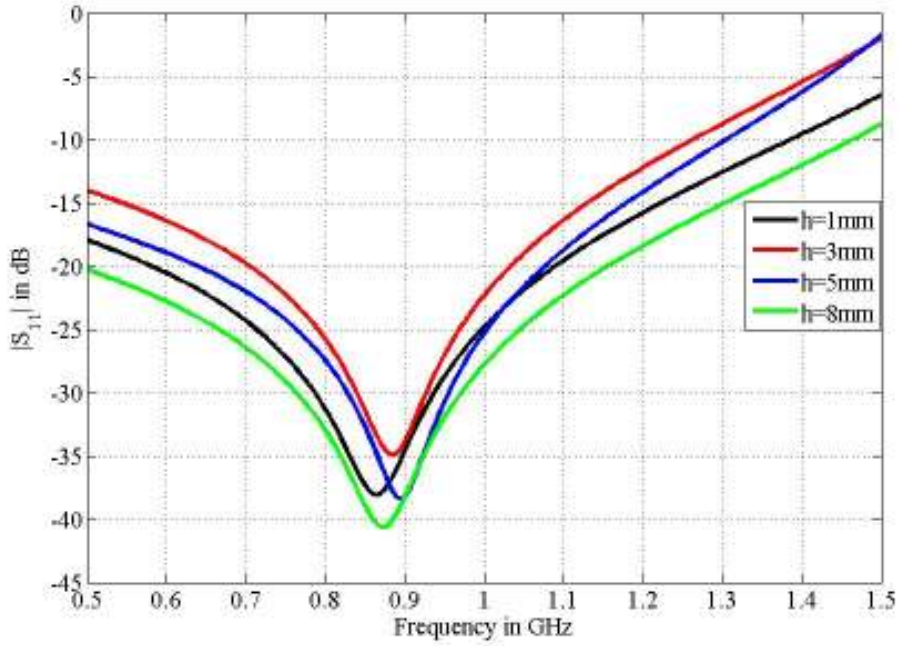
0
-5
-10
-15
-20
-25
-30
-35
-40
-45
0.5
0.6
0.7
0.8
0.9
1
1.1
1.2
1.3
1.4
1.5
|S11| in dB
Frequency in GHz
h=1mm
h=3mm
h=5mm
h=8mm

(b)

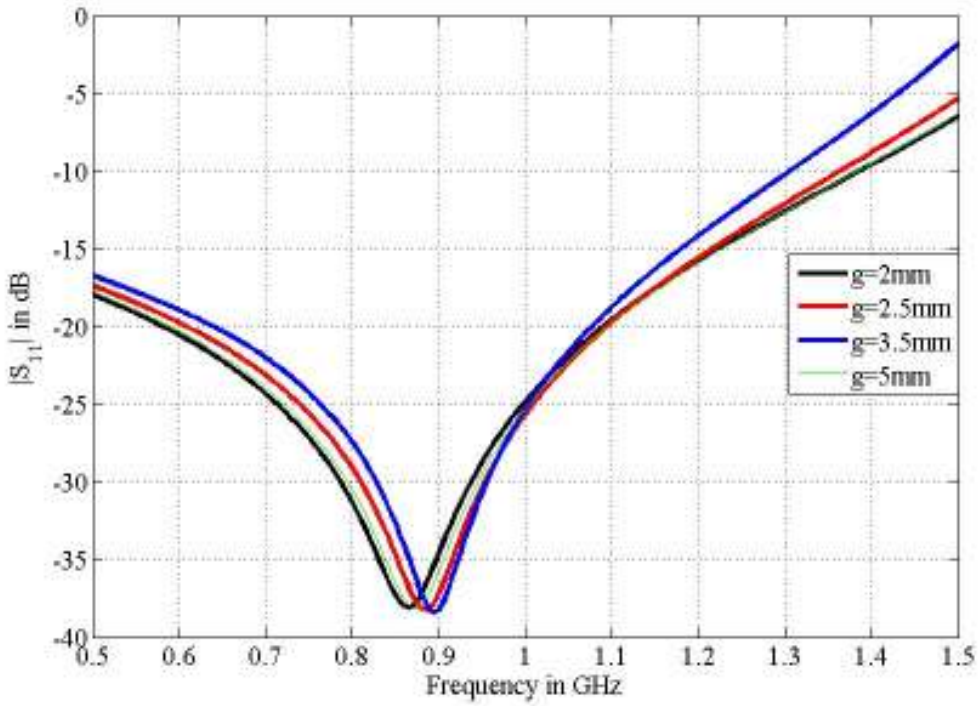

(c)

Figure 5.10:Parametric study of the reflection coefficients $|s_{11}|$ of the target antenna; (a) adjusting in e-parameter, (b) modifying in h-parameter and (c) changing in g-parameter

In contrast, the size of the parameter has a direct a peer on to the antenna's performance as well as the sensor bandwidth which can be clearly seen in Figure 5.10(b). Furthermore, from Figure 5.10(c) the g-parameter also affects the frequency and the bandwidth.

The optimum radiator gain is presented in Figure 5.11 where it can be seen that the highest gain is at 867*MHz* and around -0.25*dBi*.

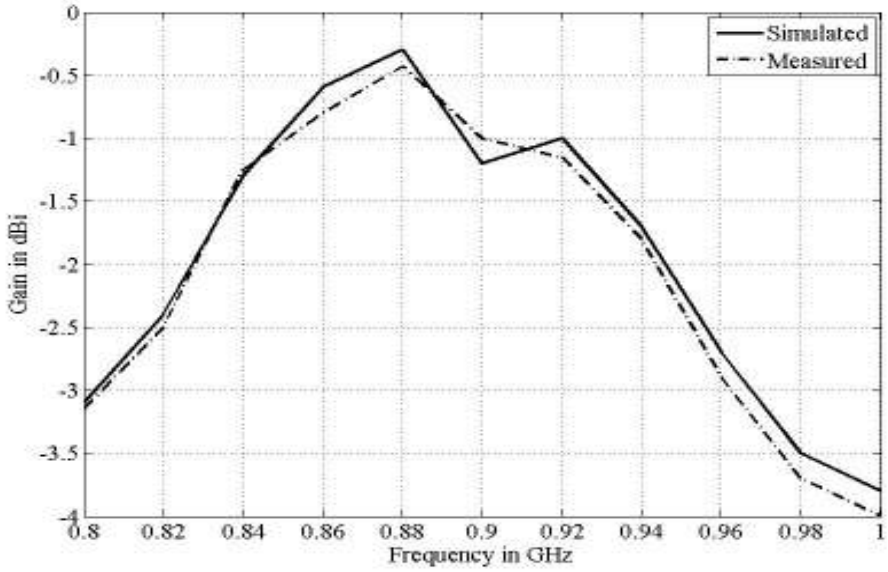

Figure 5.11:The measured and simulated gain results of the aimed design

The input impedance has been demonstrated in Figure 5.12 and found to be about $(14.9 - \text{j}136)\Omega$ at $876MHz$.

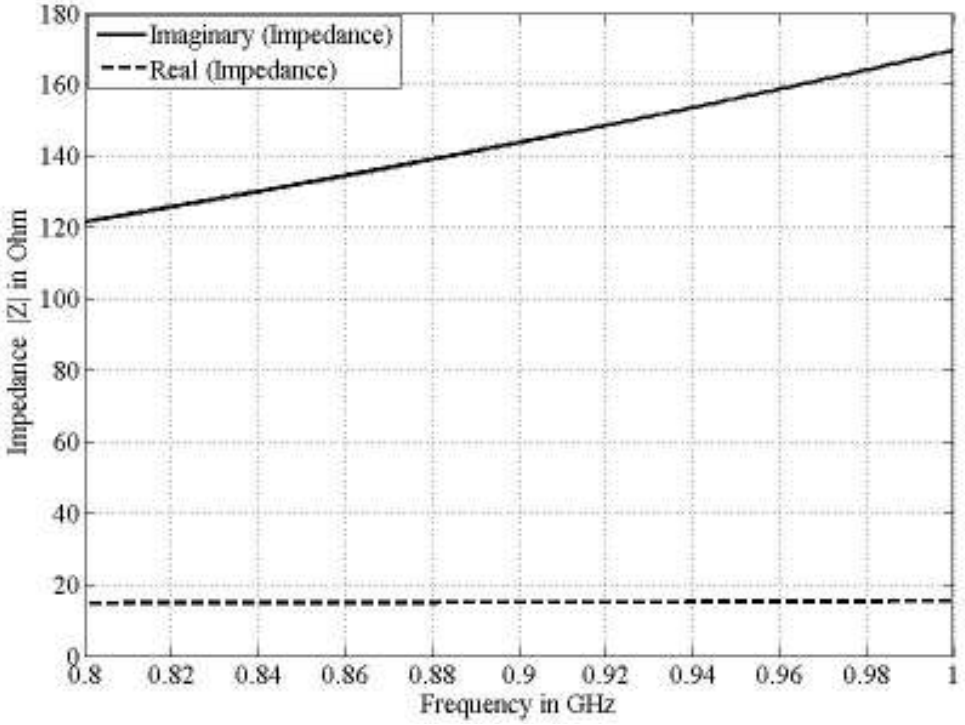

Figure 5.12:The impedance plot for Metallic T-shape RFID tag antenna.

The simulated vs. measured normalised far-field patterns results of the target RFID tag antenna in z-x , z-y and x-y planes at 876*MHz* are presented in Figure 5.13 a, b and c respectively. These fields confirmed that the antenna preserve the linear polarised omni-directional patterns.

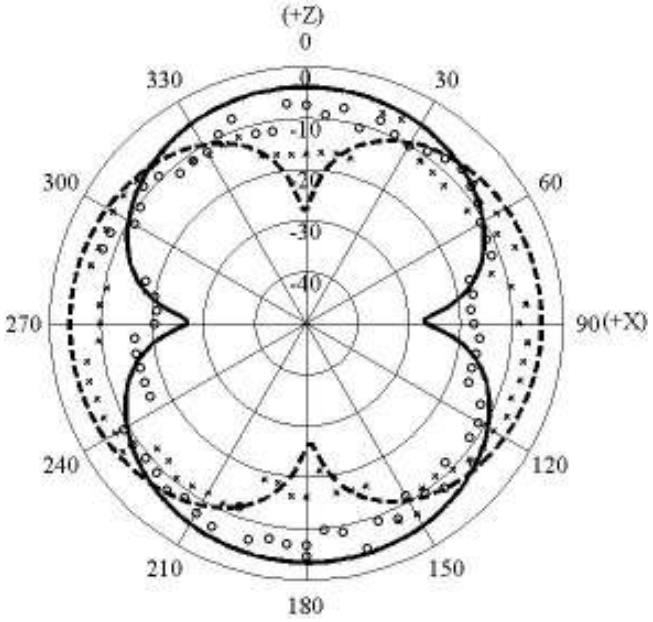

(a)

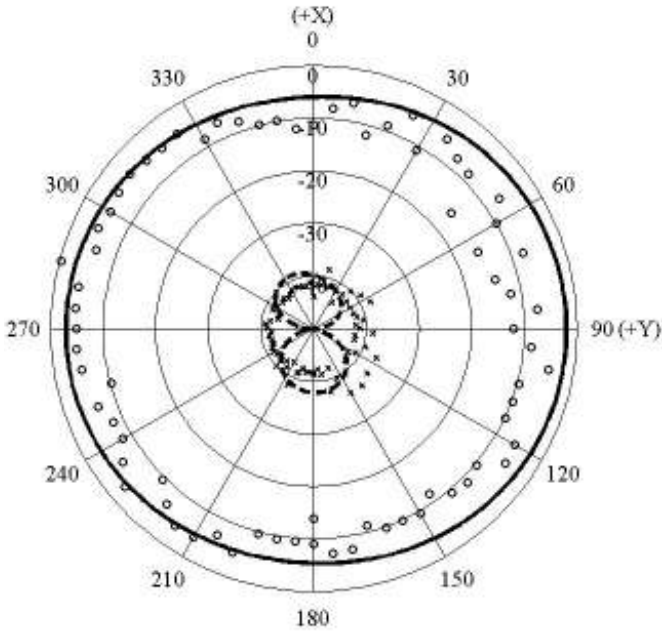

(b)

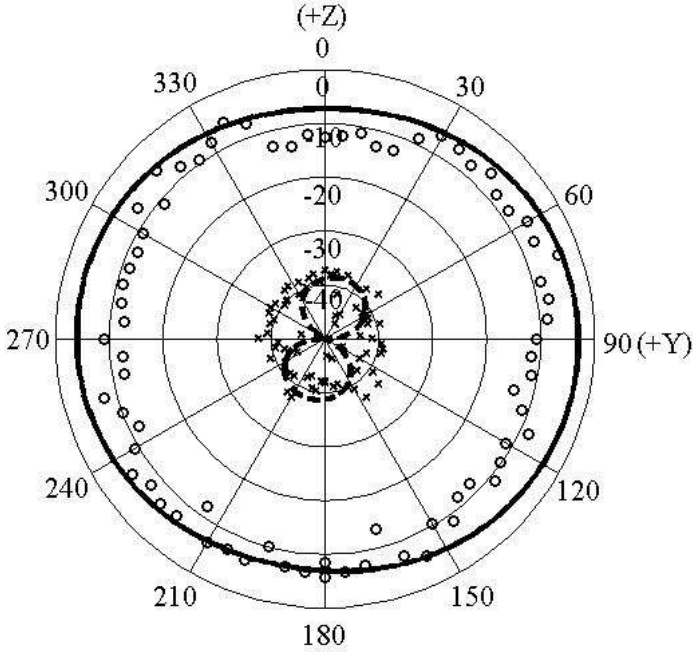

(c)

Figure 5.13:The simulated vs. measured normalised radiation patterns results of the target RFID tag's sensor in: a) *z-x* plane, b) *z-y* plane and c) *x-y* plane at 876*MHz*.
'—' simulated co-polarisation, '----' simulated cross-polarisation
'oooo' measured co-polarisation and 'xxx' measured cross-polarisation

5.4 CONCLUSIONS

In this chapter two linearly polarised antenna designs for UHF RFID application have been investigated in an environment when they are mounted on metallic conducting surfaces. The designs of the ***S*** and ***T*** antennas model, although novel, and with improved detection ranges, draw heavily on contemporary research literature. Going forward, improved simulations and a design strategy are required for this class of antenna. Detailed simulation and analysis of the tag antennas have been carried out for (867-900)*MHz* operation. The S-antenna design dimensions have been fixed at 32.5*mm*×9.5*mm*×1.6*mm* as well as T- sensor model parameters have been found 46*mm*x43.5*mm*x1.6*mm*. From simulation the S and T designs input impedance of the target transponder antenna has been found to be (14.3-j140.9)Ω and (10-j135)Ω respectively which have been normalised to 50Ω; this confirms both antennas could be good candidates for future RFID tag sensors. The final designs have tested to identify an object consisting of a metal surface, the effective detection has been found to be between 0.7 m and 1.5m.

CHAPTER SIX

DESIGN AND OPTIMISATION OF COMPACT HYBRID QUADRIFILAR HELICAL-SPIRAL RFID READER'S ANTENNA USING GENETIC ALGORITHM

6.1 INTRODUCTION

Recently, the RFID devices working on ultra high frequency (UHF) have been attracted much attention owing to the ease of the possibility of the employment in the wide of applications. It is noted that, however, the RFID reader captures a key role in multiple applications of this system through its advantages of compactness, simplicity and manoeuvrability i.e. easy to move and direct its antenna in a certain direction. A reader (detector) commonly consists of a radio frequency form which gives ability to the reader's antenna to work as a transmitter and/or a receiver to send a signal to the transponder [12-85].

In the most cases, the detector antenna uses circular polarisation in order to overcome the possibility of losing signal polarisation owing to a linear polarisation of the tag antenna [101]. Furthermore, the detector creates a magnetic oscillating field in the radio frequency range. The transponder which forms the real information carrying device of an RFID system traditionally has a coupling element and an electronic microchip. Obviously,

an RFID tag antenna has been employed as a transponder to integrate with the reader antenna within the interrogation area. In practise, load modulation utilizing a subcarrier, as well as (sub) harmonics of the reader's transmission frequency band, has been employed to transfer the instruction which has been stored in the RFID tag chip to the reader, both were limited to the serial number or more size of data. Consequently, the reader might be called a controller because it has the ability to transmit instruction from the device to the tags as well as receiving information from the tags to the device through the reader antenna. A reminder does need to be taken into account that there are passive and active RFID tags [85, 100].

From point of a passive tag antenna must noted to the RFID reader's antenna design should contain some unique characteristics. In detail in case of using passive RFID devices, the reader antenna should be designed with lower correlation coefficient level as much as possible than in a normal communication scheme. In a nutshell, the backscattered wave signal of the passive tag antenna is usually rather weak and exposed to collision with the strong reflected signal which might be emitted from reader antenna [85].

A vast majority of RFID tag antennas are formed as linear polarisation (LP), therefore, the reader antennas should be configured as circular polarisation (CP) to confirm the smoothing and easing communication between the reader and the tag antenna. In other words, the CP antenna can limit the signal losses which naturally occur due to the multipath effects among the

tags and a reader. On the whole, compact size, light weight and low profile with a CP antenna are all important characteristics for the RFID reader antenna and the separation between the reader and the tags is very critical for the RFID system performance [85].

In order to investigate a long detection range, the high gain of the reader antenna must be taken into an account especially since the emitter must be directed to the tags. Similarly, the near field radiation is another issue which needs to focused in as it clearly effects the read field length; therefore, the RF reader energy often transfers to the passive tags through magnetic near field passing via dielectric substances with very little signal reduction. From here the detect ability could be measured as the relative distance that let the reader recognise the tags. It cannot be forgotten that near field devices allow significantly smaller tags compared to ones in far field systems. This allows the spread of RFID applications into smaller items. Explicitly, in near field applications, the interaction between the RFID transponder and the receiver is dependent on inductive coupling [85, 102].

It is useful to refer to the impact of the working environment, since the RFID system has had failure in recognizing the tags in bad work environments which directly affect the signal deployment.

In most cases, the readers are able to be interfaced to a PC, robot control and so forth through peripherals using RS232, RS485 and other known tools which could be used for this purpose. It is worth mentioning that the readers have also been equipped with wireless antennas, which might be used to link the reader to a host PC [85].

In this research, a non-resonant antenna has been created through combining a spiral antenna and an axial mode helical antenna which radiates a circularly polarised (CP) wave. Due to widespread use of antenna in many applications, the design had not consider a number of criteria. These include lightweight, small size, simple configuration, low consuming power, ability to work across and beyond the whole frequency band of the device and cost of implementation.

It is worth mentioning that the physical size and operating frequency i.e. wavelength subject to be change according to vary some measurements such as radiation pattern, polarisation, input impedance and so forth. To clarify this more, let's mention an example like if the entire physical antenna parameters are increased by a factor of four then the antenna efficiency could be kept as a same value if also the operating frequency is increased by a factor of four.

6.2 SPIRAL ANTENNA

The spiral antenna can be described in a simple way as a geometrical RF antenna design which defines the surface by angles. Moreover, spiral antennas can transmit/receive over a wide range of frequencies, therefore, may can be classified as frequency independent antenna. In addition, the stability and unchanging of the radiation prototype, polarisation and impedance in a long large bandwidth has been granted excellence. It is worth mentioning that spiral antenna is essentially circularly polarised with low gain and an array of spiral antenna can be employed to raise the gain. Even in terms of size, the circumvent ring specialty gives a good choice to minimise the spiral antenna to achieve an extremely small antenna formation. Through access to the target antenna modulations, there are many shapes to design such antenna like square spiral, archimedean spiral and star spiral [85, 103].

The optimum spiral antenna types could be found via changing the number of the turns and the spacing among the arm. As for the choice of the dielectric, a thick height of the dielectric with low permittivity could be replaced with same properties by thin ones with high permittivity in order to get lightweight antenna design, but the availability and the cost of material tends to be varied along best operational performance. Indeed, the effectiveness of the antenna depends on the shape and the material [103, 104].

The spiral antennas manoeuvre in three ‘W’ methods which are rapid wave, roving wave and spongy or leaky wave. In detail, the travelling wave created on the spiral arms normally authorises for broadband completion, whereas the rapid or fast wave forms due to the mutual coupling phenomenon occurring among the arms, and the power leaks during propagation through the spiral arms to fabricate radiation produce leaky wave. In other word, the ring or band theory could give a good explanation to the spiral antenna working method. The active area i.e. the circumference of spiral is the same as the wavelength is the region which the spiral antenna theoretically radiate a signal [85].

6.3 HELICAL ANTENNA

A helical antenna is simply defined as an antenna composed of a conducting wire wound in the helix form, which is normally mounted over a ground surface. In addition, this type of antenna usually has a power source connected in middle of the ground plane and the bottom of the helix. As the target antenna described in the mode of operation, the helical antenna can work in one of two manners: normal method (broadside helix) or axial style (end-fire helix) [85].

To understand more about the broadside helix mode, the parameters of the helix i.e. the patch and diameter are significantly small when compared to the wavelength. However, electrically this type of antenna radiates a signal

likes a short dipole or monopole, and the antenna pattern is likewise similar to the omnidirectional shape with the greatest emission at right angles to the helix axis. In addition, the radiation forms as a linear polarisation parallel to the helix axis [85, 104].

In contrast, the helix dimensions of the axial technique are similar to a wavelength. Furthermore, the end-fire helix antenna operates as a directional sensor giving out a beam off the helix terminals along the antenna's axis. Therefore, this antenna works as circular polarised.

6.4 DESIGN AND OPTIMISATION OF COMPACT HYBRID QUADRIFILAR HELICAL-SPIRAL ANTENNA IN RFID APPLICATIONS USING GENETIC ALGORITHM

Simultaneously, quadrifilar helical antenna (QHA) and quadrifilar spiral antenna (QSA) are extremely capable candidates radiators for RFID applications owing to the symmetry of their geometry, the features of the balanced feeding and their capability to supply circular polarisation in excess of a wide angular area [105, 106]. In particular, the QHA, as presented Figure 6.1a has the ability to offer an extensive beam width prototype controlled to a one hemisphere and a good circular polarisation which makes the QHA an attractive and smart selection for non-tracking wireless communications and general purpose RFID tag antennas. In addition, the target model is essential to realise the necessity of the axial

ratio and front to back power ratio. Generally, the axial length of QHA is much bigger for definite applications. However, the QSAs are recognised for their capability to create an extremely wideband nearly in ideal circularly polarised radiation in excess of their occupied treatment section. Furthermore, the QSA designs as seen in Figure. 6.1(b) propose a low feature profile, in addition to the axial ratio performance and beam width; while the surface region is in use by the typical QSA design is also increased, as compared with the QHA.

Modelling compact QHA or QSA antennas for RFID applications has attracted many antenna researchers and various studies have already been demonstrated. The motivation and purpose which are taken in this chapter, is the development of a new type of uses of compact quadrafilar design in RFID devices which contains the characteristics of both QHA and QSA. Generally to explain the topic, Figure 6.1(c) clearly shows a simplified target model i.e. compact hybrid quadrifilar helical-spiral antenna (HQHSA). Obviously, the intended form is composed from both QSA and QHA. It is worth mentioning, the alimentation of the QSA from the external periphery is planned to avert the complexity and gap needs of centre feed; the QSA could be fed by externally coaxial cables. Consequently, the initial segments of the QHA is straight connected from the release end of the QSA and then generated vertically beside the QSA surface scheme. This devise is expected to decrease the axial length of the QHA as well as to minimise the

surface region of the QSA while maintaining a good axial ratio beam width coverage and power gain.

6.4.1 ANTENNA DESIGN USING GA

The formation and optimisation of the target compact hybrid quadrifilar helical-spiral antennas is created using genetic algorithms (GA). The GA is an optimisation tool that generates a random code for searching purposes that tests a fitness functions and in return a test procedure is applied for selection the optimum solution (i.e., meeting target antenna design specifications); and this will continue until reaching the maximum generation [107]. An approach of using GA in conjunction with an electromagnetic simulator has been introduced for antenna designs [108, 109]. For example, GA was applied to design wire antennas and microstrip antennas. The benefit of applying GA is that they provide fast, accurate and reliable solutions for antenna structures [110, 111].

The Genetic Algorithm driver [112], written in FORTRAN has been adopted in this work in conjunction with the industry-standard NEC2 Fortran source code [113] which was used to evaluate the randomly generated antenna samples. For comparison purpose, the proposed HQHSA together with a typical QHA and QSA were studied for optimisation with GA. In this instance, real-valued GA chromosomes have been used. Antenna parameters such as the VSWR and axial ratio (AR) are optimised at 900*MHz* operating

frequency of RFID system. Each antenna sample was computed using NEC2 source code and its results were compared with desired fitness using the following cost function 'F':

$$F = W_1 \times \left(\frac{1}{VSWR}\right) + W_2 \times AR \tag{6.1}$$

where,

$$VSWR = (1 + |\Gamma| \tag{6.2}$$

$$\Gamma = |(Z_{in} - 50)/(Z_{in} + 50)| \tag{6.3}$$

VSWR is the voltage standing wave ratio, AR is the axial ratio, Z_{in} is the input impedance, Γ is the reflection coefficient and W_1 and W_2 are the weighting coefficients. The objective was to maximise *F*. The GA was applied using the following procedure: The GA randomly chooses the initial population and then converts each antenna configuration to a file which can be read by NEC2. The NEC2 program is executed and the results will be fed back to GA for the evaluation process. This will continue till GA converges to an optimum solution.

In addition, the overall parameters of the optimal RFID reader antenna of HQHSA demonstrates the effectiveness of size reduction using this proposed antenna configuration where approximately 30% of size reduction of the axial length is achieved; as compare to the one of the optimal QHA design (see Table 6.1); whereas, it also offers more compact design in terms of the spiral surface area over a typical QSA.

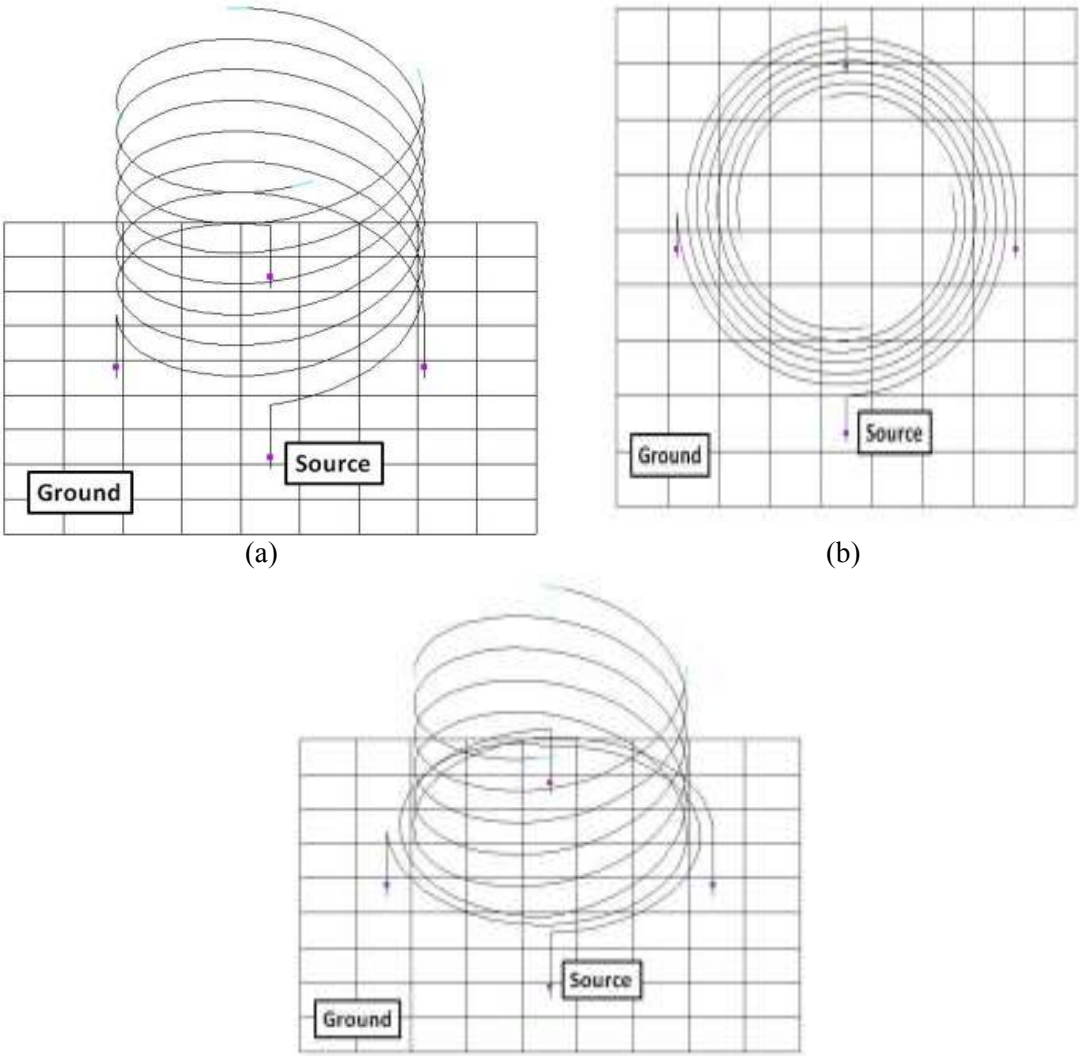

(a) (b)

(c)

Figure 6.1:Antenna configurations studied. (a) QHA, (b) QSA and (c) HQHSA

In figure 6.1, the HQHSA is clearly shown in the stages of designing and the four feeding point (red colour) has been taken place on the bottom to feed the antenna. In this design, a GA is employed to create and optimise the desired HQHSA for RFID application. In order to validate and compare the performance of the proposed design, a typical QHA and QSA are also optimised using GA as two reference designs. The GA input parameters,

antenna variables and best solutions for each one of the designs are summarised and listed in Table 6.1.

Table 6.1:Summary of GA input parameters, antenna variables and best solutions for QHA, QSA and HQHSA.

GA parameters	**QHA Design**		**QSA Design**		**HQHSA Design**	
	Parameters (*m*)	Optimum values (*m*)	Parameters (*m*)	Optimum values (*m*)	Parameters (*m*)	Optimum values (*m*)
Number of population size = 8	Pitch distance (0.015-0.025)	0.01946	No of turns (1-2.5)	2.0768	Pitch distance (0.01-0.02)	0.01982
Number of Parameters 3; 4;6	Axial length (0.3-0.5)	0.03496	Spacing between turns (0.003-0.007)	0.00482	Axial length (0.02-0.03)	0.02497
Probability of mutation =0.02	Radius of helix (0.015-0.035)	0.02270	Inner radius (0.01-0.02)	0.01850	Radius of helix/ Inner radius of spiral (0.01-0.02)	0.01891
Maximum generation =300	-	-	Outer radius (0.02-0.035)	0.02930	Outer radius of spiral (0.02-0.03)	0.02266
Number of possibilities=32768	-	-	-	-	Spacing between turns	0.001
-	-	-	-	-	No of turns	0.5
-	Radius of wires Distance above ground	0.0005 0.01	Radius of wires Distance above ground	0.0005 0.01	Radius of wires Distance above ground	0.0005 0.01

Table 6.2:Comparison of the target reader antenna performance of HQHSA, QHA and QSA

	***6dB*/*8dB* Bandwidth (*MHz*)**	**Axial Ratio angle coverage (Degree)**	**Target antenna total gain (*dBi*)**
HQHSA	40/20	170	7.3
QHA	70/50	175	7.5
QSA	70/40	120	8

6.4.2 RESULTS AND DISCUSSION

Configurations of optimal proposed HQHSA antenna with excellent VSWR and AR has been investigated within the maximum generations; antenna dimensions of the best designs are shown in Table 6.1.

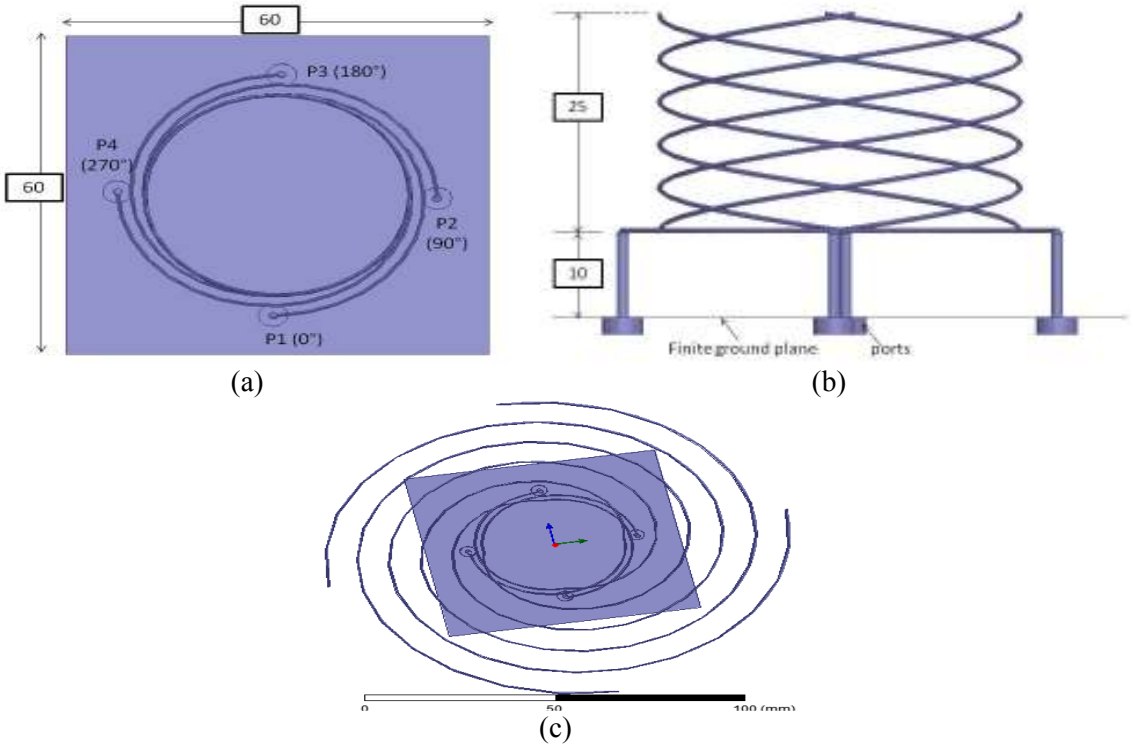

Figure 6.2:HFSS model of the GA-optimised final antenna; (a) Ground plan, (b) side view and (c) top view with wider open on the top

To verify the GA-optimised design, performance of this optimal antenna has been characterised using commercial full-wave Electromagnetic software. In this study, Ansoft HFSS (based on finite element method) is considered to cross validate the behaviour of this antenna, as Figure 6.2 presents, where a finite ground plane with dimension of 60*mm*x60*mm* is considered, the side view and the top view which shown how the antenna is wider at the top end. The reflection coefficients have been studied in Figure 6.3 and get it nearly to -18*dB* at 900*MHz*.

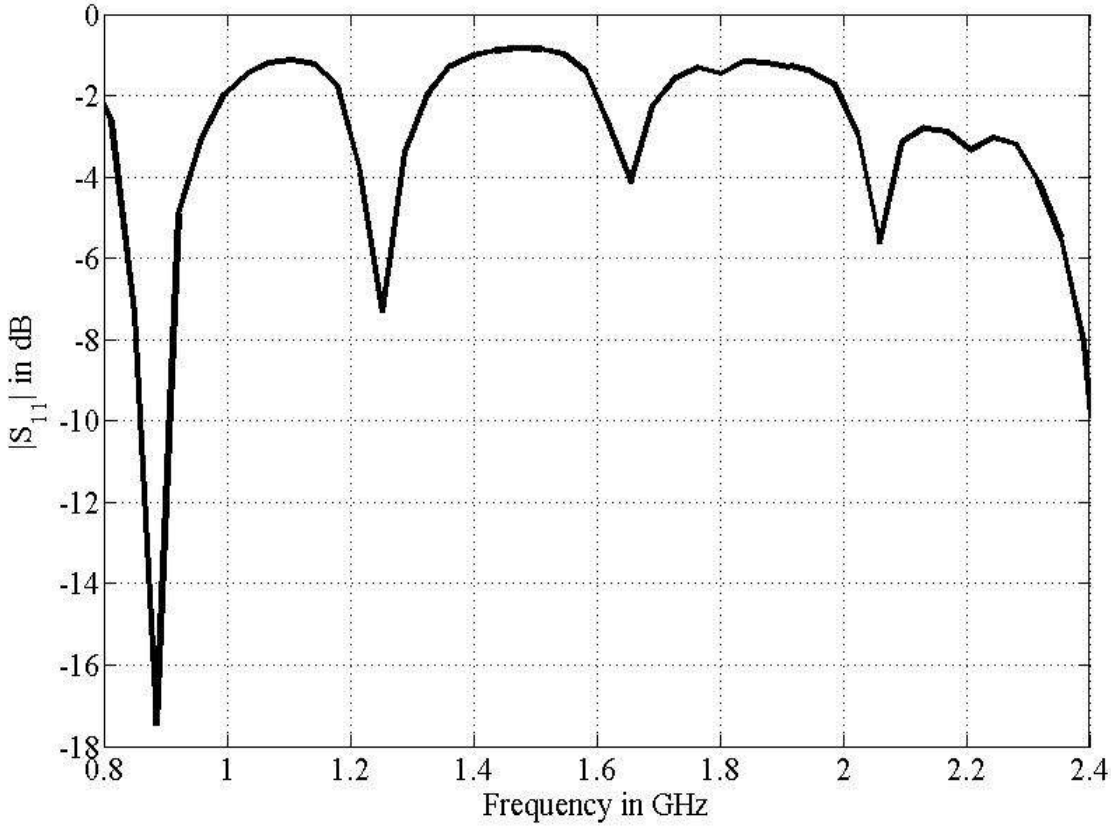

Figure 6.3:The reflection coefficients of the target design

The VSWR at the input ports of the proposed circularly-polarised antenna were calculated and compared at the RFID system frequency. Their

corresponding results are presented in Figure 6.4. As can be seen, the optimal antenna appears to have excellent impedance matching that covers the bandwidth requirements for RFID device communications. However, the antenna resonant frequency shifted slightly from the design frequency of 900*MHz*. This may be due to the fact of the size of finite ground plane considered in this study. Generally, both the simulated results are in fairly good agreement.

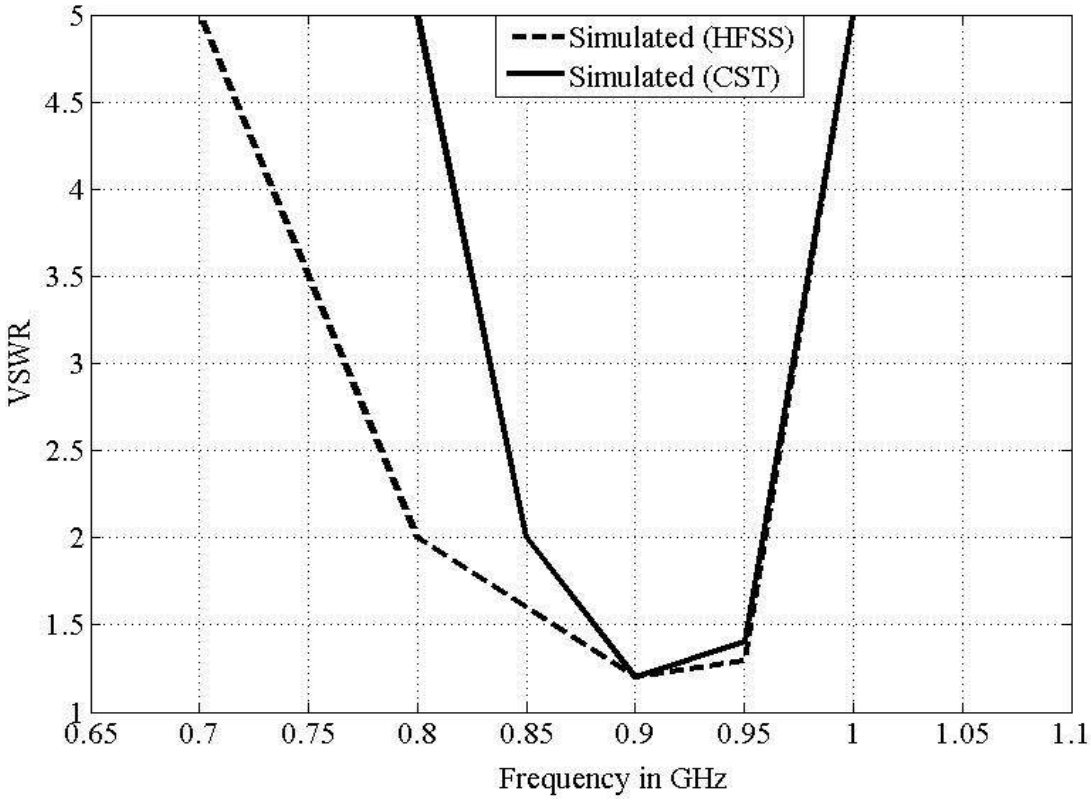

Figure 6.4:Computed VSWR from HFSS and CST software.

Figure 6.5 illustrates the axial ratio of the proposed antenna against the elevation angle θ at 900*MHz* for two vertical planes at constant Φ = 0° and Φ= 90°. The proposed antenna shows approximately ± 90° elevation angle variations for an axial ratio less than 2 dB. The observations confirm the

superior circular-polarised characteristic for the proposed antenna over a wide elevation angle.

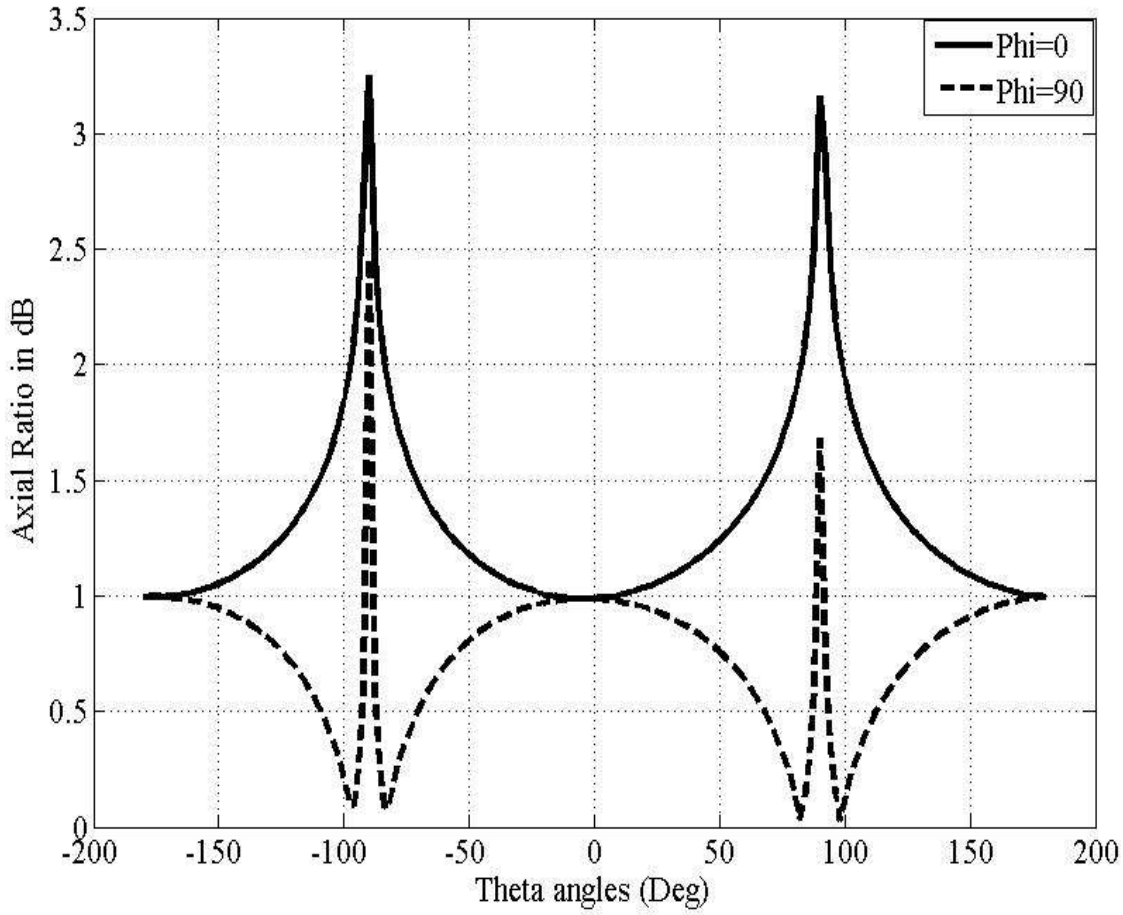

Figure 6.5:Axial ratios in *dB* against the elevation angles at 900 *MHz* at two vertical cuts: Φ = 0° and Φ = 90°.

Figure 6.6 (a and b) depicts the far field patterns of the proposed antenna at 900*MHz* for two planes similar to those plotted for the AR. As can be observed, symmetrical and identical variations were obtained for all the radiation patterns. The maximum gain of the antenna is found to be around 7dBi.

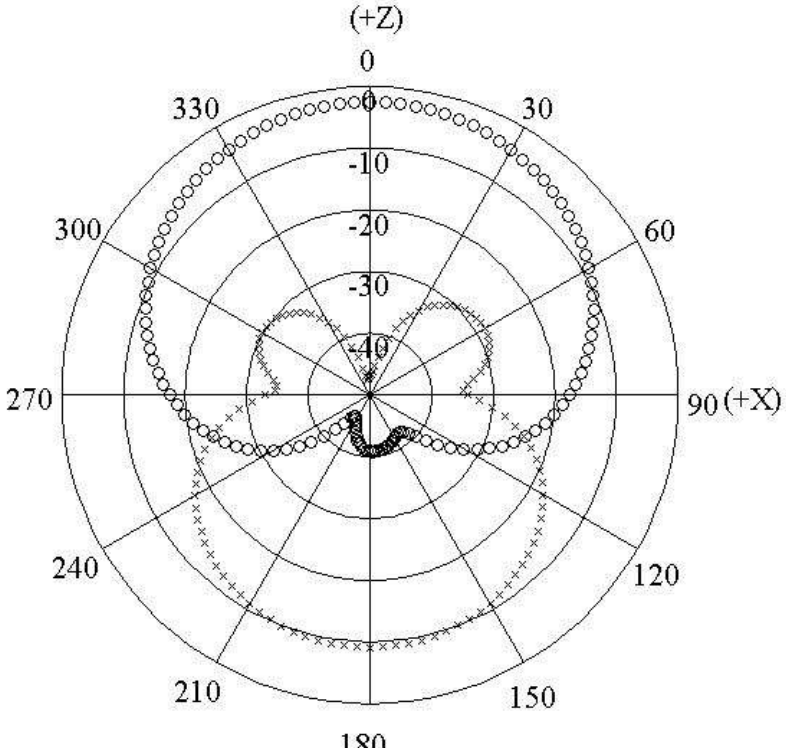

(a)

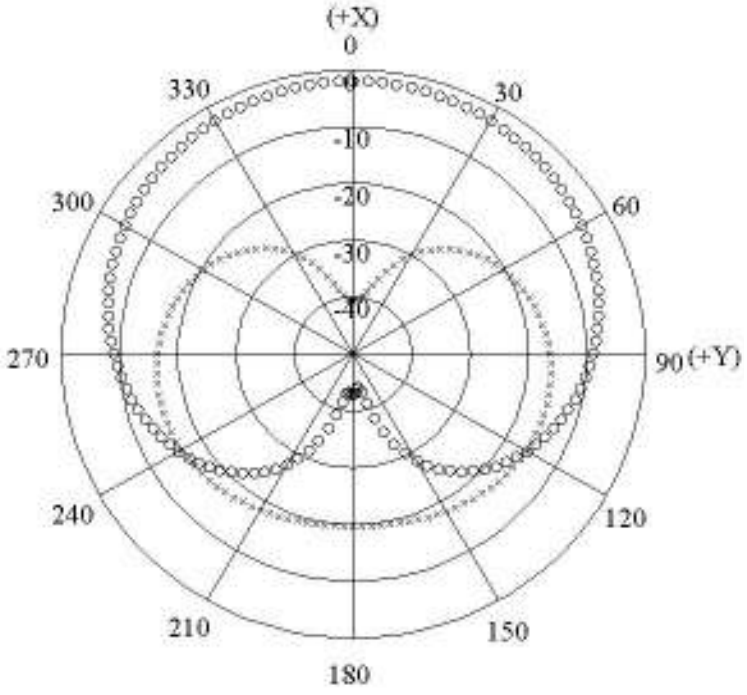

(b)

Figure 6.6:Simulated gain radiation patterns of the proposed antenna for two vertical planes; (a) Φ = 0° and (b) Φ=90°, where solid line presents left handed circular polarisation and dash line is for right handed circular polarisation. 'ooo' simulated co-polarisation and 'xxx' simulated cross-polarisation.

6.5 CONCLUSIONS

A novel circularly polarised antenna called as HQHSA is proposed. Modeling, design and optimization of this circularly-polarised hybrid quadrifilar helical-spiral antenna using Genetic Algorithms, operated for RFID reader applications have been demonstrated and discussed. The performance of the best selected antenna structure has been validated and compared via two different commercial EM simulators. The results confirm that an axial ratio of less than $2dB$ near ± 90° elevation angle at the antenna resonant frequency could be achieved with satisfactory $7dBi$ power gain. It is worth noted that the present designs proved to have better radiation performances than the manufacture product, apart from achieving small antenna size. The GA has provided its advantage in quickly finding solutions for antenna designs.

CHAPTER SEVEN

INTERACTION BETWEEN ELECTROMAGNETIC (EM) FIELD AND HUMAN BODY FOR RFID TAG ANTENNAS VIA HYBRID COMPUTATIONAL METHOD

7.1 THEORETICAL CONCEPTS

7.1.1 INTRODUCTION

Day by day the finite elements methods (FEM) have been widely utilised to design open and closed domain electromagnetic problems in scalar model in two and three dimensions (2 & 3D). Moreover, FEM has been employed to design a large category of problems by analysing up the computational field into elements of easy forms. In contrast, the function's form must be chosen; therefore, specific computer programs can be built using the basic functions to solve complex geometries. It should mention of that the elements selection needs to be carefully clarified to guarantee there is a solution for the discussion problems [3, 114].

Nevertheless, the proper energy of the FEM has been discovered in 3D volume shapes when complexity has been found when using the surface based integral equation methods with material and structural inhomogeneities.

It is clearly shown that the restriction of the numerically accurate mechanisms, nonetheless, is their capability to find a solution of huge problems that place a big load on the Central Processing Unit (CPU) memory as well as time [7]. There are numerous of electromagnetic engineering problems could be expressed and solved by partial differential equations (PDE). In contrast, the analytical methods could be used to solve a couple of the practical geometries [7].

An electromagnetic wave propagating is affected by the medium properties in which the waves are travelling in different speeds compared to the free space light speed. These changes must be taken into the account before deciding the required minimum time step. In addition, to diffuse a space of one cell needs a least amount time of $\Delta t = \Delta\chi/c_0$. Moreover, the propagation needs to allow in the diagonal direction in case of 2^{th}D simulation has been needed to obtain $\Delta t = \Delta\chi/(\sqrt{2}c_0)$. Compared to that, 3^{th}D simulation requires $\Delta t = \Delta\chi/(\sqrt{3}c_0)$.Unless otherwise specified, throughout this report has been determined Δt by (7.1):

$$\Delta t = \frac{\Delta\chi}{3.c_0} \tag{7.1}$$

In fact, 3D simulation is complicated owing to the need to use all vector fields as well as all points is in three magnitudes [3, 115, 116]. The Yee cell as presented in Figure 7.1 has been demonstrated by Kane Yee which clearly shown that the differential and integral of Maxwell's equations have been

applied in form of geometric relationship of the specific sampling of the vector components of the electric (charged) *E* and magnetic (attractive) field *H*.

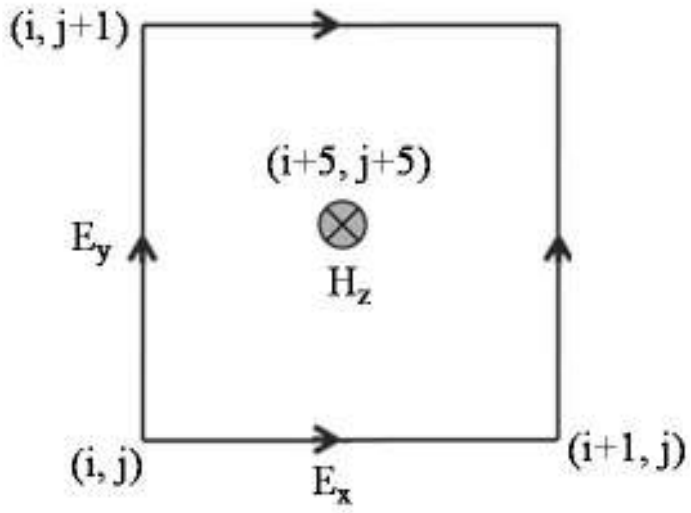

Figure 7.1:Yee Grid 2D

7.1.2 MAXWELL'S EQUATIONS IN 3D

Faraday Ampere and Gauss laws for electric and magnetic field as introduced in equation (7.2), (7.3), (7.4) and (7.5) respectively could be used to express the time (*t*) depending to the Maxwell's equations in term of differential and integral structure, imaginary, that no electrical or magnetic exporters in this part of area but could be contain a body which attract electric or magnetic field power [117, 118].

$$\frac{\partial \vec{B}}{\partial t} = -\nabla \times \vec{E} - \vec{J}_m \tag{7.2}$$

$$\frac{\partial \vec{D}}{\partial t} = -\nabla \times \vec{H} - \vec{J}_e \quad (7.3)$$

$$\nabla \times \vec{D} = 0 \quad (7.4)$$

$$\nabla \times \vec{B} = 0 \quad (7.5)$$

where, → is a sign of vector, E is the electric field (V/m = N/C), D is the electric flux density (C/m^2 = N/Vm), H is the magnetic field (A/m), B is the magnetic flux density (Wb/m^2), J_e is the electric conduction current density (A/m^2) and J_m is the equivalent magnetic conduction current density (V/m^2).

In case of using linear emitting materials, the relation between B to H also D to E could be simplified as presented in below equations (7.6) and (7.7):

$$\vec{B} = \mu\vec{H} \quad (7.6)$$

$$\vec{D} = \varepsilon\vec{E} \quad (7.7)$$

Throughout these equations, the term μ will be used to refer to the magnetic permeability (H/m = N/A^2) and ε will refer to the electric permittivity (F/m).

In such case, the characteristics of used materials are having field–independent– direction-independent and frequency-independent electric and magnetic. However, the possibility of losing the electric and magnetic which might form electromagnetic field in the substance surface so that they

appear in a type of heat energy. In particular, the corresponding attracted current to relate for the magnetic loss mechanisms has been defined in the equation (7.8) [117-119].

$$\vec{J}_m = \acute{\rho} \times \vec{H} \tag{7.8}$$

where $\acute{\rho}$ is an equivalent magnetic resistivity (Ω/m)

In addition, the equal electric current to account for the electric loss mechanisms can be found by the equation (7.9).

$$\vec{J}_e = \sigma \times \vec{E} \tag{7.9}$$

where σ is the electric conductivity (S/m)

If B and J_m are exchanged in equation (7.6), the below equations (7.10a) and (7.10b) can be defined as:

$$\frac{\partial \mu \vec{H}}{\partial t} = -\nabla \times \vec{E} - \acute{\rho}\vec{H} \tag{7.10a}$$

$$\frac{\partial \vec{H}}{\partial t} = \frac{1}{\mu} \times (\nabla \times \vec{E} - \acute{\rho}\,\vec{H}) \tag{7.10b}$$

If D and J_e are replaced in equation (7.7), then the new form of equation will be:

$$\frac{\partial \overrightarrow{\varepsilon E}}{\partial t} = -\nabla \times \vec{H} - \sigma \vec{E} \tag{7.11a}$$

$$\frac{\partial \vec{E}}{\partial t} = \frac{1}{\varepsilon} \times (\nabla \times \vec{H} - \sigma \vec{E}) \tag{7.11b}$$

Equations (7.10b) and (7.11b) can be written as the vector components of the curl operator to proceed in the next group of six associated numerical equations to Maxwell's curl equations in 3D, rectangular synchronise structure (x, y and $\mathcal{Z}$). Specifically, equations (7.12) and (7.13) are assimilated as the foundation of the finite-difference time-domain (FDTD) statistical algorithm of the common 3D items relation with electromagnetic waves.

$$\frac{\partial H_x}{\partial t} = \frac{1}{\mu} \times (\frac{\partial E_y}{\partial_{\mathcal{Z}}} - \frac{\partial E_{\mathcal{Z}}}{\partial_y} - \acute{\rho}\, H_x) \tag{7.12a}$$

$$\frac{\partial H_y}{\partial t} = \frac{1}{\mu} \times (\frac{\partial E_{\mathcal{Z}}}{\partial_x} - \frac{\partial E_x}{\partial_{\mathcal{Z}}} - \acute{\rho}\, H_y) \tag{7.12b}$$

$$\frac{\partial H_{\mathcal{Z}}}{\partial t} = \frac{1}{\mu} \times (\frac{\partial E_x}{\partial_y} - \frac{\partial E_y}{\partial_x} - \acute{\rho}\, H_{\mathcal{Z}}) \tag{7.12c}$$

$$\frac{\partial E_x}{\partial t} = \frac{1}{\varepsilon} (\frac{\partial H_{\mathcal{Z}}}{\partial_y} - \frac{\partial H_y}{\partial_{\mathcal{Z}}} - \sigma\, E_x) \tag{7.13a}$$

$$\frac{\partial E_y}{\partial t} = \frac{1}{\varepsilon} \times (\frac{\partial H_x}{\partial_{\mathcal{Z}}} - \frac{\partial H_{\mathcal{Z}}}{\partial_x} - \sigma\, E_y) \tag{7.13b}$$

$$\frac{\partial E_Z}{\partial t} = \frac{1}{\varepsilon} \times \left(\frac{\partial H_y}{\partial_x} - \frac{\partial H_x}{\partial_y} - \sigma E_Z \right) \tag{7.13c}$$

One of the many advantages of the FDTD design method is that it can be used to model complex substances. Moreover, it has a capability to gain wideband outcomes via passing excitation comparing to the other numerical mechanisms.

In fact, there is only one locative parameter for a certain point in Yee space network as demonstrated by Yee in Figure 7.2.

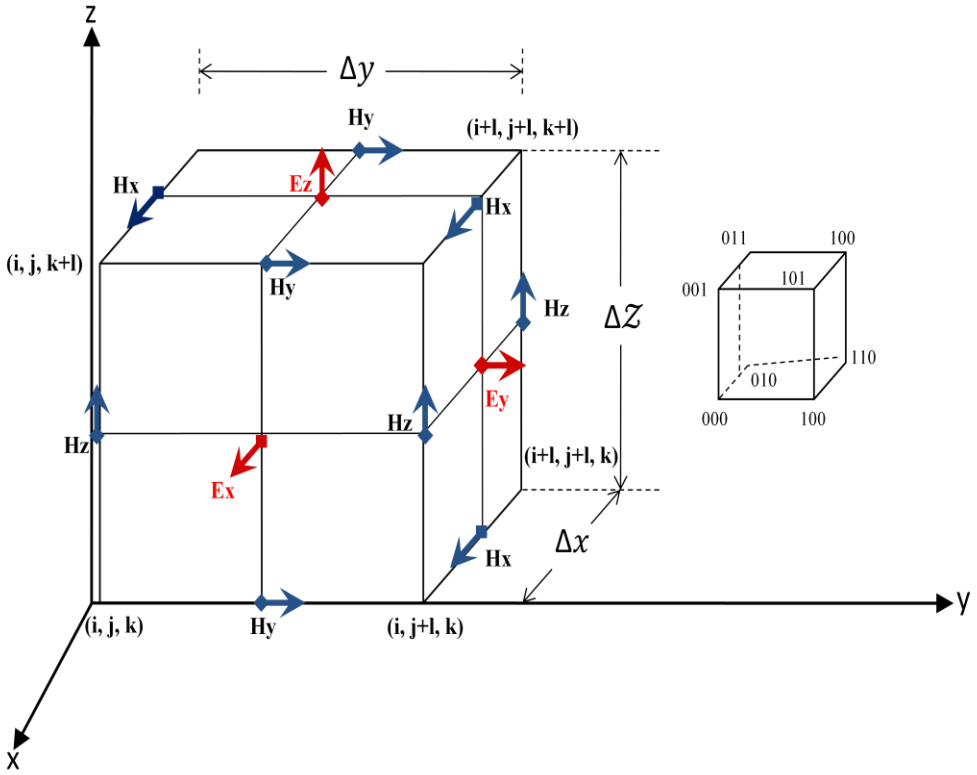

Figure 7.2:The Yee space network shows the direction of a range of field components; the electric field intensity (E) components are in the centre and magnetic induction field (H) components are in the middle of the faces

In particular, $(i, j\ and\ k)$ have been used to identify the position of each point. The follow equation (7.14) gives more clarification.

$$(i, j, k) = (i\Delta x, j\Delta y, k\Delta z) \tag{7.14}$$

From this equation, note that $(i, j\ and\ k)$ are integers; as for $(\Delta x, \Delta y, and\ \Delta z)$ are the lattice space enhancements in the $(x, y\ and\ z)$ depending on the distance and direction of the point movement. For instance, if the point moves with distance l in direction of x axis then the new location of this point would be $(i + l, j\ and\ k)$. In such case, if assumption that q stands for space and time estimated at a separate point in the web as well as discrete point in time as represent in equation (7.15).

$$q(i\Delta x, j\Delta y, k\Delta z, n\Delta t) = q^{n}_{i,j,k} \tag{7.15}$$

Where n is an integer and Δt is the time change is assumed uniform in excess of the observation time.

To clarify the Yee algorithm more, an example of one dimension (1D) space-time chart viewing middle differences for the space derivatives and leaping in excess of the time derivatives is introduced in Figure 7.3.

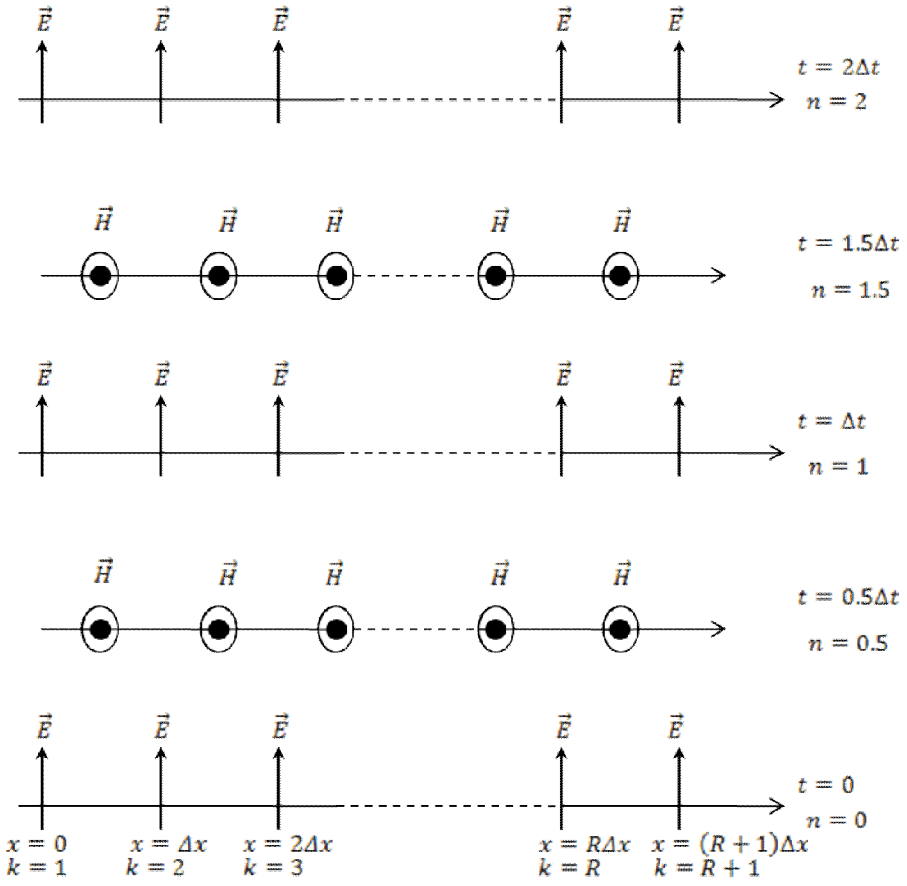

Figure 7.3:Example of one dimensional space time plan of the Yee algorithm; n is the time step and k signifies electric field node numbers

The cantered finite difference has been employed by Yee to demonstrate the space as well as time derivatives. Overall, it has indicated simply programmed and second order accurate in the area and time period additions. If assumed that his style of idiom for the fractional space derivative of in the -path which estimated at the constant time then the build equation is in (7.16).

$$\frac{\partial m}{\partial y}(i\Delta x, j\Delta y, k\Delta z, n\Delta t) = \frac{m^{n}_{i,j+\frac{1}{2},k} - m^{n}_{i,j-\frac{1}{2},k}}{\Delta y} + O[(\Delta y)^2)] \tag{7.16}$$

Clearly this equation shows a space finite difference over $\pm 1/2\Delta y$ with increasing $\pm 1/2$ in the j subscript (y-coordinate) of m. To further clarify the following example (7.17) shows the effect of increasing ± 2 in the i subscript (x-coordiante) of m, denoting a space finite difference over $\pm 2\Delta x$.

$$\frac{\partial m}{\partial x}(i\Delta x, j\Delta y, k\Delta z, n\Delta t) = \frac{m^{n}_{i+2,j,k} - m^{n}_{i-2,j,k}}{\Delta x} + O[(\Delta x)^2)] \tag{7.17}$$

In addition to that, the Yee term for the initial time partial derivative of m, demonstrated at the set space point (i, j, k), is given in equation (7.18).

$$\frac{\partial m}{\partial t}(i\Delta x, j\Delta y, k\Delta z, n\Delta t) = \frac{m^{n+1/2}_{i,j,k} - m^{n-1/2}_{i,j,k}}{\Delta t} + O[(\Delta t)^2) \tag{7.18}$$

It must be pointed out that the $\pm 1/2$ increment happens in the n evaluate (time coordinate) of m, represents the amount of a time finite difference over $\pm 1/2\Delta t$. Precisely, this information has been selected by Yee owing to realise a leapfrog algorithm in line with his $\vec{H}$ and $\vec{E}$ components in time at intervals of $1/2\Delta t$.

7.1.3 3D FINITE DIFFERENCE REPRESENTATIONS FOR MAXWELL'S EQUATIONS

In this stage, 3D finite difference could be phrased as a mathematical estimate of Maxwell's curl equations which have been discussed in equations (7.12) and (7.13). Consequently, equation (7.11b) and (7.12b) also must be taken into account. In order to simplify the idea more, instead of $\partial Hx, \partial Hy \; and \; \partial Hz$ as well as $\partial Ex, \partial Ey \; and \; \partial Ez$ will compensate similar to (7.19) [117-119]:

$$\frac{\partial Hx}{\partial t} = \frac{H_x|_{i,j,k}^{n+1/2} - H_x|_{i,j,k}^{n-1/2}}{\Delta t} \tag{7.19}$$

The same technique applies to the entire previous mentioned factor. Here should be addressed to the important issue which is H_x at time step n is not expected to be stored in the computer's memory. However, $n-1/2$ is supposed to be stored in PC's memory. Therefore, a method known as a semi-implicit estimate can be employed to solve this problem as indicated in equation (7.20).

$$H_x|_{i,j,k}^{n} = \frac{H_x|_{i,j,k}^{n+1/2} + H_x|_{i,j,k}^{n-1/2}}{2} \tag{7.20}$$

To driven the calculations, the following equation (7.21) illustrates clearly how to obtain the accurate equation for this issue.

$$\frac{H_x|_{i,j,k}^{n+1/2} - H_x|_{i,j,k}^{n-1/2}}{\Delta t} = \frac{1}{\mu_{i,j,k}} \times \begin{pmatrix} \frac{E_y|_{i,j,k+\frac{1}{2}}^{n} - E_y|_{i,j,k-\frac{1}{2}}^{n}}{\Delta z} - \\ \frac{E_z|_{i,j+\frac{1}{2},k}^{n} - E_z|_{i,j-\frac{1}{2},k}^{n}}{\Delta y} - \\ \acute{\rho}_{i,j,k} \times H_x|_{i,j,k}^{n} \end{pmatrix} \quad (7.21)$$

In the case of comparing between the two parties of the equation (7.21), note that all E magnitudes and H magnetic field occurrence because of the magnetic loss $\acute{\rho}$ are estimated at time step$'n'$. Just on a reminder, H_x is only imagined to be stored in the computer's memory at time step$n-1/2$. Therefore, equation (7.22) H_x at time step n has been estimated (semi-implicit).

$$H_x|_{i,j,k}^{n+1/2} - H_x|_{i,j,k}^{n-1/2} = \frac{\Delta t}{\mu_{i,j,k}} \times \begin{pmatrix} \frac{E_y|_{i,j,k+\frac{1}{2}}^{n} - E_y|_{i,j,k-\frac{1}{2}}^{n}}{\Delta z} - \\ \frac{E_z|_{i,j+\frac{1}{2},k}^{n} - E_z|_{i,j-\frac{1}{2},k}^{n}}{\Delta y} - \\ \acute{\rho}_{i,j,k} \times \left(\frac{H_x|_{i,j,k}^{n+1/2} + H_x|_{i,j,k}^{n-1/2}}{2} \right) \end{pmatrix} \quad (7.22)$$

Through this equation, in case of leaving this value $H_x|_{i,j,k}^{n+1/2}$ on the left side same as it is and move this amount $H_x|_{i,j,k}^{n-1/2}$ to the right direction; also taking this rate $\frac{\Delta t\, \acute{\rho}_{i,j,k}}{2\mu_{i,j,k}}$ as a common factor between them, then the new equation obtained is shown in equation (7.23).

$$H_x|_{i,j,k}^{n+\frac{1}{2}} + \frac{\Delta t\, \acute{\rho}_{i,j,k}}{2\mu_{i,j,k}} = H_x|_{i,j,k}^{n-\frac{1}{2}} - \frac{\Delta t\, \acute{\rho}_{i,j,k}}{2\mu_{i,j,k}} + \frac{\Delta t}{\mu_{i,j,k}} \left(\frac{E_y|_{i,j,k+\frac{1}{2}}^{n} - E_y|_{i,j,k-\frac{1}{2}}^{n}}{\Delta z} - \frac{E_z|_{i,j+\frac{1}{2},k}^{n} - E_z|_{i,j-\frac{1}{2},k}^{n}}{\Delta y} \right) \tag{7.23}$$

Through the apportionment of both parties to $(1 + \frac{\Delta t\, \acute{\rho}_{i,j,k}}{2\mu_{i,j,k}})$, the needed specific time stepping link for $H_x|_{i,j,k}^{n+1/2}$ is shown in equation (7.24).

$$
\begin{aligned}
&H_x|_{i,j,k}^{n+1/2} \\
&= H_x|_{i,j,k}^{n-1/2} \left(\frac{1 - \frac{\Delta t\, \acute{\rho}_{i,j,k}}{2\mu_{i,j,k}}}{1 + \frac{\Delta t\, \acute{\rho}_{i,j,k}}{2\mu_{i,j,k}}} \right) \\
&+ \left(\frac{\frac{\Delta t}{\mu_{i,j,k}}}{1 + \frac{\Delta t\, \acute{\rho}_{i,j,k}}{2\mu_{i,j,k}}} \right) \left(\frac{E_y|_{i,j,k+\frac{1}{2}}^{n} - E_y|_{i,j,k-\frac{1}{2}}^{n}}{\Delta z} - \frac{E_z|_{i,j+\frac{1}{2},k}^{n} - E_z|_{i,j-\frac{1}{2},k}^{n}}{\Delta y} \right)
\end{aligned}
\tag{7.24}
$$

Equations (7.25) and (7.26) show that the same way can be used to calculate the finite difference statements on the basis of Yee's algorithm for H_y and H_z signal specified by Maxwell's rules.

$$
\begin{aligned}
&H_y|_{i,j,k}^{n+1/2} \\
&= H_y|_{i,j,k}^{n-1/2} \left(\frac{1 - \frac{\Delta t\, \acute{\rho}_{i,j,k}}{2\mu_{i,j,k}}}{1 + \frac{\Delta t\, \acute{\rho}_{i,j,k}}{2\mu_{i,j,k}}} \right) \\
&+ \left(\frac{\frac{\Delta t}{\mu_{i,j,k}}}{1 + \frac{\Delta t\, \acute{\rho}_{i,j,k}}{2\mu_{i,j,k}}} \right) \left(\frac{E_z|_{i+\frac{1}{2},j,k}^{n} - E_z|_{i-\frac{1}{2},j,k}^{n}}{\Delta x} - \frac{E_x|_{i,j,k+\frac{1}{2}}^{n} - E_x|_{i,j,k-\frac{1}{2}}^{n}}{\Delta z} \right)
\end{aligned}
\tag{7.25}
$$

$$
\begin{aligned}
&H_z|_{i,j,k}^{n+1/2} \\
&= H_z|_{i,j,k}^{n-1/2} \left(\frac{1 - \dfrac{\Delta t\, \acute{\rho}_{i,j,k}}{2\mu_{i,j,k}}}{1 + \dfrac{\Delta t\, \acute{\rho}_{i,j,k}}{2\mu_{i,j,k}}} \right) \\
&+ \left(\frac{\dfrac{\Delta t}{\mu_{i,j,k}}}{1 + \dfrac{\Delta t\, \acute{\rho}_{i,j,k}}{2\mu_{i,j,k}}} \right) \left(\frac{\dfrac{E_x|_{i,j+\frac{1}{2},k}^{n} - E_x|_{i,j-\frac{1}{2},k}^{n}}{\Delta y} - \dfrac{E_y|_{i+\frac{1}{2},j,k}^{n} - E_y|_{i-\frac{1}{2},j,k}^{n}}{\Delta x} }{} \right)
\end{aligned}
\tag{7.26}
$$

In a comparable style, E_x, E_y and E_z have been found in equation (7.27), (7.28) and (7.29). But for this case, $\sigma E^{n+1/2}$ indicates the loss term on the right side of every equation.

$$
\begin{aligned}
&E_x|_{i,j,k}^{n+1} \\
&= E_x|_{i,j,k}^{n} \left(\frac{1 - \dfrac{\Delta t\, \sigma_{i,j,k}}{2\varepsilon_{i,j,k}}}{1 + \dfrac{\Delta t\, \sigma_{i,j,k}}{2\varepsilon_{i,j,k}}} \right) \\
&+ \left(\frac{\dfrac{\Delta t}{\varepsilon_{i,j,k}}}{1 - \dfrac{\Delta t\, \sigma_{i,j,k}}{2\varepsilon_{i,j,k}}} \right) \left(\frac{\dfrac{H_z|_{i,j+\frac{1}{2},k}^{n+1/2} - H_z|_{i,j-\frac{1}{2},k}^{n+1/2}}{\Delta y} - \dfrac{H_y|_{i,j,k+\frac{1}{2}}^{n+1/2} - H_y|_{i,j,k-\frac{1}{2}}^{n+1/2}}{\Delta z} }{} \right)
\end{aligned}
\tag{7.27}
$$

$$
\begin{aligned}
&E_y|_{i,j,k}^{n+1} \\
&= E_y|_{i,j,k}^{n} \left(\frac{1 - \frac{\Delta t\, \sigma_{i,j,k}}{2\varepsilon_{i,j,k}}}{1 + \frac{\Delta t\, \sigma_{i,j,k}}{2\varepsilon_{i,j,k}}} \right) \\
&+ \left(\frac{\frac{\Delta t}{\varepsilon_{i,j,k}}}{1 - \frac{\Delta t\, \sigma_{i,j,k}}{2\varepsilon_{i,j,k}}} \right) \left(\frac{H_x|_{i,j,k+\frac{1}{2}}^{n+1/2} - H_x|_{i,j,k-\frac{1}{2}}^{n+1/2}}{\Delta z} - \frac{H_z|_{i+\frac{1}{2},j,k}^{n+1/2} - H_z|_{i-\frac{1}{2},j,k}^{n+1/2}}{\Delta x} \right)
\end{aligned}
\tag{7.28}
$$

$$
\begin{aligned}
&E_z|_{i,j,k}^{n+1} \\
&= E_z|_{i,j,k}^{n} \left(\frac{1 - \frac{\Delta t\, \sigma_{i,j,k}}{2\varepsilon_{i,j,k}}}{1 + \frac{\Delta t\, \sigma_{i,j,k}}{2\varepsilon_{i,j,k}}} \right) \\
&+ \left(\frac{\frac{\Delta t}{\varepsilon_{i,j,k}}}{1 - \frac{\Delta t\, \sigma_{i,j,k}}{2\varepsilon_{i,j,k}}} \right) \left(\frac{H_y|_{i+\frac{1}{2},j,k}^{n+\frac{1}{2}} - H_y|_{i-\frac{1}{2},j,k}^{n+\frac{1}{2}}}{\Delta x} - \frac{H_x|_{i,j+\frac{1}{2},k}^{n+1/2} - H_x|_{i,j-\frac{1}{2},k}^{n+1/2}}{\Delta y} \right)
\end{aligned}
\tag{7.29}
$$

In 1982, the total and scattered field modulations have been recorded in the science history [3]. In particular, the simulation's result of sinusoidal stable condition has been recorded by a lot of experiences to recognise a compact signal exporter. Obviously, the widespread FDTD scattering software package has been used this formularization up to now. Actually, this logic has been determined on the linearity of Maxwell's rule as well as corruption

of the magnetic and electric fields. The following equations (7.30) and (7.31) give a clear conception about it.

$$\vec{H}_{tot} = \vec{H}_{inc} + \vec{H}_{scat} \tag{7.30}$$

$$\vec{E}_{tot} = \vec{E}_{inc} + \vec{E}_{scat} \tag{7.31}$$

Ideally, the amount of the incident wave fields $\vec{H}_{inc}$ and $\vec{E}_{inc}$ could be considered as a known value at whole space points and time steps of the FDTD lattice. On the other hand, $\vec{H}_{scat}$ and $\vec{E}_{scat}$ are unknown value of the scattered signal fields which outcome from the reaction of the incident wave with any items in the network.

The solution of 3D structure problems in electromagnetic are just one of the trouble that FMs could be functional to. Meanwhile, because of the impossibility to expand mesh of the computational domain to infinity, the boundary condition should be applied to simulate the effect of the infinite domain. On the other hand, the vector absorbing boundary conditions (ABCs) could be used to solve the radiation and scattering problems for 3D models. Here, it should be addressed that the ABC is normally employed to resection the computational area, especially when the Yee algorithm could not be used to update the tangential components of the exciting filed beside the surface boundary of the computational field [3-7].

In application after application, ABCs are very important into the problem space to carry on departing E and H fields as well as prevent them from reflecting back. In the essential statement of the FDTD method, the surrounding H values are being required to calculate the E field. The concept of employing ABCs material has been found, though, these materials did not afford enough small of boundary reflection. In particular, this is because of the substance boundary impedance has been corresponded to free space impedance at standard occurrence. While, much research was done to modify these materials, a perfectly matched layer (PML) method has been found by Berenger in 1994. In fact, PML has been used as a substance absorber; therefore, it has been indicated to supply much preferable exactness than mainly other ABCs [3, 114, 120].

Berenger assumed a “split-field” addition of Maxwell’s equations that confirms the electromagnetic signal phase rate inside the PML area is equivalent as in free space for the entire frequencies and whole angles of incidence. There is no doubt, in the PML section, a huge quantity of loss could occur, but not influencing the phase velocity. Continuously, the PML area which is wrapping the computational domain will be able to end with a perfect electric conductor (PEC). Consequently, the reflections which recovered from this PEC could be sending it again to the interior computational space; nevertheless, it is normally small. On the implementation, a PML is just “perfect” in the continuous scholar and either in discrete structure is not ideal. An abstract PML method has been

developed to use in a lot of networks with planar interfaces outside the model Yee lattice [121, 122].

Noticeably, there is a continuous change in the electronic devices development as if they are in a raise with the time speed, typical engineering investigation equipment have become out of date [32]. More and more aspects of concerned consuming devices of electrical units are owed to increase the frequency of the operation.

Regardless of whether the electrical power consumed by devices is small or large, these issues have produced huge computational areas; this in itself needs large quantity of computational facilities like memory and implementation time [3, 32]. On the other hand, the electromagnetic difficulty such as scattering, radiation, wave-guiding and so forth are not being easy to model statistically, contain and overcome or ignoring it i.e. the plurality of the asymmetrical geometries which have been found in the real devices. Moreover, it is an extremely demanding function to mount the RFID tag antenna design either on or in the human body because of its multi-dimension character. So it requires an intelligent system, like computer to model, simulate and solve these problems.

It is worth mentioning that the computational electromagnetic (CEM) is a technique which uses a digital computer to simulate and obtain numerical results for electromagnetic problems. It is observed that it is descended

from mathematical analysis and experimental observation methods. At some point, the obtained results have been confirmed by comparing the analysis and CEM results with the experimental results, or employ the analysis and/or CEM to predict the experimental results. Generally, there are two CEM numerical methods have been appeared to analysis and design the antennas. The method of moments (MoM) and finite difference time-domain (FDTD) are presented as shown in Figure 7.4 [3-7].

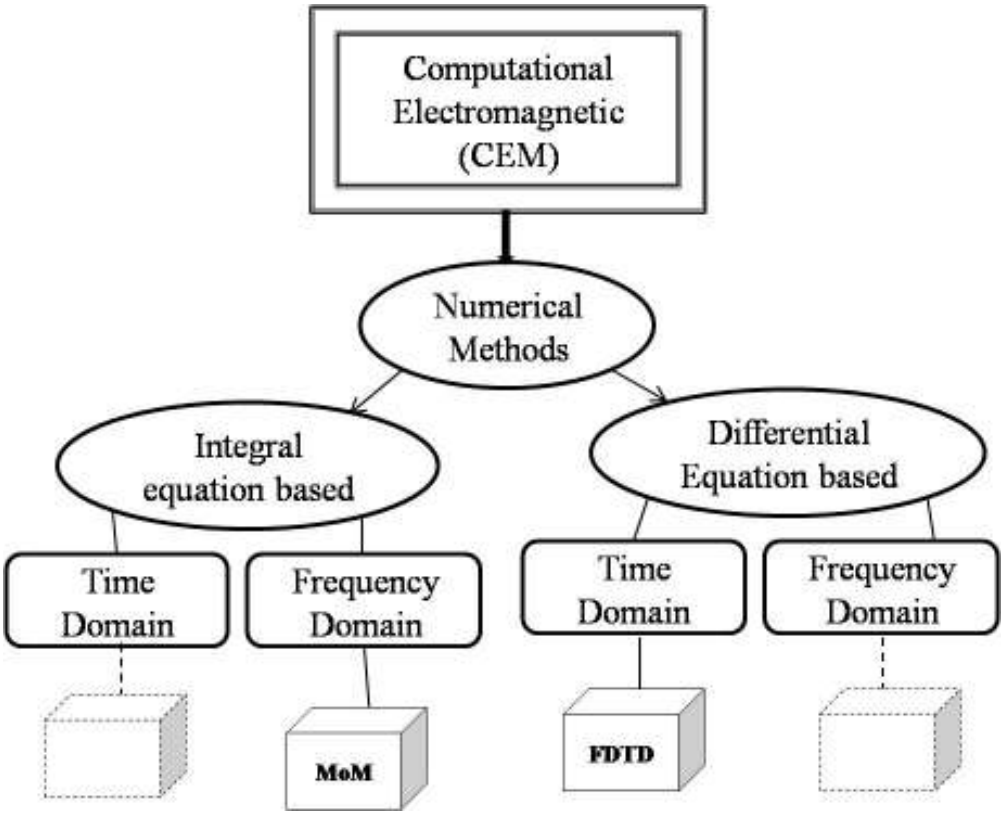

Figure 7.4:FDTD and MoM categories

As seen from Figure 7.4, the numerical methods can be seen as an integral equation based or differential equation based. Furthermore, both of them have been divided into frequency domain and time domain. In this research,

the integral equation based by employing frequency domain i.e. MoM and the differential equation based by placing the time domain i.e. FDTD been investigated [123]. It can be seen that the integral equation could be establish in term of time domain, for example, the space time integral equation; while, the differential equation based could be built with frequency domain, for example, the finite element methods (FEM). Presently the FEM have become a popular used method and it is considered the essential method in scattering problems.

In terms of the unidentified current ($I_{(z')}$), an integral equation with a structure of simultaneous linear algebraic equations can be solved by using MoM. Hence, the radiation pattern and impedance could be obtained easy owing to the recognised current.

The computational numerical methods could conquer the incapability to make similar shape solutions of Maxwell's equations below different constituent relatives of media and boundary conditions. The experimental, analytical or numerical technique has been used to solve the field problem. In reality, the numerical method has been applied before starting the experiments or practical parts. Eventually, the time loosing, the high cost, the risk, the limitation in parameter, and so forth have been avoided by implementing practical model that matches as possible the exact real time problem.. The analytical techniques are more accurate solution while the numerical methods are the estimated ones [124].

A sinusoid or a transient pulse can be used as a signal to excite the computational area. In fact, the exact frequency has been specified for most of the cases; therefore, a sinusoid source is the suitable one to use. Moreover, the using of transient pulse provides establishing the scattering response in excess of the whole bandwidth of the pulse. It is noted in a recent article [125], that the computational electromagnetic technique, Finite difference time domain (FDTD) has been used by almost all researchers to model the biological tissue.

The common finite techniques such as FDTD method and the finite element method (FEM) are second command accurate, limiting the size of the domains that could be controlled efficiently [3, 114]. In addition, Computational electromagnetic (CEM) is a widespread technique, easy to recognise and simple to implement in software. In such a system, the simulation results are able to cover a large frequency range through a single simulation run [7].

The FDTD method can be seen as a very significant procedure in wireless communications area, which could be used as a creating and general analytical device owing to its relative ease, strength and ability for holding inhomegeneity inside volumetric difficulty [3, 126]. In particular, the relation of the computational work size to the number of the individual components has been minimised. Therefore, a comparatively high resolution

of the head in a three-dimensional (3D) can be handled in a feasible timescale.

Ideally, since the head representation has been become more realistic than the handset and the antenna or the RFID tag's antenna which can be created with more and more operation degree of clarity .The reason goes back to the simplicity of the antenna representation compared to the head. In view of the fact that the FDTD technique symbolises all structures as a standard matrix of rectangular parallelepipeds, it gives a very scratchy depiction of a good building wire. Undoubtedly, it is noted that the head has been optimised by FDTD through using the hybrid designs. Whilst, the handset has been illustrated by the Method of Moments (MoM) which allows basically random shapes of conducting designs. Reference [123] describes a numerical solution utilizing the frequency-domain MoM and polynomial basis functions in a Galerkin solution. Such systems are able of simulating conducting surfaces, wire, strip and small regions of inhomogeneous dielectric. Anyway, the dielectric could not normally be optimised in this case. Consequently, it has been decided to use hybridise FDTD with integral-equation time-domain (IETD) technique in this research.

According to Ying [125], the hybrid methods confirm enhanced accuracy and practicality in conditions of computational resources at the same time while FDTD is simply functional to a small part of the whole design prototype. According to that the combining of FDTD with the frequency –

domain method of moments have been employed to overcome these problems [3, 126].

It is worth mentioning that a way has been established to create the network of the FDTD method conformal in the form of arbitrary of shaped metallic systems. Notice that the resolution should be relatively small if the finer details are epitomised. Consequently, the computer running time might be relatively long. So, the hybrid system is the best in the event that a short run times are needed.

The Finite element method (FEM) is used to locate estimated solution of partial differential equations (PDE) and integral equations. Based on the Integral Equation Methods, the purpose of this process is integrating the reaction of all the (discretised) sensor sections of the physical structure of an electromagnetic system with each of the same (discretised) sensor pieces. Commonly, it happened in sequence with the differential equation methods [126]. In fact, the far-field has been expected to found when successfully both an amplitude and phase data obtained from the near-field measurements [120].

Reference [120] reported on near- field and far-field transformation algorithm employing plane wave development which has been given and implemented to the situation of spherical near – field measurements. Commonly, the direction, location, field power, and frequency of the

practical field are depending on the substance properties of the medium ε, σ and μ.

7. 2 MODELLING AND RESULTS

The RFID antennas adopted in this study have been previously described in chapter three. The Meander antenna, Linear polarised, and a Cross RFID antenna, Circular polarised, which has been designed, investigated and implemented are reused in this chapter to test the antenna efficiencies when it is attached to the human body.

The human body model has been generated through the Fortran code. In particular, the human skin and the organs have been modelled with the nearest human specifications. Specifically, the head, tummy, chest, legs, hands and other organs have been carefully seen from the simulation results. Moreover, the six millimetres cell has been used to model the human body and the organs. In such a program, a hybrid computational method has been implemented. The efficiency models have been measured by the interaction between a meander RFID antenna placed in proximity with the human body.

The place of the mounted RFID antennas inside equivalent surface enclose has been developed in a bigger size than the maximum dimension of the tag. Undoubtedly, the antenna direction whether vertical or horizontal polarisation is affected directly by the size of the box because the proposed

antenna is in a rectangular shape. Therefore, the changing of the antenna orientation needs to change the box parameters. However, it should be taken into account that the antenna centre i.e. feeding point should be in the middle of the box. Figure 7.5 represents the program flow chart.

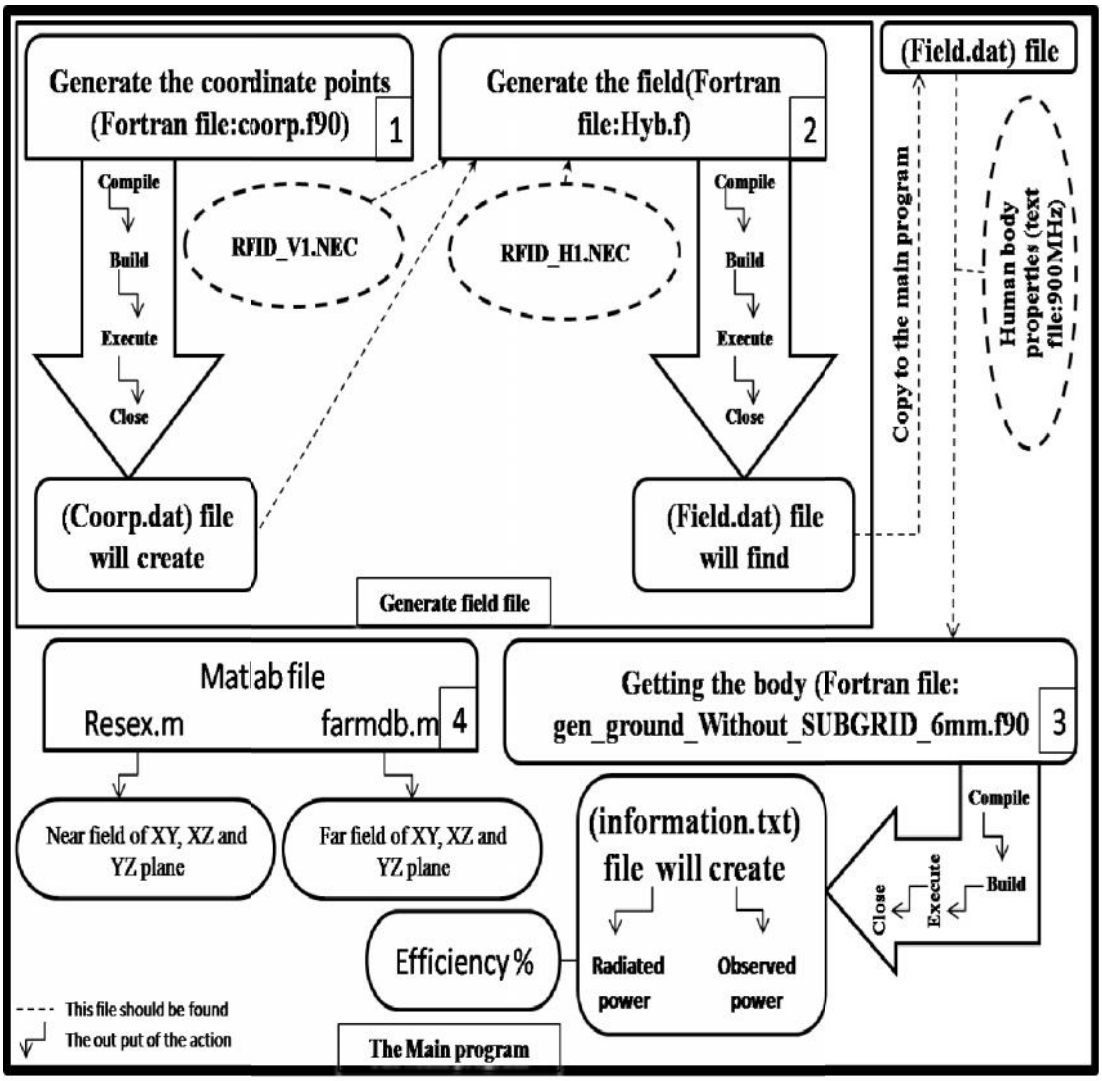

Figure 7.5:The program flow chart

Furthermore, the box location has been moved from one point to another one attached to the head, back, chest, tummy, legs and other points in the

organs. It is assumed that each region of those organs has many points on which to place the box in order to cover all of the targeted areas. Moreover, sixteen points have been taken to cover the back section of the human body, while eight points have been tested on the tummy similar to the chest. In each point, the coordinate and hybrid Fortran program have been complied, built and executed.

The NEC-files of the optimum RFID tag antenna in both polarisation (horizontal and vertical) have been placed in the same directory of the generate field folder, which consists of the coorp.f90 (this file is used to generate the surface geometry of the hygence surface) and hyb.f (this file to compute the incident fields on the hygence surface). In the begging of the program, the coordinate points have been generated by complied, built, executed the coorp.f90 file, after that, the data will transfer to the MoM code. To check the validity of this procedure, the coorp.dat file, which is the coordinate of used RFID antenna can be found in the same directory. Moreover, this file is needed in the second step as well. Secondly, the same procedure has been done with the hyb.f file, but the optimum RFID antenna (NEC file) has been located in the same directory previously. Furthermore, the horizontal and vertical RFID antenna must be found in the NEC file form and saved at the same directory. It is worth mentioning that the Field.dat file, which consists from coorp.dat and Ex,z and Hx,z as magnitude and phase value has been formed. Figure 7.6 displays the file form.

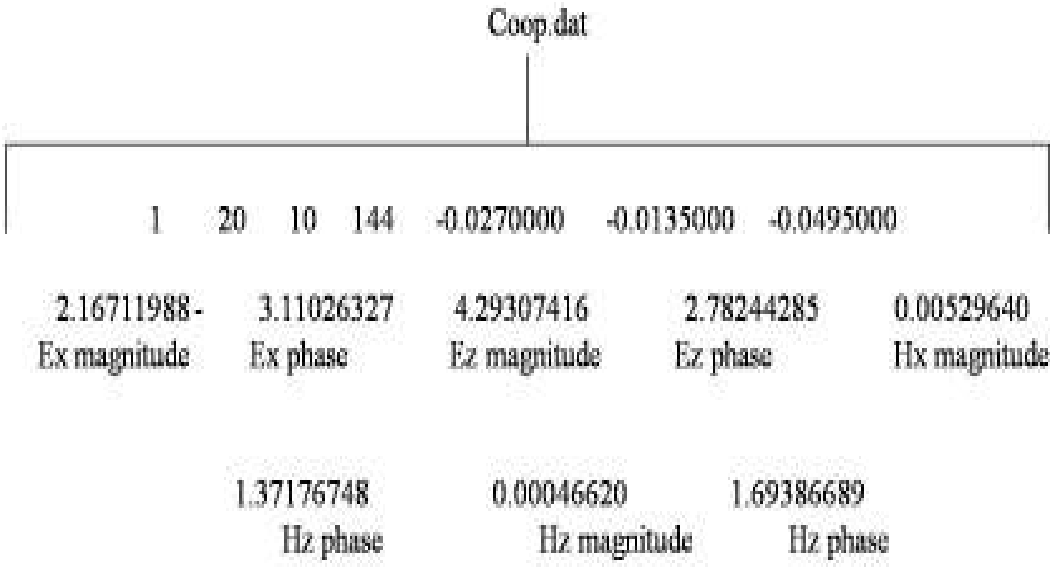

Figure 7.6: The created Field file explanation

The Ez and Hz directions inside the box are indicated in Figure 7.7 as well as Ex and Hx.

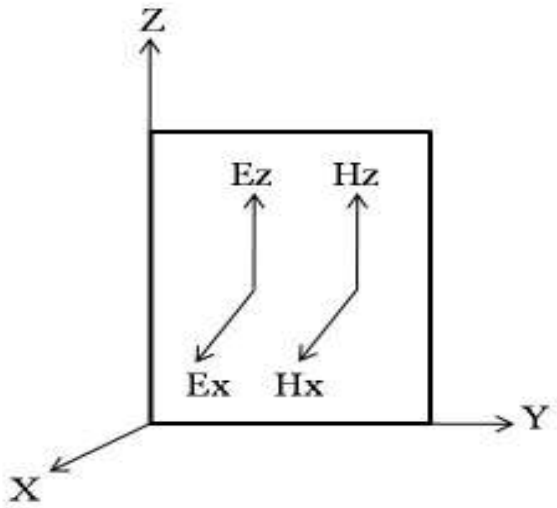

Figure 7.7:The Ez and Hz position

The modified of the 900MHz.txt file is copied to the main file directory. The gen_ground_without_sugrid.f90 file should be located at the main

program director. As a result from comply, build and execute this file, the information.txt file should be immediately created inside its directory. The electrical potential characteristics of the human body tissues at 900*MHz* with the external and internal air have been presented in Table 7.1.

Table 7.1: Tissue types and there permittivity, Conductivity and density at 900 *MHz*.

Tag No.	**Tissue name**	**Permittivity** $\boldsymbol{\varepsilon_r}$	**Conductivity** $\boldsymbol{\sigma}\ (\frac{\boldsymbol{S}}{\boldsymbol{m}})$	**Density** $\boldsymbol{\rho}\ (\frac{\boldsymbol{kg}}{\boldsymbol{m^3}})$
0	AIR.(external)	1	0	1.3
1	AIR.(internal)	1	0	1.3
2	BILE	70.19	1.838	1010
3	BODY.FLUID	68.90	1.636	1010
4	EYE.(cornea)	55.24	1.394	1076
5	FAT	5.462	0.05104	916
6	LYMPH	59.68	1.039	1040
7	MUSCOUS.MEMBRANE	46.08	0.8448	1040
8	NAILS.(toe.&.finger)	12.45	0.1433	1030
11	NERVE.(spine)	32.53	0.5737	1038
17	MUSCLE	55.03	0.9430	1047
25	HEART	59.89	1.230	1030
30	WHITE.MATTER	38.89	0.5908	1038
48	STOMACH	65.06	1.187	1050
49	GLANDS	59.68	1.039	1050
65	BLOOD.VESSEL	44.78	0.6961	1040
68	LIVER	46.83	0.855	1030
88	GALL.BLADDER	59.14	1.257	1030
108	SPLEEN	57.18	1.273	1054
110	CEREBELLUM	49.44	1.263	1038
111	BONE.(cortical)	12.45	0.1433	1990
133	CARTILAGE	42.65	0.7824	1097

142	LIGAMENTS	45.83	0.7184	1220
143	SKIN/DERMIS	41.41	0.8668	1125
148	INTESTINE.(large)	57.94	1.080	1043
152	TOOTH	12.45	0.1433	2160
160	GREY.MATTER	52.73	0.9423	1038
163	EYE.(lens)	46.57	0.7934	1053
164	LUNG.(outer)	51.42	0.858	1050
168	INTESTINE.(small)	59.49	2.165	1043
183	EYE.(sclera/wall)	55.27	1.167	1026
184	LUNG.(inner)	22	0.4567	260
188	PANCREAS	59.68	1.039	1045
189	BLOOD	61.36	1.538	1058
190	CEREBRAL.SPINAL.FLUI	68.64	2.413	1007
203	EYE.(retina)	55.27	1.167	1026
204	EYE.(aqueous.humor)	68.9	1.636	1009
207	KIDNEYS	58.67	1.392	1050
209	BONE.MARROW	5.504	0.04022	1040
227	BLADDER	18.94	0.3831	1030
228	TESTICLES	60.55	1.210	1044
253	BONE.(cancellous)	20.79	0.34	1920

The check points of RFID tag antenna position on the human body in the front and back side have been illustrated in Figure 7.8. In addition, the equivalent Huygence surface with double line meander RFID tag radiator i.e. linear polarisation for both vertical and horizontal orientations have been demonstrated as well.

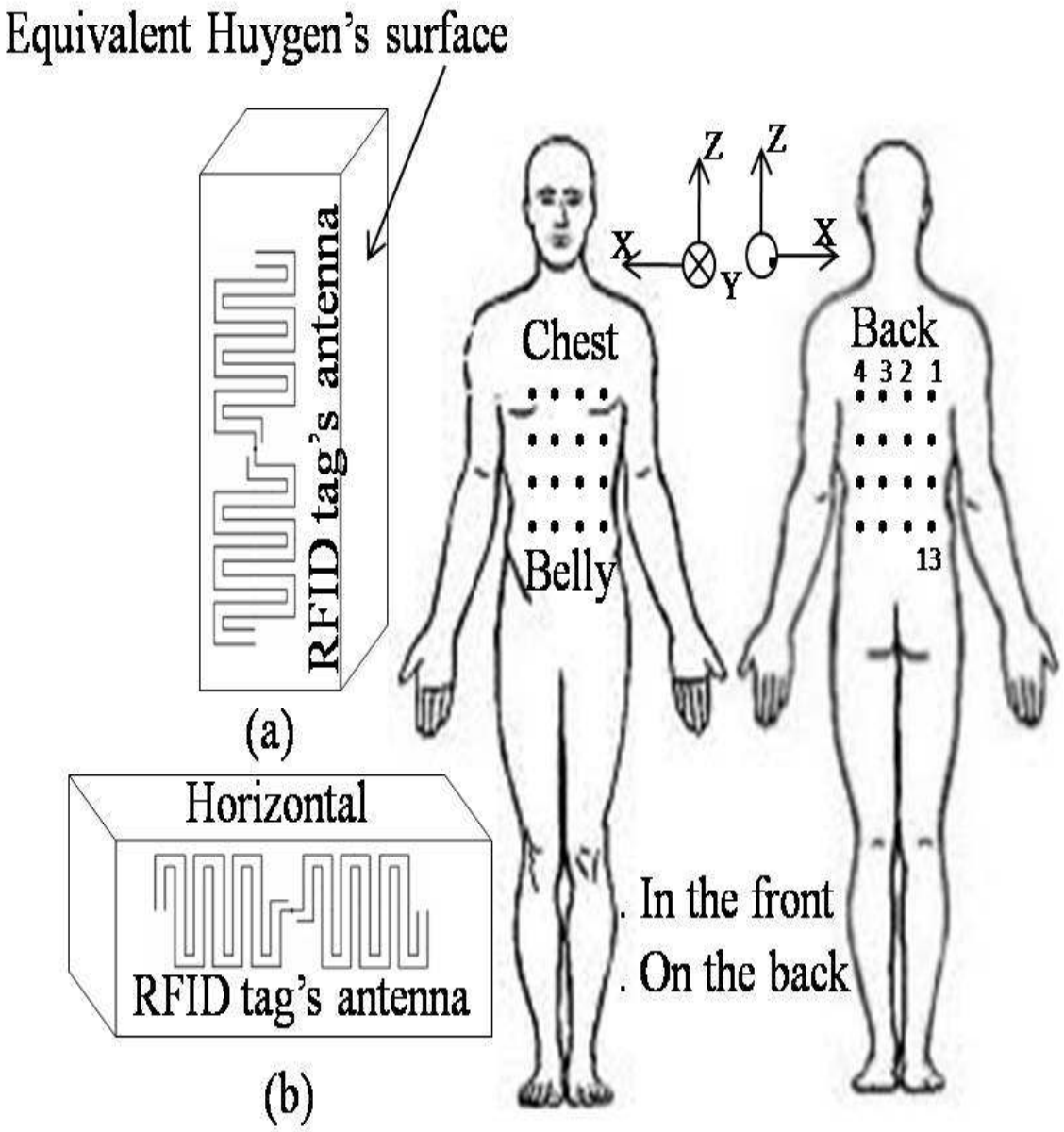

Figure 7.8:Human body design and the RFID tag's antenna positions; a) Vertical position, b) Horizontal position

The visualization of the final work program which has been prepared for the experiment i.e. the position of the human body, FDTD, PML, the ground and the RFID tag sensor summarised in Figure 7.9.

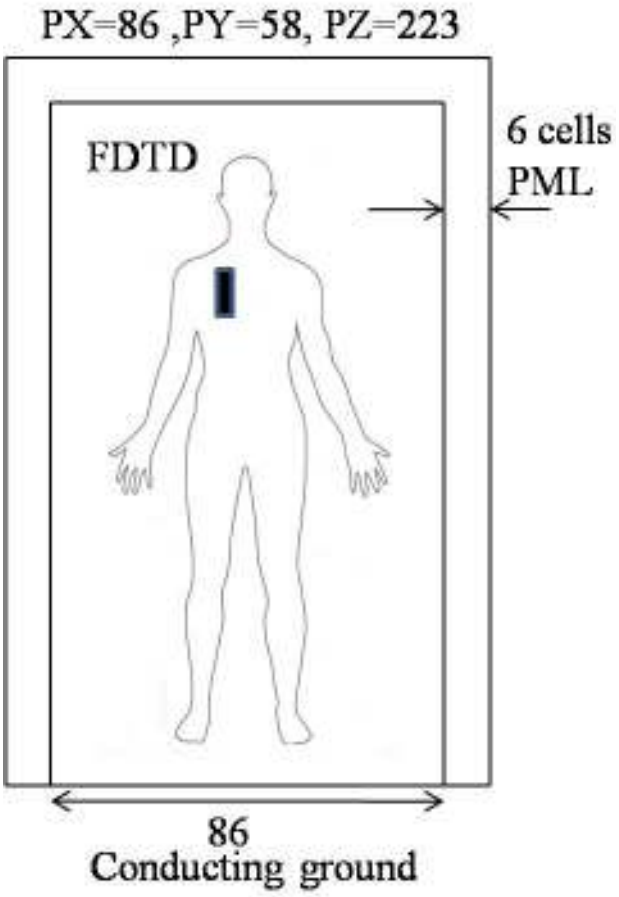

Figure 7.9:The RFID tag's antenna location and direction at the human body, FDTD and PML

7.2.1 THE HUMAN BODY DESIGN

The human body form in x-y plane at various vertical distances at cell number zc=35 near the bottom, zc=150 at the middle and the tummy while zc is about 200 have been drawn in Figure 7.10.

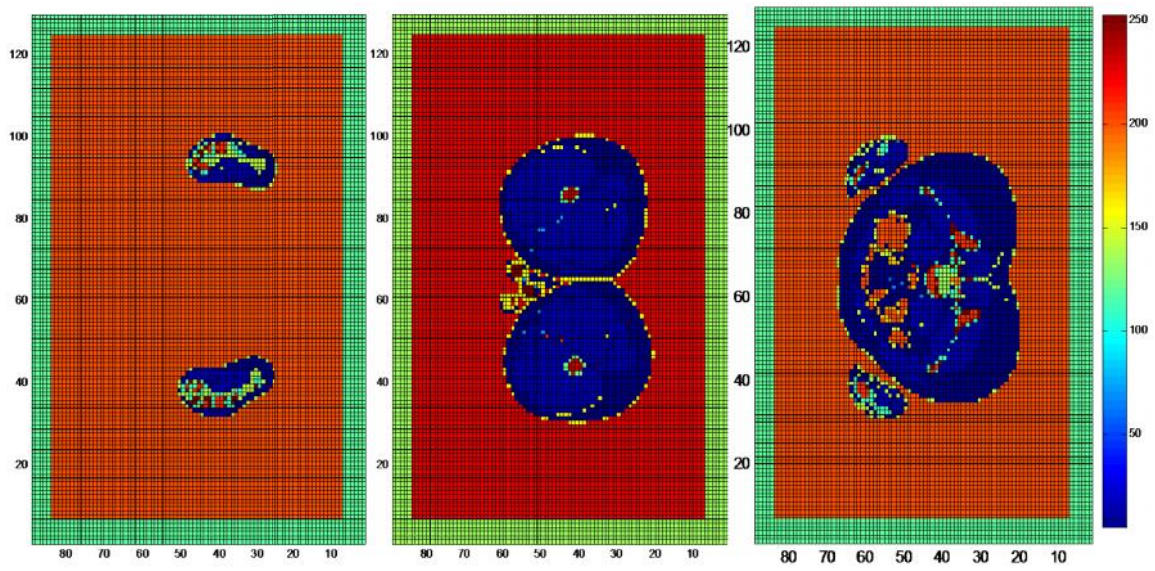

(a) (b) (c)

Figure 7.10: The human body design in x-y plane of the human body model used at (a) zc=35 near the foot, (b) zc=150 at the middle and (c) zc=200 the tummy

It is worth mentioning that the cross sections in the upper parts of the human body in different position at the top view have been taken. In order to compare different parts in the human body the x-y plane at zc is equal 220, 250 and 300 as shown in Figure 7.11; to indicate the thickness of the fat tissues that plays important role on the induced emf.

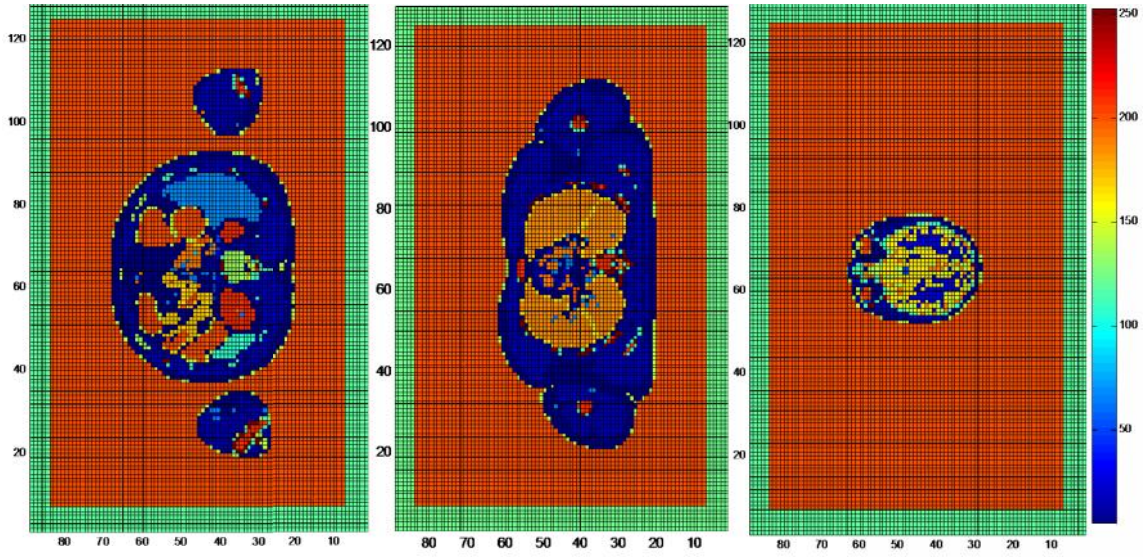

(a) (b) (c)

Figure 7.11: Different slides for xy plane at (a) zc=220 at the tummy, (b) zc=250 at the chest and (c) zc=300 the brain

The side view from the left of the human body to the right i.e. y-z plane has been explored. Therefore, Figure 7.12 expound from right till the middle which shown clearly the right shoulder at xc=110, between middle and right side at xc=50 and nearly in the middle at xc=67. As noted when x is equal to 50 the backbone and human anatomy from the middel has been photographed clearly.

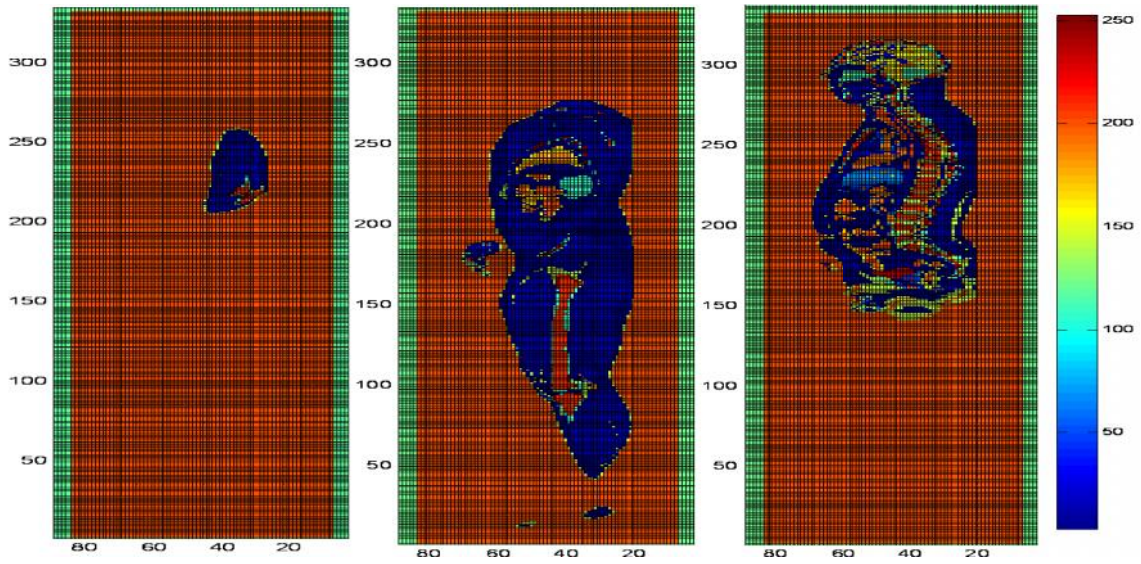

(a) (b) (c)

Figure 7.12:The human body model in y-z plane of the computation domain Cross section at: (a) xc=110 right shoulder, (b) xc=50 deeper in the right side and (c) xc=67 the middle

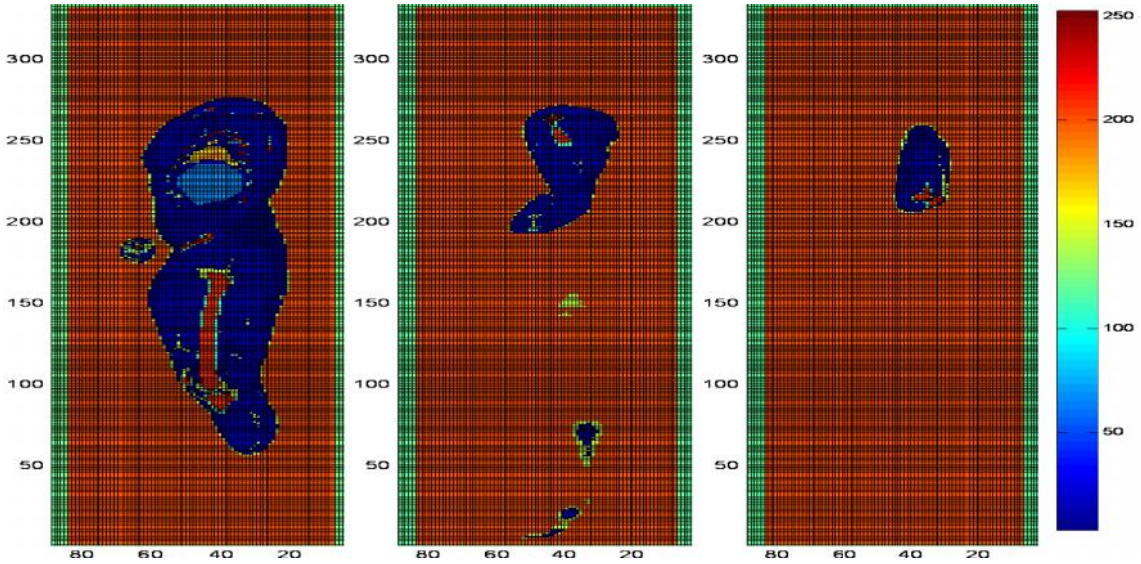

(a) (b) (c)

Figure 7.13:The human body model in y-z plane of the computation domain Cross section at: (a) xc=45 in the middle, (b) xc=35 the left foot and (c) xc=22 the left shoulder

While when xc= 45 the side view between the middle and the left side, the left foot and shoulder at xc=35 and the right shoulder at xc=22 have been represented in Figure 7.13.

The back side of the human body in term of x-z plane when y is equal to twenty (growths body background), when yc=40 in the middle has been anatomised in Figure 7.14. The lungs, rib cage, parts of vertebral column and the brain can be seen.

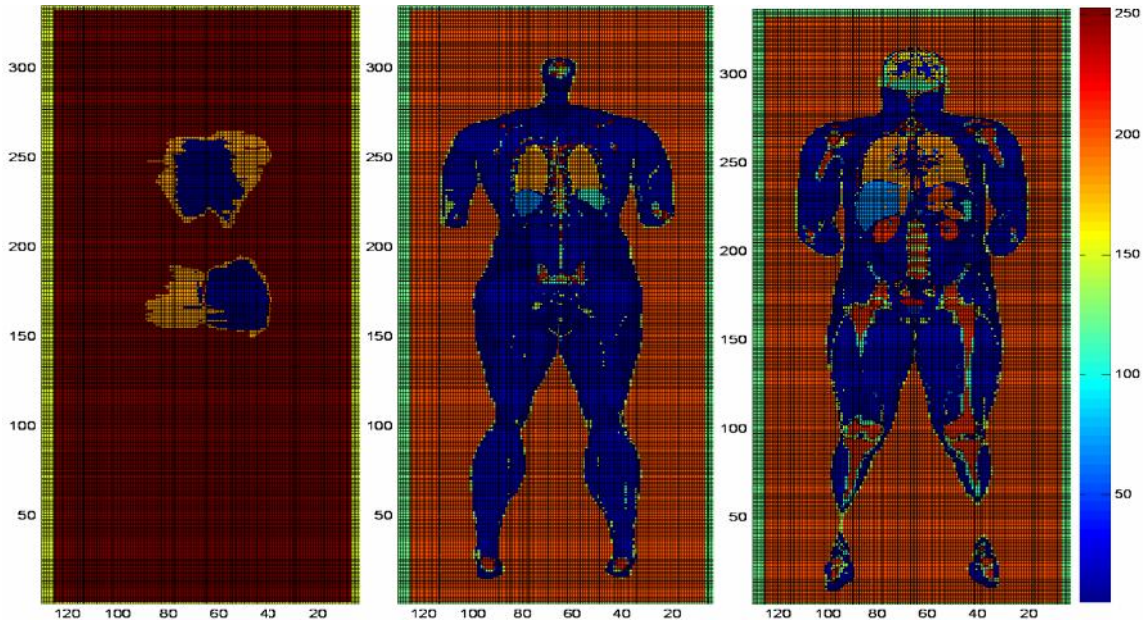

(a) (b) (c)

Figure 7.14:The human body design in x-z plane of the computation domainCross section at : (a) yc=20 the back of the human body, (b) yc=30 the back and (c) yc=40 the middle

As for the front section of x-z plane, Figure 7.15 shows the output format of the middle of the human body when yc is equal to 47. Furthermore, the

section on the front parts of the body when yc is equal to 55 and 60 has been defined and the intestine has been visible.

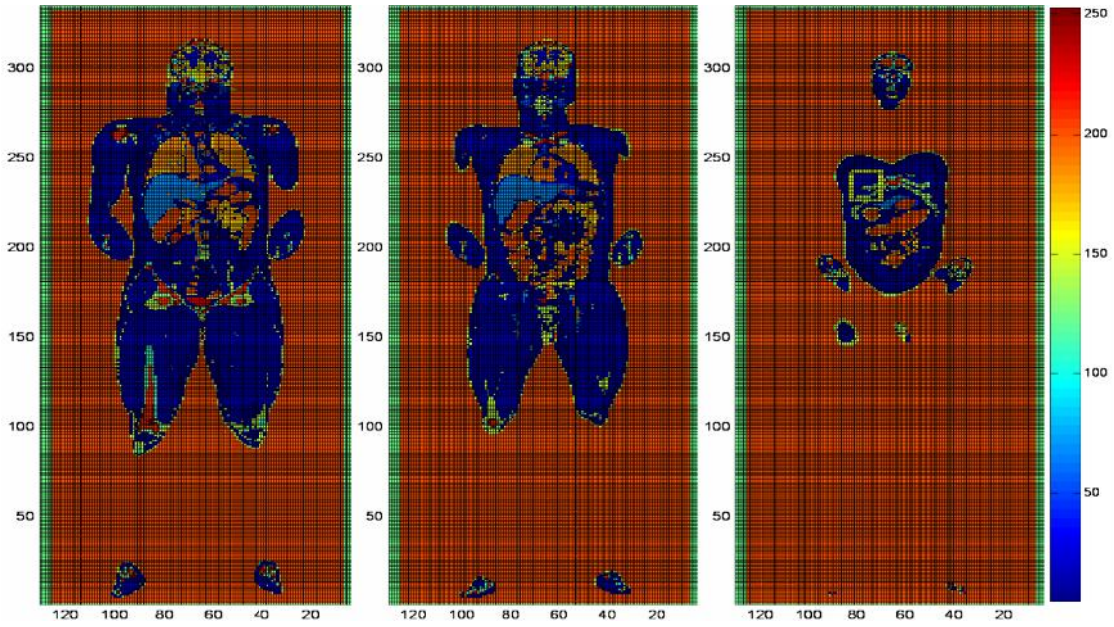

(a) (b) (c)

Figure 7.15:The human body model in x-z plane of the computation domain Cross section at: (a) yc=47 the middle, (b) yc=55 the front and (c) yc=60 the front

7.2.2 THE ELECTRIC FIELD DISTRIBUTION

The total electrical field distributions including the human body have been studied when the RFID tag antenna is mounted close to the human skin. On the whole, the intensification of the strong electric field intensity is shown in Figure 7.16 that states the total electrical electric in *dB* normalised to 1 watt input power; when the RFID tag's sensor placed at horizontal position on the back side at location point number 16. In addition, y-z, x-z and x-y plane are indicated in a, b and c consecutively.

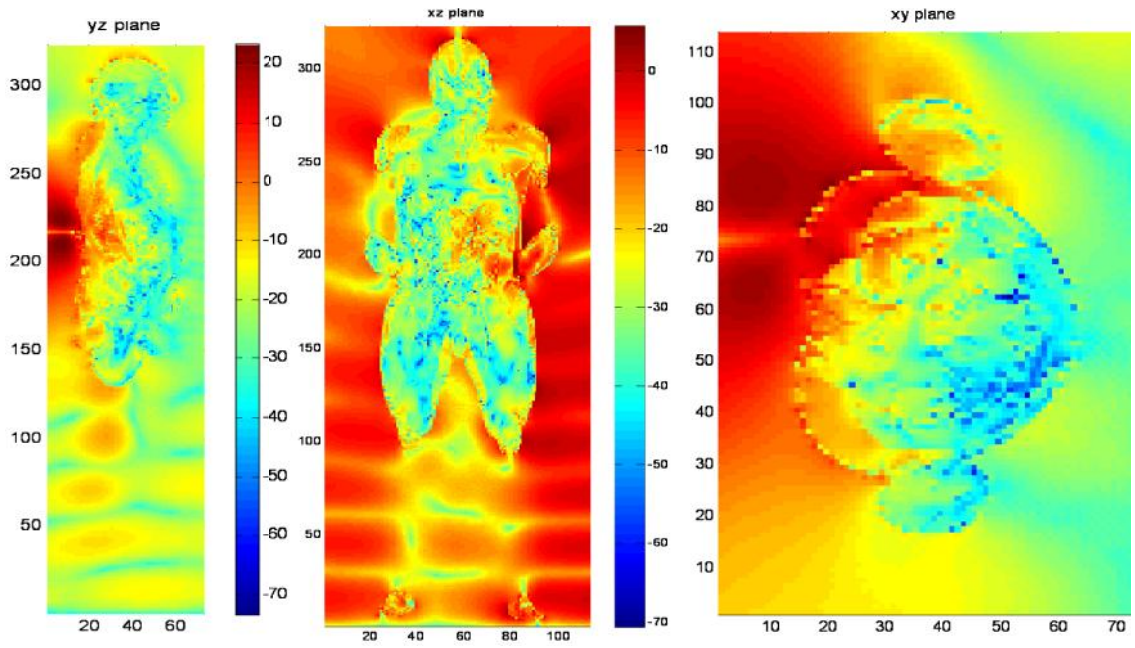

(a) (b) (c)

Figure 7.16:Total electrical fields in *dB* when the RFID tag's antenna located in horizontal position at the back of human body for location position number 16: (a) y-z plane, (b) x-z plane and (c) x-y plane

To study the situation more, the distribution of the total electrical field for back side has been observed at location position number 8 is shown in Figure 7.17.

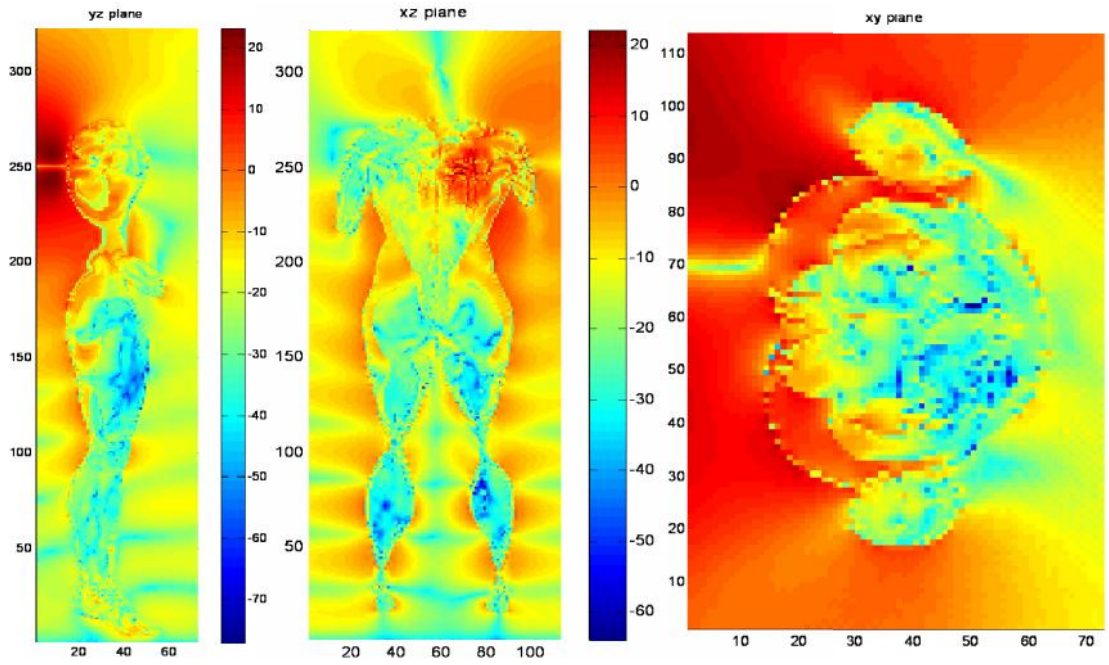

(a) (b) (c)

Figure 7.17:The Electric field distribution for horizontal polarised antenna placed at the back of the human body at location position 8.

Similarly, the electrical field distribution at the front side of the human body for location position number 5 has been demonstrated in Figure 7.18. The affect of the antenna to the human body when the sensor in vertical position such as that at chest point number 4 has been indicated in Figure 7.19; to clarify the and confirm the influence of the tag position on the electric fields intensities compared to the previous position located at the back model.

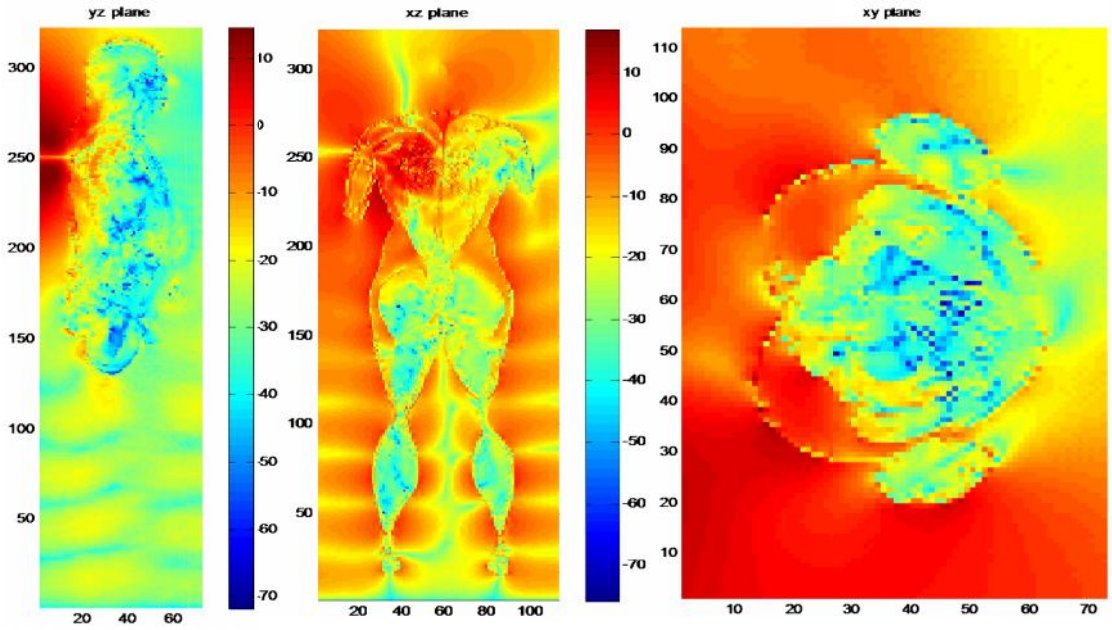

(a) (b) (c)

Figure 7.18:The Electric field distribution for vertical polarised antenna placed at the back of the human for location position 5.

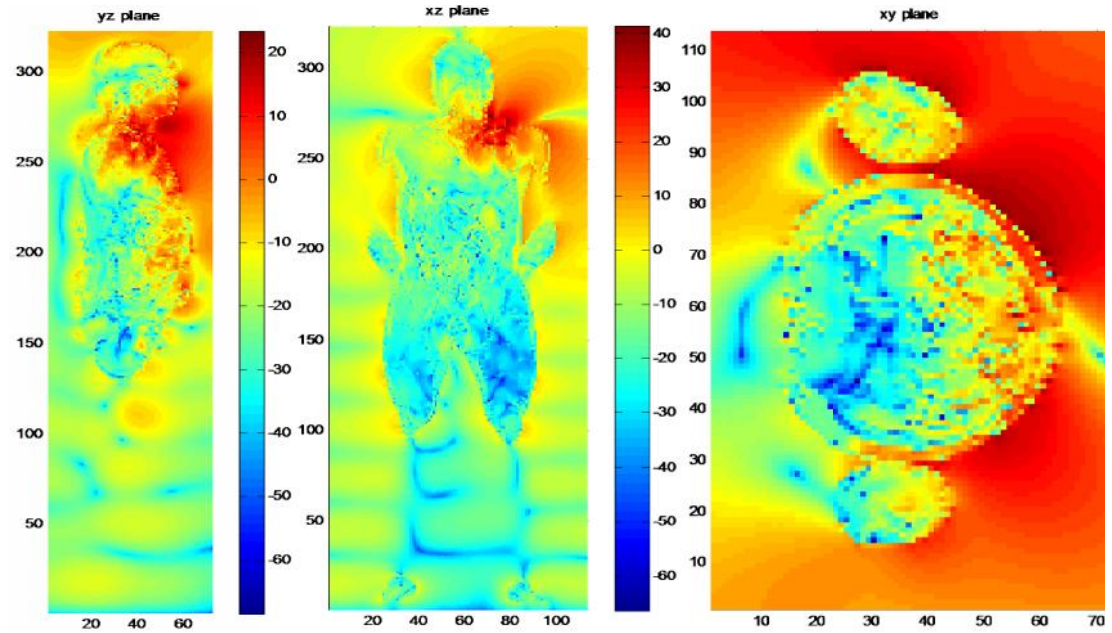

(a) (b) (c)

Figure 7.19:The Electric field distribution for vertical polarised antenna placed at the chest of the human for location position 4.

On the other hand, the effective of the circular RFID tag antenna to the human body is very challenging for this study since in most scattering problem this type of polarisation is recommended. Figure 7.20 demonstrates the field's distributions at the back side of the human body for location position 1. In addition, the field distribution at the front side whereas the tag antenna placed at chest level of location position 1 has been shown in Figure 7.21.

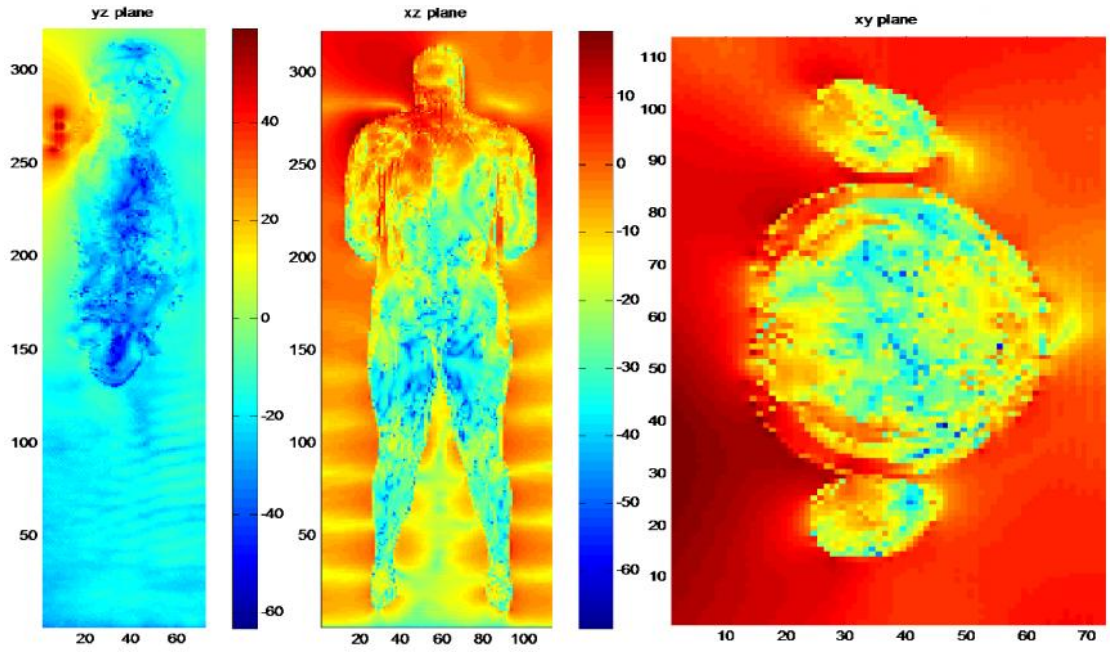

(a) (b) (c)

Figure 7.20:The Electric field distribution for circular polarised antenna placed at the back of the human for location position 1.

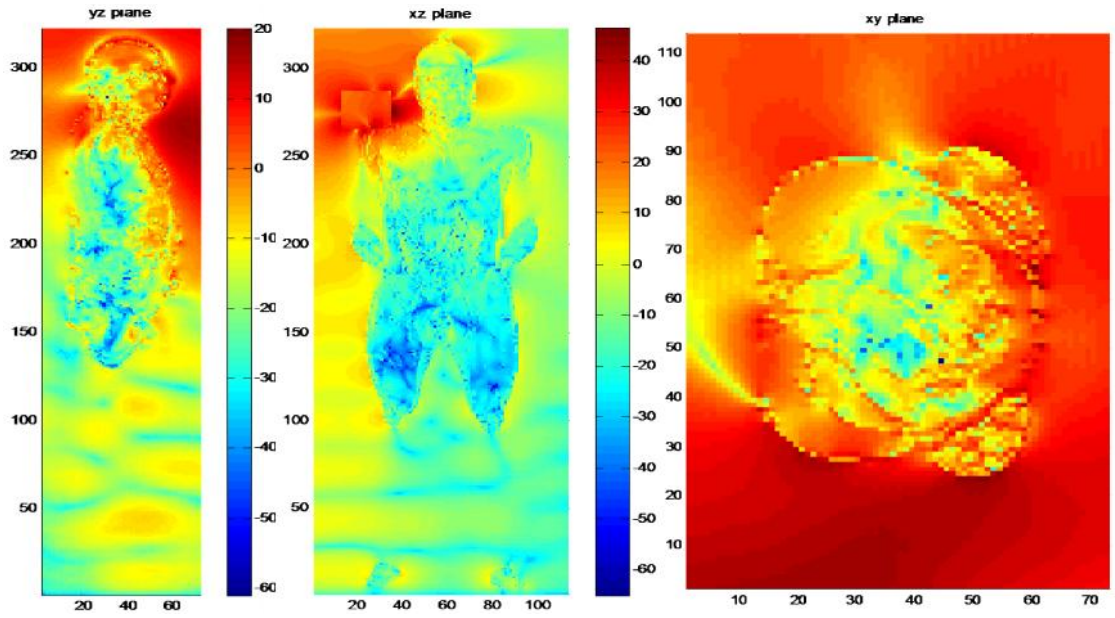

(a) (b) (c)

Figure 7.21:The Electric field distribution for circular polarised antenna placed at the chest level of the human for location position 1.

7.2.3 THE FAR FIELD PATTERN RESULTS

The far field radiation pattern for the most location positions discussed earlier has been computed. In particular, the far field at x-y, x-z and z-y planes when the target RFID tag located at the back of the human body for location position number 16 is recognised and shown in Figure 7.22.

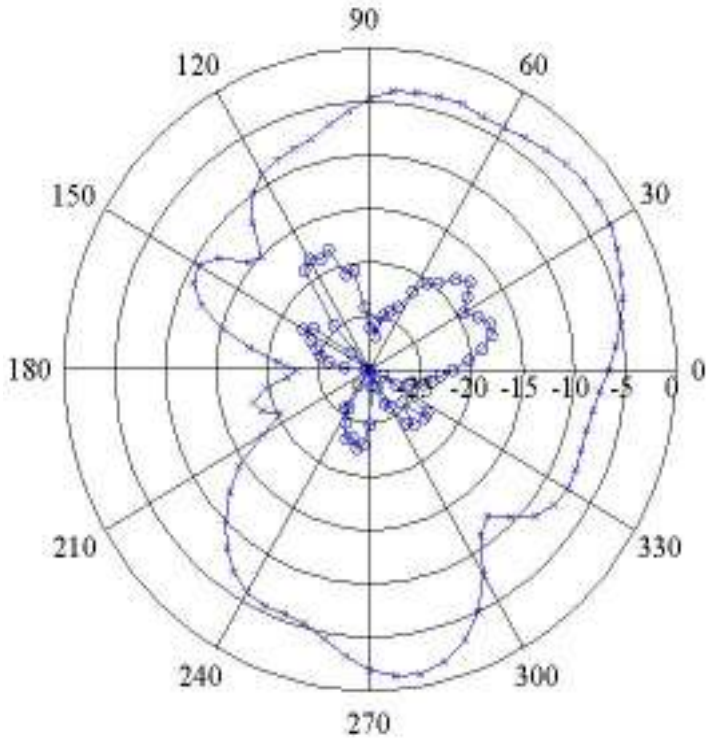
90
120
60
150
30
180
0
-25 -20 -15 -10 -5 0
210
330
240
300
270

(a)

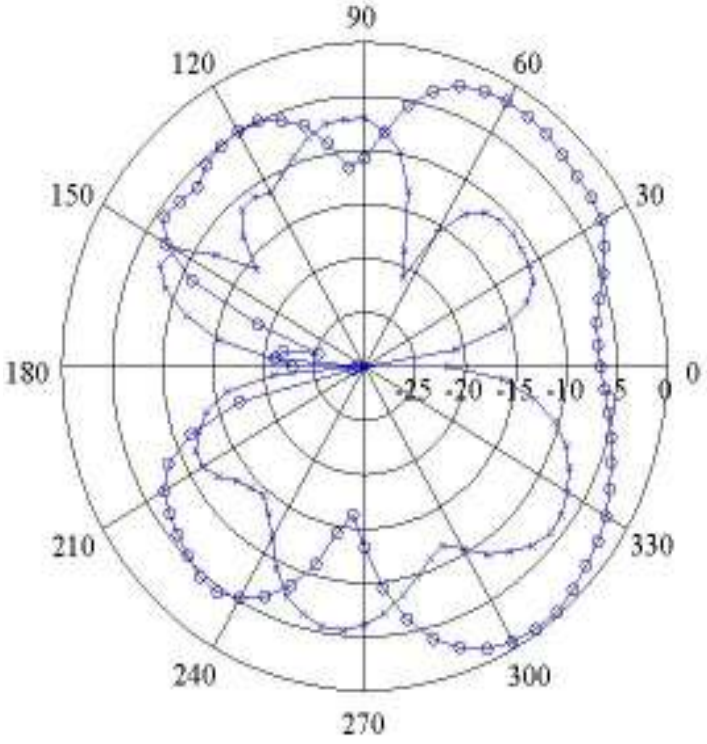
90
120
60
150
30
180
0
-25 -20 -15 -10 -5 0
210
330
240
300
270

(b)

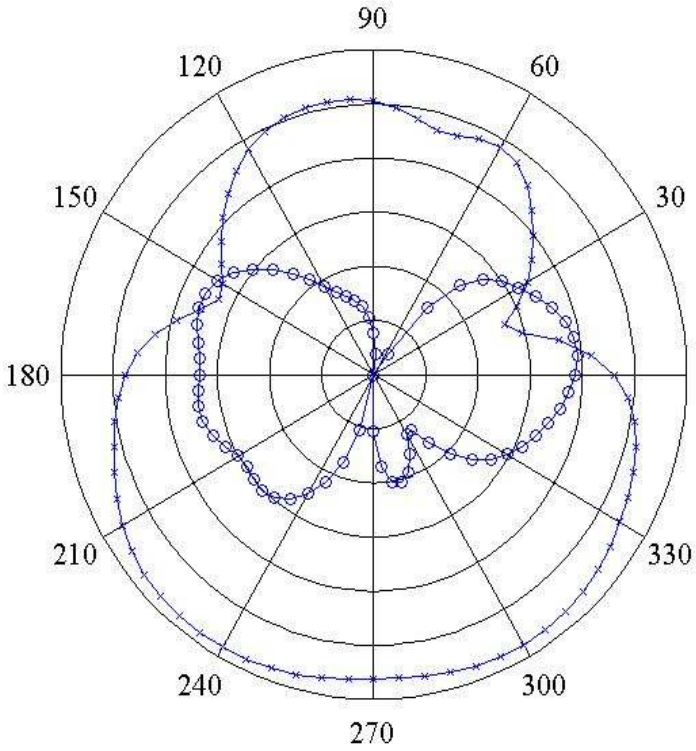

(c)

Figure 7.22:The Far field pattern for horizontal polarised antenna placed at the back of the human (location position16): (a) xy plane, (b) xz plane, (c) yz plane; 'o-o-o': Eθ, 'x-x-x': Eφ.

The far field zone for horizontal polarised RFID tag's antenna which is placed on the back of the human body for location position number 8 has been demonstrated in Figure 7.23.

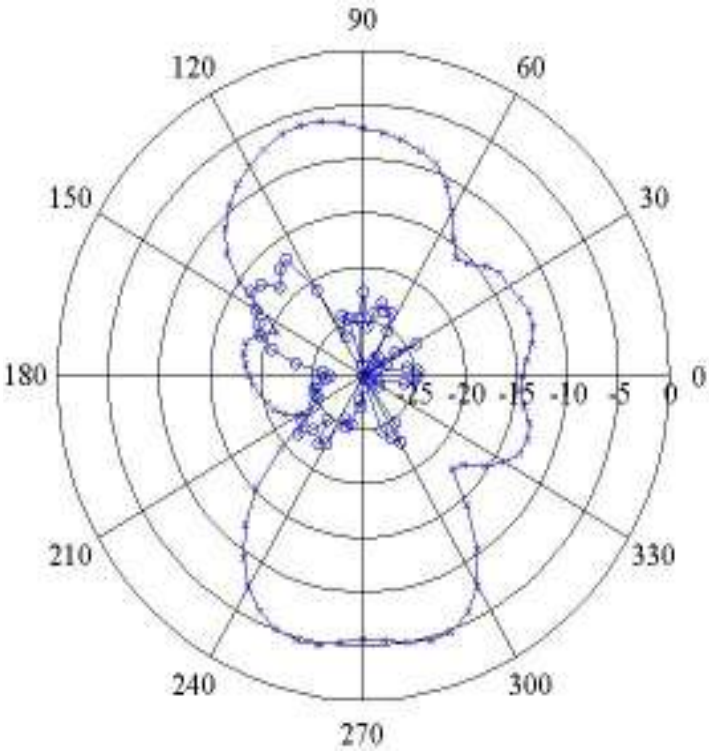
90
120
60
150
30
180
0
-25 -20 -15 -10 -5 0
210
330
240
300
270

(a)

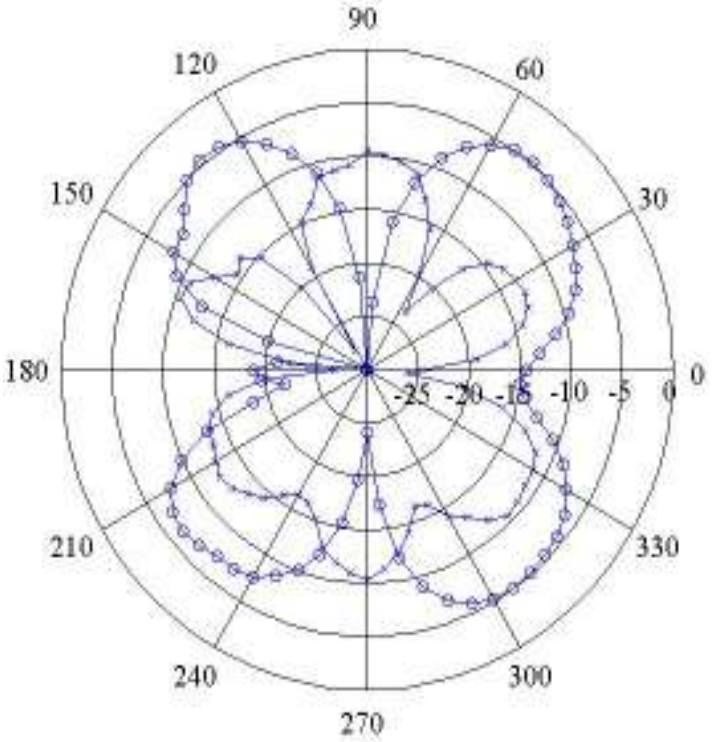
90
120
60
150
30
180
0
-25 -20 -15 -10 -5 0
210
330
240
300
270

(b)

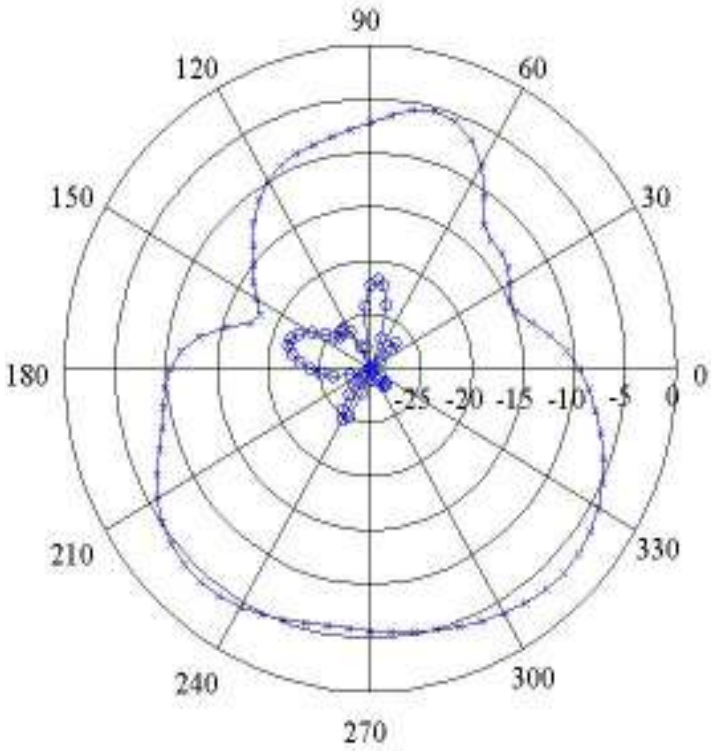

(c)

Figure 7.23:The Far field pattern for horizontal polarised antenna placed at the back of the human (position 8): (a) xy plane, (b) xz plane, (c) yz plane; 'o-o-o': Eθ, 'x-x-x': Eφ.

In term of the vertical polarised antenna, the radiation field when the antenna is placed on the back of the human body for location position number five has been indicated in Figure 7.24. In addition, another results has been taken when the antenna in position of number four which has been represented in Figure 7.25.

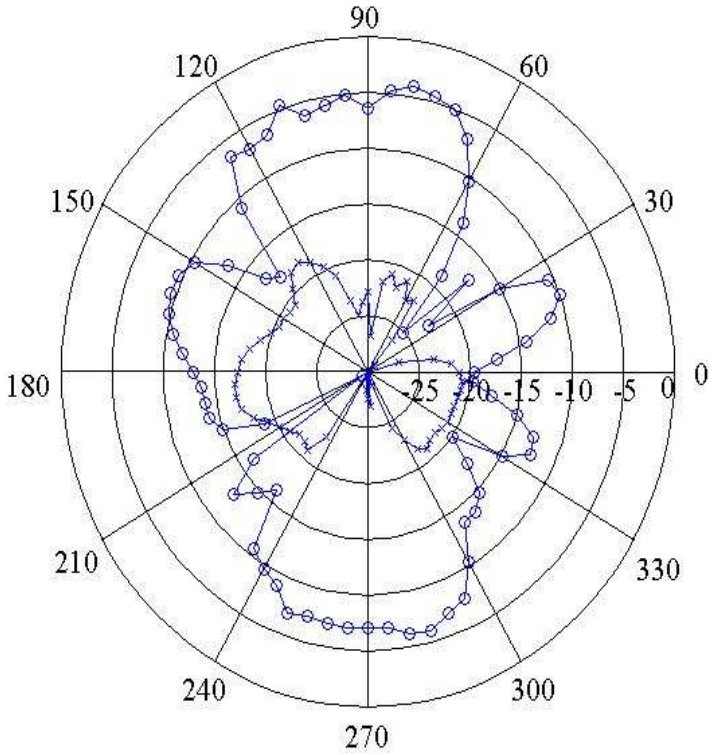
90
120
60
150
30
180
0
-25 -20 -15 -10 -5 0
210
330
240
300
270

(a)

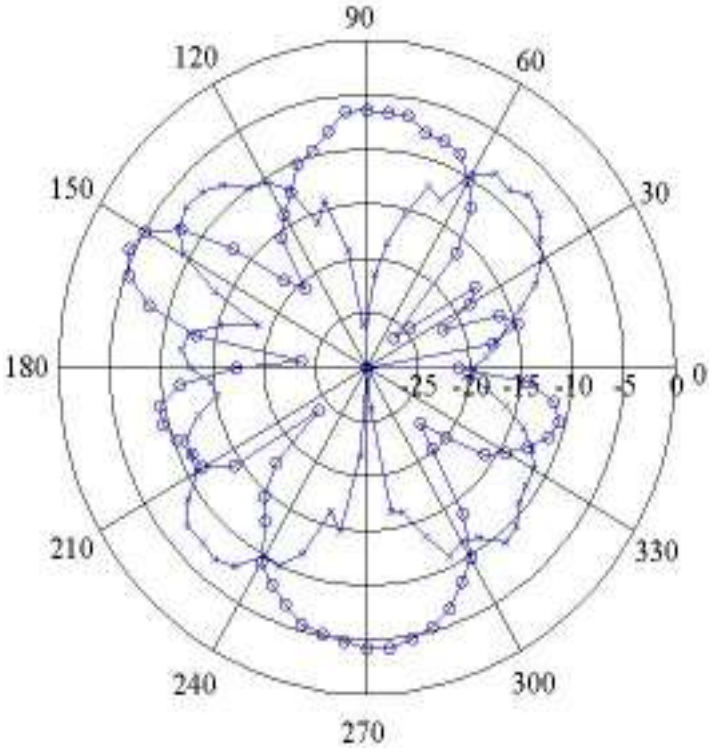
90
120
60
150
30
180
0
-25 -20 -15 -10 -5 0
210
330
240
300
270

(b)

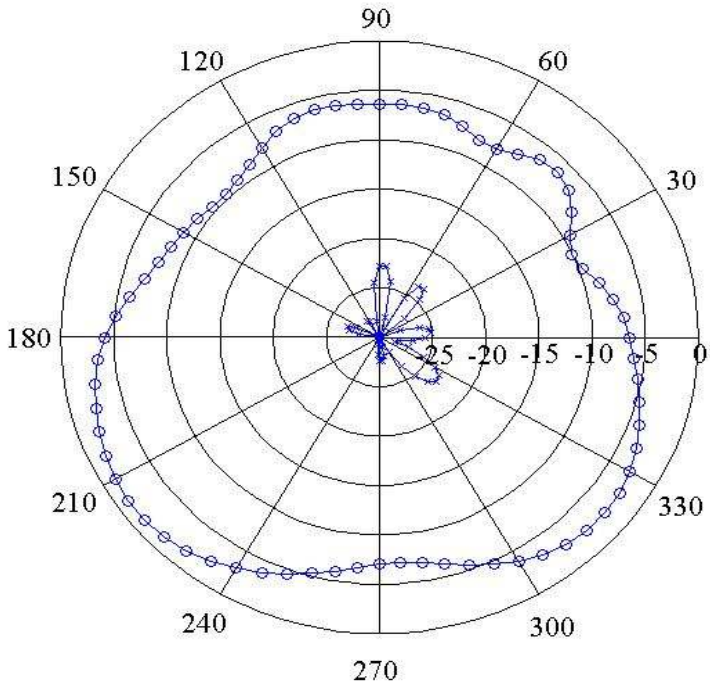

(c)

Figure 7.24:The Far field pattern for vertical polarised antenna placed at the back of the human (position 5): (a) xy plane, (b) xz plane, (c) yz plane;
'o-o-o': Eθ, 'x-x-x': Eφ.

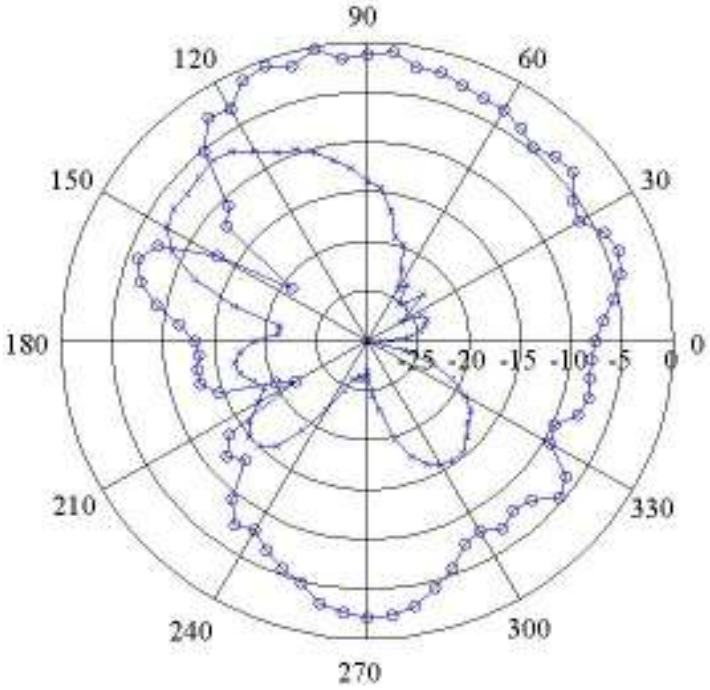

(a)

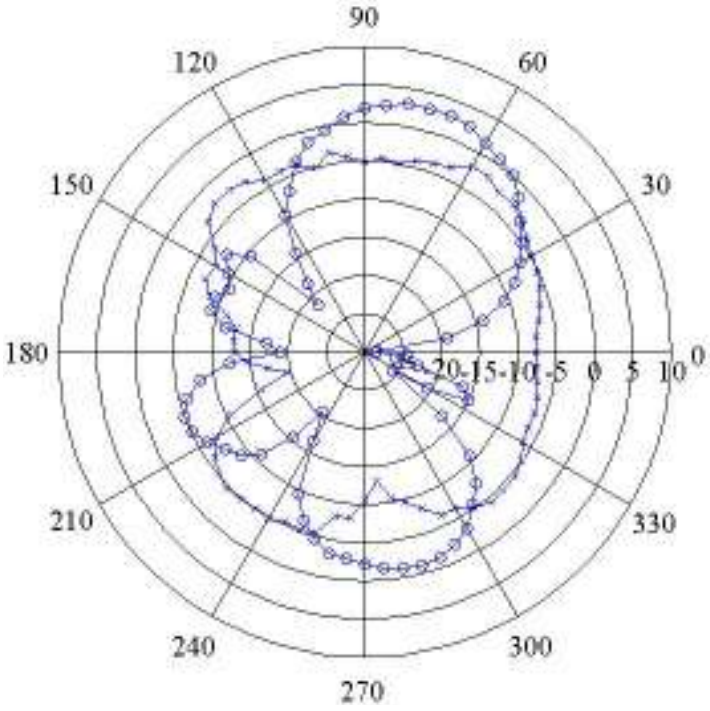

(b)

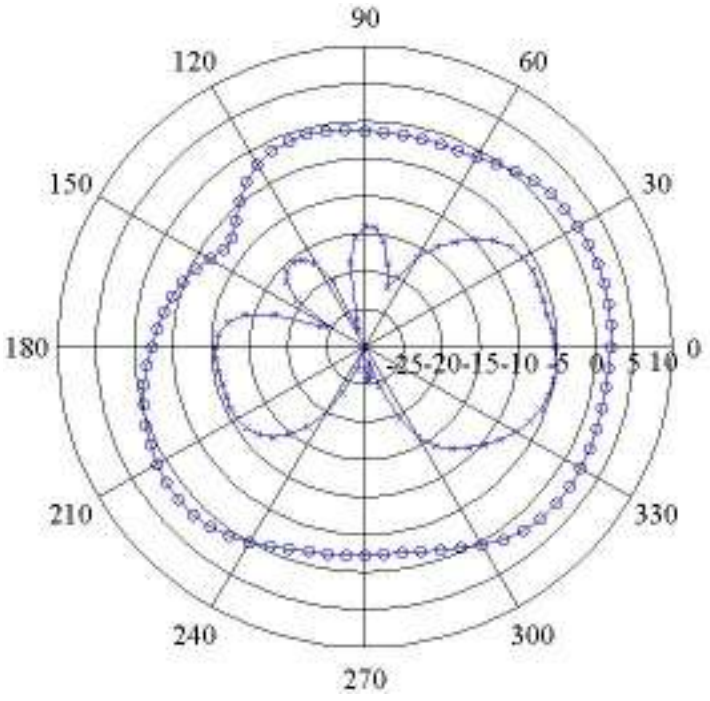

(c)

Figure 7.25:The Far field pattern for vertical polarised antenna placed at the back of the human (location position 4): (a) xy plane, (b) xz plane, (c) yz plane; 'o-o-o': Eθ, 'x-x-x': Eφ.

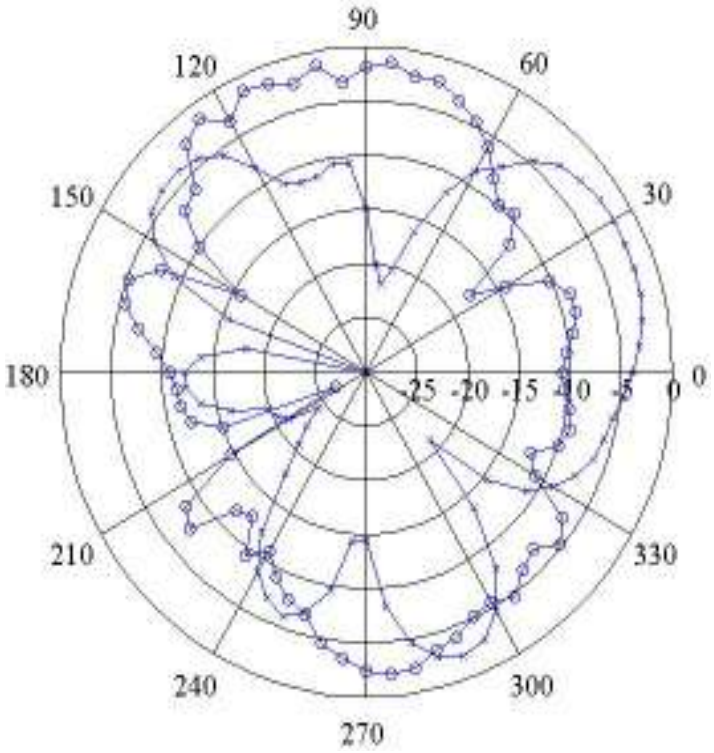
90
120
60
150
30
180
0
-25 -20 -15 -10 -5 0
210
330
240
300
270

(a)

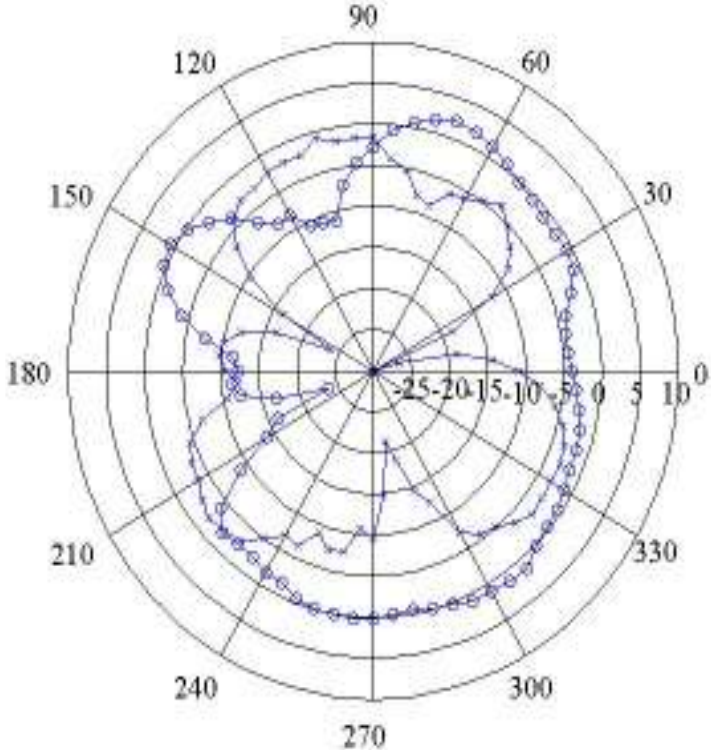
90
120
60
150
30
180
0
-25-20-15-10 -5 0 5 10
210
330
240
300
270

(b)

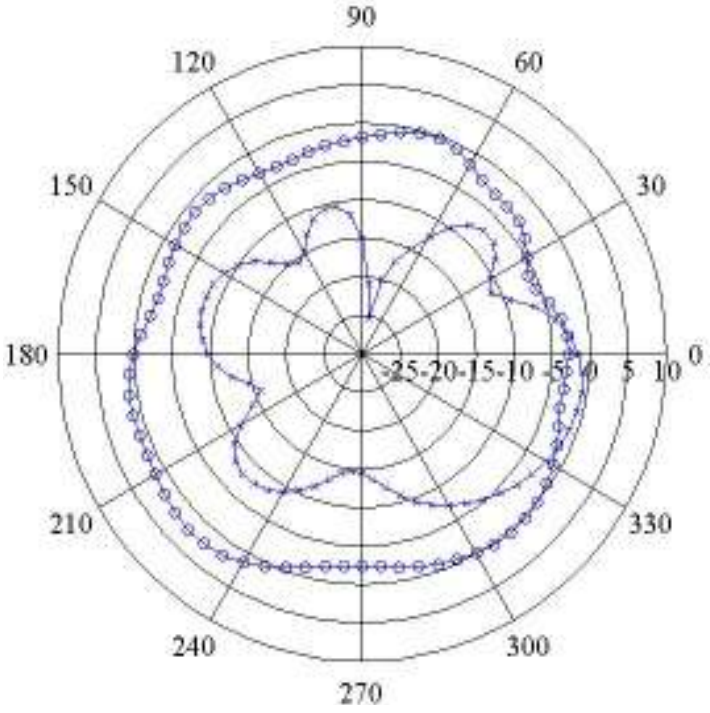

(c)

Figure 7.26:The Far field pattern for circular polarised antenna placed at the back of the human (location position1): (a) xy plane, (b) xz plane, (c) yz plane; 'o-o-o': Eθ, 'x-x-x': Eφ.

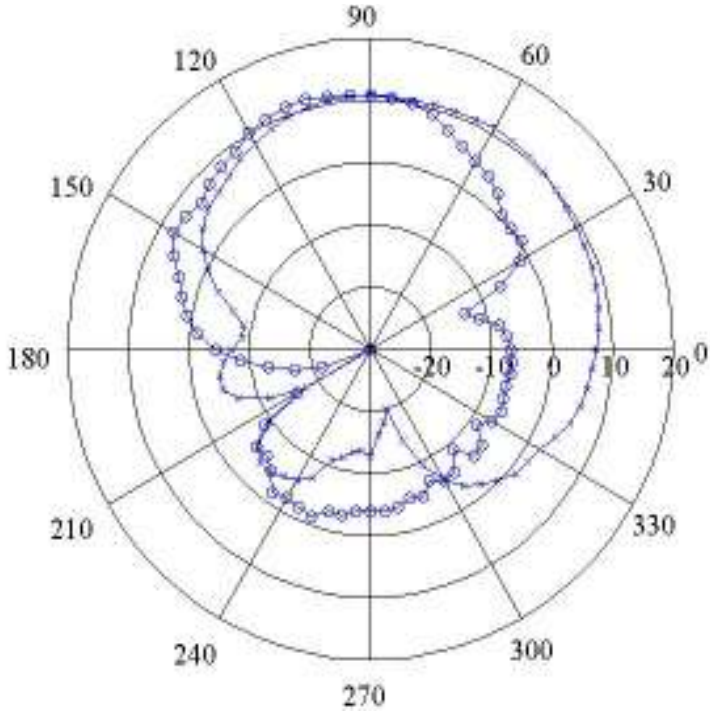

(a)

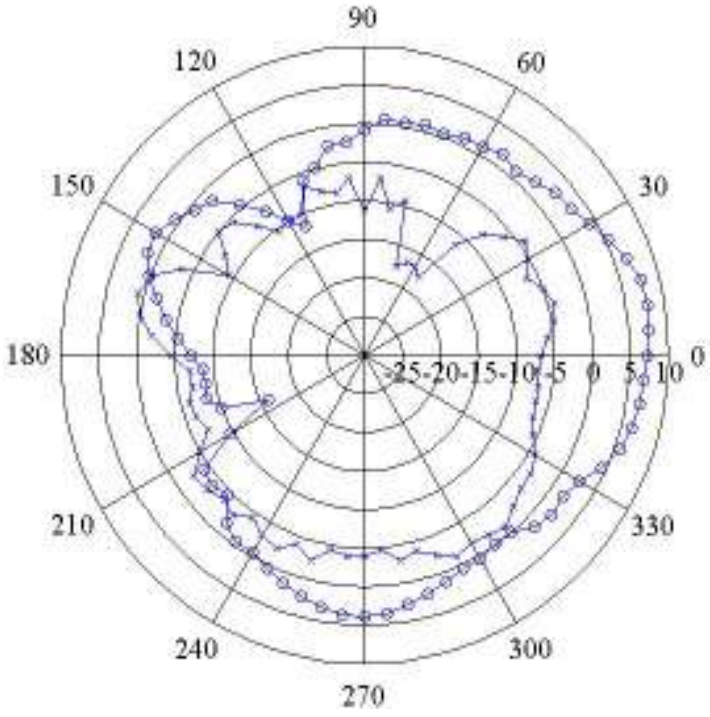

(b)

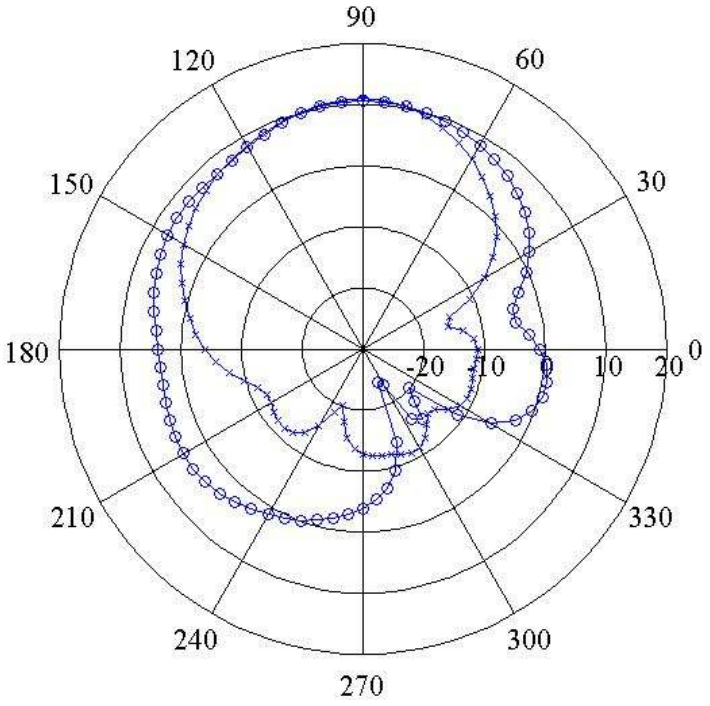

(c)

Figure 7.27:The Far field pattern for circular polarised antenna placed at the chest of the human (location position1): (a) xy plane, (b) xz plane, (c) yz plane; 'o-o-o': Eθ, 'x-x-x': Eφ.

In order to test the far field radiation pattern for the circular polarised antenna, the results of two points have been considered; the first one in the back at position one and the other in the front at chest position number one are presented in Figure 7.26 and Figure 7.27 respectively. A general comment can be concluded from all these far fields pattern that the human body plays an effective role on reducing the fields strength between 5 to 20 dBs in the direction opposite to the location of the tag antenna i.e. the pattern not facing the human tissues has less effects but not null effects.

7.2.4 CUMULATIVE DISTRIBUTION FUNCTION (CDF)

The simulated results of the absorbed energy inside the human body and the radiation power from the RFID tag's antenna are discussed in this section. The radiation efficiency of the optimum RFID tag's antenna for circular and linear polarised characterises could be calculated using equation 7.32:

$$efficiency = \frac{P_{radiated}}{P_{input} + P_{absorbed}} \tag{7.32}$$

Therefore, the CDF is studied and analysed for several antenna position on the human body. Furthermore, the power absorbed and radiation efficiency by the human body has been investigated. The information of the radiation efficiency which is gained for horizontal polarised antenna at front and back position on the human body has been combined as well to obtain the total histogram form as shown in Figure 7.28. As well as, the total of the

cumulative distribution function for same position has been plotted in Figure 7.29. In contrast, the same pattern but for the vertical polarised the histogram figure indicated in Figure 7.30 and the cumulative distribution in Figure 7.31.

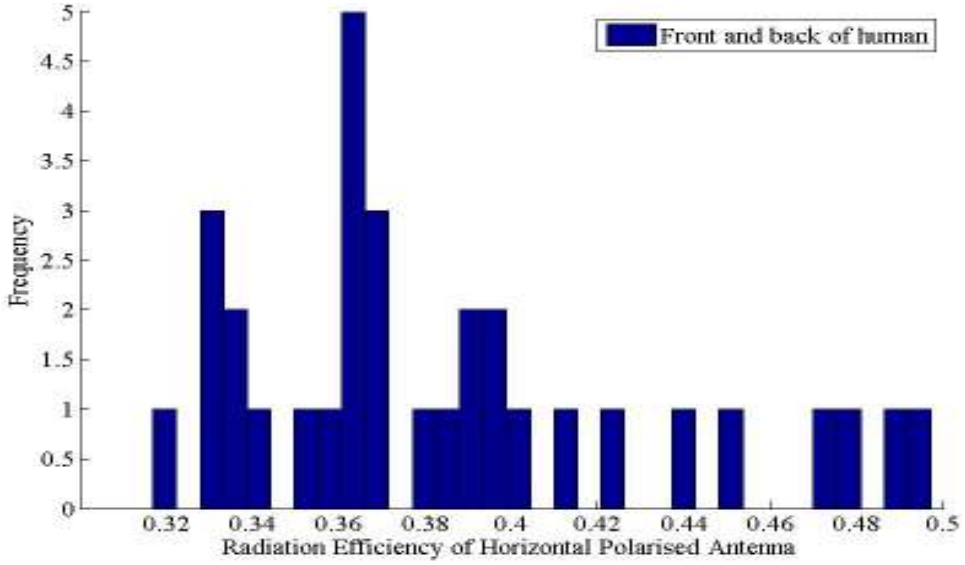

Figure 7.28:The histogram figure of both front and back position of horizontal polarised RFID tag's antenna

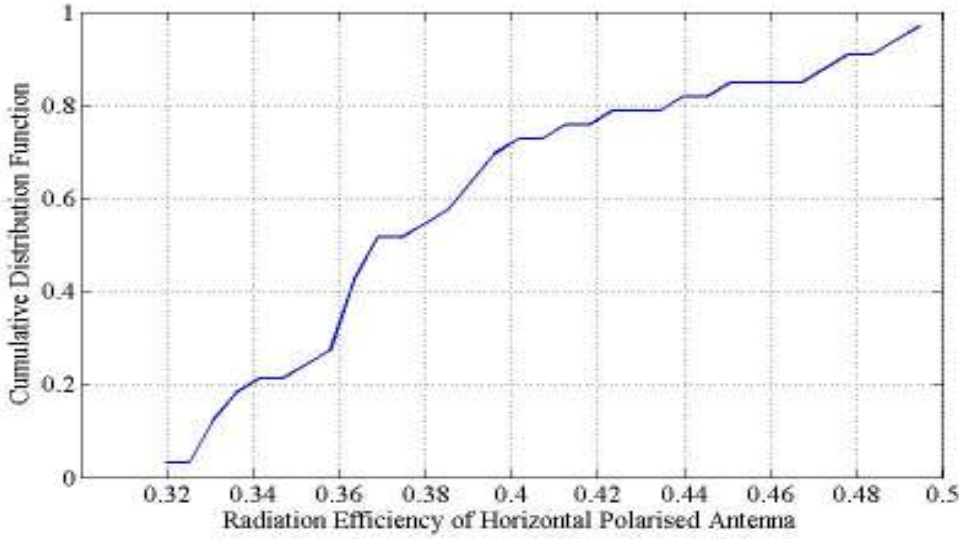

Figure 7.29:The total cumulative distribution function for front and back position of horizontal polarised antenna for radiation efficiency

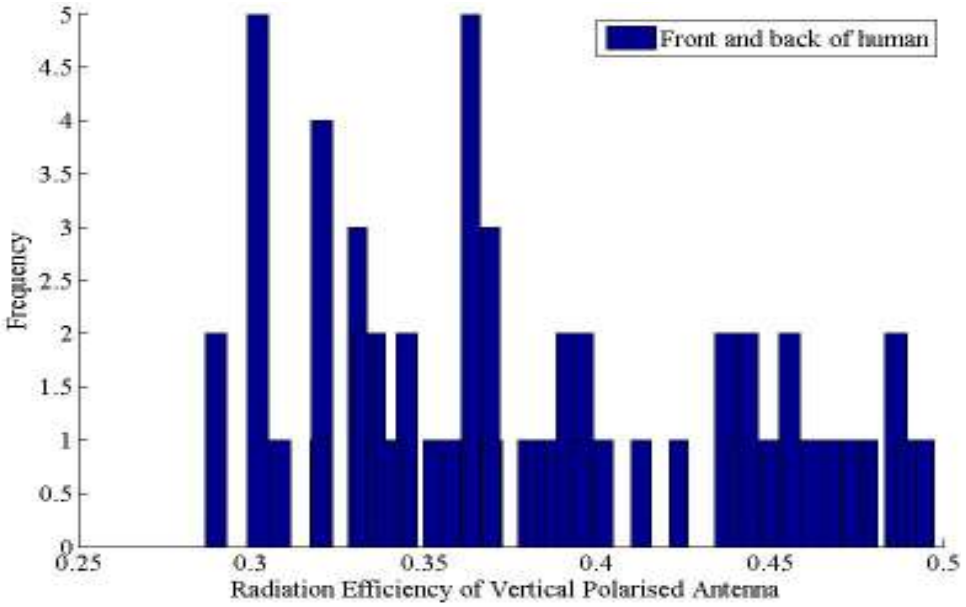

Figure 7.30:The histogram figure of both front and back position of vertical polarised RFID tag's antenna

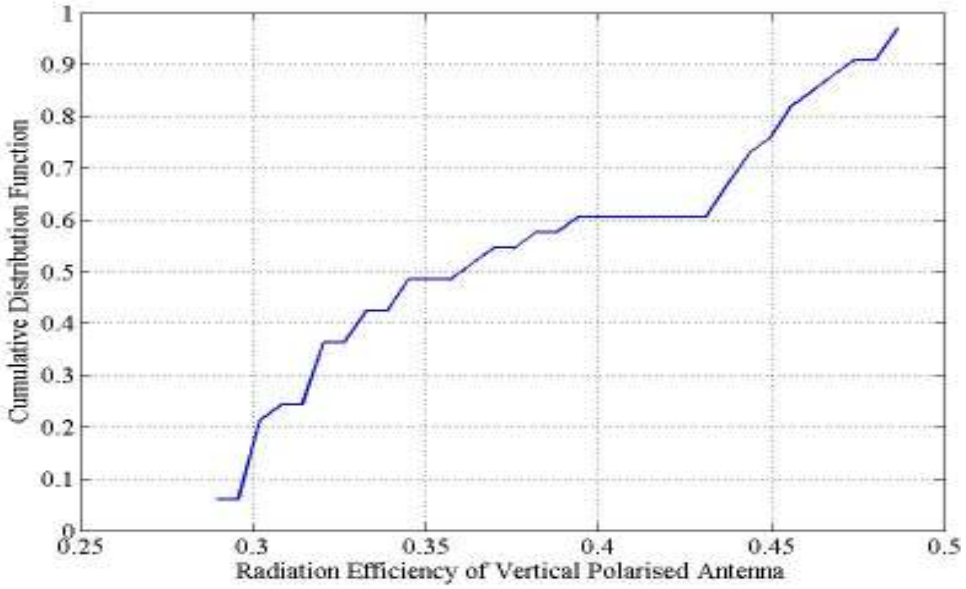

Figure 7.31:The total cumulative distribution function for front and back position of vertical polarised antenna for radiation efficiency

The absorbed power over the radiated power for horizontal polarised antenna at the front and the back of the human body has been calculated. The histogram form is presented in Figure 7.32 and the total cumulative

distribution function is reported in Figure 7.33. Moreover, the histogram scheme and the total cumulative distribution function for the vertical polarised antenna have been evaluated in Figure 7.34 and Figure 7.35 consecutively. The CDF of the radiation efficiencies for vertical and horizontal polarisations are comparable to each other and they look quite similar; this is clearly indicates that the polarisation of small tag antenna size has no too much influence on radiation efficiency for both cases. This is also applied to the CDF of the variations on the P_{abs}/P_{rad} ratio.

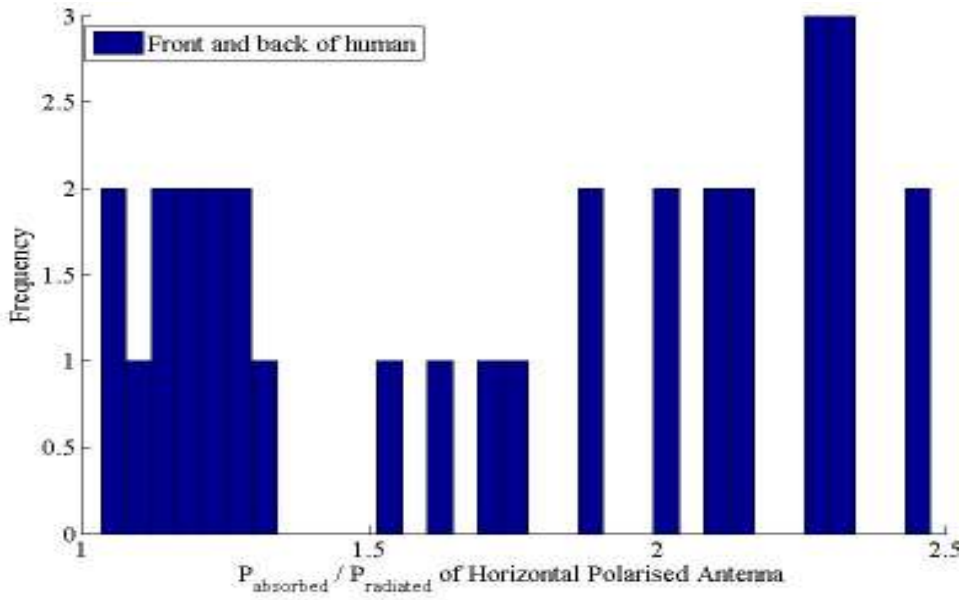

Figure 7.32:The histogram figure of both front and back position of horizontal polarised RFID tag's antenna $P_{absorbed}/P_{radiated}$

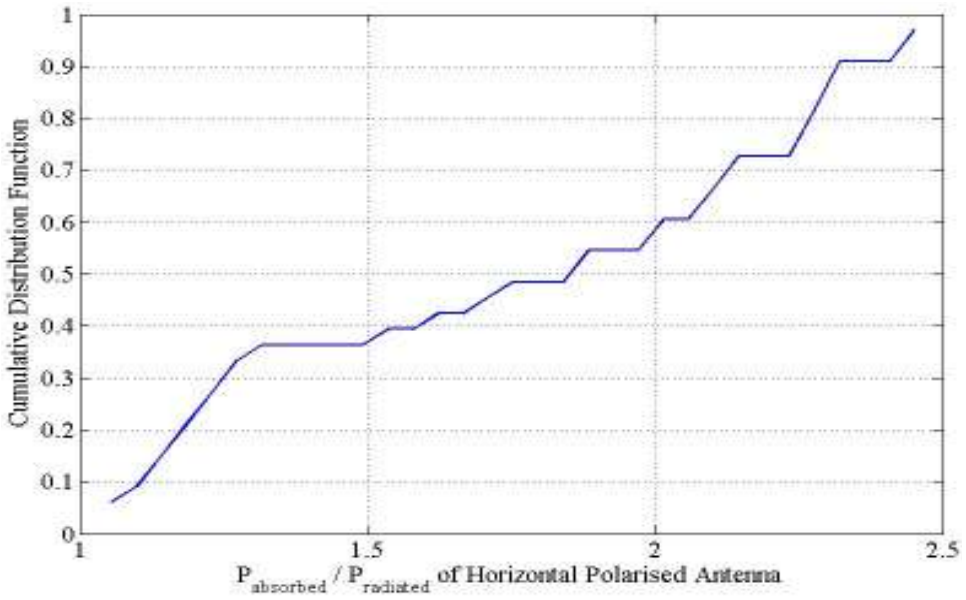

Figure 7.33:The total cumulative distribution function for front and back position of Horizontal polarised antenna for radiation efficiency ($P_{absorbed}/P_{radiated}$)

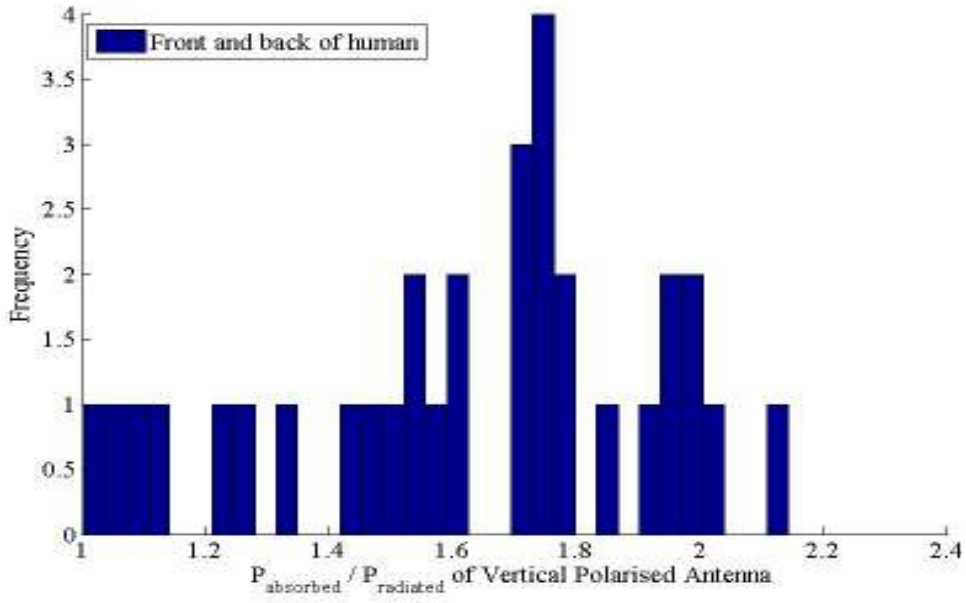

Figure 7.34:The histogram figure of both front and back position of vertical polarised RFID tag's antenna $P_{absorbed}/P_{radiated}$

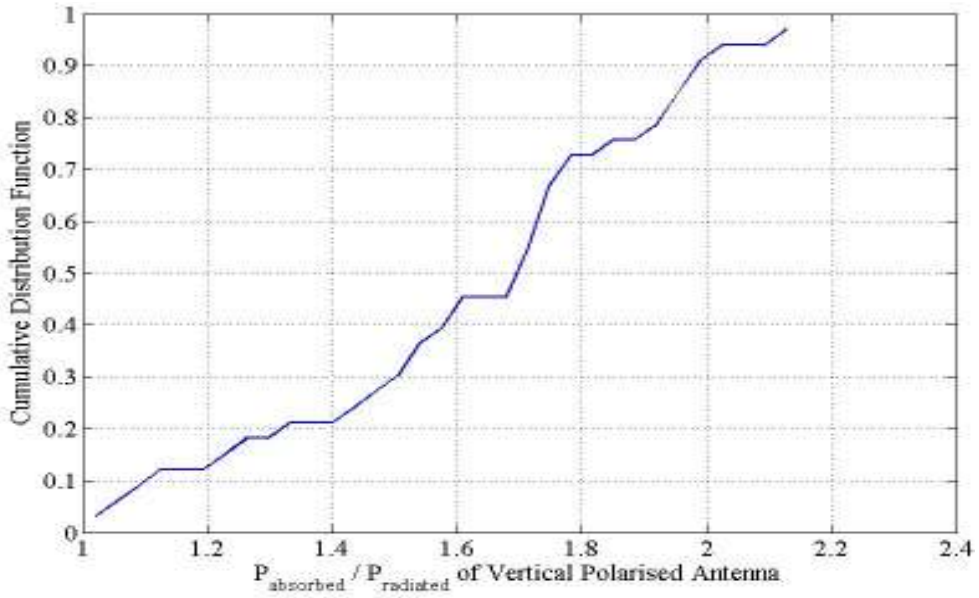

Figure 7.35:The total cumulative distribution function for front and back position of vertical polarised antenna for radiation efficiency($P_{absorbed}/P_{radiated}$)

7.3 CONCLUSION

A hybrid MOM-FDTD has been applied for model of the human body interaction with linear and circular polarised RFID tag antennas. In particular, sixteen points on the front of the human body and sixteen on the back have been studied. The MOM/FDTD method has been successfully adopted to generate the electrical and magnetic field as created by the antenna in free space and then applied to the FDTD domain where the human model is present. The human body of over 48 tissue layers has been modelled at propinquity to the RFID tag's antenna working at 900*MHz*. The near and the far field radiations have been studied for the horizontal, the vertical and the circular polarised antennas for 32 different locations. In addition, CDF of radiation efficiency and the ratio of the absorbed and the radiated power of the antenna at different location on the human body have been computed.

CHAPTER EIGHT

CONCLUSIONS AND SUGGESTIONS FOR FUTURE WORK

8.1 CONCLUSION

The main and the primary objective of this work which done in this report are the discussion, development and analysis of the RFID tag and reader antennas. These studies have focused in general to expansion the size, quality, polarisation, detection range, environment, its impact to the human body and so forth. In general, various RFID tag antenna shapes and the practical experiences have been explored to see the effect on performance.

A novel RFID tag and reader antennas have been improved the detection range for various expected applications. In addition, the target RFID sensors have been modelled to amendment the tag operation when placed on surface items which having a different electric properties. the RFID tag and RFID reader sensor have been designed using the Genetic Algorithm (GA) via Ansoft High Frequency Structural Simulator (HFSS), the Computer Simulation Technology (CST), Fortran and the Matlab software. It is worth mentioning that the simulation results have been taken. Subsequently, most of the models have been made and tested in laboratory to obtain measured results. In term of verifying of the results, the simulation results and the measurement results for the target designs have been compared and substantial convergence has been observed between them. As for the impact

of the RFID tag antenna in linear and circular polarisation to the human body, the simulation results show the effects on the human body.

One of the major opportunities for RFID technology is their successful implementation that improve the quality of service, track and correct errors. Furthermore, the range of the applications is potentially very wide, but significant areas of application might include distributing and managing the activities of professional applications. RFID could ensure that only authorised people have access to places and systems but could also be used to guarantee that the correct resources are delivered to the relevant locations and are utilised in the prescribed manner. Such RFID systems are comparatively new technologies but are nevertheless widespread and among several applications and general location based services.

Novel designs of several RFID tag antennas have been designed to operate as linear and circular polarised sensors. Two software packages have been used for modelling the fundamental concepts and design optimisation; in addition to an in house source code utilising the GA optimisation method. Summaries and conclusions for chapters three to seven are presented as follows:

In Chapter 3, linearly polarised (LP) meander line and circularly polarised (CP) cruciform antennas have been simulated and configured with the aid of a genetic algorithm (GA) based optimiser. The optimisation strategy

adopted here uses a FORTRAN driver for the GA in conjunction with the NEC-2 source code. The designed studies have been subjected to various constraints and cost functions; the final outputs produce good input impedance matching to the RFID chip input port.

Linearly polarised (LP) RFID tag antenna designs are investigated in Chapter 4. Single and double equally spaced meander line antennas structures are selected. Moreover, the loop effecting to the tag's results has been explained. The simulated electric field distribution for most of the models has been presented. In each case the design concept is to obtain maximal angular readability from a dipole-like radiation pattern. The various candidates were cross validated using HFSS (finite element, reduced order modelling) and Microwave Studio (finite integration, transient), constructed and measured. The measurements show close agreement with the various simulations. The basic symmetry of the first design is used to calculate the input impedance of the tag. The results show a good impedance match which required for the Higgs IC. The refection coefficient $|S_{11}|$ for all designs which include in this chapter has been found from -30 and above with efficiency up to seven metres. Naturally, the designs option all operate in the European UHF band.

In Chapter 5, the possibility of implementing RFID tag antennas over metallic surfaces is considered. Results for *S* and *T* type RFID tags are obtained for the UHF band. Initial simulation work is carried out using

HFSS. The effects of the antenna substrate as well as the conducting surface must be fully characterised in these simulations to fully gauge the impact on the RFID performance. Furthermore, the simulated and measured gain results have been sketched for both designs and have been shown nearly convergence. To find the optimum design, the parametric study has been applied. In contrast, looping around the chip has been successfully investigated as a means of improving the reading range.

The design and optimisation of compact hybrid quarifilar helical-spiral RFID readers antenna using GA has been proposed in Chapter 6. In particular, the optimum reader's antenna dimensions have been modelled using HFSS software and transferred to CST software in order to compare the results. Furthermore, the axial ration has been calculated as $2dB$ near $\pm 90^0$ and above than $7dBi$ power gain.

Chapter 7 explains the interaction among Electromagnetic (EM) Field and Human body for RFID tag's antennas via Hybrid Computational Method. Obviously, a hybrid MoM-FDTD-without sub-grading has been functional and the near and far fields affection has been studied. A total of 32 points distributed to the back and front of the human body, the linear (vertical and horizontal) and circular polarisation antenna mounted on the surface of mentioned points and the required results have been observed. In addition, the CDF of the radiation efficiency and the ratio of the absorbed and radiated energy have been analysed.

8.2 SUGGESTIONS FOR FUTURE WORK

The RFID devices grant a novel standard technology in tracking and transferring information. As most of RFID system applications are still in the stages that need to be further development and adopted by limited features.

It will be the great potential if the future studies focus intensely in the RFID technology integration with other technology system such as GPS, personal equipment and so forth. Admittedly, the RFID price must be taken in consider the thinking to decrease to the lowest possible and increases the encryption security. Therefore, in the future the research will be highlighting to employ the RFID method everywhere on everything and installed at all building entrance to track data or item or personal with controlling the access to the data and the power of the information i.e. fully privacy.

In fact, the work presented in this report has tried to determine the factors which affect the RFID tag antenna design against the detection reading range. The presented designs have involved the study of the characteristics of RFID tags antenna performances subject to several applications. Actually, in order to continue this research, the future tasks are given as following:

- Study the effectiveness of RFID performance, vs. changes in the operating environment, construction materials and dielectric composition and so forth. In addition, dual polarised RFID tag's antenna mounted on complex dielectric structure could be studied to overcome the fading, dead spots and drop-outs signal. Therefore, the week antenna radiation could be switched by stronger emitting signal antenna [127. 128].
- Model and improve the operation of circular polarisation RFID tag and reader antennas and implement the required measurements [129].
- Design and implement a miniaturised RFID tag antenna mounted on metallic surface. Investigate existing and new RFID tag antennas on real time developments for multi applications.
- Employment the RFID tags in the sewer infra structure to warn the maintenance company as sending Email or SMS or call in case of any block in manhole or inside the homes.
- Write a program to control the RFID reader information and use it to apply in different application. In contrast, the cognitive radio (CR) method is good technology could be utilised in the RFID system as writing or editing suitable software defined radio (SDR) as dealing with spread spectrum. Therefore, the control to give identity and authorising to the user, out power, encrypt or decrypt signals and so forth. Furthermore, the federal communication commission (FCC) might be benefit for RFID technology to get the public people to use the unused RF spectrum i.e. white spaces [130].

- Think to increase the chip memory to transfer plethora of data that give option to save more information about the tagged object.
- Modify some of the mentioned RFID design antennas to be operated for 2.4 and 2.5 GHz i.e. Wireless local area networks WLAN.
- In case to increase the optimizing data speed and decrease the communication errors, applying the MIMO system (Multi Input, Multi output) for RFID application in order to decrease the multipath. Observance of RFID applications, the MISO (Multi Input, Single Output) or SIMO (Single Input, Multi Output) could be utilised.
- Work on expand the current studies and research developments to gain much possibility to implement this device in a wider applications.

REFERENCES

[1] J. Symonds, J. Ayoade and D. Parry, Auto-identification and ubiquitous computing applications: RFID and Smart Technologies for Information Convergence, Information Science Reference (an imprint of IGI Global). Hershey, New York, 2009.

[2] K. Finkenzeller, RFID handbook: fundamentals and Applications in Contact less Smart Cards and identification. Chichester, England, Hobbken, N.J.Wiley, 2003.

[3] B. Glover and H. Bhatt, RFID Essentials. Beijing, Farnham, CA:O'Reilly, Jan. 2006.

[4] Y. Zuo, "Survivable RFID Systems: Issues, Challenges and Techniques", *IEEE Trans. on Systems*, Man, and Cybernetics—Part C: Applications and Reviews, vol.40, no.4, pp. 406-418, July 2010.

[5] K. Fyhn, R. M. Jacobsen, P. Popovski, A. Scaglione, and T. Larsen, "Multipacket reception of passive UHF RFID tags: A communication theoretic approach," *IEEE Transactions on Signal Processing*, vol. 59, pp. 4225-4237, 2011.

[6] P. D'Arco and A. De Santis, "On ultralightweight RFID authentication protocols," *IEEE Transactions on Dependable and Secure Computing*, vol. 8, pp. 548-563, 2011.

[7] S. Garfinkel and B. Rosenberg, RFID: applications, security, and privacy. Addison-Wesley, 2006.

[8] C. R. Medeiros, J. R. Costa, and C. A. Fernandes, "RFID reader antennas for tag detection in self-confined volumes at UHF," *IEEE Antennas and Propagation Magazine*, vol. 53, pp. 39-50, 2011.

[9] A. R. Jimenez Ruiz, F. Seco Granja, J. C. Prieto Honorato, and J. I. Guevara Rosas, "Accurate pedestrian indoor navigation by tightly coupling foot-mounted IMU and RFID measurements," *IEEE Transactions on Instrumentation and Measurement*, vol. 61, pp. 178-189, 2012.

[10] X. Xu, G. Lin, W. Jianping, X. Guoliang and S. C. Cheung, “Read More with Less: An Adaptive Approach to Energy-Efficient RFID System”, *IEEE Journal on Selected Areas in Communications*, vol.29, no.8, pp. 1684-1697, Sep. 2011.

[11] W.-J. Yoon and S.-H. Chung, "ISS-TCA: An identified slot scan-based tag collection algorithm for performance improvement in active RFID systems," *IEEE Transactions on Industrial Electronics*, vol. 59, pp. 1662-1672, 2012.

[12] E. Vahedi, V. Shah-Mansouri, V. W. S. Wong, I. F. Blake, and R. K. Ward, "Probabilistic analysis of blocking attack in RFID systems," *IEEE Transactions on Information Forensics and Security*, vol. 6, pp. 803-817, 2011.

[13] V. Antti, Raisanen and A. Lehto, Radio Engineering for Wireless Communication and Sensor Application. Artech House, Boston, London, 2003.

[14] R. J. Marhefka and D. D. Kraus, Antennas for all applications, 3rd ed. New York, Mcgraw-Hill, 2002.

[15] B.-S. Choi, J.-W. Lee, J.-J. Lee, and K.-T. Park, "A hierarchical algorithm for indoor mobile robot localization using RFID sensor fusion," *IEEE Transactions on Industrial Electronics*, vol. 58, pp. 2226-2235, 2011.

[16] I. Bahl, Lumped Elements for RF and Microwave Circuits. Artech House, INC, Boston, London, 2003.

[17] S. Preradovic, S. M. Roy and N. C. Karmakar, “RFID System Based on Fully Printable Chipless Tag for Paper-/Plastic-ltem Tagging”, *IEEE Antennas and Propagation Magazine*, vol.53, no.5, pp.15-32, Oct. 2011.

[18] W. A. Davis and K. K. Agarwal, Radio Frequency Circuit Design, John Wiley & Sons, INC., 2nd ed. New York, Chichester, 2001.

[19] P. G. Garter, Electromagnetic waves-Microwave components and devices, 1st ed. TJ Press, UK, 1990.

[20] J. Yin, J. Yi, M. K. Law, Y. Ling, M. C. Lee, K. P. Ng, B. Gao, H. C. Luong, A. Bermak, M. Chan, W.-H. Ki, C.-Y. Tsui, and M. Yuen, "A system-on-chip EPC Gen-2 passive UHF RFID tag with embedded temperature sensor," 445 Hoes

Lane / P.O. Box 1331, Piscataway, NJ 08855-1331, United States, 2010, pp. 2404-2420.

[21] L. Sang-Do, M. Shin and K. Hyoung-Jun, “EPC vs IPv6 mapping mechanism”, presented at ICACT2007, ICACT, Korea, Feb. 2007, pp.1243-1245.

[22] Y. Tikhov and J. H. Won, "Impedance-matching arrangement for microwave transponder operating over plurality of bent installations of antenna," Electronics Letters, vol. 40, pp. 574-575, 2004.

[23] G. Marrocco, "The art of UHF RFID antenna design: Impedance-matching and size-reduction techniques," *IEEE Antennas and Propagation Magazine*, vol. 50, pp. 66-79, 2008.

[24] P. S. Hall and Y. Hao, Antennas and propagation for body-centric wireless communication. Artech house, INC., Oct. 2006.

[25] J. D. Krarus and R. J. Marhefka, Antennas for all applications. Mcgraw-Hill Higher Education, New York, 3rd ed., 2002.

[26] W. C. Gibson, The Method of Moments in Electromagnetics. Taylor & Francis Group, LLC, the United States of America, 2008.

[27] T. M. Millington and N. J. Cassidy, "Improving the accuracy of FDTD approximations to tangential components of the coupled electric and magnetic fields at a material interface," *IEEE Transactions on Antennas and Propagation*, vol. 59, pp. 2924-2932, 2011.

[28] A. Freni, P. De Vita, P. Pirinoli, L. Matekovits, and G. Vecchi, "Fast-factorization acceleration of MoM compressive domain-decomposition," *IEEE Transactions on Antennas and Propagation*, vol. 59, pp. 4588-4599, 2011.

[29] R. A. Abd-Alhameed, P. S. Excell, J. A. Vaul, and M. A. Mangoud, "Hybrid treatment for electromagnetic field computation in multiple regions," Electronics Letters, vol. 34, pp. 1925-1926, 1998.

[30] M. A. Mangoud, R. A. Abd-Alhameed, N. J. McEwan, P. S. Excell, and E. A. Abdulmula, "SAR reduction for handset with two-element phased array antenna

computed using hybrid MoM/FDTD technique," *Electronics Letters*, vol. 35, pp. 1693-1694, 1999.

[31] R. A. Abd-Alhameed, P. S. Excell, and M. A. Mangoud, "A hybrid computational electromagnetics formulation for simulation of antennas coupled to lossy and dielectric volumes," *IEEE Transactions on Broadcasting*, vol. 50, pp. 253-259, 2004.

[32] K. N. Ramli, R. A. Abd-Alhameed and D. Zhou, "Interaction between electromagnetic field and human body for dual band balanced antenna using hybrid computational method", *Presented at Antennas and Propagation Conference (LAPC), Loughborough*, Nov. 2010, pp. 449-452.

[33] L. O'Gorman and T. Pavlidis, "Auto ID technology: from barcodes to biometrics", *IEEE Robotics & Automation Magazine*, vol.6, no1, pp. 4-6, March 1999.

[34] J. Swartz, "The growing 'magic' of automatic identification", *IEEE Robotics & Automation Magazine*, vol.6, no.1, pp.20-23, 56, March 1999.

[35] J. Landt, "The history of RFID," *IEEE Potentials*, vol. 24, pp. 8-11, 2005.

[36] H.-M. Sun and W.-C. Ting, "A Gen2-based RFID authentication protocol for security and privacy," *IEEE Transactions on Mobile Computing*, vol. 8, pp. 1052-1062, 2009.

[37] J. A. Rodriguez-Rodriguez, M. Delgado-Restituto, J. Masuch, A. Rodriguez-Perez, E. Alarcon, and A. Rodriguez-Vazquez, "An ultralow-power mixed-signal back end for passive sensor UHF RFID transponders," *IEEE Transactions on Industrial Electronics*, vol. 59, pp. 1310-1322, 2012.

[38] M. Pelissier, J. Jantunen, B. Gomez, J. Arponen, G. Masson, S. Dia, J. Varteva, and M. Gary, "A 112 Mb/s full duplex remotely-powered impulse-UWB RFID transceiver for wireless NV-memory applications," *IEEE Journal of Solid-State Circuits*, vol. 46, pp. 916-927, 2011.

[39] P. Wei, W. Che, Z. Bi, C. Wei, Y. Na, L. Qiang, and M. Hao, "High-efficiency differential RF front-end for a Gen2 RFID tag," *IEEE Transactions on Circuits and Systems II: Express Briefs*, vol. 58, pp. 189-194, 2011.

[40] R. A. Abd-Alhameed, D. Zhou, Y. Ma, M. S. Alkhambashi, C. H. See, M. M. Abusitta, and P. S. Excell, "Equal-spaced rectangular meander-line antenna RFID tag design for UHF band," in 3rd International Conference on Internet Technologies and Applications, *ITA 09*, September 8, 2009 - September 11, 2009, Wrexham, Wales, United kingdom, 2009, pp. 426-430.

[41] S.-C. Jung, M.-S. Kim, and Y. Yang, "Baseband noise reduction method using captured TX signal for UHF RFID reader applications," *IEEE Transactions on Industrial Electronics*, vol. 59, pp. 592-598, 2012.

[42] J. W. Lee and B. Lee, "Design of high-Q UHF radio-frequency identification tag antennas for an increased read range," *IET Microwaves*, Antennas and Propagation, vol. 2, pp. 711-717, 2008.

[43] J. Ryoo, J. Choo, and H. Choo, "Novel UHF RFID tag antenna for metallic foil packages," *IEEE Transactions on Antennas and Propagation*, vol. 60, pp. 377-379, 2012.

[44] N. Konstantinou, “Expowave: An RFID Anti-Collision Algorithm for Dense and Lively Environments”, *IEEE Trans. on Communications*, vol.60, no.2, pp.352-356, Feb. 2012.

[45] Y. Zuo, "Survivability experiment and attack characterization for RFID," *IEEE Transactions on Dependable and Secure Computing*, vol. 9, pp. 289-302, 2012.

[46] H. B. Chung, H. Mo, N. Kim, and C. Pyo, "An advanced RFID system to avoid collision of RFID reader, using channel holder and dual sensitivities," *Microwave and Optical Technology Letters*, vol. 49, pp. 2643-2647, 2007.

[47] L. Kang, K. Wu, J. Zhang, H. Tan, and L. M. Ni, "DDC: A novel scheme to directly decode the collisions in UHF RFID systems," *IEEE Transactions on Parallel and Distributed Systems*, vol. 23, pp. 263-270, 2012.

[48] X. Qing and Z. N. Chen, "Proximity effects of metallic environments on high frequency RFID reader antenna: Study and applications," *IEEE Transactions on Antennas and Propagation*, vol. 55, pp. 3105-3111, 2007

[49] P. V. Nikitin, K. V. S. Rao, R. Martinez, and S. F. Lam, "Sensitivity and Impedance Measurements of UHF RFID Chips," *IEEE Transactions on Microwave Theory and Techniques*, vol. 57, pp. 1297-1302, 2009.

[50] J. Gao, J. Siden and H. Nilsson, “Printed Electromagnetic Coupler With an Embedded Moisture Sensor for Ordinary Passive RFID Tags”, *IEEE Electron Device Letters*, vol.32, no.12, pp. 1767-1769, Dec. 2011.

[51] T. Bjorninen, M. Lauri, L. Ukkonen, R. Ritala, A. Z. Elsherbeni, and L. Sydanheimo, "Wireless measurement of RFID IC impedance," *IEEE Transactions on Instrumentation and Measurement,* vol. 60, pp. 3194-3206, 2011.

[52] S. Rao and D. Daniel, “Evaluation of the State of Passive UHF RFID: An Experimental Approach”, *IEEE systems journal*, vol.1, no.2, pp. 168-176, Dec.2007.

[53] S.-L. Chen, K.-H. Lin, and R. Mittra, "A measurement technique for verifying the match condition of assembled RFID tags," *IEEE Transactions on Instrumentation and Measurement,* vol. 59, pp. 2123-2133, 2010.

[54] Alien Technology Corp., (2008, Jan). Morgan Hill CA, USA. Available: http://www.alientechnology.com. [Accessed: 25 May 2010].

[55] Soe-Mile F. Nee, (2000).Polarisation Measurement, U. S., Naval Air Warfare Centre. [Online ebook]. Available: spb, www.autex.spb.ru/download/wavelet/books/sensor/CH60.PDF. [Accessed: 01 \Jan 2011].

[56] Y. K. Jung and B. Lee, “Dual-Band Circularly Polarised Microstrip RFID Reader Antenna Using Metamaterial Branch-Line Couple”, *IEEE Trans. on Antennas and Propagation*, vol.60, no.2, pp.786-791, Feb. 2012.

[57] J. Liu, Z.-J. Zhang, and Y. Yang, "Performance enhancement of subspace detection with a diversely polarized antenna," *IEEE Signal Processing Letters,* vol. 19, pp. 4-7, 2012.

[58] E. Doumanis, G. Goussetis, J. L. Gomez-Tornero, R. Cahill, and V. Fusco, "Anisotropic impedance surfaces for linear to circular polarization conversion," *IEEE Transactions on Antennas and Propagation*, vol. 60, pp. 212-219, 2012.

[59] H. Makimura, Y. Watanabe, K. Watanabe, and H. Igarashi, "Evolutional design of small antennas for passive UHF-band RFID," 445 Hoes Lane / P.O. Box 1331, Piscataway, NJ 08855-1331, United States, 2011, pp. 1510-1513.

[60] I. Chen and C. Peng, “Compact Modified Pentaband Meander-Line Antenna for Mobile Handsets Applications,” *IEEE Antennas and Wireless Propagation Letters*, vol.10, pp. 607-610, 2011.

[61] W.-T. Hsieh and J.-F. Kiang, "Small broadband antenna composed of dual-meander folded loop and disk-loaded monopole," *IEEE Transactions on Antennas and Propagation*, vol. 59, pp. 1716-1720, 2011.

[62] C. Occhiuzzi, C. Paggi and G. Marrocco, “Passive RFID Strain-Sensor Based on Meander-Line Antennas”, *IEEE Trans. on Antennas and Propagation*, vol.59, no.12, pp. 4836-4840, Dec. 2011.

[63] Y. Dong and T. Itoh, "Substrate integrated composite right-/left-handed leaky-wave structure for polarization-flexible antenna application," *IEEE Transactions on Antennas and Propagation,* vol. 60, pp. 760-771, 2012.

[64] D. M. Monro, Fortran 77. British library Cataloguing in Publication Data, London, 1982.

[65] T. Weise, (2009). Global Optimization Algorithms – Theory and Application, 2nd ed. [Online eBook].Available: Weise, http://www.it-weise.de/ Ver. 2009, [Accessed: 02 March 2012].

[66] J. Leech, T. K. Boon, G. Yassin, P. Kittara and S. Wangsuya, “Experimental Investigation of a Low-Cost, High Performance Focal-Plane Horn Array”, *IEEE Trans. on Terahertz Science and Technology*, vol.2, no.1, pp. 61-70, Jan. 2012.

[67] L. D. S. Coelho, T. C. Bora, and L. Lebensztajn, "A chaotic approach of differential evolution optimization applied to loudspeaker design problem," 445 Hoes Lane / P.O. Box 1331, Piscataway, NJ 08855-1331, United States, 2012, pp. 751-754.

[68] L. Cen, Z. L. Yu, W. Ser, and W. Cen, "Linear aperiodic array synthesis using an improved genetic algorithm", *IEEE Transactions on Antennas and Propagation,* vol. 60, pp. 895-902, 2012.

[69] D. Kim, J. Ju, and J. Choi, "A mobile communication base station antenna using a genetic algorithm based fabry-perot resonance optimization", *IEEE Transactions on Antennas and Propagation*, vol. 60, pp. 1053-1058, 2012.

[70] C. Hua and R. Zheng, "Robust topology engineering in multiradio multichannel wireless networks", *IEEE Transactions on Mobile Computing*, vol. 11, pp. 492-503, 2012.

[71] Y. Zhou, C.-H. Woo, and Y. Zheng, "Magneto-electric coupling in a multiferroic tunnel junction functioning as a magnetic-field-effect transistor", *IEEE Transactions on Nanotechnology*, vol. 11, pp. 77-81, 2012.

[72] E. E. Altshuler, "Design of a vehicular antenna for GPS/IRIDIUM using a genetic algorithm", *IEEE Transactions on Antennas and Propagation*, vol. 48, pp. 968-972, 2000.

[73] B. Glover and H. Bhatt., RFID Essentials. Beijing, Farnham, CA:O'Reilly, Jan. 2006.

[74] Arlon Materials for Electronics, (2007) Rev E. Arlon Materials for Electonics Division. [Online]. Available: www.arlon-med.com. [Accessed: 01 Sept. 2012].

[75] M. S. Alkhambashi, D. Zhou, R. A. Abd-Alhameed, C. H. See, Z. Zainal Abidin, K. N. Ramli, et al., "Meander-line antenna design for UHF RFID tag using a genetic algorithm," Presented at Progress In Electromagnetics Research Symposium, March 23-27, Beijing, China, 2009, pp.1253-1256.

[76] Chemtronics Technical Data Sheet, (2010, Feb.). Chemical Product and Company Information, 8125 Cobb Centre Drive, Kemesaw, GA 30152, 1-770-4244888. [Online]. Available: http://www.technitool.com/content/resources/MSDS/237CH204.pdf. [Accessed: 22 April 2009].

[77] S. K. Sharma, and L. Shafai, "Performance of a Novel Ψ-Shape Microstrip Patch Antenna with Wide Bandwidth", *IEEE Antennas and Wireless Propagation Letters*, vol.8, pp. 468-471, 2009.

[78] W. Kin-Lu and C. Chih-Hua, "WLAN Chip Antenna Mountable Above the System Ground Plane of a Mobile Device", *IEEE Trans. on Antennas and Propagation*, vol.53, no.11, pp. 3496-3499, November 2005.

[79] D. M. Nashaat, H. A. Elsadek, and H. Ghali, "Single feed compact quad-band PIFA antenna for wireless communication applications", *IEEE Transactions on Antennas and Propagation*, vol. 53, pp. 2631-2635, 2005.

[80] Alien Technology, (2007, Jan). Hardware Setup Guide, [Online]. Available: http://www.alientechnology.com. [Accessed: 16 April 2010].

[81] The High Frequency Structure Simulator (HFSSTM Ver. 11), User Manual, Ansoft Corporation, Pittsburgh (USA). Available: http://www.ansoft.com/products/hf/hfss/, (part of the ANSYS Group). [Accessed: 01 Jan 2009].

[82] A. Ren, C. Wu, Y. Gao, and Y. Yuan, "A robust UHF near-field RFID reader antenna", *IEEE Transactions on Antennas and Propagation*, vol. 60, pp. 1690-1697, 2012.

[83] Y. Okano, "A simple shape broad and planar antenna adaptable to RFID-tag", *IEEE Transactions on Antennas and Propagation*, vol. 54, pp. 1885-1888, 2006

[84] Computer Simulation Technology Corporation, CST Microwave Studio, Version 5.0, Computer Simulation Technology Corporation, Germany.

[85] S. Ahson and M. Ilyas, RFID Handbook, Applications, Technology, Security and privacy. Taylor &Francis Group LCC, 2008.

[86] M. Jo, H. Y. Youn, S.-H. Cha, and H. Choo, "Mobile RFID tag detection influence factors and prediction of tag detectability", *IEEE Sensors Journal*, vol. 9, pp. 112-119, 2009.

[87] X. Qing, C. K. Goh, and Z. N. Chen, "Impedance characterization of rfid tag antennas and application in tag co-design", *IEEE Transactions on Microwave Theory and Techniques*, vol. 57, pp. 1268-1274, 2009.

[88] S.-K. Kuo and L.-G. Liao, "An analytic model for impedance calculation of an RFID metal tag", *IEEE Antennas and Wireless Propagation Letters*, vol. 9, pp. 603-607, 2010.

[89] T. Deleruyelle, P. Pannier, M. Egels, and E. Bergeret, "An RFID tag antenna tolerant to mounting on materials," 445 Hoes Lane - P.O.Box 1331, Piscataway, NJ 08855-1331, United States, 2010, pp. 14-19.

[90] H.-W. Son and G.-Y. Choi, "Orthogonally proximity-coupled patch antenna for a passive RFID TAG on metallic surfaces", *Microwave and Optical Technology Letters*, vol. 49, pp. 715-717, 2007.

[91] H. Kwon and B. Lee, "Compact slotted planar inverted-F RFID tag mountable on metallic objects", *Electronics Letters*, vol. 41, pp. 1308-1310, 2005.

[92] K. H. Kim, J. G. Song, D. H. Kim, H. S. Hu, and J. H. Park, "Fork-shaped RFID tag antenna mountable on metallic surfaces", *Electronics Letters*, vol. 43, pp. 1400-1402, 2007.

[93] J. S. Kim, W. Choi, and G. Y. Choi, "UHF RFID tag antenna using two PIFAs embedded in metallic objects", *Electronics Letters*, vol. 44, pp. 1181-1182, 2008.

[94] C. Sung-Lin and L. Ken-Huang, "A Slim RFID Tag Antenna Design for Metallic Object Applications", *IEEE Antennas and Wireless Propagation Letters*, vol.7, pp.729-732, Nov. 2008.

[95] D. Kim and J. Yeo, "Low-profile RFID tag antenna using compact AMC substrate for metallic objects", *IEEE Antennas and Wireless Propagation Letters*, vol. 7, pp. 718-720, 2008.

[96] J. D. Griffin, G. D. Durgin, A. Haldi, and B. Kippelen, "RF tag antenna performance on various materials using radio link budgets", *IEEE Antennas and Wireless Propagation Letters*, vol. 5, pp. 247-250, 2006.

[97] B. Gao and M. M. F. Yuen, "Passive UHF RFID packaging with electromagnetic band gap (EBG) material for metallic objects tracking", *IEEE Transactions on Components, Packaging and Manufacturing Technology*, vol. 1, pp. 1140-1146, 2011.

[98] G. Kapoor and S. Piramuthu, "Single RFID tag ownership transfer protocols", *IEEE Transactions on Systems, Man and Cybernetics Part C: Applications and Reviews*, vol. 42, pp. 164-173, 2012.

[99] L. Catarinucci, D. De Donno, R. Colella, F. Ricciato, and L. Tarricone, "A cost-effective SDR platform for performance characterization of RFID tags", *IEEE Transactions on Instrumentation and Measurement*, vol. 61, pp. 903-911, 2012.

[100] J.-Y. Jung, C.-W. Park, and K.-W. Yeom, "A novel carrier leakage suppression front-end for UHF RFID reader," in MINI-SPECIAL ISSUE ON 2011 RADIO FREQUENCY INTEGRATED CIRCUITS (RFIC) SYMPOSIUM, 445 Hoes Lane / P.O. Box 1331, Piscataway, NJ 08855-1331, United States, 2012, pp. 1468-1477.

[101] F. Paredes, G. Zamora, J. Bonache, and F. Martin, "Dual-band impedance-matching networks based on split-ring resonators for applications in RF identification (RFID)", *IEEE Trans. Microw. Theory Tech.,* vol.58, no.4, pp. 1159–1166, Apr. 2011.

[102] W.-I. Son, M.-Q. Lee, and J.-W. Yu, "Module integrated antenna with circular polarization for mobile UHF RFID reader", *IEEE Transactions on Microwave Theory and Techniques,* vol. 59, pp. 1157-1165, 2011.

[103] F. Paredes, G. Zamora, F. J. Herraiz-Martinez, F. Martin, and J. Bonache, "Dual-band UHF-RFID tags based on meander-line antennas loaded with spiral resonators," *IEEE Antennas and Wireless Propagation Letters*, vol. 10, pp. 768-771, 2011.

[104] D. Zhou, S. Gao, R. A. Abd-Alhameed, C. Zhang, M. S. Alkhambashi, and J. D. Xu, "Design and optimisation of compact hybrid quadrifilar helical-spiral antenna in GPS applications using Genetic Algorithm," in 6th European Conference on Antennas and Propagation, *EuCAP 2012*, March 26, 2012 - March 30, 2012, Prague, Czech republic, 2012.

[105] N. Padros, J. I. Ortigosa, J Baker, M. F. Iskander and B. Thornber, "Comparative study of high-performance GPS receiving antenna designs", *IEEE Trans. on antennas and propagation*, vol.45, no.4, pp. 698-706, 1997.

[106] R. A. Abd-Alhameed, M. Mangoud, P. S. Excell, and K. Khalil, "Investigations of polarization purity and specific absorption rate for two dual-band antennas for satellite-mobile handsets," *IEEE Transactions on Antennas and Propagation*, vol. 53, pp. 2108-2110, 2005.

[107] D. E. Goldberg, Genetic Algorithms in Search, Optimization and Machine Learning. Addison-Wesley, 1997.

[108] J. M. Johnson and Y. Rahmat-Samii, "Genetic Algorithms in Engineering Electromagnetics" *IEEE Antennas and Propagation Magazine*, vol.39, no.4, pp.7-21, 1997.

[109] D. Zhou, S. Gao, R. A. Abd-Alhameed, C. Zhang, M. S. Alkhambashi, and J. D. Xu, "Design and optimisation of compact hybrid quadrifilar helical-spiral antenna in GPS applications using Genetic Algorithm," in 6th European Conference on Antennas and Propagation, *EuCAP 2012*, March 26, 2012 - March 30, 2012, Prague, Czech republic, 2012.

[110] E. E. Altshuler and D. S. Linden, "Wire-antenna designs using genetic algorithms", *IEEE Antennas and Propagation Magazine*, vol. 39, pp. 33-43, 1997.

[111] R. A. Abd-Alhameed, D. Zhou, and P. S. Excell, "A wire-grid adaptive-meshing program for microstrip-patch antenna designs using a genetic algorithm [EM Programmer's Notebook]", *IEEE Antennas and Propagation Magazine*, vol. 51, pp. 147-151, 2009.

[112] D. L. Carroll, FORTRAN Genetic Algorithm Driver, Version 1.7. [Online]. Available: http://www.staff.uiuc.edu/~carroll/ga.html. [Accessed: 12 Nov 1998].

[113] G. L. Burke and A. J. Poggio, Numerical Electromagnetics Code (NEC)-Method of Moments. Lawrence Livermore Laboratory, Livermore, CA, 1981.

[114] M. M. Ilic, M. Djordjevic, A. Z. Ilic, and B. M. Notaro, "Higher order hybrid FEM-MoM technique for analysis of antennas and scatterers", *IEEE Transactions on Antennas and Propagation*, vol. 57, pp. 1452-1460, 2009.

[115] S.-Y. Hyun and S.-Y. Kim, "3-D thin-wire FDTD approach for resistively loaded cylindrical antennas fed by coaxial lines", *IEEE Transactions on Antennas and Propagation*, vol. 58, pp. 4095-4099, 2010.

[116] D. M. Sullivan, Electromagnetic Simulation using the FDTD Method The institute of Electrical and Electronics Engineers, New York, 2000.

[117] H. E. Abd-El-Raouf, "A class of finite difference time domain (FDTD) techniques for solving large electromagnetic structures," in 2006 *International RF and Microwave Conference,* RFM, September 12, 2006 - September 14, 2006, Putrajaya, Malaysia, 2006, pp. 301-305.

[118] L. John, C. Arindam and C.K. Leo, “Finite element method for electromagnetic: Antenna, Microwave Circuits and Scattering Application”, *IEEE antenna & propagation society*. Wiley, Jun 1998.

[119] W .L. Stutzman and G. A. Thiele, Antenna theory and design. pp 20, 2012.

[120] C. H. Schmidt, M. M. Leibfritz, and T. F. Eibert, "Fully probe-corrected near-field far-field transformation employing plane wave expansion and diagonal translation operators", *IEEE Transactions on Antennas and Propagation*, vol. 56, pp. 737-746, 2008.

[121] T. Luciano, Alessandra E., Advances in Information Technologies for Electromagnetics. 2006.

[122] B.-Z. Wang, Y. Wang, W. Yu, and R. Mittra, "A hybrid 2-D ADI-FDTD subgridding scheme for modeling on-chip interconnects", *IEEE Transactions on Advanced Packaging*, vol. 24, pp. 528-533, 2001.

[123] R. A. Abd-Alhameed, P. S. Excell, and J. A. Vaul, "Currents induced on wired I.T. networks by randomly distributed mobile phones - A computational study", *IEEE Transactions on Electromagnetic Compatibility,* vol. 48, pp. 282-286, 2006.

[124] P. A. Mason, W. D. Hurt, T. J. Walters, J. A. D'Andrea, P. Gajsek, K.L. Nelson, et al., "Effects of frequency, permittivity, and voxel size on predicted specific absorption rate values in biological tissue during electromagnetic-field exposure", *IEEE Trans. on Microwave Theory and Techniques*, vol.48 ,no.11, pp. 2050 – 2058, 2000.

[125] W. Ying, S. Safavi-Naeini, S. K. Chaudhuri, "A hybrid technique based on combining ray tracing and FDTD methods for site-specific modelling of indoor radio wave propagation", *IEEE Trans. on Antennas and Propagation*, vol.48 , no.5 , pp. 743 –754, 2000.

[126] T. Luciano. and E. Alessandra, Advances in Information Technologies for Electromagnetics, Springer, The Netherlands, Dordrecht, 2006.

[127] I. T. E. Elfergani, R. A. Abd-Alhameed, C. H. See, T. Sadeghpour, J. M. Noras, and S. M. R. Jones, "Small size tuneable printed F-slot antenna for mobile handset applications", *Microwave and Optical Technology Letters*, vol. 54, pp. 794-802, 2012.

[128] H. Wegleiter, B. Schweighofer, C. Deinhammer, G. Holler and P. Fulmek "Automatic Antenna Tuning Unit to Improve RFID System Performance", *IEEE*

Trans. on Instrumentation and Measurement, vol.60, no.8, pp. 2797-2803, Aug. 2011.

[129] Nasimuddin, Z. N. Chen, and X. Qing, "Asymmetric-circular shaped slotted microstrip antennas for circular polarization and RFID applications", *IEEE Transactions on Antennas and Propagation*, vol. 58, pp. 3821-3828, 2010.

[130] Garber and Lee, "news Briefs*", IEEE Journals and Magazines*, Computer, vol.45, no.3, pp. 18-20, 2012.

Selected Author's publications

A Novel RFID Tag Antenna Mountable on Metallic Objects

M.S. Alkhambashi[#1], A.S. Hussaini[*2], R.A.Abd-Alhameed[#1], C.H. See[#1], J.M. Noras[#1], M.B. Child[#1], J. Rodriguez[*2]
[#]Mobile and Satellite Communications Research Centre University of Bradford,
Bradford, West Yorkshire, BD7 1DP, UK
[1]{msaalkha, r.a.a.abd, c.h.see, j.m.noras, m.b.child} @bradford.ac.uk
[*]Instituto de Telecomunicações – Aveiro, Portugal
[2]{ash@av.it.pt, jonathan@av.it.pt}

***Abstract*—This paper investigates the design of UHF RFID tagging antennas mounted on, or in close proximity, with a conducting surface. Detailed simulation and analysis of the tag antenna was carried out for 900 MHz operation. The antenna dimensions were fixed at 32.5 mm × 9.5 mm × 1.6 mm. From simulation the input impedance of the target transponder antenna was found to be (14.3-j140.9) Ω, normalized to 50 Ω. The final design was tested to identify an object consisting of a metal surface, the effective detection was found to be between 0.7 m and 1.2 m.**

Keywords- passive RFID tag; antenna; conducting surface; measurment

I. INTRODUCTION

RFID tagging technologies are a rapidly becoming a ubiquitous form of auto-identification in a range of applications in logistics, commerce, and environmental infrastructure. This popularity stems from the ability to track objects and associated information on static or moving objects quickly and in multiple data types. Typical data transfer times are less than 100 ms [1-3]. RFID devices can be deployed in awkward environments, although practical limitations. RFID devices are capable of being implemented in physically awkward environments, although there are some practical limitations in this respect. Thus far commercial and logistic applications have tended to dominate the field, e.g. access control (tollgates) and product or component tracking; there is also a rapidly developing biomedical applications field.

RFID systems involve a radio transponder (the 'tag') and reader or interrogator. The RF antenna is a key part of the system, and often presents a serious design challenge as it must have a direct connection to the tag's ASIC (application specific integrated chip). The ASIC input impedance always presents a capacitive reactance. It follows that the reactive nature of the tag antenna must be properly realized as the complex conjugate of the ASIC input impedance to enable the maximum transmission using the RF power induced from the tag. Microstrip antennas have an obvious attraction for such applications. They may be easily constructed with given radiation and polarization properties, and made to work in most normal operating environments [4-6]. This work is concerned with overcoming the difficulties of identifying a given passive tag in close proximity with metal surfaces. Recent work in this area includes the possible use of EBG material [7] and the integration of a tag with aluminum foil packaging [8].

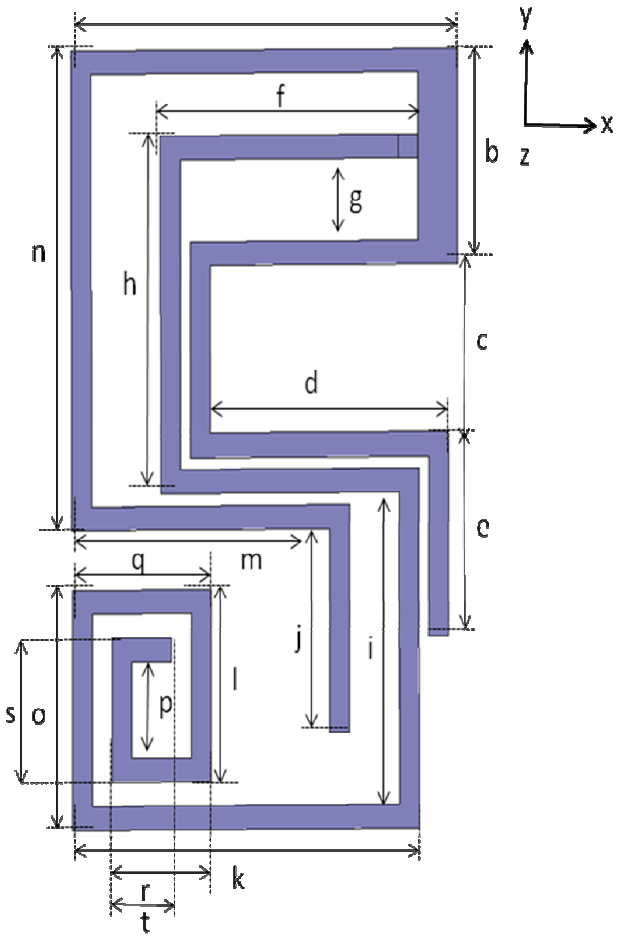

Figure 1a. RFID tag antenna for metal surface: the proposed (S)- Shape antenna's geometry.

II. RFID TAG'S ANTENNA MODEL

The target frequency band and RF specification is the European UHF RFID band, which has a centre frequency of 900 MHz and a bandwidth of 3 MHz. The ASIC selected for this tag IC design is a Higgs IC, which has been designed to

follow the EPCglobal Class-1 Gen-2 specification, therefore, the used input impedance is (15 + j140) Ω. Instead of a standard meander line antenna, an S-shaped printed line antenna has been designed using the FR4-epoxy substrate which has a permittivity of 4.5 and loss tangent of 0.017 at 900 MHz. Moreover, 1.6 mm substrate thickness has been employed. Consequently, the first cut dimensions have been found from simulation using HFSS [9]. Indeed, a candidate structure with principal linear dimensions of 32.5 mm × 19.5 mm has been prototyped and illustrated in Figure 1. Furthermore, for more details about the intended design dimensions see Table 1.

Figure 1b. RFID tag antenna for metal surface: antenna prototype with Alien chip (Higgs-2).

TABLE I. PARAMETERS OF THE PROPOSED RFID TAG'S ANTENNA

Parameter	Value mm	Parameter	Value mm
a	19.5	***K***	17.5
b	9	***L***	8
c	0.5	***M***	13
d	12	***N***	20
e	8.5	***O***	10
f	13	***P***	4
g	0.5	***Q***	7
h	14.9	***R***	5
i	13	***S***	6
j	8.5	***T***	2

III. PROTOTYPE RESULTS AND DISCUSSIONS

The antenna has been connected with the tag IC, and preliminary distance detection tests have been carried out. As a result of the tag antenna input impedance has been optimized as (14.3 – j 140.9) Ω, at a desired frequency such as 900 MHz which is commonly normalized to 50 Ω throughout the whole RFID band. In contrast, the detection rate has been measured and found is greater than 75 cm.

For comparison, the simulated (HFSS) and measured antenna's result of reflection coefficients have been visualized and depicted in the Figure 2. Obviously, the measured results have been shown agree well with simulated results. In contrast, the simulated gain performance has been given in Figure 3.

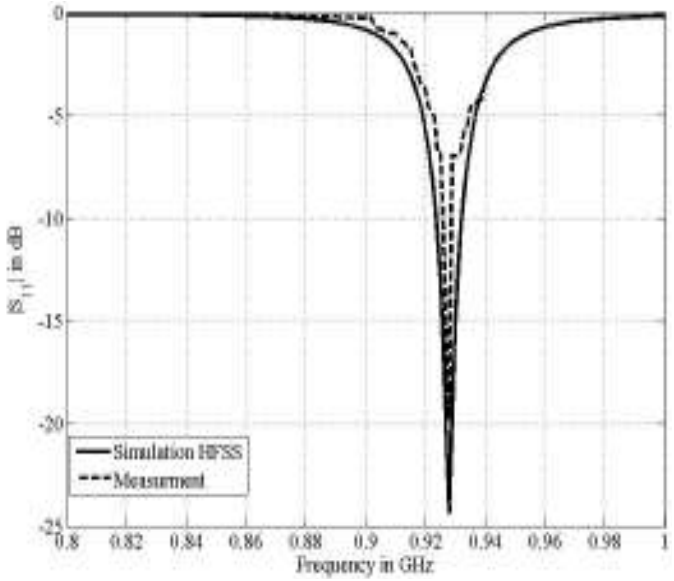

Figure 2. REFECTION COEFFICIENT |S11| FOR THE OPTIMISED DESIGN

As observed from Figure 3, the gain factor of such tag's antenna when placed on the metallic surface has been presented. It is worth mentioning that the detection rate could be decreases a few times compared to the normal range of tag's when its work in the non-conducting surface. Indeed, the simulated and measured results have been obtained and looked closer to each other.

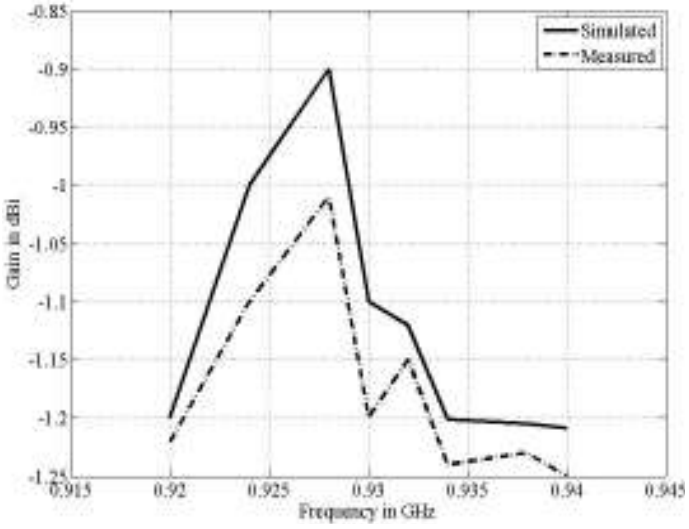

Figure 3. Simulated gain of proposed RFID tag's antenna design

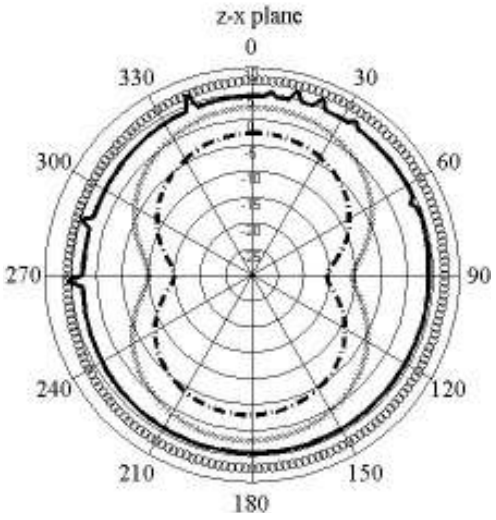

(a)

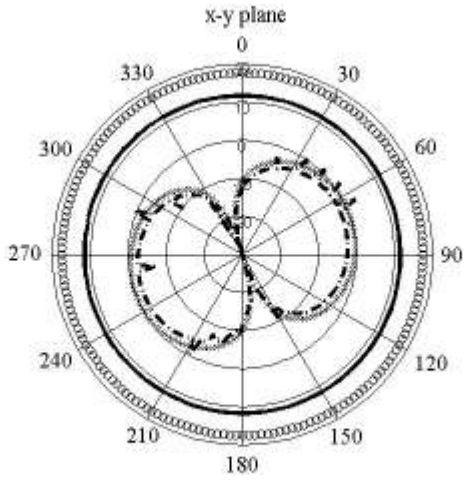

(B)

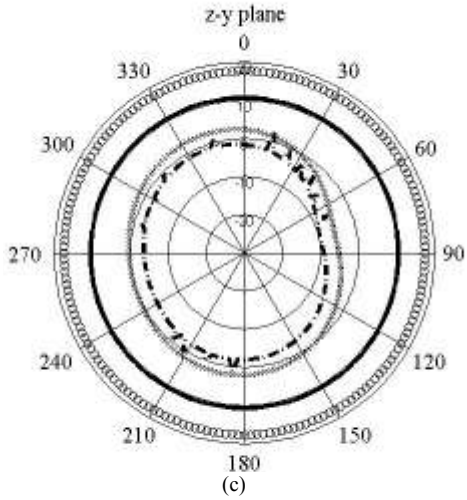

(c)

Figure 4. The simulated and measured normalized radiation patterns results of the optimum RFID tag's antenna in: a) *z-x* plane, b) *x-y* plane and c) *z-y* plane at 900MHZ.
'oo' simulated co-polarization, 'xx' simulated cross-polarization,
'—' measured co-polarization and '-.-.-'measured cross-polarization.

The computed antenna patterns were compared with the measurement results, see Figure 4, (a, b and c) which shows the z-x, x-y and z-y planes, respectively. The results are fully consistent with one another, in particular the z-x and x-y planes demonstrate a typical omni-directional pattern. The current distribution was computed within the simulation, see Figure 7, it can be seen that the maximum current is distributed about the feed point.

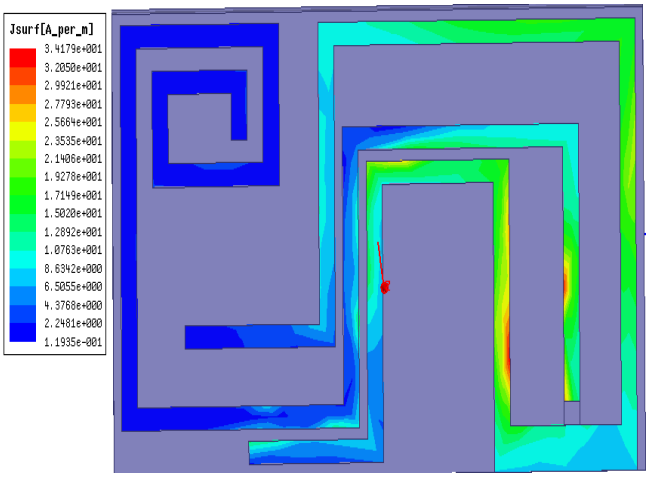

Figure 5. The current distribution of the tag's antenna at 900MHz.

IV. CONCLUSION

The design of a mountable RFID tag has been presented for UHF frequencies and situations where the tag is expected to be in close proximity of metallic surfaces. Detailed electromagnetic simulation of the antenna tag sub-system indicated an impedance of (14.3 – j140.9) Ω at 900 MHz. The tag antenna has been tested using an Alien ALR8800 RFID reader, the detection range is found to be better than 75 cm. The radiation patterns in the z-x and z-y planes are omni-directional, and the characteristics are similar to those of a dipole antenna.

ACKNOWLEDGMENT

MSA would like to acknowledge the technical support from the School of Engineering workshop.

REFERENCES

[1] S. Ahson and M. Ilyas, "RFID Handbook, Applications, Technology, Security and privacy", Taylor &Francis Group LCC, 2008.

[2] S. Chen, K.-H. Lin and R. Mittra, "A Measurement Technique for Verifying the Match", *IEEE Transactions on Instrumentation and Measurement*, vol. 59, no. 8, pp.2123-2133, Aug. 2010.

[3] M. Jo, *et al*, "Mobile RFID Tag Detection Influence Factors and Prediction of Tag Delectability", *IEEE Sensors Journal*, vol. 9, no. 2, pp .112-119, Feb. 2009.

[4] X. Qing, C.K. Goh and Z.N. Chen; "Impedance Characterization of RFID Tag Antennas and Application in Tag Co-Design", *IEEE Transactions On* Microwave Theory and Techniques, vol. 57, no. 5, pp. 1268 – 1274, May 2009.

[5] S. Kuo, L. Liao, "An Analytic Model for Impedance Calculation of an RFID Metal Tag", IEEE Antennas and Wireless Propagation Letters, vol. 9, pp. 603-607, 2010.

[6] T. DeJeruyell, et al., "An RFID Tag Antenna Tolerant to Mounting on Materials", *IEEE Antennas and Propagation Magazine,* vol. 52, no. 4, pp. 14-19, Aug. 2010.

[7] B. Gao and M. M. F. Yuen, "Passive UHF RFID Packaging with Electromagnetic Band Gap (EBG) Material for Metallic Objects Tracking", *IEEE Transactions On Components, Packaging And Manufacturing Technology*, vol. 1, no. 8, pp. 1140-1146, Aug. 2011.

larger than the bandwidth of the PDs. The fundamental frequencies used were 10 GHz and 10.1 GHz, and the result of the measurement of the UTC-PD at 40 mA is shown in Figure 3 (right inset). The two tone measurements were repeated for different photocurrents, and the results are presented as the OIP3 versus the photocurrent in Figure 4(a). The OIP3 of the UTC-PD was found to be increasing with bias voltage, and therefore a bias −6 V was chosen, which was found to be the largest safe voltage. The increase of the OIP3 with voltage is consistent with results of [8]. Because of the dynamic range limitations of the ESA, the measurements of PIN-PD and the UTC-PD were limited to photocurrents between 5 and 13 mA, and 15 and 40 mA, respectively. The UTC-PD had about 15–20 dB larger OIP3 in this measurement range. The measurements of the linearity and noise can be added together under the assumption that the photodetector is limiting the link, as mentioned in the introduction, and thus, the SFDR can be calculated and is plotted as a function of photocurrent in Figure 4(b). As a consequence of the high OIP3 of the UTC-PD, the SFDR is more than 10 dB higher than for the PIN-PD.

4. DISCUSSION AND CONCLUSIONS

In our experiment, we observed only a minor increase in CNR when operating the UTC-PD at photocurrents beyond what the PIN-PD could handle. However, the CNR could be increased with higher OSNR and larger photocurrents. From a linearity point of view, it is a great benefit to use the UTC-PD compared with the PIN-PD because of their opposite behavior of the OIP3. The result that the UTC-PD's OIP3 increasing with photocurrent is consistent with previously published results [8]. This is explained by the self-bias effect improves the RF response with increased photocurrent and that the space-charge effect is not dominant. The OIP3 is over 16 dB better for the UTC-PD compared with the PIN-PD. If the dynamic range is considered for the UTC-PD, we have that both the noise floor and the OIP3 are increasing with photocurrent but at different rate. The optimum dynamic range is given by the SFDR, which then is a function of photocurrent. However, it can be concluded that it is beneficial to use the UTC-PD as the increase in OIP3 nearly counteracts the increase of the noise floor and thereby only results in minor decrease of SFDR with increased photocurrent.

In conclusion, we have compared the linearity and the performance in realistic noise environment of a typical UTC-PD and a commercial PIN-PD. It is found that it is beneficial to use a UTC-PD compared with a PIN-PD, as the UTC-PD has superior OIP3, which even increases with photocurrent. Thus, the SFDR of the UTC-PD decreases very slowly with high photocurrents compared to the PIN-PD.

REFERENCES

1. C.H. Cox, III, Analog optical link: Theory and practice, Cambridge University Press, Cambridge, U.K., 2004.
2. V. Urick, M. Rogge, P. Knapp, L. Swingen, and F. Bucholtz, Wide-band predistortion linearization for externally modulated long-haul analog fiber-optic links, IEEE Trans Microwave Theory Tech 54 (2006), 1458–1463.
3. E. Ackerman, Broad-band linearization of a Mach-Zehnder electro-optic modulator, IEEE Trans Microwave Theory Tech 12 (1999), 2271–2279.
4. G. Betts, Linearized modulator for suboctave-bandpass optical analog links, IEEE Trans Microwave Theory Tech 12 (1994), 2642–2649.
5. R.B. Welstand, S. Pappert, C.K. Sun, J.T. Zhu, Y.Z. Liu, and P.K.L. Yu, Dual-function electroabsorption waveguide modulator-detector for optoelectronic transceiver applications, IEEE Photon Technol Lett 11 (1996), 1540–1542.
6. V. Urick, M. Rogge, F. Bucholtz, and K. Williams, The performance of analog photonic links employing highly compressed erbium-doped fiber amplifiers, IEEE Trans Microwave Theory Tech 7 (2006), 3141–3145.
7. K. Williams, L. Nichols, and R. Esman, Photodetector nonlinearity limitations on a high-dynamic range 3 GHz fiber optic link, J Lightwave Technol 2 (1998), 192–199.
8. T. Ohno, H. Fukano, Y. Muramoto, T. Ishibashi, T. Yoshimatsu, and Y. Doi, Measurement of intermodulation distortion in a uni traveling carrier refracting-facet photodiode and a p-i-n refracting-facet photodiode, IEEE Photon Technol Lett 3 (2002), 375–377.
9. M. Gustavsson, P.O. Hedekvist, and P.A. Andrekson, Uni-travelling-carrier photodiode performance with X-band modulation at high optical power, IEEE Microwave Wireless Compon Lett 5 (2005), 297–299.
10. T. Ishibashi, T. Furuta, H. Fushumi, S. Kodama, H. Ito, T. Nagatsuma, N. Shimuzu, and Y. Miyamoto, InP/InGaAs uni-traveling-carrier photodiodes, IEICE Trans Electron E83-C (2000), 938–949.
11. G.P. Agrawal, Fiber-optic communication system,2nd ed., Wiley, New York, NY, 1997.

DESIGN OF DUAL-BAND QUADRIFILAR SPIRAL ANTENNAS FOR SATELLITE-MOBILE HANDSETS

R. A. Abd-Alhameed,[1] D. Zhou,[1] C. H. See,[1] P. S. Excell,[2] M. M. Abusitta,[1] M. S. Alkhambashi,[1] and N. J. McEwan[1]

[1] Mobile and Satellite Communications Research Centre, Bradford University, Bradford, West Yorkshire, BD7 1DP, United Kingdom; Corresponding author: r.a.a.abd@bradford.ac.uk

[2] The Glyndwr University Wrexham, Wrexham, Wales, LL11 2AW, United Kingdom

Received 7 July 2009

ABSTRACT: *A novel quadrifilar spiral antenna is proposed for use in personal communications mobile terminals exploiting the "big low earth orbit" (big-LEO) satellite system (uplink 1.61–1.63 GHz; downlink 2.48–2.5 GHz). Feeding of the antenna from the outer periphery is proposed, to avoid the complexity and space requirements of a centre feed; an externally fed antenna can also be fed either by coaxial cables or stripline. Moreover, the hybrid phasing network and the matching network (if required) can be located outside and possibly printed in the same plane as the antenna structure. Versions of the design were investigated using the method of moments and in hardware realizations. These had a finite ground plane with air dielectric between the spirals and the ground plane. Performance suitable for satellite mobile system applications was demonstrated, including dual-band matching.* © 2010 Wiley Periodicals, Inc. Microwave Opt Technol Lett 52: 987–990, 2010; Published online in Wiley InterScience (www.interscience.wiley.com). DOI 10.1002/mop.25090

Key words: *quadrifilar spiral antenna (QSA); circular polarization; antennas; personal satellite communications*

1. INTRODUCTION

Spiral antennas are particularly known for their ability to produce a very wideband almost a perfect circularly polarized radiation over their full coverage region [1–5]. As a result of this polarization characteristic and the ability to produce a broad zenith-directed pattern, spiral antennas are popular for their use in satellite mobile communication handsets [2, 6, 7]. This concept was developed for personal communication antennas for "a big low earth orbit" (big-LEO) satellite system mobile terminal,

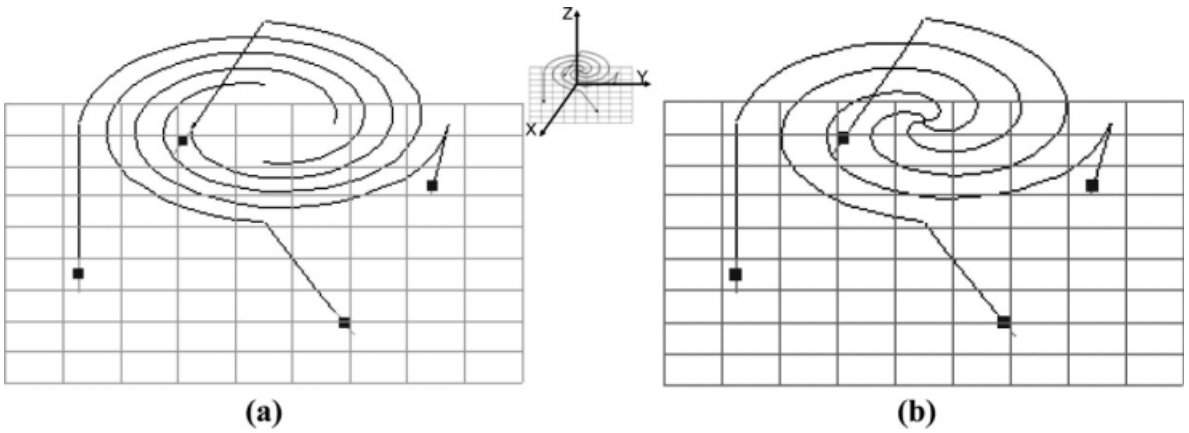

Figure 1 Basic geometry of quadrifilar spiral antennas fed from outside; (a) QSA with free (unconnected) inner ends and (b) QSA with connected inner ends

TABLE 1 Geometrical Data for Quadrifilar Spiral Antennas

Inner End Connection	Free	Connected
Wire radius (m)	0.00025	0.00025
Spiral height (m)	0.0175	0.018
Number of turns	1.42	1.3
Spacing between turns (m)	0.013	0.0159
Inner start radius of spiral (m)	0.017	0
End radius of spiral (m)	0.0278	0.028
Spiral constant (m/radian)	0.248	0.253

using the uplink and downlink bands of 1.61–1.63 GHz (L band) and 2.48–2.5 GHz (S band) respectively [7]. Earlier and recent studies [2, 5] for single, dual, and quadrifilar spirals were restricted by the need to feed the antennas from the centre. This causes additional constraints on the size and the mutual coupling between the feeding ports. These problems have been solved here by applying the feeding ports on the outside, thus avoiding the complexity and space requirement of a centre feed. An externally fed antenna also offers the option of feeding either by coaxial cables or stripline and the hybrid phasing and the matching networks can be located outside and possibly printed in the same plane as the antenna structure. This study was performed on a finite ground plane of dimensions 6×6 cm^2 with air dielectric between the spirals and the ground plane for convenience (a solid dielectric version would be significantly smaller). An industry-standard frequency-domain MoM program was used for computer simulations.

2. CONFIGURATION OF QUADRIFILAR SPIRAL ANTENNAS

Quadrifilar spiral antennas (QSAs) consist of four separate spiral arms, each rotated by 90° with respect to its neighbors (Fig. 1). The feed signal for each of the arms is 90° out of phase with respect to its neighbors. The Archimedean spiral configuration [5] with small pitch turns was adopted and fitted within a 6×6 cm^2 planar area. The area can be varied, subject to meeting the required antenna performance for personal satellite services. In addition, some extra spacing between the wires should be allowed to prevent degradation by proximity effects between closely parallel wires [8]. Figure 2 shows photos of the antennas.

The antenna is designed to provide circular polarization in the elevation angular region from zenith to ±60° in both the L and S bands (range 1.61–1.63 GHz and 2.48–2.5 GHz). The dual band antenna should provide a maximum voltage standing

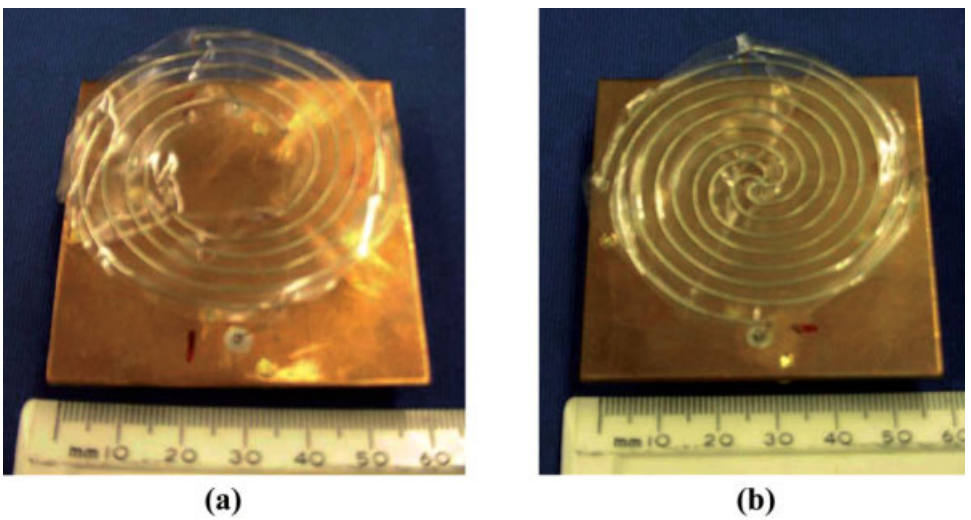

Figure 2 Prototypes of quadrifilar spiral antennas; (a) QSA with free inner ends and (b) QSA with connected inner ends. [Color figure can be viewed in the online issue, which is available at www.interscience.wiley.com]

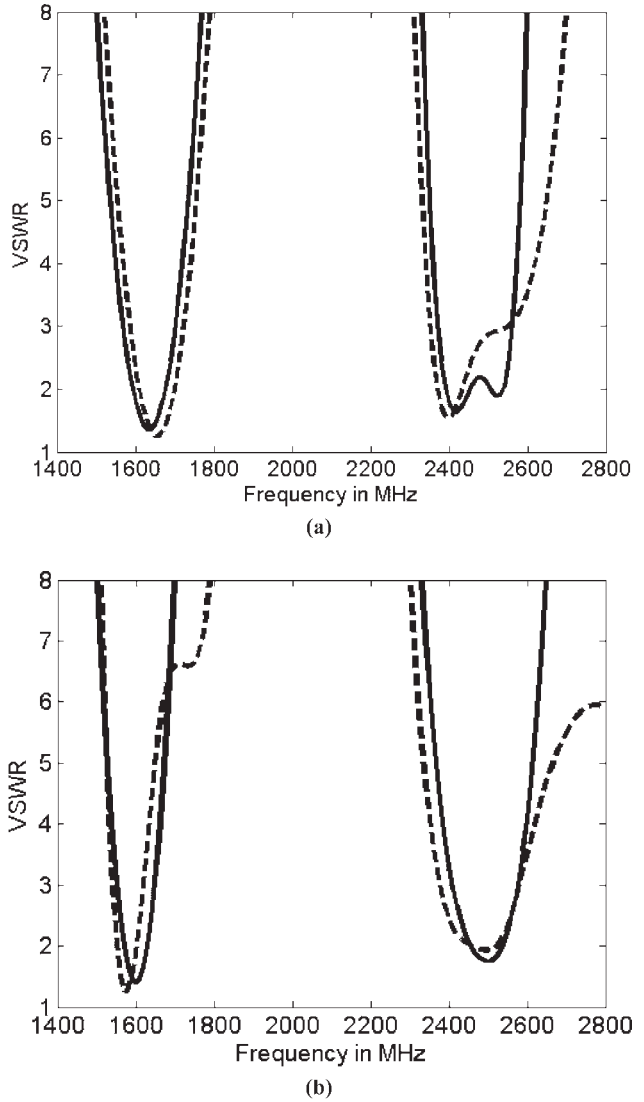

Figure 3 Simulated and measured voltage standing wave ratio versus the operating frequency for QSAs; (a) with free inner ends and (b) with connected inner ends, (simulated: "_____," measured: "---------")

wave ratio (VSWR) of 2:1 over the whole range of the bands and also a reasonable power gain exceeding 3 dB at L band and 5 dB at S band.

3. SIMULATED AND MEASURED RESULTS

The antenna analysis software NEC-Win Pro [9] was used to predict the antenna performance. It was assumed that the spiral conductors and the finite ground were perfectly conducting. A range of parameters was tried to find the design with optimum characteristics. Different discretization segment lengths were also tested to evaluate the stability of the results. The antenna parameters were shown in Table 1. The feeding lines to the spiral arms were tilted by 33° from the normal to the ground plane to improve the circular polarization performance. The arms were fed using a hybrid network that provided the required voltages with approximately equal amplitude and appropriate phase [10].

The simulated and measured VSWR at one of the input ports (for other ports were approximately similar [11]), axial ratio, and power gain for a QSA with free inner ends [Fig. 1(a)] are shown in Figures 3(a), 4(a), and 5 respectively. Similarly, the results of the shorted-arm version QSA [Fig. 1(b)] are presented in Figures 3(b), 4(b), and 5. The measured results correspond well with the desired computed behavior. The relative bandwidths of VSWR $\leq$ 2.5 of the free inner QSA at 1.6 and 2.48 GHz are 8.1 and 8% respectively. Similarly for the shorted-arm QSA at 1.6 and 2.48 GHz they are 5 and 7.2% respectively. These results were encouraging because they showed a reasonable agreement with the required specifications. The measured return losses, 16.2 dB at 1.6 GHz and 12.7 dB at 2.5 GHz, for the free inner ends and 13.03 dB at 1.6 GHz and 11.3 dB at 2.5 GHz for the shorted-arms version were in good agreement with the performance required. The measured imaginary part of the input impedance was close to zero at the working frequencies, whereas the real parts, 49.6 and 39.2 Ω at 1.6 and 2.48 GHz, respectively for a free inner end QSA and 60 and 68 Ω at 1.6 and 2.48 GHz, respectively for the shorted-arms version, are acceptable for practical operation in a 50 Ω system.

The maximum degradation in axial ratio at 1.61 GHz for free inner ends and shorted-arms QSAs were around 2.0 dB over the elevation range ±45° as shown in Figures 4(a) and 4(b) respectively. For the shorted-arms QSA the variation of axial ratio with elevation angle at 2.485 GHz was quite similar to that in the 1.61 GHz band [Fig. 4(b)], whereas for the free inner ends version it was 3.6 dB over ±45° elevation angle as shown in Figure 4(a).

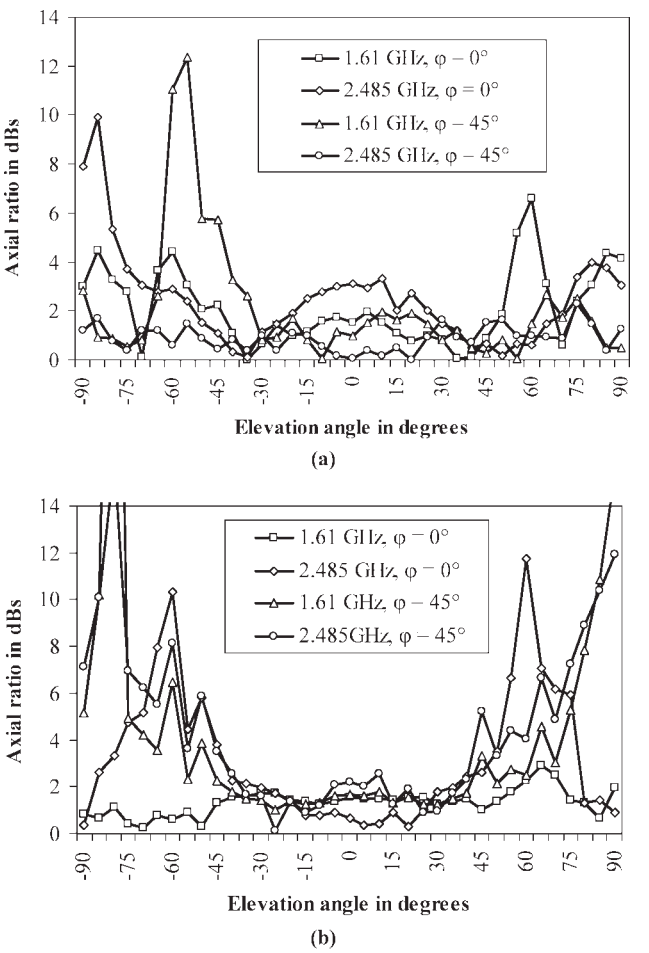

Figure 4 Axial ratio of QSAs versus the elevation angle at two azimuth angles ($\varphi = 0°$ and $\varphi = 45°$) and for two operating frequencies (1.61 and 2.485 GHz); (a) with free inner ends and (b) with connected inner ends

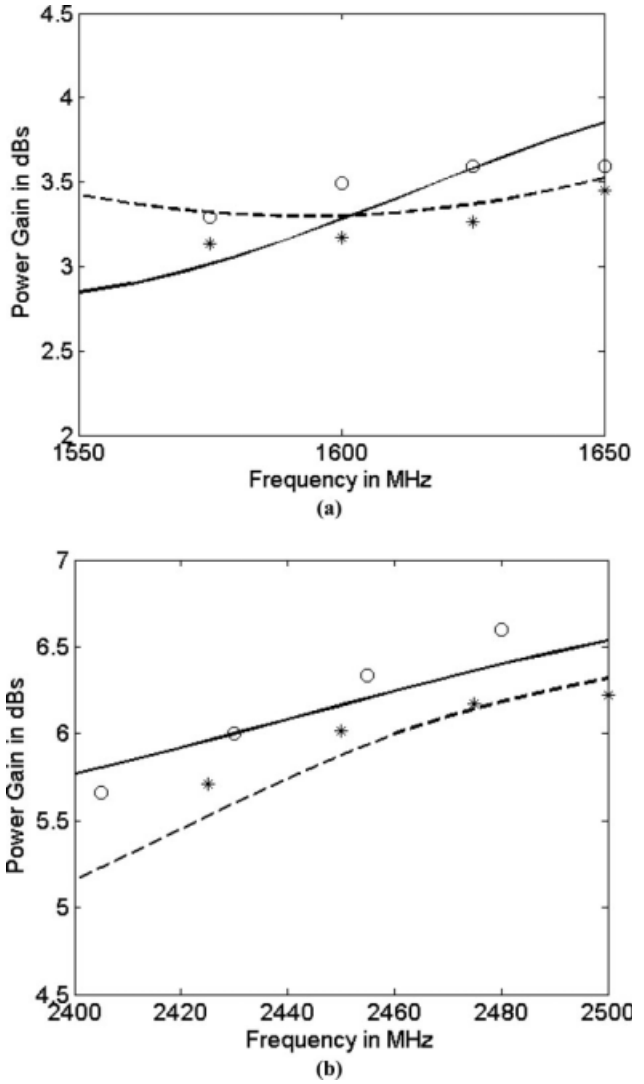

Figure 5 Simulated and measured power gain versus the operating frequency of the QSAs; (a) L band and (b) S band. (Free inner ends: simulated "_____," measured "o o o"; connected inner ends: simulated "---", measured "* * *")

Figure 5 illustrates the calculated and measured antenna gain in the broadside direction ($\varphi = 0°$, $\theta = 0°$) for the two antennas shown in Figure 2, over L and S bands. The measured results are clearly in quite reasonable agreement with the computed ones. It is also seen that the gain variations are fairly symmetrical for the free inner ends and the shorted-arms QSAs in the two bands under considerations. It should be noted that the measured power gain for each frequency band in the measurement plots has been compensated in offline analysis for the insertion loss of the feeding network As can also be observed in Figure 5, the measured gains for both antennas varied between 2.8 and 3.8 dBi over the entire L band; and between 5.2 and 6.8 dBi over the entire S band. These results are quite promising and encouraging for practical deployment.

4. CONCLUSIONS

QSAs of traditional form have been limited by the need for feeding at the centre, causing extra constraints on the size and the mutual coupling between the feeding ports. These problems have been overcome by locating the feeding ports on the outside of the spirals. This allows the QSA arms to be connected at the centre, thus providing extra space for long spiral arms. Such an antenna can be fed by microstrip lines and can allow integration with phasing and matching networks in the same plane. Measured results showed excellent agreement with method-of-moments simulations. The antennas demonstrate the basic viability of the designs as low-profile antennas for dual-band satellite-mobile handsets: it is to be expected that much smaller designs could be created by using suitable solid dielectrics between the spirals and the ground plane.

REFERENCES

1. H. Nakano, S. Okuzawa, K. Ohishi, H. Mimaki, and J. Yamauch, A curl antenna, IEEE Trans Antennas Propag 41 (1993), 1570–1575.
2. J.S. Colburn and Y. Rahmat-Samii, Quadrifilar-curl antenna for the Big-LEO mobile satellite service system, IEEE Antennas Propag Soc Int Symp Dig 2 (1996), 1088–1091.
3. T.W. Hertel and G.S. Smith, Analysis and design of two-arm conical spiral antennas, IEEE Trans Electromagn Compat 44 (2002), 25–37.
4. M. McFadden and W.R. Scott, Analysis of the equiangular spiral antenna on a dielectric substrate, IEEE Trans Antennas Propag 55 (Part 2) (2007), 3163–3171.
5. H. Nakano, S. Sasaki, H. Oyanagi, and J. Yamauchi, Cavity-backed Archimedean spiral antenna with strip absorber, IET Microwaves Antennas Propag 2 (2008), 725–735.
6. R.A. Abd-Alhameed, M.A. Mangoud, P.S. Excell, and J.A. Vaul, Investigation of SAR and polarisation purity of satellite mobile handset, IEEE Trans Antennas Propag 53 (2005), 2108–2110.
7. D. Zhou, R.A. Abd-Alhameed, C.H. See, P.S. Excell, and E.A. Amushan, Design of quadrifilar helical and spiral antennas in the presence of mobile handsets using genetic algorithms, In Proceedings of the First European Conference on Antennas and Propagation, session 3PA1, no. 122, Nice, France, November 2006, pp. 6–10
8. G. Smith, Proximity effect in systems of parallel conductors, J Appl Phys 43 (1972), 2196–2203.
9. NEC-Win Pro Antenna analysis software, Version 1.1, Nittany Scientific Inc., USA.
10. S.M. Daddish, R.A. Abd-Alhameed, and P.S. Excell, New designs for dual band antennas for satellite-mobile communications handsets, ACES J 3 (2000), 248–258.
11. J.S. McLean, Balancing networks for symmetric antennas: Part 2 Practical implementation and modelling, IEEE Trans Electromagn Compat 46 (2004), 24–32.

RECTANGULAR M-PRS STRUCTURE FOR SECTORAL BASE STATION ANTENNA WITH VERTICAL POLARIZATION

Mohamad Hajj, Emmanuel Rodes, Dina Serhal, Hassan Chreim, Eric Arnaud, and Bernard Jecko
XLIM-CNRS UMR 6172, Faculté des Sciences et Techniques, 123 Avenue Albert Thomas, 87060 Limoges, France;
Corresponding author: mohamad.hajj@xlim.fr

Received 15 June 2009

ABSTRACT: *This article presents a new method to realize sectoral antennas for base station by incorporating metallic partially reflecting surface (M-PRS). The main idea consists in inserting simple radiating elements, as patches, inside a Fabry-Perot cavity resonator. This consists of a ground plane, where the feeding system rests covered by a rectangular M-PRS. A patch array is used as a feeding structure to enhance directivity and radiation bandwidth. A rectangular M-PRS*

Meander-line Antenna Design for UHF RFID Tag Using a Genetic Algorithm

D. Zhou, **R. A. Abd-Alhameed**, **C. H. See**, **M. S. Alkhambashi**,
Z. Zainal Abidin, **K. N. Ramli**, **M. M. Abusitta**, **and M. Usman**
Mobile and Satellite Communications Research Centre
University of Bradford, Bradford, West Yorkshire, BD7 1DP, UK

Abstract— In this paper, a simple planar meander-line tag antenna for RFID application at UHF band designed and optimized using genetic algorithms (GA). The meander-line tag antenna dimensions were optimized and evaluated using GA in collaboration with NEC-2 source code. Configuration of optimal antenna with excellent impedance value at 900 MHz frequency band was found within the maximum generation. The simulated input impedance of the GA-optimised tag antenna has shown good agreement with the targeted impedance value. Moreover, the capabilities of GA are shown as an efficient optimisation tool for selecting globally optimal parameters to be used in simulations with an electromagnetic antenna design code, seeking convergence to designated specifications.

1. INTRODUCTION

In recent years Radio Frequency Identification (RFID) has become very popular in many commercial applications such as access control, animal tracking, security, and toll collection, because of its ability to track moving objects and its low-cost implementation [1, 2]. A typical RFID system is always made up of two components, including the tags (transponders) and readers (interrogators). A tag comprises an antenna and an application-specific integrated circuit (ASIC, or microchip) that is given a unique electronic product code. The antennas, as a key part of the system, enable the tag or reader to send and receive the signals. Readers are devices that read tags, and they equipped with antennas, a transceiver, and a processor (server with software system). The tag antenna design is quite challenging. This is because tag antenna is required directly connected to the tag IC, whose input impedance always presents capacitive reactance in nature. It means that the reactance part of tag antenna has to be designed and optimised to be complex conjugate impedance of tag IC in order to realize the maximum transmission using RF power induced from the antenna tag.

In this paper, an approach of using Genetic Algorithm (GA) in cooperation with an electromagnetic simulator was adopted to design and optimise the RFID tag antenna for UHF band. The benefit of applying GA is that it provides fast, accurate and reliable solutions for antenna structures. Genetic algorithm driver [3], written in Fortran, was adopted in this work in conjunction with the industry-standard NEC-2 Fortran source code [4], which was used to evaluate the randomly generated antenna samples. A meander-line antenna configuration was proposed in this study in order to achieve a tag design with compact size at UHF band. A Higgs IC [5], designed to follow EPCglobal Class-1 Gen-2 specification, was selected for the tag IC, input impedance of which was found to be $(12.2 - j135)\,\Omega$ at 900 MHz.

2. GENETIC ALGORITHM

Genetic algorithms are stochastic search procedures orchestrated by natural genetics, selection and evolution. They are modelled on Darwinian concepts of natural evolution thus making them more inspiring during use [6]. After it's first introduction in 1960's by J. Holland, it has become an efficient tool for search, optimization and machine learning, but in the pre-GA era, concepts of it had been looming and applied in game playing and pattern recognition [7]. Over the recent years, it has proven to be a promising technique for different optimizations, designs and control applications.

An approach of using GA in cooperation with an electromagnetic simulator has been introduced for antenna designs and has become increasingly popular recently [8]. For example, GA have been employed to design wire antennas [9, 10] and microstrip antennas [11]. The benefit of applying GA is that they provide fast, accurate and reliable solutions for antenna structures. Genetic algorithm driver [3], written in Fortran, was adopted in this work in conjunction with the industry-standard NEC-2 Fortran source code [4], which was used to evaluate the randomly generated antenna samples.

Several antenna designs using GA in authors' previous study [12, 13] has shown that the GA was successfully proved as an efficient optimizer tool that can be adopted and used to search and find the quicker solutions for complex antenna design geometries.

A flow chart to represent the easiest way in which the GA optimizer coordinates its functions is represented in Fig. 1. The algorithm randomly initiates its population and converts the parameters of the initiated individuals into a file in a card format which can be called by NEC-2 to determine the performance of these individuals. The results from NEC-2 are fed again to the GA engine to evaluate individual fitness if the maximum value is obtained for convergence, if otherwise the whole process is repeated until optimal results are produced.

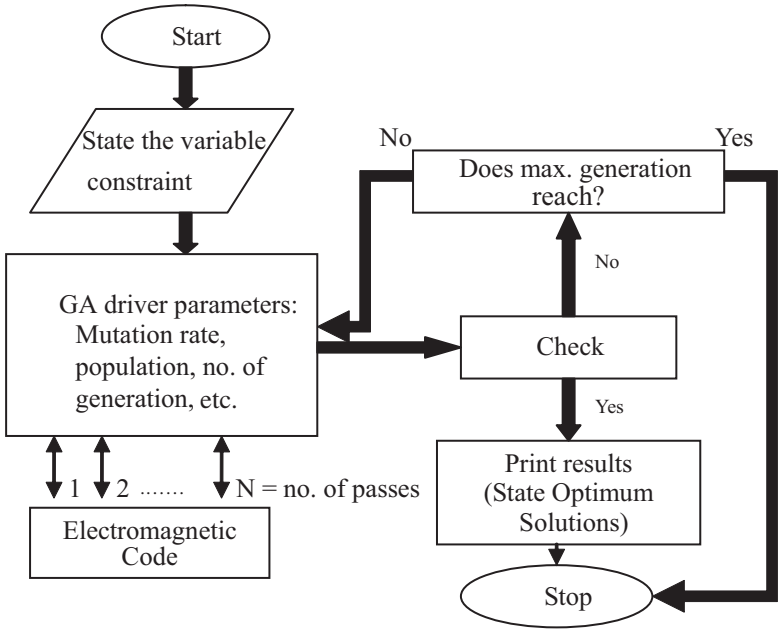

Figure 1: Flow chart of the genetic algorithm adopted in this study.

3. SIMULATION RESULTS AND DISCUSSION

A meander-line antenna configuration, as shown in Fig. 2, was proposed in this study in order to achieve a tag design with compact size at UHF band. Moreover, a paralleled meander line arrangement was used to enhance the impedance bandwidth for the proposed design. A Higgs IC [5], designed to follow EPCglobal Class-1 Gen-2 specification, was selected for the tag IC, input impedance of which was found to be $(12.2 - j135)\,\Omega$ at 900 MHz.

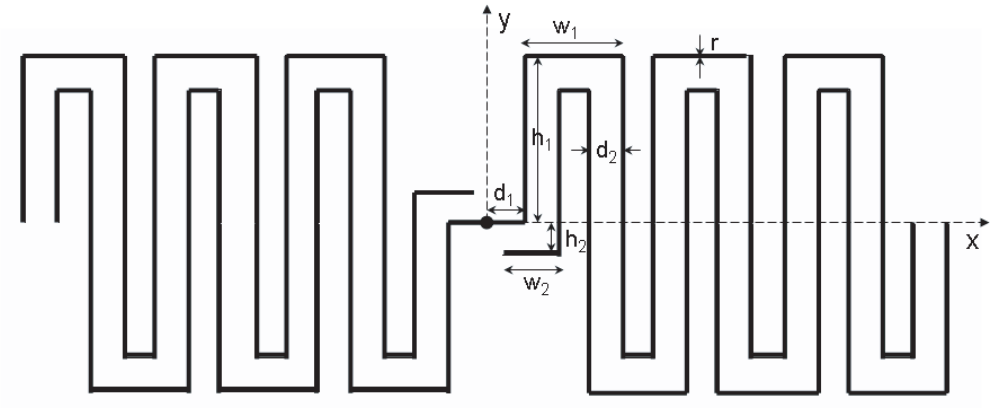

Figure 2: The new RFID antenna tag model.

Table 1 presents the GA input parameters in which the possible range of parameters magnitudes

were shown. There are seven parameters used to define the proposed tag antenna, including a matching circuit (i.e., parameters w_2 and h_2). For this optimisation, real-valued GA chromosomes were used. The optimisation of input impedance of the proposed tag antenna at 900 MHz band is considered inside the GA cost function. The randomly generated antenna configurations were evaluated for maximum fitness using a cost function. The computation time consumed for each of the erratically generated antenna samples only took a few seconds, according to the different combination of length, width and height of the patch antenna selected for comprising the antenna configuration. This was achieved by using a PC: 2.8 Pentium IV of 1 GB RAM.

Table 1: Summary of GA input parameters, antenna variables and best solutions.

GA parameters	GA-optimised RFID passive tag antenna	
	Parameters (m)	Optimal (m)
	Feeding wire length (d_1) (0.0025–0.0025)	0.0025
No. of population size = 4,	Spacing between wires (d_2) (0.001–0.003)	0.00222
No. of parameters = 7,	Outer wire width (w_1) (0.006–0.01)	0.00651
Probability of mutation = 0.02,	Matching wire width (w_2) (0.0015–0.0055)	0.00372
Maximum generation = 250,	Outer wire height (h_1) (0.005–0.015)	0.01110
No. of possibilities = 32768,	Matching wire height (h_2) (0.001–0.003)	0.00214
	Wire radius (r) (0.0002–0.0002)	0.0002

The geometry configuration of the optimal antenna was found within the maximum generations and the best solutions are listed in Table 1. It is notable the overall dimension ($l \times w$) of the optimal tag antenna is 62×22 mm. The obtained input impedance of the optimal tag antenna was found to be $(10.5+j135.2)\,\Omega$. For validation, the performance of the GA-optimised tag antenna was evaluated and validated with another commercial EM simulator and simulated results of the antenna input impedance from 800 MHz to 1000 MHz was analysed and presented in Fig. 3. Moreover, comparison of the simulated return loss of the GA-optimised RFID tag antenna was shown in Fig. 4. As can be seen, the optimal tag antenna features wide impedance bandwidth with respect to the tag IC impedance and enables to fully cover the allocated UHF frequency band for RFID application from 860 MHz to 960 MHz. Radiation patterns of the proposed tag antenna were also investigated. The radiation patterns in the zx plane and zy plane at 900 MHz were studied and the corresponding normalised results were presented in Fig. 5. As can be see, the optimal antenna has a dipole-like pattern, as expected. The maximum antenna gain was found to about 1.5 dB. The results are encouraging for practical implementation of this tag antenna.

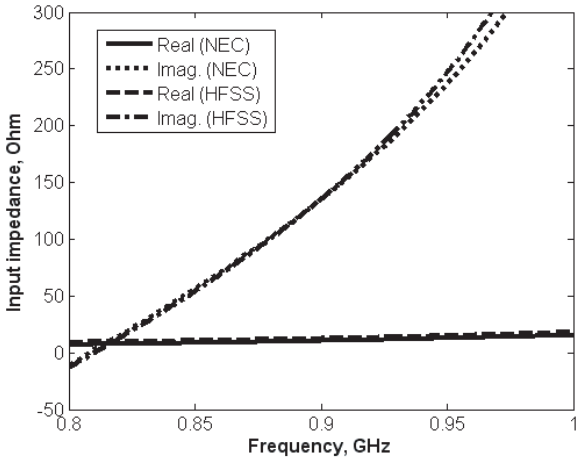

Figure 3: Simulated input impedance of the optimal RFID tag antenna.

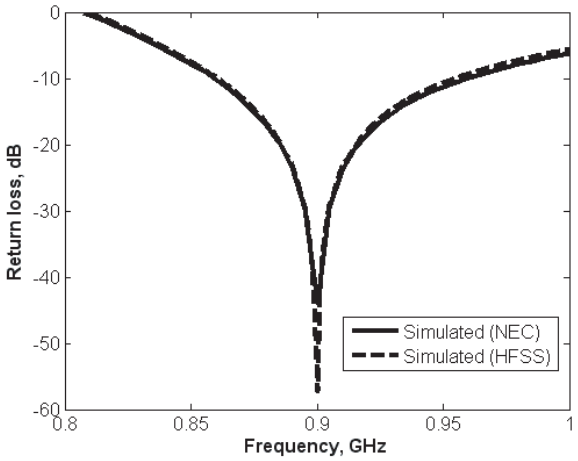

Figure 4: Comparison of return loss for the optimal RFID tag antenna.

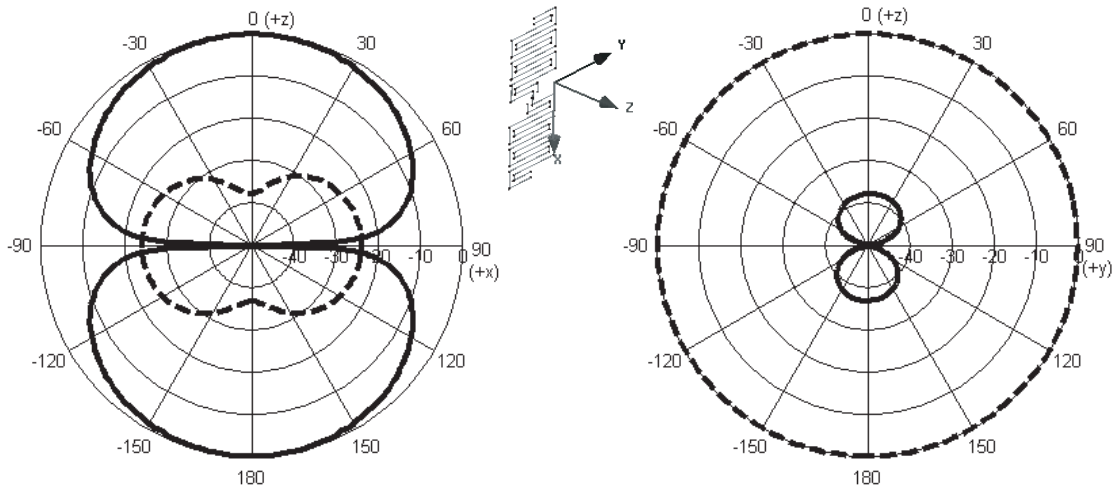

Figure 5: Radiation patterns of the proposed GA-optimized tag antenna for 900 MHz at: (left) zx plane; (right) zy plane; '—' measured E_θ and '- - - -' measured E_ϕ.

4. CONCLUSIONS

A novel design for the design and optimisation of RFID tag antennas with linear polarisation by use of genetic algorithms has been presented. A FORTRAN code genetic algorithm driver was adopted in this work in conjunction with the industry-standard NEC-2 FORTRAN source code, which was used to evaluate the randomly generated antenna samples. The results of the optimum designs of the proposed antennas exhibit good input impedance matching as required by the RFID IC. The presented examples show the capability of the proposed program in antenna design using GA and the results are encouraging for practical implementation of this tag antenna for UHF RFID applications.

REFERENCES

1. Finkenzeller, K., *RFID Handbook*, 2nd ed., John Wiley & Sons, Chichester, Ltd., 2004.
2. Bhatt, H. and B. Glover, *RFID Essentials*, O'Reilly, January 2006.
3. Carroll, D. L., FORTRAN Genetic Algorithm Driver, Version 1.7, download from: http://www.staff.uiuc.edu/ carroll/ga.html, 12/11/98.
4. Burke, G. L. and A. J. Poggio, "Numerical Electromagnetics Code (NEC)-method of moments," Lawrence Livermore Laboratory, Livermore, CA, 1981.
5. http://www.alientechnology.com.
6. Coley, D. A., *An Introduction to Genetic Algorithms for Scientists and Engineers*, World Scientific, Singapore, 1999.
7. Ammar, H. H. and Y. Tao, "Fingerprint registration using genetic algorithms," *IEEE Symposium on Applications Specific Systems and Software Engineering Technology*, 148–154, March 2000.
8. Rahmat-Samii, Y. and E. Michielssen, "Electromagnetic optimization by genetic algorithms," John Wiley & Sons, Canada, 1999.
9. Altshuler, E. E. and D. S. Linden, "Wire-antenna designs using genetic algorithms," *IEEE Antennas Propag. Mag.*, Vol. 39, 33–43, 1997.
10. Jones, E. A. and W. T. Joines, "Design of Yagi-Uda antennas using genetic algorithms," *IEEE Transactions on Antennas and Propagation*, Vol. 45, No. 9, 1386–1392, 1997.
11. Liu, W.-C., "Design of a CPW-fed notched planar monopole antenna for multiband operations using a genetic algorithm," *IEE Proc. — Microw. Antennas Propag.*, Vol. 152, No. 4, 273–277, 2005.
12. Zhou, D., R. A. Abd-Alhameed, C. H. See, P. S. Excell, and E. A. Amushan, "Design of quadrifilar helical and spiral antennas in the presence of mobile handsets using genetic algorithms," *Proceedings of the European Conference on Antennas and Propagation: EuCAP 2006*, Session 3PA1, No. 122, Nice, France, November 6–10, 2006.
13. Zhou, D., R. A. Abd-Alhameed, and P. S. Excell, "Bandwidth enhancement of balanced folded loop antenna design for mobile handsets using genetic algorithms," *PIERS Online*, Vol. 4, No. 1, 136–139, 2008.

EQUAL-SPACED RECTANGULAR MEANDER-LINE ANTENNA RFID TAG DESIGN FOR UHF BAND

R.A. Abd-Alhameed[1], D. Zhou[1], Y. Ma[1], M.S. Alkhambashi[1], C.H. See[1], M.M Abusittta[1] and P.S. Excell[2]

[1] Mobile and Satellite Communications Research Centre,
University of Bradford, Bradford, West Yorkshire, BD7 1DP, UK
[2] Centre for Applied Internet Research,
Glyndŵr University, Wrexham, LL11 2AW, Wales, UK
r.a.a.abd@bradford.ac.uk, d.zhou2@bradford.ac.uk, y.ma7@bradford.ac.uk,
m.s.alkhambashi@bradford.ac.uk, c.h.see2@bradford.ac.uk,
m.m.abusitta@bradford.ac.uk, p.excell@glyndwr.ac.uk

ABSTRACT

Design and testing of an equal-spaced rectangular meander-line antenna (ESRMLA) for RFID tag applications in the European UHF band 865-868 MHz is presented. The tag antenna was modelled and analysed using two established electromagnetic simulator packages. For validation, a prototype tag antenna was constructed and tested. The input impedance of the proposed antenna was verified against the simulated data results and the measured and simulated results were found to be in good agreement. The tag has a compact size (63.2 mm x 21.9 mm) and shows excellent impedance matching to the typical input impedance of an RFID integrated circuit chip.

KEYWORDS

RFID, Antenna design, Electromagnetic simulation, Printed antennas

1.0 INTRODUCTION

RFID is an automatic identification method, relying on storing and remotely retrieving data using devices called RFID tags or transponders. The RFID tag is often represented as a substitute for the traditional bar code [1, 2], but it has much wider ramifications since, in addition to being readable at a greater distance and through opaque material, it can also be remotely modified and even, potentially, reprogrammed. The technology requires some degree of cooperation between an RFID reader (interrogator) and a tag (transponder). A tag comprises an antenna and an application-specific integrated circuit (ASIC, or microchip) that is given a unique electronic product code. The antennas, as a key part of the system, enable the tag or reader to send and receive the signals: in addition, the RF power transmitted from the reader is normally required to power the circuit in the tag, so avoid the need for batteries.

Readers are devices that read tags, and they are equipped with antennas, a transceiver, and a processor (server with software system). The tag antenna design is quite challenging, because the antenna is required to be directly connected to the tag integrated circuit (IC), whose input impedance always presents a capacitive reactance. This means that the reactance part of the tag antenna output impedance has to be designed and optimised to be the complex conjugate impedance of that of the IC in order to realize the maximum transmission efficiency using RF power induced from the antenna. In recent years, many novel RFID tag antennas with compact size have been successfully demonstrated [3-9] in the open literature.

In this paper, an equal-spaced meander-line RFID tag antenna was investigated, working in a UHF band (860-960 MHz), but intended for compliance with the European UHF band 865-868 MHz. The rectangular meander-line antenna (MLA) is simple in its architecture and it is popular because of its low cost of production and low profile. A Higgs IC [10], designed to follow EPCglobal Class-1 Gen-2 specification [11], was selected for the tag IC whose input impedance was found to be 12.2-j135 Ω at 900 MHz [12].

2.0 ANTENNA DESIGN

The geometrical configuration of the proposed compact ESRMLA RFID tag is shown in Fig. 1, which illustrates the basic structure together with dimensional notations. The proposed antenna is composed of two strips having multiple but equal meanders, where the horizontal lines control the radiation resistance and the vertical lines acts as storage of electric energy and loss resistance. As can be seen in Fig. 1, the antenna is composed of two meander-shaped strips which were analysed as being perfectly electrically conducting (PEC). The MLA has transmission-line current between meander lines, which also have radiation coupling. These transmission lines do not contribute to the radiating power and instead produce losses (R_R and R_L). An ESRMLA with the meander-line shape is able to resonate at much lower frequencies than in the case of a straight dipole of the same height. The ESRMLA is required to be characterised to achieve optimum conjugate impedance with respect to the tag IC input impedance: to provide some design flexibility it was chosen to be mounted on a foam dielectric substrate with relative permittivity of ε_r= 1.1. The design aimed to accommodate the European UHF RFID band, requiring 3 MHz bandwidth around a centre frequency of f_c = 867 MHz, the antenna being designed with its first resonance at this frequency.

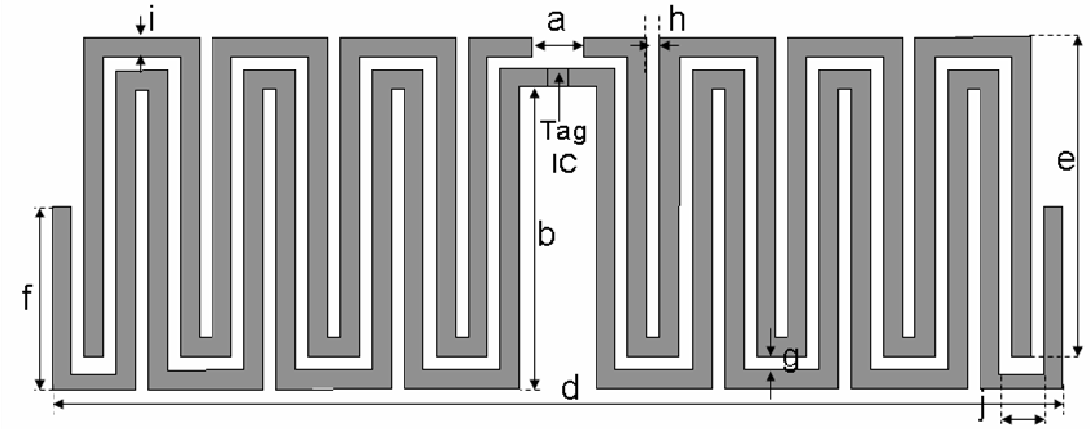

Fig.1 Configuration and important parameters of the proposed RFID tag antenna.

It was found during the model-based design process that the antenna input impedance or matching can be adjusted or optimised by changing antenna length (parameter e) and by varying the spacing of the gaps between lines (parameters h and g – chosen to be equal). In addition, the feed position also plays a vital role in controlling the resonant frequency for the proposed MLA design.

3.0 SIMULATION, RESULTS AND DISCUSSION

A MLA configuration, as shown in Fig. 1, was proposed in order to achieve a tag design with compact size at UHF band. Moreover, a paralleled meander line arrangement was used to enhance the impedance bandwidth for the proposed design. The geometry configuration of the optimal antenna was found with the aid of Ansoft HFSS simulator [13] and the optimum parameters are listed in Table 1. The return loss at 867.5 MHz is -40.81 dB, as shown in Fig. 2

and the input impedance of the optimal tag antenna was found to be 14.21-j134 Ω as shown in Fig. 3.

Table 1 Optimum parameter values (see Fig 1).

a	3.2mm	f	11.5mm
b	19mm	g	0.9mm
c	4.8mm	g	0.8mm
d	63.2mm	i	1.2mm
e	19.8mm	j	2.8mm

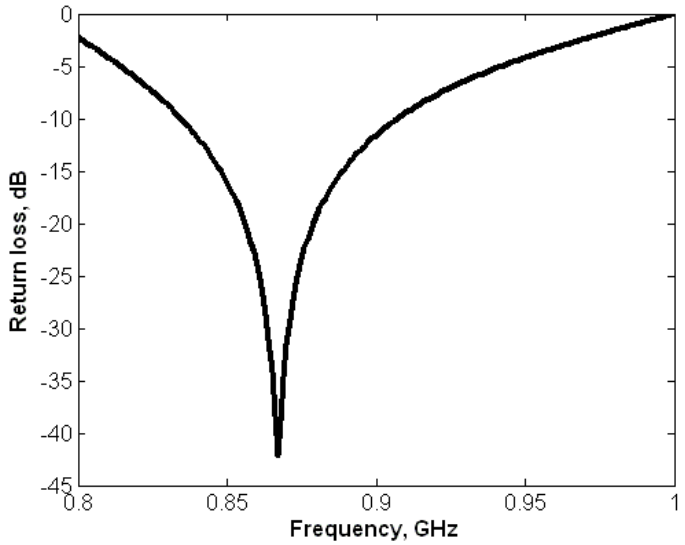

Fig.2 Simulated RFID tag antenna return loss.

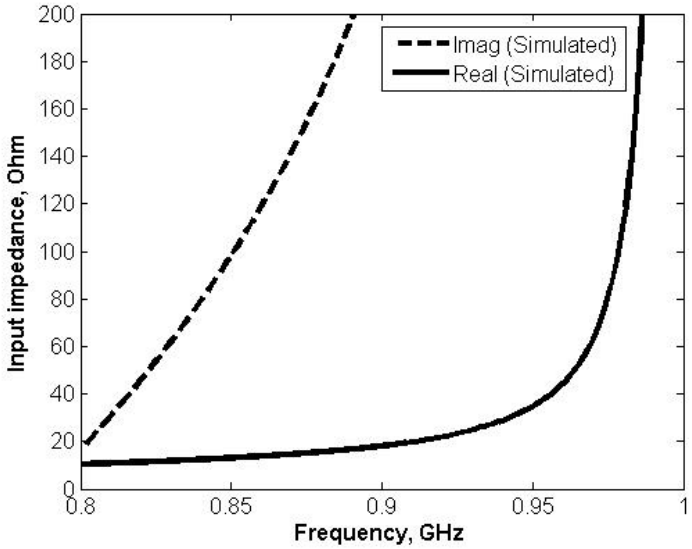

Fig. 3 Simulated RFID tag input impedance.

For validation, the performance of the proposed optimal tag antenna was evaluated and validated with the CST Microwave Studio simulation software [14]: simulated results of the antenna input impedance from 800 MHz to 1000 MHz were analysed. The comparative input impedance locus from both packages for the antenna at frequencies of interest was plotted on a Smith Chart (see Fig. 4). This shows that the simulated input impedance achieved at 867 MHz was found to be 11.2-j80.6 Ω (using CST Microwave Studio software) and was 14.4-j134.8 Ω using HFSS. The results show fairly good agreement using the two different packages.

A prototype of the proposed tag antenna was fabricated and tested. The measured input impedance of the antenna was obtained using mirror image theory since the proposed design has a symmetrical structure. Therefore, only half of the antenna, operating as a monopole over a very large square ground plane, was used in this measurement, where each lateral length of the ground plane is greater than 3λ (wavelength in free space). The resultant measured input impedance is shown in Fig. 4, in which it is also compared to two calculated values obtained from the two different EM simulators.

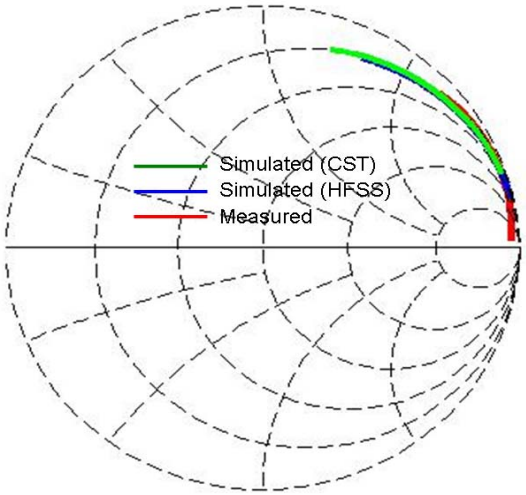

Fig. 4 Comparison of input impedance on Smith Chart using HFSS, CST Microwave Studio, and measurement.

The radiation patterns in the E-plane (z-x plane) and H-plane (z-y plane) at 867 MHz were studied and the corresponding normalised results are presented in Fig 5. The radiation pattern of the proposed antenna is an omnidirectional radiation pattern in the H-plane and doughnut shape pattern in the E-plane with linear polarisation, very like the case for a typical dipole antenna. The maximum antenna gain was found to be about 1.7 dBi and 1.5 dBi for z-y and z-x planes, respectively.

The present foregoing simulated results are quite well suited for practical implementation of this tag antenna (see Fig. 6). These encouraging results may lead to further practical investigation of the maximum detection distance of the RFID reader using the proposed tag design and the commercial Alien Technology UHF tags [10].

CONCLUSIONS

A design for a linear polarized RFID tag antenna based on equally-spaced meander line has been presented. The antenna was shown to have a dipole-type radiation pattern, giving readability over the maximal range of angles. The antenna can be directly matched to the arbitrary complex impedance of a tag chip, and appropriate bandwidth characteristics can be obtained by properly adjusting the characteristic impedance of the incorporated two-strip transmission line. The simulated performance for the proposed design was compared and

verified using two different electromagnetics software simulators. The results exhibit good input impedance matching, as required by the Higgs IC. The obtained results are acceptable for practical implementation in RFID tag antennas using the European UHF band.

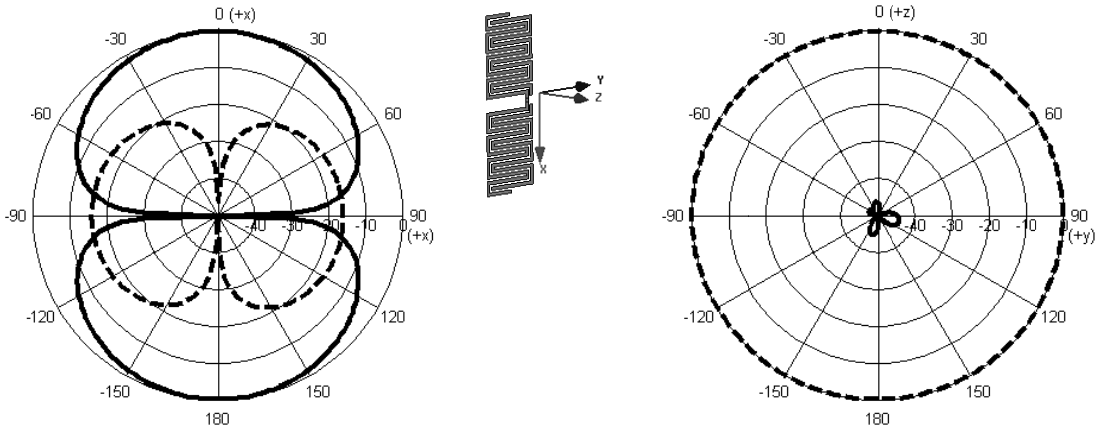

Fig. 5 Radiation patterns of the proposed antenna for 867 MHz in: (left) z-x plane; (right) z-y plane, where '——' measured E_θ and '- - -' measured E_ϕ.

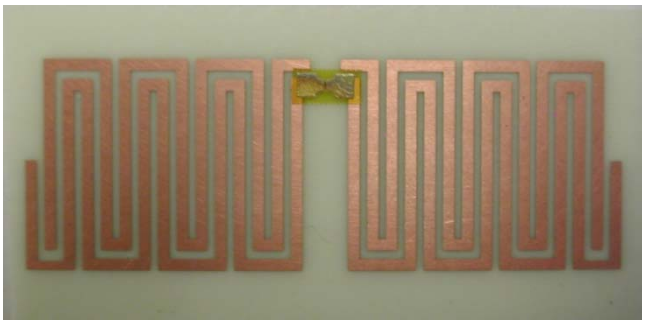

Fig. 6. The prototype RFID tag with the designed antenna and integrated IC.

References

[1] Finkenzeller K., RFID Handbook, 2nd edn. Chichester: John Wiley & Sons, Ltd, 2004.

[2] Bhatt H.and Glover B., RFID Essentials, O'Reilly, January 2006.

[3] Marrocco G., "The art of UHF RFID antenna design: impedance matching and size-reduction techniques", IEEE Antennas and Propagation Magazine, vol. 50, no. 1, pp. 66-79, Jan. 2008.

[4] Choi W., Son H.W., Shin C., Bae J.-H. and Choi G., "RFID tag antenna with a meandered dipole and inductively coupled feed", IEEE Antennas and Propagation Society, International Symposium, pp. 619-622, July 2006.

[5] Keskilammi M. and Kivikoski M., "Using text as a meander line for RFID transponder antennas", IEEE Antennas and Wireless Propagation Letters, vol. 3, pp. 372-374, 2004.

[6] Rao K.V.S., Nikitin P.V. and Lam S.F., "Antenna design for UHF RFID tags: a review and a practical application", IEEE Trans. Antenna Propag., vol. 53, no. 12, pp. 3870-3876, 2005.

[7] Marrocco G., "Gain-optimized self-resonant meander line antennas for RFID applications", IEEE Antennas and Propagation. Lett., vol. 2, pp. 302-305, 2003.

[8] Marrocco G., "The art of UHF RFID antenna design: impedance-matching and size-reduction techniques", IEEE Antennas and Propag. Magazine, vol.50, no.1, pp.66-79, Feb. 2008.

[9] Noguchi, K., Mizusawa M., Yamaguchi T., and Okumura Y., "Increasing the bandwidth of a meander line antenna consisting of two strips", IEEE Antennas and Propagation Soc. Int. Symp. Digest, vol.4, pp. 2198-2201, 2003.

[10] Alien Technology Corp., Morgan Hill CA, USA. http://www.alientechnology.com

[11] Electronic Product Code global organization (EPCglobal), "Class 1 Generation 2 UHF Air Interface Protocol Standard", http://www.epcglobalinc.org/standards/uhfc1g2

[12] Zhou D., Abd-Alhameed R.A., See C.H., Alkhambashi M.S., Zainal Abidin Z., Ramli K.N., Abusitta M.M. and Usman M., "Meander-line antenna design for UHF RFID tag using a genetic algorithm", Progress In Electromagnetics Research Symposium, March 23-27, Beijing, China, 2009.

[13] High Frequency Structure Simulator, Version 11, Ansoft Corporation, USA.

[14] CST Microwave Studio software, Version 5.0, Computer Simulation Technology Corporation, Germany.

Ninth Informatics Workshop for Research Students Bradford UK ISBN 978 1 85143 251 6

Accurate Hybrid Computational Electromagnetics Techniques

K.N. Ramli, R.A. Abd-Alhameed, D. Zhou, P.S. Excell, C.H. See, Z. Zainal Abidin, M.S. Alkhambashi, M.M. Abusitta and H. Xu

***Abstract*—An approach to hybridization, linking the Method of Moments, the Finite Difference Time Domain method and subgridded FDTD regions is presented. This hybrid method is capable of analysing a system of multiple discrete regions by employing the Principle of Equivalent Sources to excite the coupling surfaces and then using a linear field-interpolation method. The method is developed to suit RFID model analysis for both near- and far-field applications.**

***Index Terms*—FDTD, MoM, Hybrid Method, RFID, Equivalent Surface.**

I. Introduction

The demand for efficient and accurate field modelling tools for electromagnetic (EM) problems is constantly growing. The various numerical methods can be divided into several categories. One possible division can be made, based on the domain in which the procedure is applied: time domain methods and frequency domain methods [1, 2].

The applications of these two classes of methods mainly depend on the type of problems to be solved and on the form of the required solution, e.g. impulse response or harmonic solution. It is clear that results can be moved from one domain approach to the other by applying a direct or inverse Fourier transform, applying the proper care to avoid aliasing and to ensure causality. However, there are deeper issues of stability which may also influence the decision on which method to use. A second possible classification for numerical methods is based on the type of formulation used: differential formulation and integral formulation.

This paper focuses on one differential method and one integral method, as shown in Fig. 1. The former is the Finite-Difference Time-Domain (FDTD) method which is a discrete time-domain differential formulation of Maxwell's equations that includes another embedded subgridding FDTD method (SGFDTD) to model small complex structures inside a normal FDTD method. The integral method is the 'Method of Moments' (MoM), most widely used in the frequency domain. The objective of this work is to explore subgridding inside the hybrid combinations between these two methods and apply the combined method to different EM scattering applications such as those found in RFID communication systems.

Manuscript received May 9, 2008.

The authors are with the Mobile and Satellite Communication Research Centre, University of Bradford, Bradford BD7 1DP, U.K. (e-mail: k.n.b.ramli@bradford.ac.uk; r.a.a.abd@bradford.ac.uk).

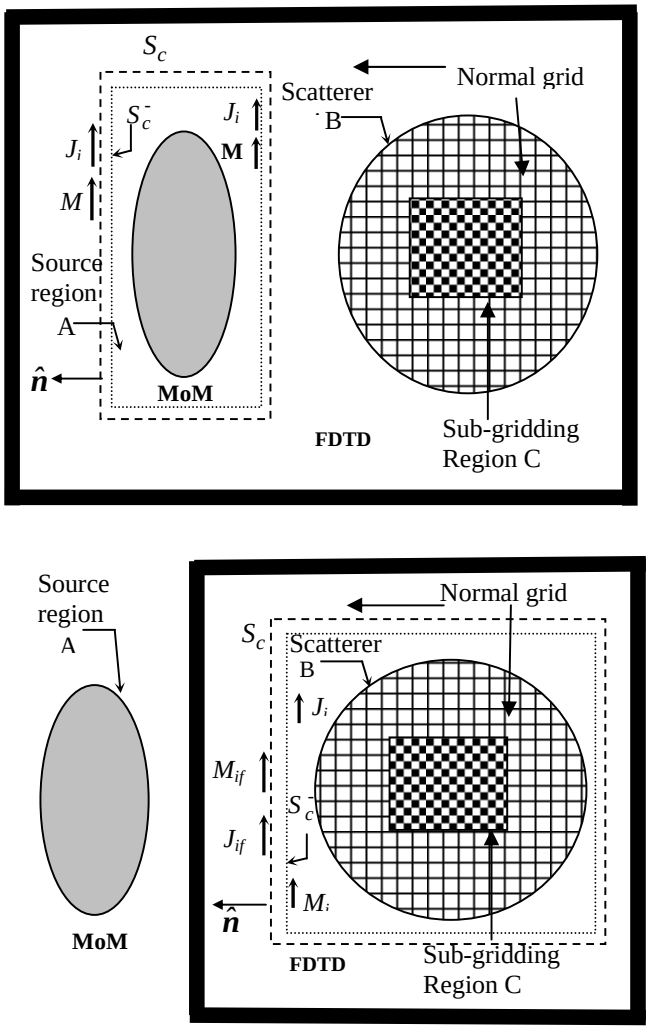

Fig. 1 Hybrid MoM/FDTD/SGFDTD configuration for the single source and scatterer geometries; (top) Near field application, (bottom) Far field application.

II. Method Implementation and Results

A computer program was written to implement the analysis method given in previous section. The new code was a modified version of the authors' work presented in [3], in which the subgridding technique is included [4]. The following example was chosen to validate the method accuracy.

A 900 MHz centre-fed half-wavelength dipole was considered as a transmitter source that represents as example of the RFID reader, whereas the RFID tag was considered as a small half-wavelength meander antenna, as shown in Fig. 2.

Two different distances between the source and the tag were studied and discussed. Two separate simulations were undertaken for each case, one with the far field application and other with near field application as shown in Fig. 1. The parameters used are summarized in Table 1.

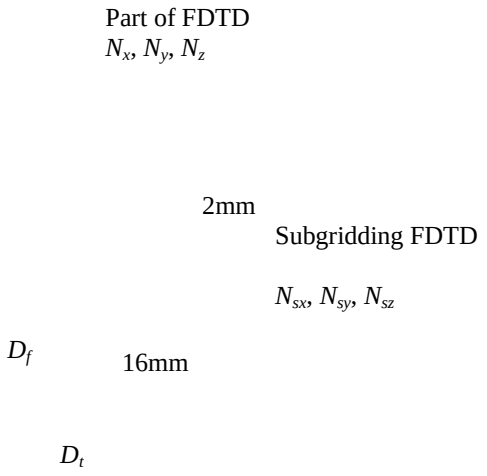

Fig. 2 FDTD/SGFDTD basic geometry.

TABLE I
INPUT PARAMETERS TO THE HYBRID METHOD

Formulation	Far Fields	Near Fields
FDTD problem space	20 × 20 × 30	20 × 40 × 30
Huygens surface	16 × 16 × 26	4 × 4 × 30
FDTD volume (cm^3)	24 × 24 × 36	24 × 48 × 36
FDTD cell size and time step	12 mm, 16.8 ps	12 mm, 16.8 ps
No. of the FDTD PML cells	8	8
Subgridding cells	5 × 5 × 15	5 × 5 × 15
Subgridding FDTD cell size and time step	2 mm, 2.8 ps	2 mm, 2.8 ps
The operating frequency	900 MHz	900 MHz
D_t: distance between the centres of transmitter and the sensor	33 cm	6 cm
D_f: distance between the centre of the sensor to the subgridding FDTD boundary	8 mm	8 mm

The transmitter is a dipole of half wavelength and radius 0.0025 wavelength.

The field distribution over an *xz* plane 2 cm distant from the sensor (scatterer) for near field and far field techniques is shown in Fig. 3. The plane size considered here was 20 cm × 16 cm for *x* and *z* axes respectively. The far field and near field techniques were checked for comparisons of one antenna geometry i.e. D_t was fixed to 6 cm for both techniques, the fields were found identical to the one shown in Fig. 3. Both methods show a good stability and the results were convergent within four iterations. However, the total field components was found ±2% when compared to results computed using NEC2 software.

III. CONCLUSIONS

Multiple-region hybrid techniques with frequency-domain Method of Moments, Finite-Difference Time-Domain and subgridding were proposed and investigated. The method was validated for far field and near field applications. The present computational electromagnetics technique gave stable and accurate results which is a step towards validation of complex hybrid theory problems such as are found in RFID applications in which the tag sensors are placed or mounted on dielectric or conducting materials.

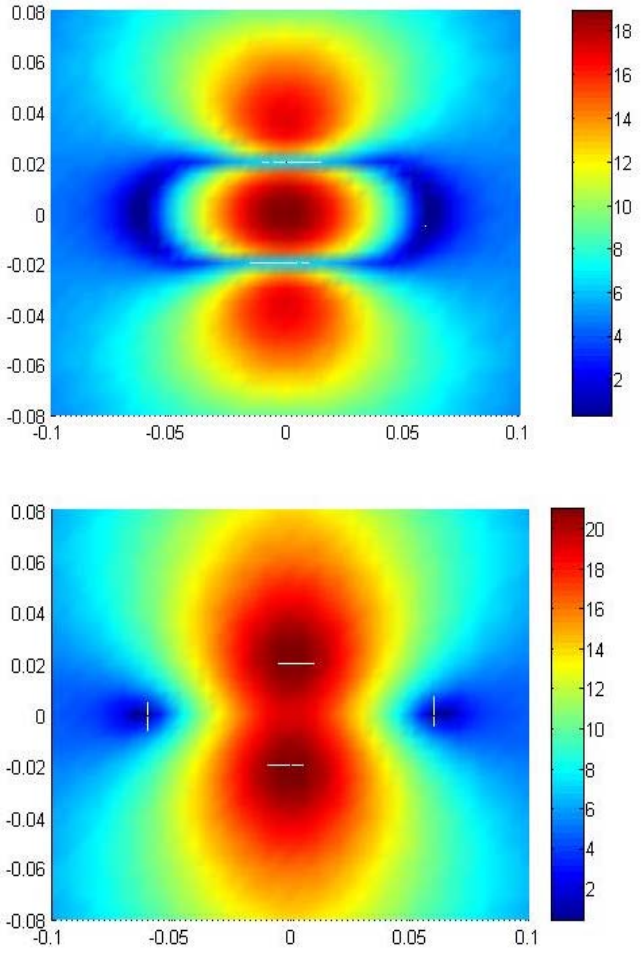

Fig. 3 The distribution of the E_z and E_{total} field components in dB at 2 cm away from the sensor, using near field technique; (top): E_z, (bottom): E_{total}.

REFERENCES

[1] A. Taflove and S. C. Hagness, Computational Electrodynamics: The Finite-Difference Time-Domain Method, 3rd ed. Boston, MA: Artech House, 2005.

[2] K. S. Yee, "Numerical solution of initial boundary value problems involving Maxwell's equations in isotropic media," IEEE Transactions on Antennas and Propagation, vol. AP-14, pp. 302-307, 1966.

[3] Abd-Alhameed, R.A., Excell, P.S and Mangoud, M.A.: 'Broadband antenna response using hybrid technique of frequency domain of MoM and FDTD', ACES Journal on Computational of Electromagnetics', vol. 20, No. 1, March 2005, pp. 70-77.

[4] C.H. See, R.A. Abd-Alhameed, R.S. Zadeh and P.S. Excell, 'FDTD Subgridding Scheme for Bioelectromagnetics Application', URSI Symposium, University of Portsmouth, Commission B, 2-3 July, 2007, UK, pp. 11.

Interaction of EM Fields to the Human Body Using MoM-FDTD-SGFDTD Hybrid Computational Method

[1,2]K. N. Ramli, [2]R. A. Abd-Alhameed, [2]Y. A. S. Dama, [2]M. S. A. Alkhambashi, [2]M. B. Child, [3]P. S. Excell
[1]Faculty of Electrical and Electronic Engineering, Universiti Tun Hussein Onn Malaysia (UTHM)
86400 Batu Pahat, Johor, Malaysia, khairun@uthm.edu.my
[2]Mobile and Satellite Communications Research Centre
University of Bradford, Bradford, BD7 1DP, UK, r.a.a.abd@bradford.ac.uk
[3] Glyndŵr University, Wrexham, LL11 2AW, Wales, UK, p.excell@glyndwr.ac.uk

Abstract—**This paper describes the application of a new hybrid method of moments, with generic and sub-gridded finite-difference time-domain approach (MoM–FDTD–(SG)FDTD) for modelling the interaction between an applied excitation placed in close proximity with an inhomogeneous human body model. The source is provided by a small low frequency RFID antenna tag, operating at 900 MHz. Near and far fields performance for the antenna are assessed for different placements over the body. The cumulative distribution function of the radiation efficiency and the absorbed power are presented, and discussed.**

Keywords: hybrid computational methods; sub-gridding; RFID antenna; cumulative distribution function; radiation efficiency

I. INTRODUCTION

The development of hybrid electromagnetic codes for precise calculation of electromagnetic fields within, or in close proximity, to anisotropic and inhomogeneous dielectric media, such as the human body, is a key ingredient on the development of medical and on body RF applications. Electromagnetic fields are induced inside any biological system when illuminated by an EM wave, and the wave is scattered externally [1-4]. Such computations place considerable demands on computational resources, hence the need for fast and efficient formulations, which are not limited to generic 'best in class' solutions. Several hybrid approaches have been suggested for a variety of electromagnetic problems, ranging from the highly specific, to the very general. For example, a genetic algorithm (GA) implementation of a multi-structure method of moments analysis (MS-MoM-GA) has been proposed by Arnaud-Cormos [5] for the optimization of antenna performance, including the feed network. Becker and Hansen [6] proposed a multi-temporal resolution (time domain) approach to the method of moments, including the geometrical theory of diffraction, for calculation of the transient fields radiated from antennas placed on large bodies. Hybridization of FEM and MoM has also been advocated [7], and has been rigorously evaluated for general scattering patterns. A hybrid time domain technique linking FEM and MoM with FDTD has been suggested for general complex problems [8].

This paper describes the application of a hybrid method of moments, with generic and sub-gridded finite-difference time-domain approach (MoM–FDTD–(SG)FDTD) for modelling the interaction between a low frequency RFID antenna tag and a various regions in close proximity to the trunk, and back of a detailed human body model. The "Visible Man" model is used for these studies [9]. The operating frequency of the antenna is 900 MHz. The near and far field properties of the antenna are evaluated for various body placements and full characterization of the antenna performance is given in terms of the polarization state, absorbed power and radiated power. The radiating efficiency of the antenna in proximity to the body may be inferred from these calculations, and a simple statistical picture is presented.

II. MODIFIED TOTAL/SCATTERED FIELD FORMULATION

The near field antenna data is obtained from a basic MoM computation and embedded into a more general FDTD simulation environment using a modified total/scattered field formulation, this is illustrated in outline by the schematic in Fig. 1.

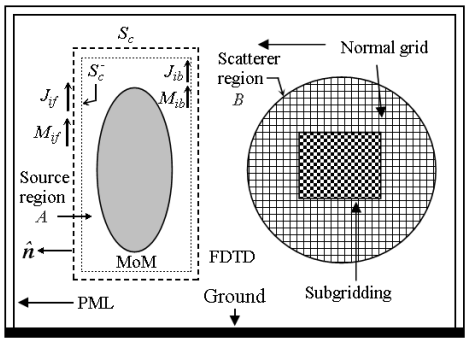

Figure 1. Modified total and scaterred field region for hybrid method.

These near field values, $E|_{MoM}$ and $H|_{MoM}$, are substituted over the five faces of the rectangular equivalent (Huygens') surface. Note, one of the faces corresponds to the finite ground plane in which the electric field vanishes. This modified total/scattered field formulation is used to exchange the scattered and total field regions. In this case, the fields inside and outside the Huygens' surface are considered to be the scattered field, and the total field region, respectively. Solutions from this formulation only exist if the source is smaller than the size of the scatterer. The 1-D updating equations for the electric and

magnetic field components are modified using an "outside surface boundary" treatment.

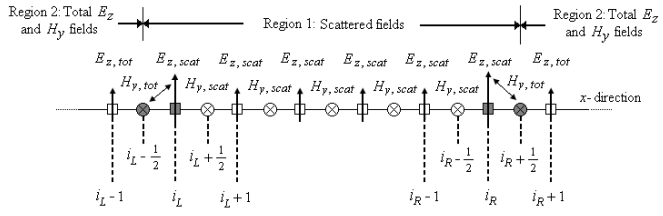

Figure 2. Modified total and scattered field components for one-dimensional hybrid method (outside *H* surface method).

This may be illustrated by examining the 1-D transverse magnetic (TM) field case, as in Fig. 2. The method divides the *x*–directed array of E_z and H_y components into Region 1 (scattered fields) and Region 2 (total fields) by a virtual surface. At this surface, there exists a special set of E and H components (grey in the diagram), these four field components are E_z at i_L and i_R and H_y at ($i_L - ½$) and ($i_R + ½$), the subscripts are for left and right, respectively. The surface of the special H field components (surface current J) is situated on the outside of the FDTD Huygens' surface grids. The boundary E_z and H_y updating equations are given by:

$$E_z\big|^{n+1}_{scat,i_L} = E_z\big|^{n}_{scat,i_L} + \frac{\Delta t}{\varepsilon_o \Delta}\left(H_y\big|^{n+1/2}_{scat,i_L+1/2} - H_y\big|^{n+1/2}_{tot,i_L-1/2}\right) + \frac{\Delta t}{\varepsilon_o \Delta} H_y\big|^{n+1/2}_{MoM,i_L-1/2} \quad (1)$$

$$H_y\big|^{n+1/2}_{tot,i_L-1/2} = H_y\big|^{n-1/2}_{tot,i_L-1/2} + \frac{\Delta t}{\mu_o \Delta}\left(E_z\big|^{n}_{scat,i_L} - E_z\big|^{n}_{tot,i_L-1}\right) + \frac{\Delta t}{\mu_o \Delta} E_z\big|^{n}_{MoM,i_L} \quad (2)$$

$$E_z\big|^{n+1}_{tot,i_R} = E_z\big|^{n}_{tot,i_R} + \frac{\Delta t}{\varepsilon_o \Delta}\left(H_y\big|^{n+1/2}_{scat,i_R+1/2} - H_y\big|^{n+1/2}_{tot,i_R-1/2}\right) - \frac{\Delta t}{\varepsilon_o \Delta} H_y\big|^{n+1/2}_{MoM,i_R+1/2} \quad (3)$$

$$H_y\big|^{n+1/2}_{scat,i_R+1/2} = H_y\big|^{n-1/2}_{scat,i_R+1/2} + \frac{\Delta t}{\mu_o \Delta}\left(E_z\big|^{n}_{tot,i_R+1} - E_z\big|^{n}_{tot,i_R}\right) - \frac{\Delta t}{\mu_o \Delta} E_z\big|^{n}_{MoM,i_R} \quad (4)$$

The subscripts "tot" and "scat" stand for total and scattered fields, respectively, ε_o is the electric permittivity in F/m, μ_o is the magnetic permeability in H/m, Δt is the time, and Δx is the FDTD cell size. Equations (1)-(4) are the 1-D total/scattered field FDTD formulations which generate the equivalent effects of the plane wave at one surface interface.

III. Source Excitation

The antenna used to develop this model is described in [10], this is basically a simple meander–line antenna. The antenna structure is composed from two strips, each with multiple equal meanders, where the horizontal dimensioning controls the radiation resistance, and the vertical dimensioning controls the antenna capacitance, and resistive losses. The antenna design was optimised for 900 MHz operation, using a genetic algorithm running in conjunction with the NEC source code [11]. The design criteria for this antenna require a good operating efficiency for use in proximity to the human body.

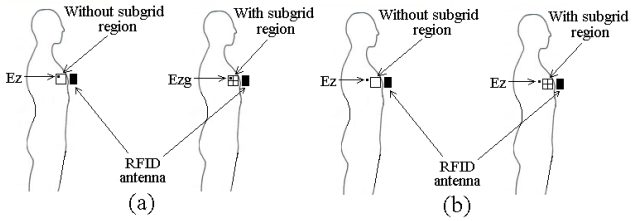

Figure 3. Observed field is located: (a) Inside subgrid, (b) Outside subgrid.

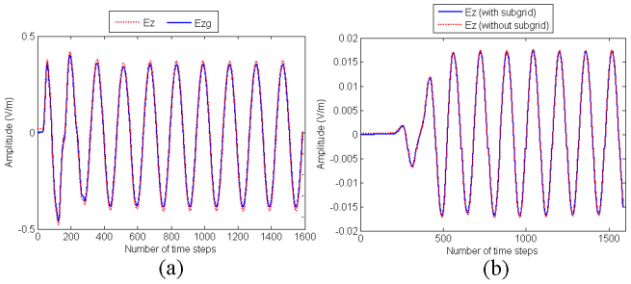

Figure 4. The electric field variation: (a) Inside subgrid region (E_{zg}) and at normal grid (E_z) (b) E_z Outside subgrid region.

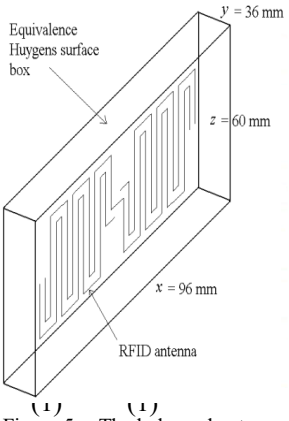

Figure 5. The balanced antenna with the equivalent Huygens box.

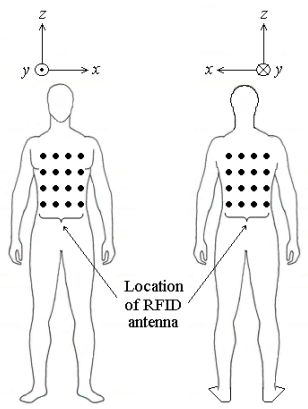

Figure 6. Human body model and the balanced antenna locations.

IV. Validation of Subgrid Scheme

The sub-gridding was validated with reference to two specific cases. Case 1 considered the observed field located within the sub-gridding region, with and without the sub-gridding present, see Fig. 3(a). Case 2 considered the observed field located outside the sub-gridding region, with and without sub-gridding present, see Fig. 3(b). The calculation volume was excited by the antenna tag at 900 MHz, and the electric fields are compared for both cases at each point. The electric fields in the sub-gridded region (E_{zg}), and the normal grid (E_z) for Case 1 are found to be identical, see Fig. 4(a). Case 2 were also found to be identical, see Fig. 4(b).

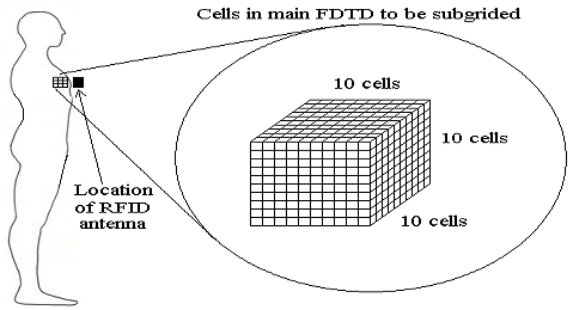

Figure 7. Subgrid cells of 10×10×10 FDTD cells are taken inside the human body.

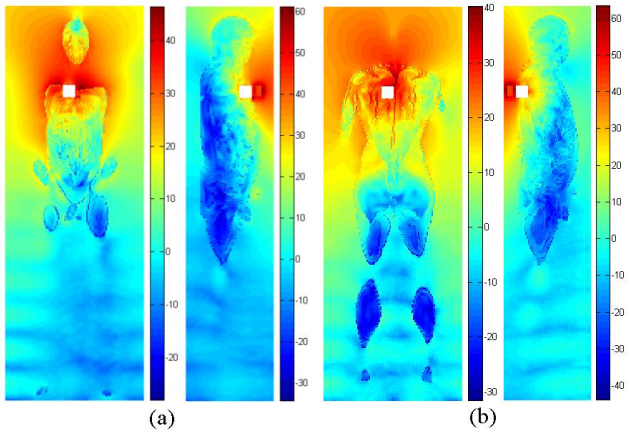

Figure 8. Electric field distribution (dB scale) for horizontally polarized antenna: (a) Front, (b) Back.

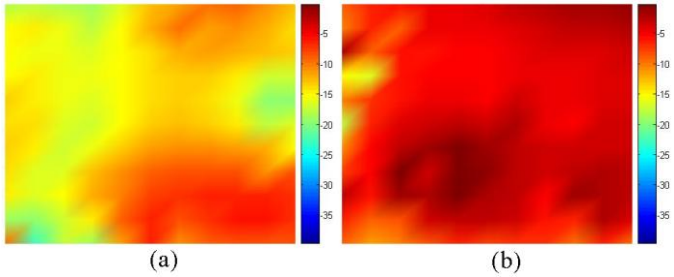

Figure 9. Electric field distribution (dB scale) inside subgrid region for horizontal polarized antenna: (a) Front, (b) Back.

V. THE HYBRID ANALYSIS

The simulation begins by defining a Huygens' surface around the antenna. The equivalent electric and magnetic sources on the surface are produced for each time step from the free space electric and magnetic fields of the antenna using NEC [11]. This field data becomes the input source for the FDTD code, the computation volume is 118×77×327 FDTD cells, and the Huygens' box is set at 16×4×10 FDTD cells for the horizontal polarization (Fig. 5). FDTD is applied over the whole calculation volume, the time step is set for 6 ps, and a six cell PML is used to terminate the calculation volume. The distance between the antenna Huygens surface box and human body is fixed at 12.0 cm (2 FDTD cells). The equivalence principle is operated using the hybrid procedure described in [12], and the coarse and fine grain cell sizes (dx=dy=dz) are 6.0 mm and 3.0 mm, respectively. The scatterer fields are obtained at each time step, and the equivalent surface currents on the Huygens surface are also obtained. The equivalent surface currents are also used to work back to the source to obtain the induced currents on it.

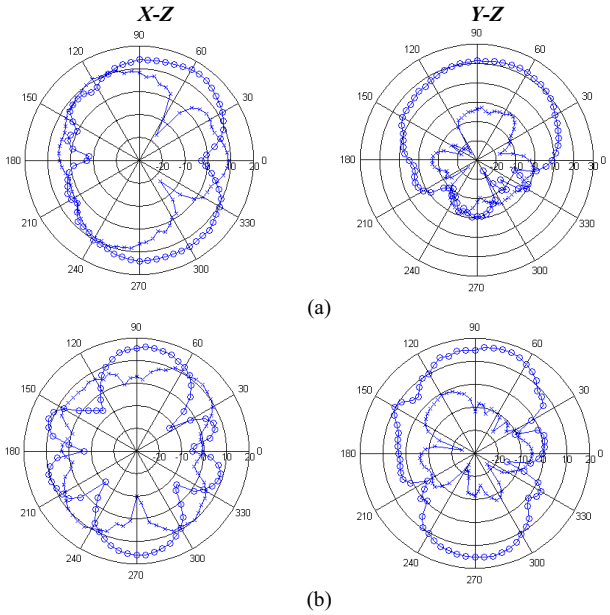

Figure 10. Far field patterns for vertically polarized antenna at *x-z* and *y-z* planes (a) Front, (b) Back; 'o-o-o': E_θ, 'x-x-x': E_ϕ.

A. Near and Far Fields Simulation

The near and far fields of the antenna are calculated and analyzed for the various locations in order to build up a realistic picture of the antenna performance while in close proximity with the human body. As shown in Fig. 6, a total of 32 locations were investigated, 16 on the back and 16 on the front. Sub-gridding was carried out within the human body model space, for the near field analysis, using 10×10×10 FDTD cells, see Fig. 7. In other words, sub-gridding volume in length was 60×60×60 mm. Fig. 8 shows the electric field distributions (using an equivalent dB scale) in the immediate neighbourhood, and the interior, of the body model, in the x–z and y–z planes, for the horizontal polarization state. Fig. 9 shows the electric field distribution inside the sub-gridded region for the x–z plane (dB scale, again). Further simulations were performed using the same antenna locations for the vertical polarization state, these were found to be comparable with the horizontal state.

The electric field distributions obtained in the neighbourhood of the human body model were almost the same regardless of whether the antenna tag was horizontally or vertically polarized. A similar observation was also produced within the sub-gridded region. The electric fields were very strong when the antenna tags are located close to the body, as indicated by the red colourization in the plots. Fig. 10 shows the far field radiation pattern for the antenna (in vertical

polarization) at the front and back of the human body model. The underlying computation was normalised to 1 W input power. The variation in the far field patterns implies that the field distributions are more concentrated in the direction facing the normal antenna axis, and away from the body. The field magnitude is reduced by between 10 dB to 20 dB due to the tailing effect of the body. Once again, the field distributions for the horizontally polarized state were quite similar to the vertical state, and are not reproduced here.

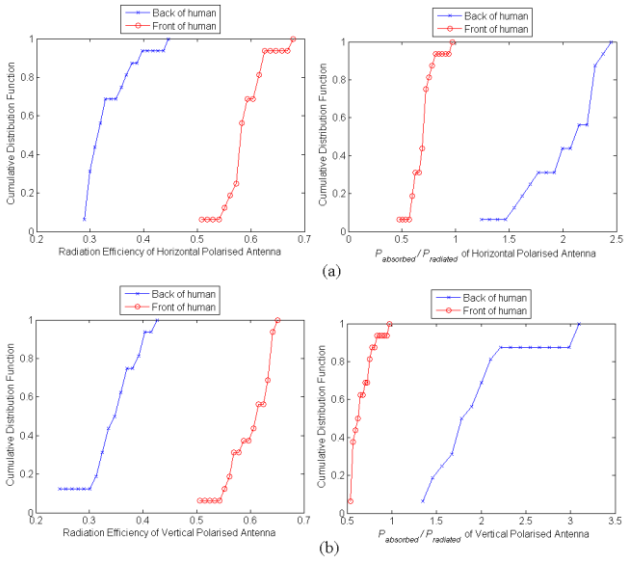

Figure 11. The CDF of the radiation effeciency and $P_{absorbed}/P_{radiated}$: (a) Horizontal polarization, (b) Vertical polarization.

B. *Cumulative Distribution Function (CDF)*

The absorbed and radiated powers generated within the human body model were obtained online during the simulations, from which the radiation efficiency of the antenna may be inferred. The cumulative distribution function (CDF) was calculated for each location in order to estimate the probability of the power absorbed and radiation efficiency with respect to location over the human body, see Fig. 11. The radiation efficiency values increase as the antenna moves from the back to the front of the body. The antenna achieves a mean radiation efficiency of 43% for both polarization states when the antenna is located on the front of the human body model, in contrast with the back positions.

VI. CONCLUSION

The bio-electromagnetic interaction between the human body, and a short range 900 MHz RFID tag antenna, located in close proximity to the body, has been developed with the aid of a hybrid MoM–FDTD–(SG)FDTD code. The inhomogeneous body properties were represented using the Visible Man model. The functional performance of the antenna was characterised in terms of the horizontal and vertical polarization states for tags distributed over thirty two distinct body locations. In addition, near and far field distributions were computed. The CDF of the radiation efficiency and the ratio of absorbed power over radiated power of the antenna was obtained for the set of body locations. This approach to the model definition, and performance analysis, should better enable future studies of antenna tags for medical and on–body communication applications with realistic forecasts of the impact of the body on antennas, both in face–on and oblique body locations.

ACKNOWLEDGEMENTS

K. N. Ramli would like to thank the Ministry of Higher Education Malaysia, and Universiti Tun Hussein Onn Malaysia (UTHM), for their financial support.

REFERENCES

[1] M. Abalenkovs, F. Costen, J. P. Berenger, and A. Brown, "Application of huygens subgridding technique to human body modelling," Antennas and Propagation Society International Symposium, pp. 1-4, 2008.

[2] A. Sani, Y. Zhao, Y. Hao, A. Alomainy, and C. Parini, "An efficient FDTD algorithm based on the equivalence principle for analyzing onbody antenna performance," IEEE Transactions on Antennas and Propagation, vol. 57, pp. 1006-1014, 2009.

[3] Y. Z. Sani, A. Y. Hao, S.-L. Lee, and G.-Z. Yang, "A simulation environment for subject-specific radio channel modeling in wireless body sensor networks," *Sixth International Workshop on Wearable and Implantable Body Sensor Networks (BSN 2009), Berkeley, CA*, pp. 23-28, 2009.

[4] J.-H. Jung, S.-W. Kim, Y.-S. Kim, and S.-Y. Kim, "Electromagnetic propagation from the intestine-ingested source in the human body model," IEEE Transactions on Antennas and Propagation, vol. 58, pp. 1683-1688, 2010.

[5] D. Arnaud-Cormos, R. Loison, and R. Gillard, "Fast multistructure method of moments combined with a genetic algorithm (MSMoM/GA) for efficient optimization of printed antennas," IEEE Antennas and Wireless Propagation Letters, vol. 6, pp. 172-174, 2007.

[6] A. Becker and V. Hansen, "A hybrid method combining the multitemporal resolution time-domain method of moments with the time-domain geometrical theory of diffraction for thin-wire antenna problems," IEEE Transactions on Antennas and Propagation, vol. 54, pp. 953- 960, 2006.

[7] M. M. Ilic and B. M. Notaros, "Computation of FEM-domain fields in the higher order hybrid FEM-MoM solution," IEEE Antennas and Prop. Society International Symposium (APSURSI), pp. 1-4, 2010.

[8] A. Monorchio, A. R. Bretones, R. Mittra, G. Manara, and R. G. Martin, "A hybrid time-domain technique that combines the finite element, finite difference and method of moment techniques to solve complex electromagnetic problems," IEEE Transactions on Antennas and Propagation, vol. 52, pp. 2666-2674, 2004.

[9] P. A. Mason, W. D. Hurt, T. J. Walters, J. A. D'Andrea, P. Gajsek, K. L. Ryan, D. A. Nelson, K. I. Smith, and J. M. Ziriax, "Effects of frequency, permittivity, and voxel size on predicted specific absorption rate values in biological tissue during electromagnetic-field exposure," IEEE Transactions on Microwave Theory and Techniques, vol. 48, pp. 2050-2058, 2000.

[10] D. Zhou, R. A. Abd-Alhameed, C. H. See, M. S. Alkhambashi, Z. Zainal Abidin, K. N. Ramli, and M. M. Abusitta, "Meander-line antenna design for UHF RFID tag using a genetic algorithm," Progress in Electromagnetics Research Symposium, Beijing, China, pp. 1253-1256, 2009.

[11] G. J. Burke and A. J. Poggio, "Numerical electromagnetics code (NEC): method of moments," US Naval Ocean Systems Centre, Rep. No. TD116, 1981.

[12] R. A. Abd-Alhameed, P. S. Excell, C. H. See, D. Zhou and K. N. Ramli, "Accurate field distribution models for RFID applications using hybrid computational electromagnetics techniques," Progress in Electromagnetics Research Symposium, Cambridge, USA, pp. 436-442, 2008.